Enantioselective Synthesis of Pretomanid
&
Investigations of Raman Spectroscopy for Through-Tube Monitoring of Reactions

By

Tho H. Tran
B.S. Chemistry, *summa cum laude with honors*
University of Houston, 2014

Submitted to the Department of Chemistry in Partial Fulfillment
of the Requirements for the Degree of

DOCTOR OF PHILOSOPHY IN CHEMISTRY

at the

Massachusetts Institute of Technology

June 2019

Signature of Author: Signature redacted
Department of Chemistry
May 29, 2019

Signature redacted

Certified by:
Timothy F. Jamison
Robert R. Taylor Professor of Chemistry
Thesis Supervisor

Signature redacted

Accepted by:
Robert W. Field
Haslam and Dewey Professor of Chemistry
Chair, Departmental Committee on Graduate Studies

This doctoral thesis has been examined by a committee in the Department of Chemistry as follows:

Signature redacted

Professor Rick L. Danheiser _____
Thesis Committee Chair
A. C. Cope Professor of Chemistry

Signature redacted

Professor Timothy F. Jamison _____
Thesis Supervisor
Robert R. Taylor Professor of Chemistry

Signature redacted

Professor Mohammad Movassaghi _____
Thesis Committee Member
Professor of Chemistry

For Diana, family, and friends.

Enantioselective Synthesis of Pretomanid

&

Investigations of Raman Spectroscopy for Through-Tube Monitoring of Reactions

By

Tho Tran

Submitted to the Department of Chemistry on May 30, 2019
in Partial Fulfillment of the Requirements for the Degree of Doctor of Philosophy in Chemistry

Abstract

Chapter 1: Enantioselective Synthesis of Pretomanid

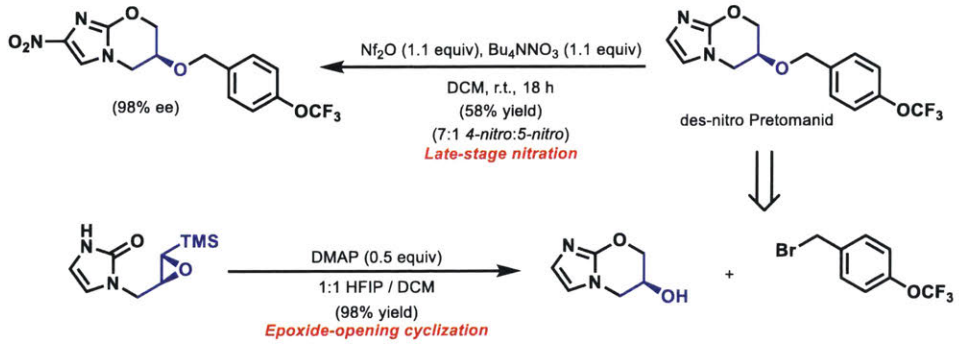

Pretomanid is a potential cornerstone active pharmaceutical ingredient for the treatment of tuberculosis (TB). It is found in several advanced clinical trials and can possibly treat all forms of TB. In this report, we discuss the development of a novel synthesis of pretomanid through a selective epoxide-opening cyclization and late-stage nitration. This route offers a new strategy to access the core of pretomanid and avoids the necessity of the explosive starting material.

Chapter 2: Investigations of Raman Spectroscopy for Through-Tube Monitoring of Reactions

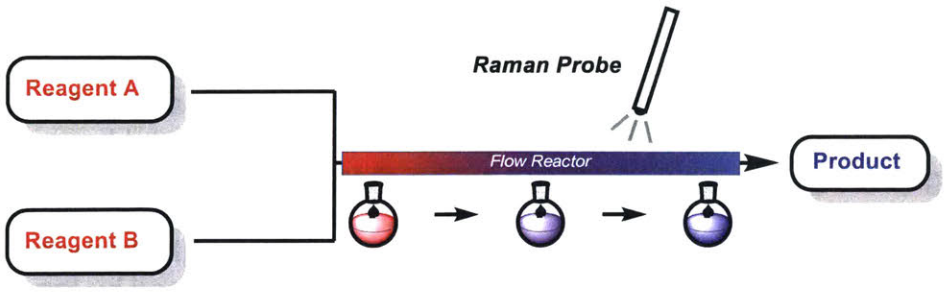

Continuous-flow chemistry has seen expansive growth and thus requires powerful new analytical techniques. The current commonly-used analytics involve inline analysis at a single point, which can hinder analysis. In this report, we demonstrate the utility of the MarqMetrix TouchRaman probe for reaction monitoring through a continuous-flow reactor. The reactions studied were ring-closing metathesis, benzyne generation, and ketene generation.

Acknowledgements

I have been so lucky to have the privilege of working with and getting to know so many wonderful, talented people throughout my academic career. Overall, I have learned so much from those around me and I thank them for their support and inspiration.

As I reflect back on my graduate career, I find myself with a completely different perspective compared to when I first step foot at MIT. As a scientist, I have grown so much through the rigorous training offered by the chemistry department and by being in Tim's lab. As a person, I have developed a better understanding of the importance of mental wellness through my training as a ChemREFS and through the many discussions with other passionate people. I am constantly impressed by the amount of people at MIT that strive to make our community a more inclusive and caring environment for everyone.

First and foremost, I thank Prof. Timothy F. Jamison for accepting me into his research team and for his mentorship throughout my graduate career. I still remember my first interaction with him, which was when he called me to inform me that I had been accepted into MIT. Little did I know that I would be part of his laboratory about a year later. As a member, I appreciate the trust and faith that Tim placed in me when I proposed the synthesis of pretomanid as a second year. For the entirety of the project, Tim has been exceptional in offering guidance and valuable feedback that has made me into a much better scientist. Furthermore, Tim has provided me with intellectual freedom to pursue my own curiosities; thus, allowing me to diversify my skillset. I thank Tim for the laboratory environment that he has carefully created. The culture has been wonderful in terms of support, kindness, and intellect.

I thank Prof. Rick L. Danheiser for not only being my committee chair but also as someone that I have had the opportunity to work with on multiple occasions. I have learned so much from his classes, our insightful discussions, and our annual meetings. I thank Prof. Mohammad Movassaghi for serving on my committee and for his thoroughness in providing me with suggestions, insight, and advice on my thesis.

Within the Jamison group, I like to thank all the past and present colleagues for their camaraderie and support throughout my graduate career: Dr. Anne-Catherine Bédard, Dr. Justin Lummiss, Dr. Long Nguyen, Dr. Tim Monos, Dr. Rachel Beingessner, Dr. Preston MacQueen, Dr. Wai-Chung Fu, Dr. Kelley Danahy, Dr. Jessica Weber, Dr. Liam Kelly, Hyowon Seo, Mary Grace Russel, Katie McGeough, Christopher Breen, Sarah Jane Mear, Grace Ahlqvist, Corshai Williams, Erica Flear, Tabrez Alam, Aria Fodness, Dr. Jon Jowarski, Dr. Peter Morse, Dr. Evan Styduhar, Dr. Pedro Garcia Barrantes, Dr. André Yvon-Bessette, Prof. Alexandra Strom, Dr. Charles Ocampo, Dr. Aaron Beedermann, Dr. Jamie Chen, Dr. Laurel Heckman, Dr. T. Andrew McTeague, Dr. Rob Ziegler, Dr. Rob Hicklin, Dr. Ashley Longstreet, Dr. Satapanawat Sittihan, Dr. Hideki Moriguchi, Dr. Elizabeth Kelley, Prof. Frank Leibfarth, Dr. Matthew Katcher, Dr. Toma Halkina, Dr. Christina Dai, Dr. Sarah Tasker, Dr. Eric Standley, Prof. Erin Podlesney, Prof. Zhi He, Dr. Doris Lee, Amanda Wicker, Martin Johansen, Cedrick

Veryser, Cody Schurter, and Felix Strieth-Kalthoff. They have been amazing to work with!

In particular, I thank Dr. Anne-Catherine Bédard for her mentorship and support through my toughest times. Her wisdom and caring nature has taught me so much to become a better person and a better scientist. Similarly, I thank my past mentors, Dr. Charles Ocampo, Dr. Evan Styduhar, Dr. Alexandra Strom, and Dr. Long Nguyen for their support in developing my skills as a scientist.

I thank Dr. Justin Lummiss for being a wonderful friend and collaborator on the Raman project. His knowledge in chemistry and creative approaches to solving problems has taught me so much on becoming a better scientist.

I thank my cohort, Dr. Jessica Weber, Amanda Wicker, Dr. Kelley Danahy, Dr. Liam Kelly, and Dr. Hyowon Seo, for being part of our self-proclaimed team "TBDMS." I enjoyed our many brunches and support group sessions! I couldn't have gotten through graduate school without them.

Outside of the Jamison lab, I have met so many wonderful and talented people. In particular, I thank Pulkit Shamshery for being my best friend throughout my career. He was literally the first person I became friends with in Boston. I thank Julia Zhao for her support and kindness. I thank Jiun-Le (Edward) Shih for his friendship throughout my time at MIT. I appreciate his continued mentorship and selfless character.

I thank my family for their incredible support throughout my stay at MIT. I thank my late grandma for her love and care throughout my life. She has sacrificed so much for my education and I hope to make her proud as the first to graduate in our family from both college and graduate school. I thank my amazing mom and dad for believing in me and allowing me to pursue my passion in chemistry. They have worked so hard throughout their lives to see their children succeed and to have a better life than they did. I appreciate all that they do. I thank my sister for her love and care. I have learned so much from her incredible resilience through the toughest times and how to overcome any obstacle. Finally, I thank Dr. Diana M. Dang, who has been my foundation from the very beginning. Her continued support and love has provided with me with everything I needed to become a better person. She has been inspirational in terms of her work ethics and her motivation to constantly improve. I look forward to what we can accomplish together in the future.

Table of Contents

List of Abbreviations

μW	microwave
Ac	acetyl
API	active pharmaceutical ingredient
Bz	benzoyl
Bn	benzyl
Bu	butyl
cat.	catalyst
DA	Diels-Alder
DCM	dichloromethane
DCE	1,2-dichloroethane
Ddn	deazaflavin-dependant nitroreductase
DHP	dihydropyran
DIBAL	diisobutylaluminum hydride
DS	drug-sensitive
ee	enantiomeric excess
FDA	Food and Drug Administration
FM	lipid-rich foamy cells

h	hour
HG II	Hoveyda-Grubbs 2nd generation catalyst
HIV	human immunodeficiency virus
HMDS	hexamethyldisilazane
IR	infrared
MDR	multi-drug resistant
MGC	multinucleated Langhans giant cell
MP	macrophage
Mtb	*Mycobacterium tuberculosis*
NDA	new drug application
PG	protecting group
PPTS	pyridinium *p*-toluenesulfonate
RCM	ring-closing metathesis
TBAF	tetrabutylammonium fluoride
t-Bu	*tert*-butyl
TEA	triethylamine
TFAA	trifluoroacetic anhydride
TB	tuberculosis

TBME	*t*-butyl methyl ether
TBS	*tert*-butyldimethylsilyl
TMS	trimethylsilyl
Ts	toluenesulfonyl
WHO	World Health Organization
XDR	extensively drug resistant

Chapter One

Enantioselective Synthesis of Pretomanid

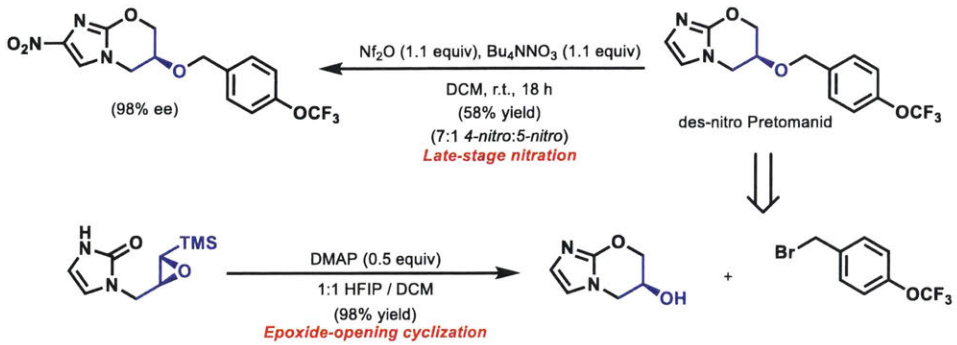

Abstract

Pretomanid is a potential cornerstone active pharmaceutical ingredient for the treatment of tuberculosis. It is found in several advanced clinical trials and can possibly treat all forms of TB. In this report, we discuss the development of a novel synthesis of pretomanid through a selective epoxide-opening cyclization and late-stage nitration. This route offers a new strategy to access the core of pretomanid and avoids the necessity of the explosive starting material.

1.1 Tuberculosis

1.1.1 General Introduction

Tuberculosis (TB) is a major global health problem and is one of the leading causes of death worldwide.[1] In 2017, there were 10 million new cases and 1.6 million deaths from the airborne disease caused by the bacillus *Mycobacterium tuberculosis*. Consequently, the World Health Organization (WHO) has declared TB as a persistent global health emergency. While the disease is fully treatable, the current multiple-drug treatment is lengthy and cumbersome, often requiring six or more months to have full efficacy.[6,7,8] Furthermore, the standard treatment is incompatible with HIV-regimens, causing further complication in disadvantaged regions where both HIV and TB are prevalent. Recently, there has been a rise in multi-drug resistant (MDR)-TB, and even extensively-drug resistant (XDR)-TB due to the poor compliance that often accompanies the outdated regimen. Therefore, it is critical that new and original therapies for TB are developed.

Pretomanid has emerged as a promising API in several clinical studies within the TB drug pipeline, including one that is currently under review for approval by the FDA.[9,10] Pretomanid is part of a recently discovered nitroimidazole drug class with a novel mechanism of action towards TB. In the *M. tuberculosis* cell, it first binds to an F_{420}-deazaflavin-dependent nitroreductase and is then subsequently activated to generate des-nitro pretomanid and nitrous acid.[14] The released nitrous acid then disproportionates into nitric oxide and will undergo anaerobic killing mechanism through nitric oxide poisoning of the cytochrome *c* oxidase. Pretomanid has additionally

displayed aerobic killing mechanism through inhibition of mycolic acid biosynthesis. These pathways resolve the issues from the current treatment in that poly- and multi-drug resistant TB strains are susceptible. Furthermore, the developing treatments involving pretomanid do not interfere with HIV medications.

Herein, we propose a novel, enantioselective synthesis of pretomanid through a challenging epoxide-opening cyclization followed by a late-stage nitration. This proposed route addresses many issues from existing routes such as avoiding an expensive, explosive starting material.[17]

1.1.2 What is tuberculosis?

Tuberculosis (TB) is the leading cause of death due to a single infectious disease, above HIV.[1] As a result, the World Health Organization (WHO) has declared this disease as a global health emergency. While estimates have varied, at least 1.7 billion people,* or 23% of the world's population, is infected. In 2017 alone, TB took the lives of an estimated 1.3 million people among those without HIV and an estimated 300,000 among those with HIV.[1] The most afflicted nations are generally those that reside in developing regions such as sub-Saharan Africa and southern Asia, according to incidence rates (Figure 1).[1] A disparaging view is through the case fatality ratio† (CFR) where variations in access to proper TB treatment and facilities can be seen (Figure 2). In other words, if people were treated in a timely manner with high quality care, then the CFR would be low despite a

* Approximately 5-10% will develop active TB during their lifetime.
† CFR – case fatality ratio, defined as the number of TB deaths divided by the estimated number of incident cases in the same years, expressed as a percentage.

high incidence rate. Unfortunately, this is not the case in nearly all heavily afflicted regions.

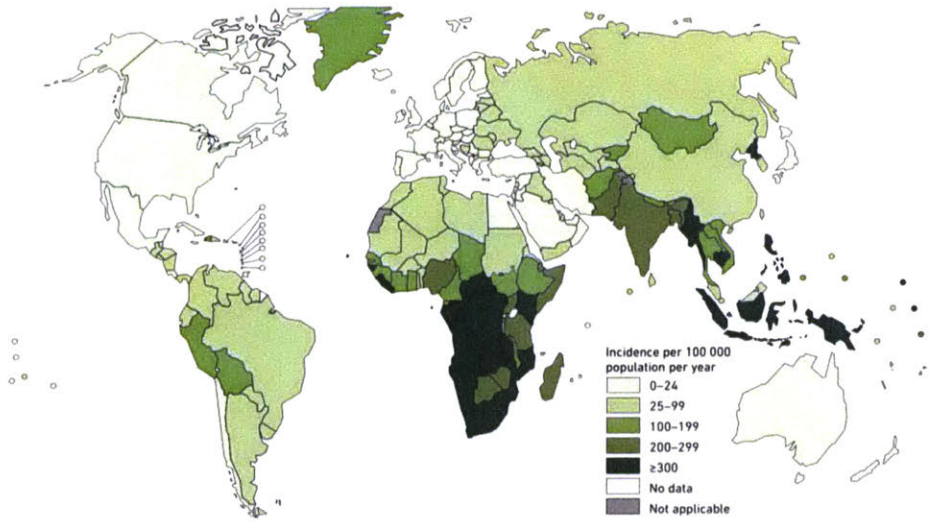

Figure 1. TB incidence rates per 100,000 population. (Image retreived from 2018 WHO TB report[1])

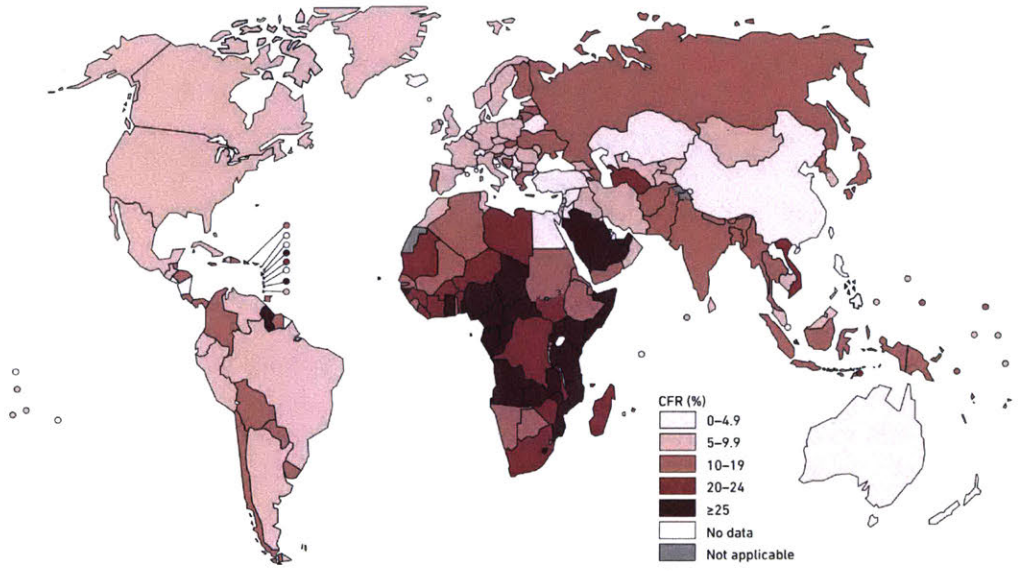

Figure 2. Case fatality rates (CFR) including HIV-negative and HIV-positive people by region. (Image retreived from 2018 WHO TB report[1])

1.1.3 Mycobacterium tuberculosis

Tuberculosis was discovered to be caused by the bacterium *Mycobacterium tuberculosis*, or Mtb, in 1882 by Robert Koch.[2] Since then, Mtb has been studied extensively and can exist within a host as two forms: active and latent.[3] The active form is what we commonly perceive as tuberculosis. In this form, the symptoms are present and can include fever, fatigue, persistent coughing, and haemoptysis or the coughing of blood. A common misconception with TB is that the Mtb infection is limited to only the lungs; however, the infection[‡] can spread throughout the body. In the active form, the bacteria is highly contagious via aerosol transmission. The latent form, by contrast, is completely symptom-free and innocuous. However, this form has the potential to develop into the active form in 5-10% of the cases and therefore poses a great risk.[4]

Upon exposure to the bacteria, Mtb will infect the human host through respiration where the bacteria will travel to the lower respiratory tract (Figure 3).[3] As Mtb lodges itself within the lungs, the alveolar macrophages (MP) will recognize this through its various receptors and will initiate uptake of the bacteria. Other pathways, such as the release of cytokines, T-cells, and B-cells are promoted to help with the bacteria envelopment (Figure 3a). These self-propagating processes initiate the recruitment of more immune cells to the infection site (Figure 3b) and will ultimately lead to the formation of granulomas known as multinucleated Langhans giant cells (MGCs) or differentiate into lipid-rich foamy cells (FM) (Figure 3c). Ironically, the creation of these granulomas creates a microenvironment at which the bacteria can survive without

---

[‡] Denoted as *extrapulmonary tuberculosis* and occurs in 15-20% of cases.

damage over long periods of time. At this point, Mtb exists as its latent stage, possibly for decades, until environmental factors, such as HIV infection or immune deficiency, or genetic factors, allow the bacteria to activate. [5] Its activation will result in the death of the infected macrophages leading to a necrotic zone called caseum due to its milky appearance (Figure 3d). Ultimately, the structure will disintegrate allowing exit of the bacteria, which will spread to other parts of the lungs and body and will lead to the formation of new lesions. The infection can additionally spread to other hosts through release of infected droplets via coughing (Figure 3e).

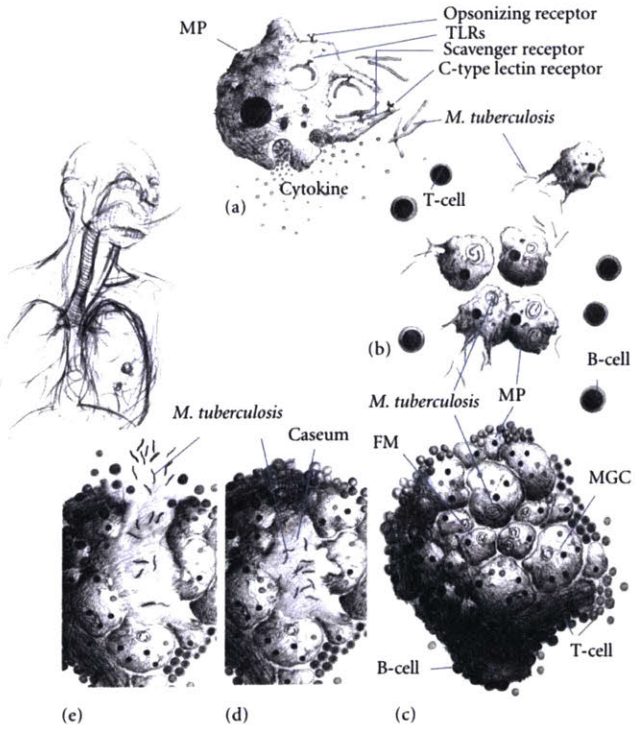

Figure 3. a) Macrophage response upon exposure to Mtb. b) More macrophages are recruited, along with other helpers from the immune system. c) Formation of MGCs or differentiation into FMs to allow for Mtb to exist in the latent form. d) Environmental or genetic triggers that causes death of the infected macrophages. Latent TB transitions into its active form. E) Mtb is released as the active form and spreads throughout the host and transmitted into the atmosphere. (Image retrieved from ref 3C)

1.1.4 Current global landscape of tuberculosis therapeutics and associated drawbacks

An effective method to treat tuberculosis is through multi-drug therapeutics.[6] The current state-of-the-art first-line treatment dates back to the late 1960s and has seen minor variations since then.[7] For active, drug-sensitive (DS) TB, the drug therapies will be a minimum two-month intensive phase of rifampicin (**4**), isoniazid (**3**), ethambutol (**1**), and pyrazinamide (**2**) followed by minimum four-month continuation phase of rifampicin and isoniazid (Figure 4). This lengthy treatment, which may last up to 2 years, and the combination of active pharmaceutical ingredients (APIs) has been determined to be the most effective and efficacious towards eradicating both forms of Mtb from the body. However, there is a chance of relapse due to residual latent Mtb.

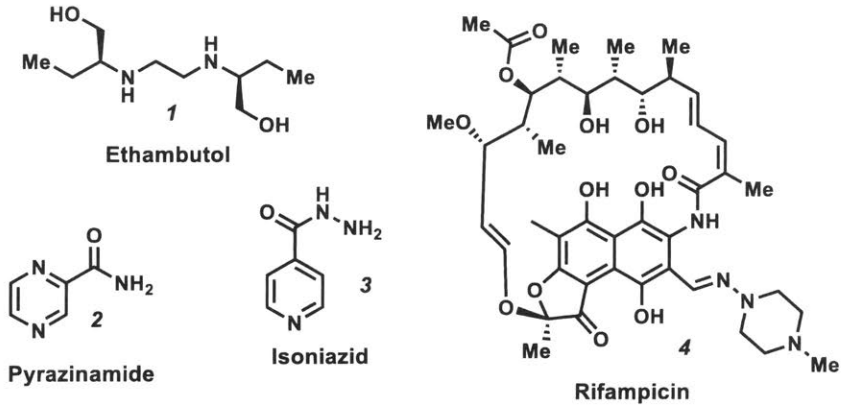

Figure 4. Typical APIs used as the first-line treatment of active, drug-sensitive TB.

The treatment is typically complicated with many adverse effects; in particular, liver injuries are frequent enough that close monitoring is necessary. As a result, TB is incredibly difficult to cure in developing regions due to both the required trained personnel and the amount of resources to carry out the treatment to ensure complete Mtb removal. Furthermore, the standard treatment is incompatible with HIV-regimens; thus, treatment for those also infected comes with many complications.[8]

In the past few decades, there has been a rise in drug-resistant Mtb strains. Of the 10 million new cases in 2017, 558,000 of those cases developed drug resistance to *at least* one of the APIs within the standard treatment.[1] Multi-drug resistant (MDR) TB has seen an overall increase in incidences rate in virtually all countries and is defined as having resistance to at least isoniazid and rifampicin, the two most effective APIs against Mtb. The most fatal drug resistant form is known as extensively drug-resistant (XDR) TB and is defined as having resistance to not only isoniazid and rifampicin but also to any fluoroquinolone and any of the injectable second-line aminoglycosides (Figure 5).[7]

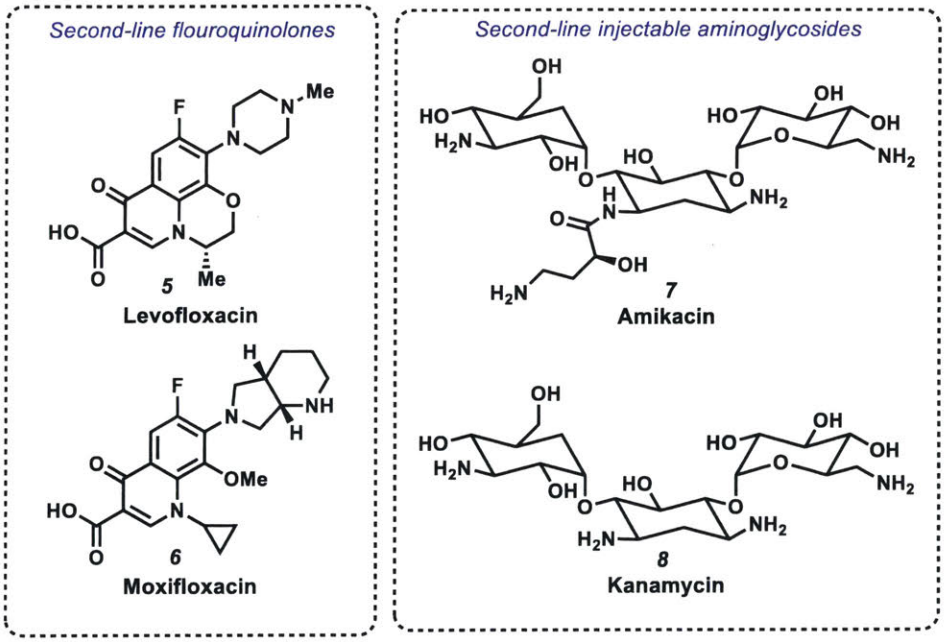

Figure 5. Second-line TB treatment examples of fluoroquinolones and injectable aminoglycosides.

1.1.5 The Global End TB Strategy set forth by WHO and the United Nations

From 2000 to 2015, there were considerable national and global efforts to reduce the burden of tuberculosis.[1] The WHO and United Nations have devised an "End TB Strategy" with three overarching, high-level indicators that are as follows:

- the number of TB deaths per year
- the TB incidence rate (new cases per 100 000 population per year)
- the percentage of TB-affected households that experience catastrophic costs as a result of TB disease

In this strategy, target milestone goals with several levels of accountability were set to solidify efforts that will ultimately lead to the eradication of the TB epidemic by 2035. The most immediate milestones, set for 2020, are to have a 35% reduction in TB deaths and a 20% reduction in TB incidence. From Figure 6, there has been a steady global decrease in both annual mortality rates and annual incidence rates from the year 2000 up to 2017. Sadly, these rates are not decreasing fast enough to reach the 2020 milestones.

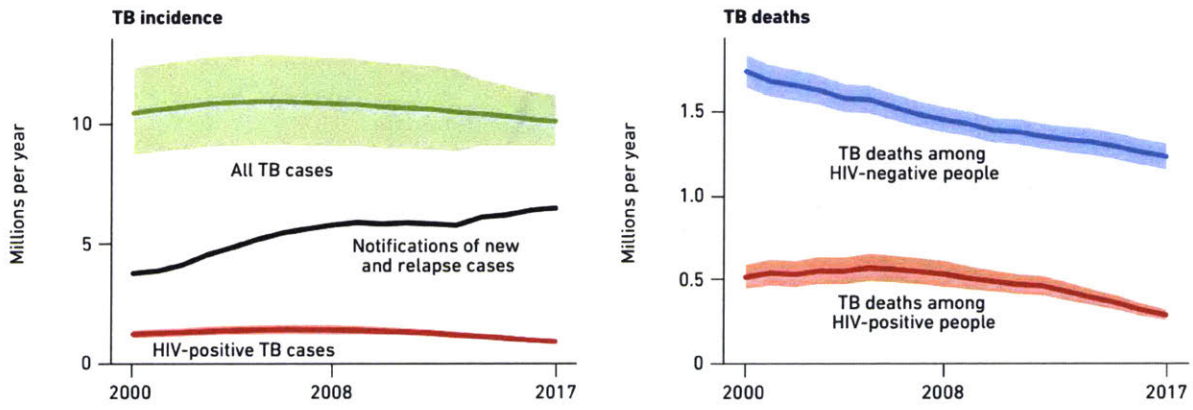

Figure 6. (Left) TB incidence rates on the decline for all TB cases, notifications of new and relapse cases, and HIV-positive TB cases. (Right) TB mortality rates among HIV-negative and HIV-positive people on the decline. (Image retreived from 2018 WHO TB report[1])

The ambitious goal to eliminate the TB epidemic by 2035 comes with many challenges that range from the worldwide presence of tuberculosis to the compounded difficulties of treatment and the rise of drug resistant strains. The global community have

taken on these challenges with full force and the future without TB is entirely possible. One immediate solution is the development of newer and more effective therapies.

1.2 Pretomanid as a promising new anti-TB active pharmaceutical ingredient

1.2.1 Pretomanid in promising emerging therapeutics

Pretomanid has emerged as a potential cornerstone API to be used in the treatment of not only drug-sensitive Mtb but also drug-resistant Mtb due to its unique biological activities. As of March 8, 2019, pretomanid is currently under review by the FDA to be approved as an orphan drug[§] under the new drug application (NDA)[**] submitted by the TB Alliance[††].[9] As a new chemical entity and a member of a class of compounds known as nitroimidazooxazines, pretomanid has appeared in 20 clinical trials spanning 14 countries. The current regimen under review is known as BPaL and is comprised of **b**edaquiline (**11**), **p**retomanid (**9**), and **l**inezolid (**10**) (Figure 7). In the clinical trial Nix-TB, where BPaL was used, 89% of participants with XDR-TB or those with treatment intolerant or nonresponsive MDR-TB was shown to have favorable outcomes. Furthermore, pretomanid is present in two other advanced phase III clinical trials known as SimpliciTB and ZeNix for the treatment of DS/MDR-TB and MDR/XDR-

---

§ An orphan drug is a pharmaceutical agent developed to treat rare medical conditions which would not be profitable to produce without government assistance. This assignment of orphan status to such diseases and drugs has spurred many medical breakthroughs that would have never been discovered.

** An NDA includes data gathered from animal studies and human clinical trials, and is a formal proposal for a new pharmaceutical to be sold in the US. On June 6, 2019, the FDA Antimicrobial Drugs Advisory Committee will host a public discussion for NDA 212862.

†† The Global Alliance for TB Drug Development is a not-for-profit organization dedicated to finding faster-acting and affordable drug regimens to fight TB. The TB Alliance utilizes innovative science and works with several partners around the globe to ensure equitable access to faster, better TB cures.

TB, respectively.[10] In these trials, the treatments are generally easier to administer (i.e. oral as opposed to injection) and are much shorter in length when compared to the current state-of-the-art. Moreover, there are no antagonistic interactions with current HIV-regimens.

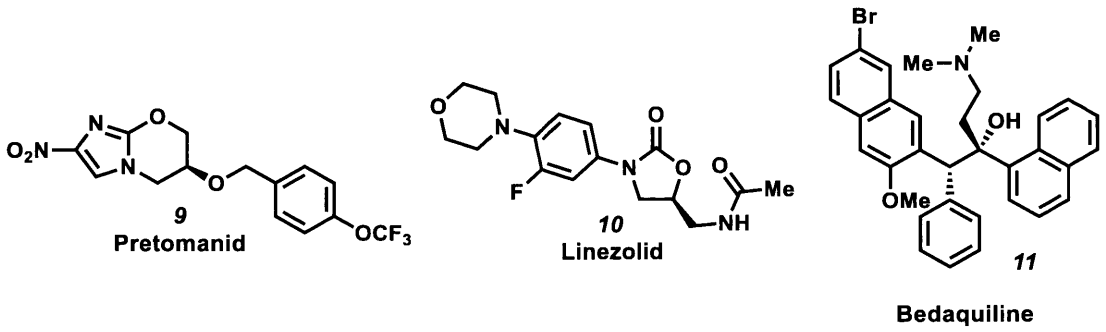

Figure 7. BPaL (bedaquiline, pretomanid, linezolid) currently under review to be approved by the FDA.

1.2.2 Structure development and mechanism of action

Pretomanid (**9**) exists in several high profile clinical trials. Accordingly, this has resulted in many studies on how the molecule behaves within the body. As a nitroimidazole, the development of pretomanid (**9**) can be traced back several decades.[11] The first appearance of such possible chemical entities to be used as drugs was metronidazole or Mtz (**12**) (Figure 8). Further structure-activity relationship (SAR) studies lead to CGI-17341 (**13**) and eventually PA-824, now known as pretomanid.[12] From these studies, delamanid (**14**) was discovered as a potent second-line option against MDR-TB; however, the treatments come with many adverse drug reactions.[13]

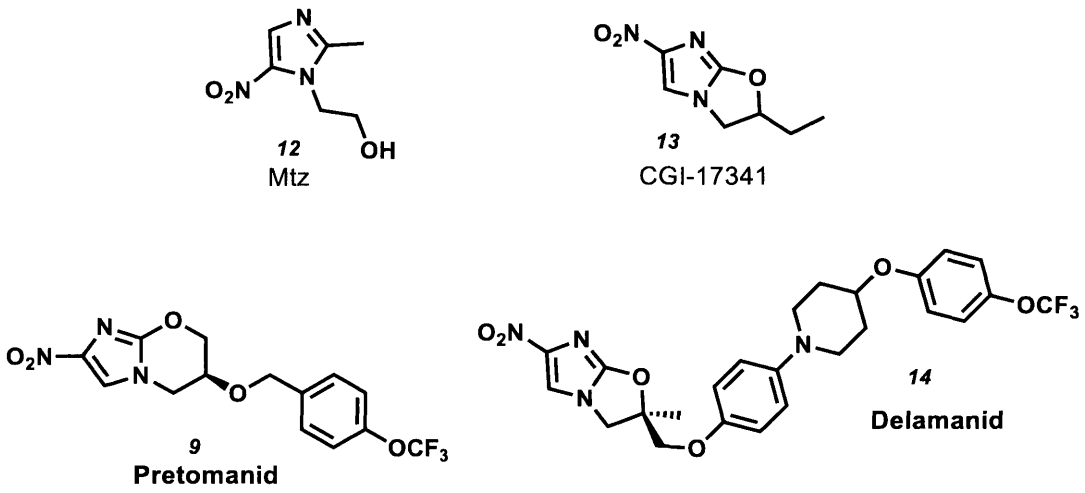

Figure 8. Mtz (**12**) as the first potential candidate as a nitroimidazole. Many SAR studies lead to CGI-17341 (**13**) and eventually pretomanid (PA-824) (**9**) and delamanid (**14**) as anti-TB candidates.

In 2008, Singh and coworkers discovered that pretomanid (**9**) proceeds through *two* possible mechanisms, effectively targeting both active, replicating Mtb and latent, non-replicating Mtb (Figure 9).[14] While the mechanism of actions are still under active investigation, it is likely to behave as a prodrug[‡‡]. In the aerobic pathway of active, replicating Mtb, pretomanid has been shown to disrupt the formation of mycolic acids, major constituents of the cell envelope of Mtb. The mycolic acids are critical for the integrity of Mtb's cell wall, and therefore, replication is prevented.

For the anaerobic pathway that targets latent Mtb, pretomanid is activated by a deazaflavin-dependant nitroreductase (Ddn) and cofactor F_{420} (Ddn:F_{420}) found within Mtb's cell wall. Through a very specific binding, pretomanid is reduced to generate toxic nitrogen species, such as nitric oxide, that react with cytochromes within Mtb to interfere with electron flow and disrupt ATP homeostasis. This process requires a very powerful

[‡‡] A prodrug is a medication or compound that is metabolized into a pharmacologically active drug.

reductant not commonly found in mammals. In fact, Ddn:F_{420} is an enzyme that is common to microoorganisms and extremophiles.

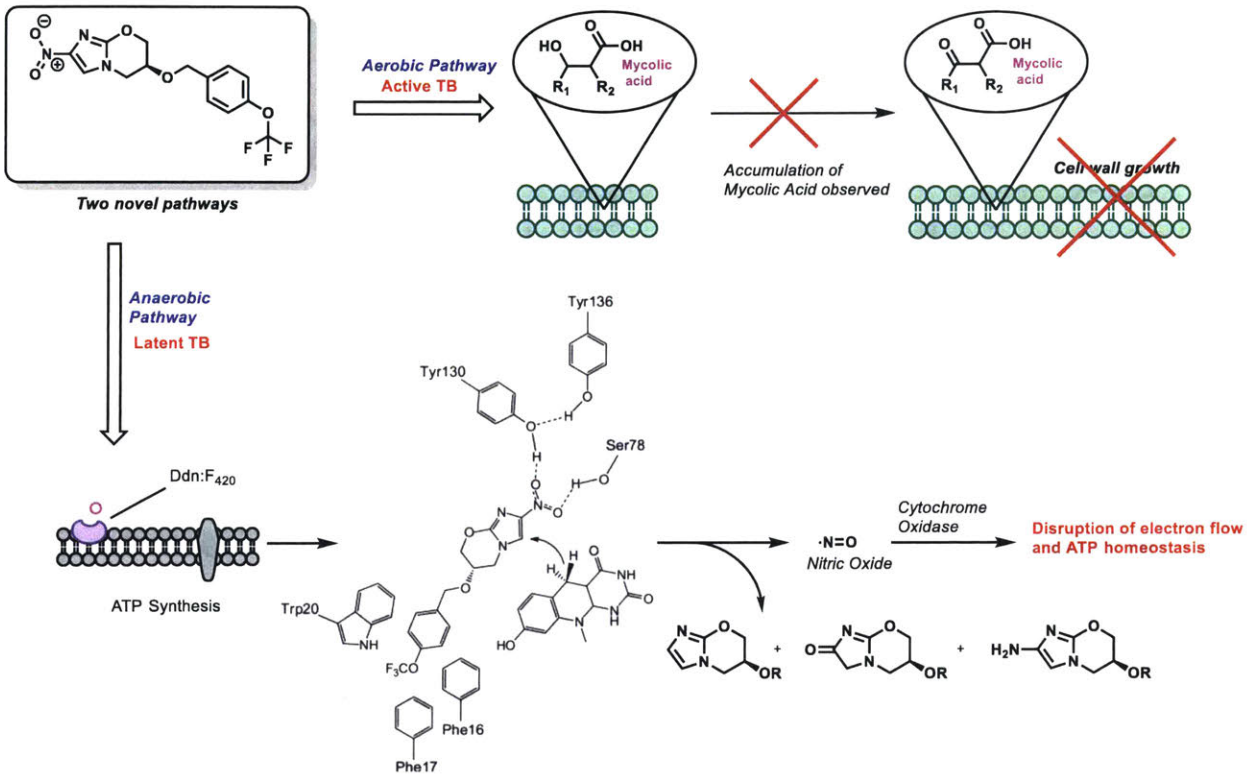

Figure 9. Two possible mechanisms of action for pretomanid (**9**) that effectively targets both active and latent Mtb.

These biological activity studies explain why pretomanid has shown such promise in clinical trials for the treatment of all forms of Mtb. The dual nature of its biological activity allows it to successfully treat both latent and active forms of Mtb. Furthermore, these unique biological pathways allows it to target MDR- and XDR-TB.

1.2.3 Current syntheses

Given the importance of pretomanid, a viable, novel synthetic route is necessary to meet supply demands. The original synthesis of **9** by Baker and coworkers was performed in a five-step linear sequence (Scheme 1A).[15,16] First, imidazole **15** was used

to open epoxide **16** to furnish alcohol **17**. Then, protection of alcohol **17**, followed by cleavage of the silyl ether and concomitant cyclization, furnished oxazine **18**. Finally, deprotection of **18** followed by benzylation with **19** provided pretomanid (**9**). Though relatively concise, the sequence suffers from the use of an explosive 2,4-dinitroimidazole (**15**) as starting material,[17] and two protecting group manipulations to access the oxazine core **18**. Moreover, the synthesis required four chromatographic separation steps, and as a result, its practicality on scale was limited. However, with pretomanid (**9**) being a possible new cornerstone treatment for TB, much work has been devoted to improve the costs and efficiency of the route, including a nonexplosive variant to **15**, a solventless modification, and a butanoyl group in lieu of the TBS group.[18,19,20]

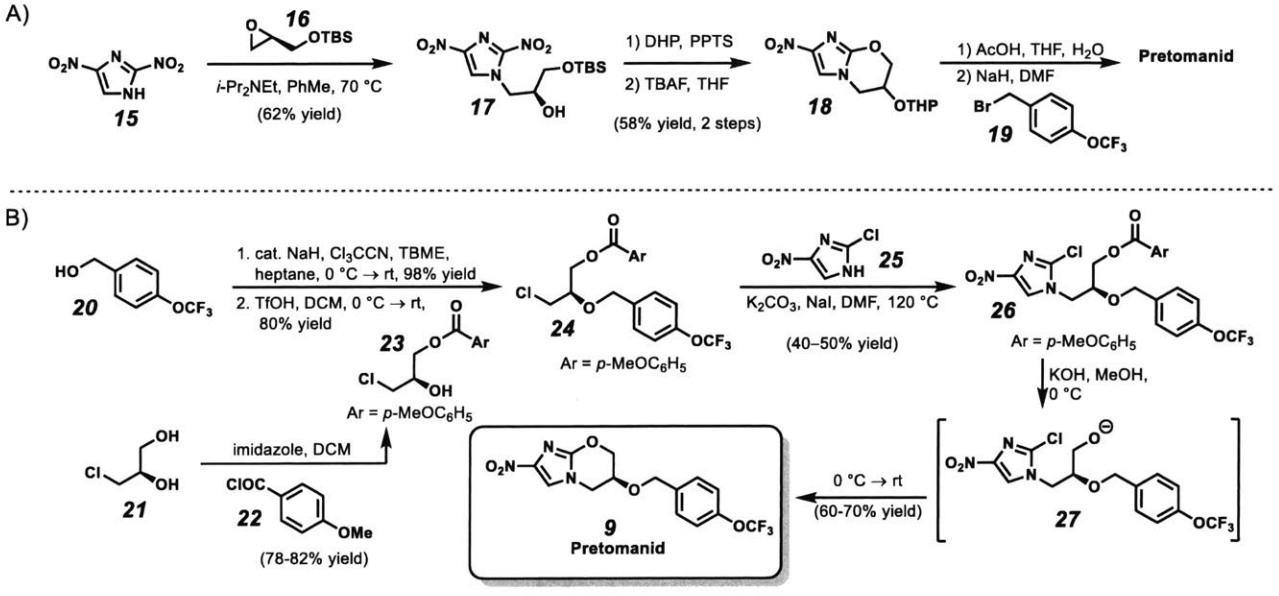

[a]DHP = 3,4-dihydro-2H-pyran; PPTS = pyridinium *p*-toluenesulfonate.

Scheme 1. A) Original route by Baker and coworkers. B) Sorensen route.

In 2010, the Sorensen group developed a convergent synthesis that accessed to pretomanid in a convergent four step sequence (Scheme 1B).[21] First, alcohol **20** was

converted into its trichloroacetimidate derivative and reacted with alcohol **23**, which was formed through a benzoylation of diol **21**, to give chloride **24**. Then, chloride displacement of **24** with nitroimidazole **25** gave imidazole **26**. Finally, saponification and subsequent cyclization provided pretomanid (**9**). A notable feature was the use of recrystallization for all except the last step, which required chromatographic purification, allowing the route to be suitable for kilogram-scale production.

In both of these routes, a recurrent issue was the use of the explosive dinitroimidazole **15**. In both the modified industrial route and the Sorensen route, the problem was circumvented by using a chloride variant which reduce the detonation potential. However, the chloride variant **25** comes directly from dinitroimidazole **15** through a laborious, dangerous, and hazardous route requiring high temperatures and concentrated acids (Scheme 2). Starting from imidazole (**28**), two tandem nitrations under harsh acidic conditions provided a highly explosive 1,4-dinitroimidazole (**30**). Then, a thermally promoted 1,5-shift in chlorobenzene furnished 2,4-dinitroimidazole (**15**). Prolonged heating in hydrochloric acid and chlorobenzene allowed for successful exchange of the nitro group to provide chloride product **25**.

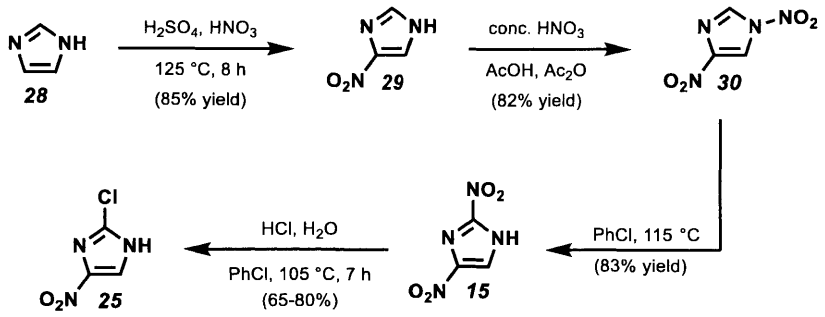

Scheme 2. Synthesis of 2,4-dinitroimidazole (**15**) and 2-chloro-4-nitroimidazole (**25**).

While these routes offer many advantages, there are many potential areas for improvement. One potential area is avoiding the use of explosive dinitroimidazole **15**. In addition, since the overall cost and number of steps to access pretomanid is a major factor for its future production at a much larger scale, a safer route that can access the oxazine core more rapidly from cheap, simple starting materials would offer a great advantage. Therefore, a new synthesis that addresses these challenges while advancing modern chemical techniques is needed.

1.3 Synthesis of Pretomanid

1.3.1 Proposal and retrosynthetic analysis

Herein we propose a novel route to pretomanid (**9**). Shown retrosynthetically in Scheme 3, we envision that **9** will be accessed through a selective nitration of des-nitro pretomanid (**31**). Des-nitro pretomanid (**31**) can then come from trapping of the alkoxide of oxazine **32** with benzyl bromide **19**. To form oxazine **32**, imidazolone **34** will undergo a bis-alkylation with dielectrophilic epichlorohydrin (**33**). This route offers benefits over the existing routes in its brevity and its absence of any protecting group manipulations. The starting material imidazolone **34** can be accessed from inexpensive commodity chemicals such as tartaric acid and urea. In addition, epichlorohydrin (**33**) can be accessed readily from biomass.[22,23]

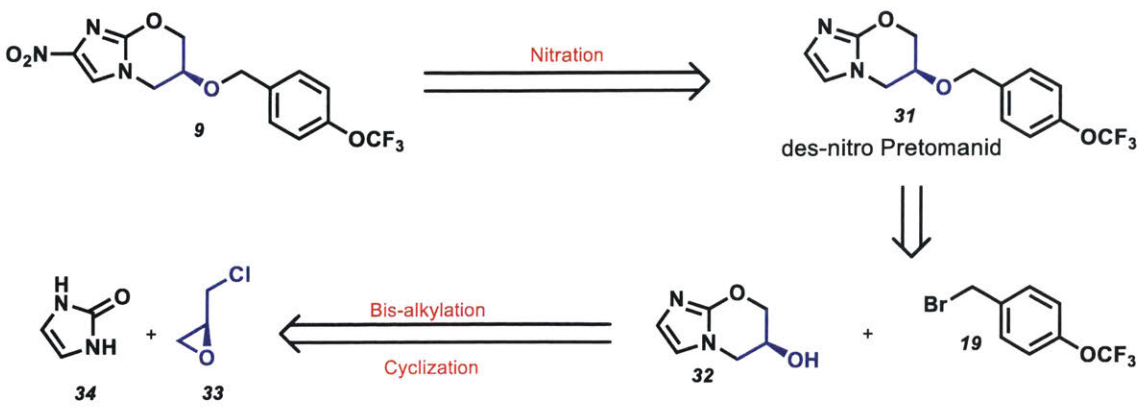

Scheme 3. Retrosynthetic analysis of pretomanid (**9**) through epoxide-opening cyclization and late-stage nitration.

1.3.2 Synthesis of analytical standards to aid investigation

In order to analyze the reactions in the proposed synthesis, oxazine **32** and des-nitro pretomanid (**31**) were obtained through a scaled-up, modified route by Singh and coworkers.[14A] To begin, racemic silyl ether **16** was synthesized in quantitative yield from glycidol **35** (Scheme 4).[24] Next, we treated (±)-**16** with K_2CO_3 and 2-nitroimidazole (**36**) to give alcohol **37** in 73% yield. Protection of alcohol **37** with 3,4-dihydro-2*H*-pyran (DHP) and pyridinium *p*-toluenesulfonate (PPTS) gave protected diol **38** in 84% yield.

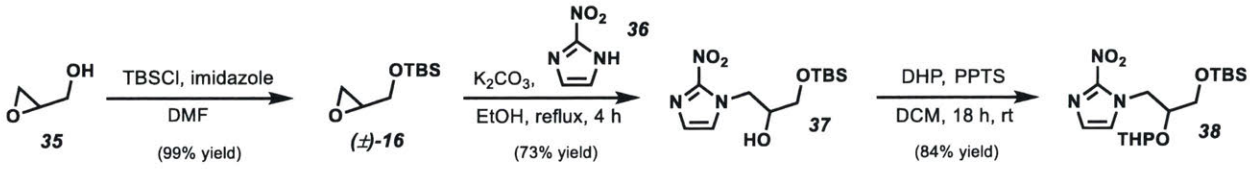

Scheme 4. Synthesis of protected diol **38**.

From there, we pursued formation of the oxazine core of des-nitro pretomanid (**31**). From protected diol **38**, cleavage of the TBS group followed by ring-closing via S_NAr would have to occur to form **39** (Table 1). The reported conditions required treatment with TBAF to cleave the silyl ether and then super-heating THF in a sealed

vessel at 125 °C to force the ring closure. For comparison, the cyclization occurred readily at room temperature for the synthesis of **18** involving either the dinitrated (**17** to **18**, Scheme 1A) or chloronitrated variant (**26** to **9**, Scheme 1B). Therefore, having the electron-withdrawing nitro group at the 4-position likely activates the imidazole ring towards S_NAr to a large extent. When the conditions were attempted, yields of less than 20% were consistently observed upon isolation (Table 1, entry 1). The low yields may be due to side reactions from the prolonged inefficient thermal heating under high pressure. Therefore, an alternative would be to investigate the reaction conditions under microwave irradiation as it has been shown to be more efficient in bulk heating.[25] It was found that subjecting **38** with TBAF followed by microwave irradiation at 130 °C gave **39** in 43% yield in 2 h (entry 2). The reaction time was then shortened to control for possible product decomposition and **39** was isolated in 78% yield within 5 minutes (entry 3). To ensure that ring-closing had indeed occurred, HMBC analysis was performed and key interactions of C8 with H7 and H5 were observed.

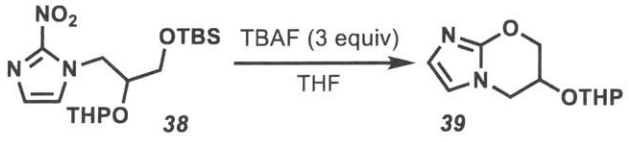

38 *39*

Entry	Conditions	Yield[a]
1	125 °C, 18 h, sealed vessel	<20% (65%)[b]
2	130 °C, 2 h, μW	43%
3	130 °C, 5 min, μW	78%

[a] isolated yield via column chromatography. [b](reported yield).

HMBC Analysis

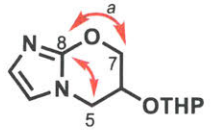

C8 with H5 and H7

Table 1. Cyclization of **38** to give protected oxazine core **39.**

We then sought to complete the synthesis of des-nitro pretomanid (**31**) from **39**. First, deprotection of **39** was performed with acetic acid in aqueous THF. We discovered that simple trituration with DCM gave (±)-**32** in 80% yield (Figure 10) and this methodology expedited purification. With oxazine (±)-**32** in hand, benzylation with **19** would give us the desired des-nitro pretomanid (**31**). Repeating the reported procedure provided **31** in 36% yield (Table 2, entry 1). Switching to THF gave less than 10% yield, likely from the poor solubility of (±)-**32** (entry 2). Since TBAI is a known phase-transfer catalyst,[26] product may have been lost to the aqueous layer during extraction due to the emulsion that formed. An alternative was to use NaI; however, low yields were still observed (<10%) (entry 3). When the additive was omitted, **31** was formed in a synthetically useful yield (72%) (entry 4).

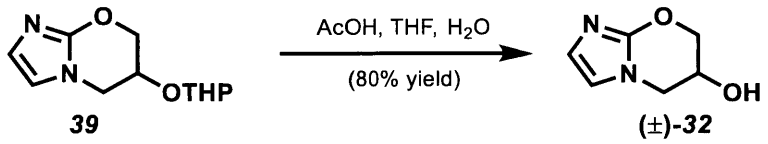

Figure 10. THP deprotection.

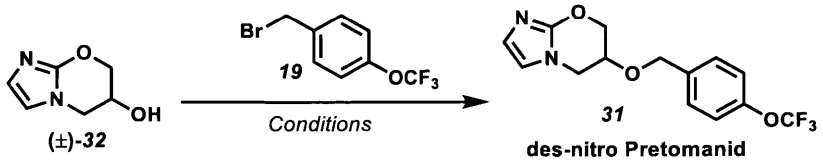

Entry	Solvent	Base	Additive	Temperature	Time	Yield
1	DMF	NaH	TBAI	0 °C→ rt	5 h	36% (56%)[a]
2	THF	NaH	TBAI	0 °C→ rt	5 h	<10%
3	DMF	NaH	NaI	0 °C→ rt	5 h	<10%
4	DMF	NaH	-	rt	5 h	72%

[a] (reported yield).

Table 2. Benzylation conditions of oxazine(±)-**32**.

When basic conditions using amines such as Hünig's base were studied, we observed the unexpected epoxide product **41** in quantitative yield (Figure 11).

Presumably, under these basic conditions, the imidazole 3-nitrogen of the oxazine core (±)-**32** is more nucleophilic than the hydroxyl group. Therefore, with adequate heating, alkylation at nitrogen will occur to give intermediate **40** followed by ring-opening to relieve the positive charge. A similar ring-opening of the oxazine core was reported by Thompson and coworkers about a year after this discovery was made with AcCl as the nitrogen activator.[27, §§]

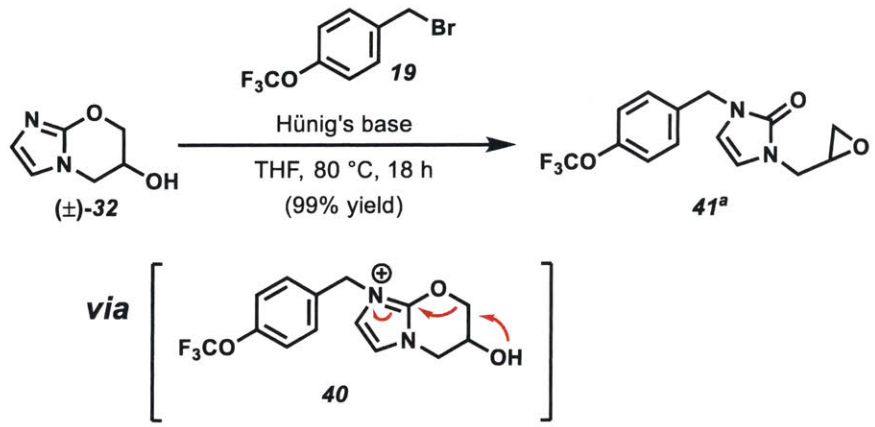

[a] Characterized through mass-spectrometry and NMR experiments such as ^{1}H NMR, ^{13}C NMR, ^{19}F NMR, HMBC, HSQC, and COSY.

Figure 11. Unexpected rearranged product with Hünig's base.

From our proposed bis-alkylation cyclization, we anticipate that the 5-membered oxazole **43**[***] is a possible side product. We have learned from the formation of oxazine (±)-**32** that the conditions will likely require an alkoxide intermediate and high heat to promore S_NAr. In addition, we anticipate that the cyclization will be faster as we are forming a 5-membered ring over a 6-membered ring. Thus, we were able to obtain TBS-protected oxazole **42** from **37** in 57% yield under refluxing NaH in dioxane (Table 3, entry 1). We then attempted homogeneous conditions under microwave conditions with

§§ The rearranged product was discovered in 2016.
*** To be discussed in greater detail in Section 1.3.5. Structure shown in Table 4.

NaO*t*-Bu as the base and obtained **42** in 71% yield (Table 3, entry 2). NaO*t*-Bu was chosen to prevent possible intermolecular S_NAr side reactivity that may occur with smaller, more nucleophilic bases. HMBC analysis confirmed that it was indeed the oxazole core that was formed. Interesting, we were not able to observe a correlation between the 3° proton (H3) and central carbon (C1). When modeling the structure via molecular mechanics 2 (MM2) calculations, we found that the dihedral angle was approximately 104° and would therefore be very weak or undetectable according to the Karplus relationship.[28] From there, the last step was remove the TBS group. To our surprise, this proved more challenging than simply using TBAF conditions from before, which only provided **43** in 20% yield (Table 4, entry 1). The likely cause for the low yields was possibly due to the oxazole product **43**'s affinity to TBS-F or tetrabutylammonium cation and its low solubility in organic solvents. Therefore, we utilized conditions from the Kishi protocol to remove the ammonium cation but only trace product was observed (entry 2). [29] This result could be attributed to the formation of a strong ionic bond between protonated oxazole and sulfonyl anion found on the surface of the DOWEX 50WX8-400 resin (Figure 12). Next, acidic conditions were attempted with only starting material recovered (entry 3). The best result was avoiding work-up completely and gave **43** in 85% yield (entry 4).

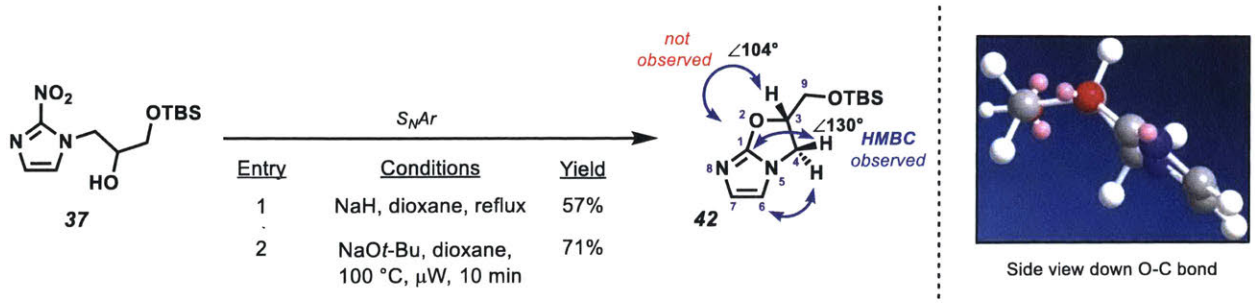

Entry	Conditions	Yield
1	NaH, dioxane, reflux	57%
2	NaO*t*-Bu, dioxane, 100 °C, μW, 10 min	71%

Table 3. Synthesis of TBS-oxazole **42**, a possible by product from epoxide-opening cyclization.

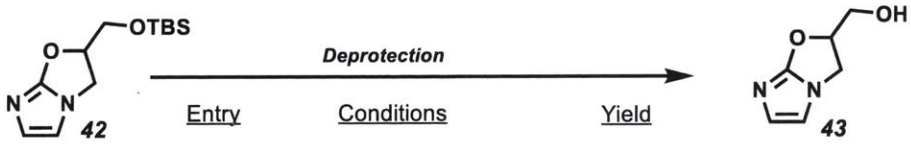

Entry	Conditions	Yield
1	TBAF, DCM, w/up	20%
2	TBAF, DCM, Kishi protocol	Trace product
3	TsOH (.2 equiv), MeOH, DCM	NR
4	TBAF, DCM, no w/up	85%

Table 4. Desilylation conditions to give oxazole **43**.

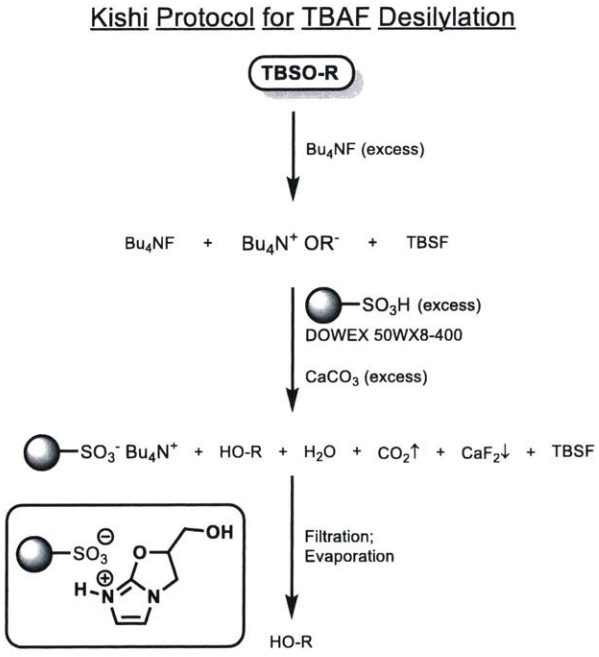

Figure 12. Attempted Kishi protocol for desilylation of TBS-protected oxazole **43.**

We have successfully synthesized important analytical standards, such as oxazine (±)-**32**, oxazole **43**, and des-nitro pretomanid **31** for the analysis of our bis-alkylation cyclization conditions (Figure 13). Given that we have sufficient access to des-nitro pretomanid **31**, our best course of action was to establish selective nitration conditions.

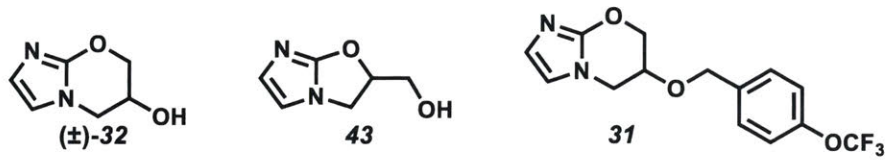

Figure 13. Important analytical standards, such as (±)-**32**, **43**, and **31**, successfully synthesized.

1.3.3 Studies on selective late-stage nitration

In order for our synthesis to be successful, the nitration must be selective for the 4-position of imidazole over all other possibilities including the 5-position and the phenyl ring (Figure 14).[30] Another challenge may be activation positions alpha to heteroatoms that may result in unwanted reaction pathways. Since we had access to des-nitro pretomanid to perform these studies, we decided to pursue this step prior to cyclization.

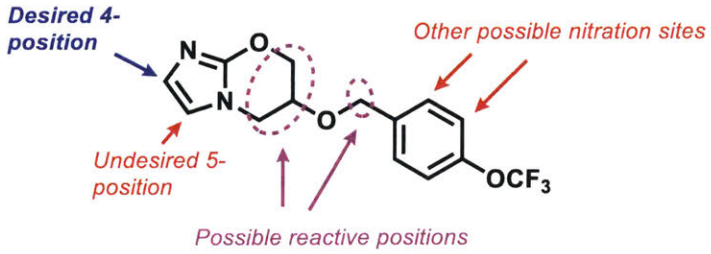

Figure 14. Possible selectivity issues with **31** under nitration conditions.

From Table 5, classic nitration conditions with fuming nitric acid and sulfuric acid resulted in only complex mixtures (entry 1).[31] This is not surprising given strongly acidic and oxidizing conditions that **31** must withstand. A more mild standard nitration

condition involving acetic anhydride and nitric acid gave only trace amounts of products, determined by mass spectrometry.[32] From these results, we sought more controlled conditions that could form the nitronium ion reliably.

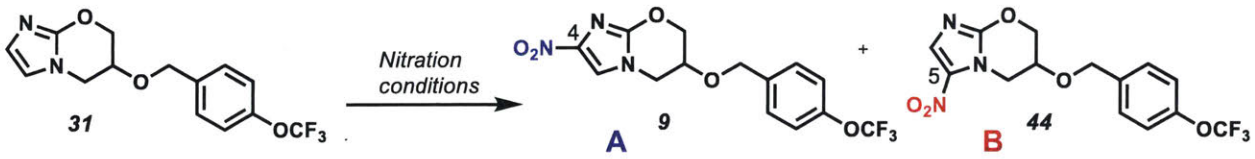

Entry[a]	Nitration conditions	Temperature	Solvent	Yield	Regiomeric Ratio (A:B)
1[c]	Fuming HNO_3 / H_2SO_4	0 °C	*neat*	Complex mixture	ND
2	Ac_2O / HNO_3	0 °C → rt	Ac_2O	Trace	ND
3	TFAA/Bu_4NNO_3 (1 equiv)	-78 °C → rt	DCM	trace	ND
4	TFAA/Bu_4NNO_3 (1 equiv)	0 °C → 30 °C	DCM	trace	ND
5	TFAA/Me_4NNO_3 (1 equiv)	rt	DCM	0%	ND
6	Tf_2O/Bu_4NNO_3 (1 equiv)	rt	DCM	56%	1.7:1
7	Tf_2O/Bu_4NNO_3 (1 equiv)	rt	DCE	61%	1.8:1
8	Tf_2O/Bu_4NNO_3 (0.5 equiv)	rt	DCE	44%	1.1:1
9	Tf_2O/Bu_4NNO_3 (2 equiv)	rt	DCE	Complex mixture	ND
10	Ts_2O/Bu_4NNO_3 (0.5 equiv)	rt	DCE	Complex mixture	ND
11	Ms_2O/Bu_4NNO_3 (1 equiv)	rt	DCE	SM	ND
13	Ms_2O/Bu_4NNO_3 (1 equiv)	40	DCE	20% conv.	ND
14	Nf_2O/Bu_4NNO_3 (1 equiv)	rt	DCE	53%	6.5:1

[a] All reactions were rune for 18 h unless otherwise noted. [b] 1 h reaction time.

Table 5. Late-stage nitration conditions of **31**.

The nitronium ion has been known to be formed through activation of a tetraalkylammonium nitrate by an acylating reagent such as trifluoroacetic anhydride (TFAA) (Figure 15).[33] This method would allow for mild nitration conditions and possibly limit side reactivity. Additionally, the nature of the nitronium counterion may affect

selectivity based on a study of the nitration of 5,8-dichloroisoquinolines by Walker and coworkers.[34] From the reported conditions by Shackelford and coworkers, we were able to observe trace products with TFAA and tetrabutylammonium nitrate at low to moderate temperatures (Table 5, entries 3 and 4). We then investigated the nature of the nitronium counterion and found tetramethylammonium counterion was insufficient due to its decreased solubility (entry 5). Based on the proposed intermediates from Figure 15, the anionic partner will likely have a strong effect on the nitronium ion's reactivity. Therefore, Tf_2O provided both the isomers in 56% yield in a 1.7:1 ratio, favoring the desired regioisomer (entry 6). Importantly, no other nitration products were observed. When DCM was switched DCE, we observed a minor increase to both the yield and selectivity (entry 7). From there, an excess amount of nitronium ion was discovered to give complex mixtures (entry 9) while a sub-stoichiometric amount provided higher yield with lower selectivity (entry 8). Other anhydrides were investigated such as Ms_2O and Ts_2O but resulted in either complex mixtures of starting material (entries 10-13). Upon closer inspection of Tf_2O, it can be inferred that the significantly low pK_a may be important for the activation of the nitronium ion when compared to other anions of the respective anhydride. In other words, if we consider intermediate **45** to exist somewhere along a gradient between being completely ionic to being completely covalent, then it is likely that the trifluoromethanesulfonate anion favors the ionic state (Figure 16). As a result, the nitronium ion is more activated towards nitration. Nonafluorobutanesulfonic anhydride, a variant of Tf_2O that is commercially available, was then used and provided the products in 53% yield and a 6.5:1 selectivity, favoring pretomanid as the major product.

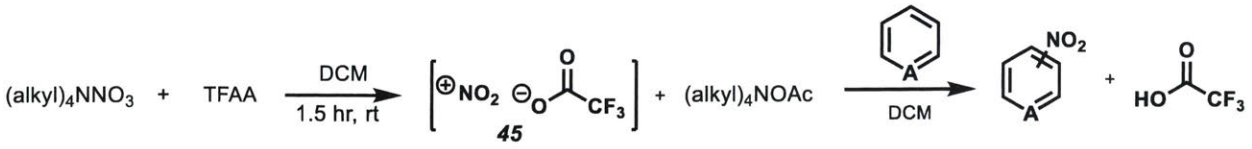

Figure 15. Formation of nitronium ion via activation of nitrate anion with an acylating reagent.

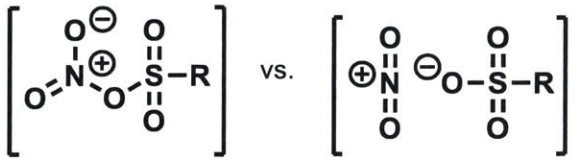

in situ nitronium formation

Figure 16. Covalent vs ionic nature of nitronium ion – counter ion relationship of intermediate **45**.

To explain the much higher selectivity of nitration via Nf_2O versus Tf_2O, we explored the following rationales (Figure 17). First, the 4-position of imidazole is more electronically rich due to the donating nitrogen at position one. This is supported from the first nitration event shown from the nitration of imidazole (Scheme 2). Another possibility is that the 5-position is more sterically hindered, where the larger nitronium – nonfluorobutanesulfonate pair may have higher difficulty accessing.

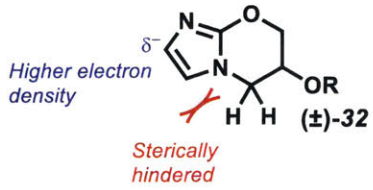

Figure 17. Possible rationales to explain selectivity for the 4-poosition over the 5-position of imidazole.

With our selective, late-stage nitration achieved, we then set out to investigate the unprecedented, challenging tandem bis-alkylation cyclization to form the crucial oxazine core of pretomanid.

1.3.4 Synthesis of imidazolone **34**

Before we investigate our proposed key steps of the bis-alkylation epoxide-opening, we must establish large scale (>10 g) reaction conditions that provide us with adequate amounts of our starting material, imidazolone **34**. Therefore, we commenced our synthesis with construction of imidazolone **34** from urea (**46**) and tartaric acid (**47**).[35] A reported method for the formation of **34** used neat sulfuric acid at 80 °C to access **48** followed by decarboxylation (Table 6). When the procedure was replicated, the short reaction time gave <10% yields for the first step, compared to the reported 53% (entry 3). Prolonging the reaction time to 18 h gave a slightly improved yield of 21% (entry 4). Since time did not increase the yield to an appreciable extent, we reasoned that varying the temperatures may be necessary. At 80 °C, the heat may be causing competing undesired reaction pathways; thus, lower temperatures were investigated. However, no conversion of starting material was observed at 60 °C after 1 h or 24 h (Table 1, entries 1 & 2). Upon heating to 100 °C for 2 h, **48** was obtained in a 32% yield (entry 5). By simply extending the reaction time to 5 h, we were pleased to isolate **48** in 86% yield (entry 6). Heating the reaction higher to 120 °C reduced yields to 19% and less than 5% at 2 h and 5 h, respectively (entries 7 & 8). With **48** in hand, we then subjected it to aqueous K_2CO_3 at reflux to give imidazolone **34** in 80% yield (Figure 18). Imidazolone **34** was found to be challenging to isolate from the decarboxylation and isolated material often contained potassium salts as impurities.

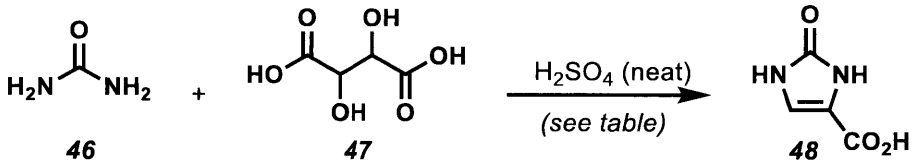

46 47 48

Entry[a]	Temperature (°C)	Time (h)	Yield[b]
1	60	1	SM
2	60	24	SM
3	80	1	<10% (53%)[c]
4	80	18	21%
5	100	2	32%
6	100	5	86%
7	120	2	19%
8	120	5	<5%

[a] All reactions were run in 2 M with respect to **46**. [b]Characterized by ^{1}H and ^{13}C NMR.[c] (reported yield).

Table 6. Synthesis of carboxyl imidazolone **48**.

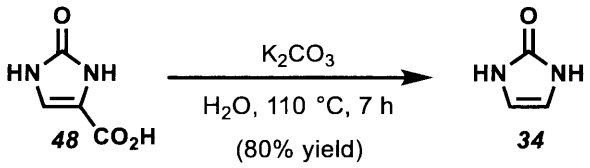

48 34

Figure 18. Decarboxylation to access imidazolone **34**.

Our next approach was to form urea derivative **50** from amine **49** followed by condensation in acid to give imidazolone **34** (Scheme 5a).[36] The first step was successful and provided urea derivative **50** in 51% yield from amine **49** and potassium cyanate at a 32 g scale. However, subjecting urea derivative **50** under various concentrations of sulfuric acid and temperatures, no condensation product was isolated and only minor amounts of hydroxyl imidazolone **52** was observed. Mechanistically, this step is likely very sluggish and polymerization may have occurred resulting in the lack of yield after release of ethanol (Scheme 5b).

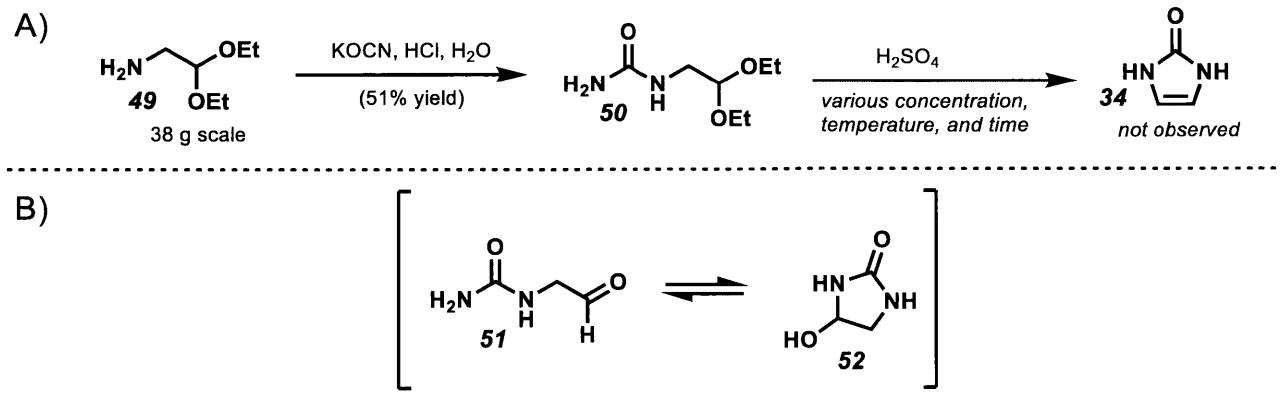

Scheme 5. Attempts to synthesize imidazolone **34** from amine **49**.

While these previous two routes offered low-cost starting materials to provide imidazolone **34**, we were discouraged by the large potential waste from the use of concentrated sulfuric acid. Therefore, we sought a different approach that excluded the use of acid altogether. Our chosen method was through the chemoselective reduction of hydantoin **53**, an incredibly cheap starting material (Table 7).[37] This two-step process involved addition of DIBAL to hydantoin at 0 °C followed by overnight stirring. Of note, other reductants were investigated such as $NaBH_4$ and $LiAlH_4$ but only starting material or complex mixtures resulted, respectively. The reaction was then quenched with 10% H_2O in MeOH and refluxed for another 24 h to first break apart the aluminum complex **54** followed by condensation to provide imidazolone **34** in 88% yield. The solid alumina byproducts were simply filtered off. While this process is slow, scales up to 20 g have been performed and reaction yields are generally between 88%-95%. This reaction was then attempted in a continuous-flow process but with hydantoin **53** having limited solubility in THF and severe clogging observed upon quenching, it was not pursued further. Regardless, with a large scale synthesis of imidazolone accomplished, we then set our focus towards investigating cyclization conditions to access oxazine core (±)-**32**.

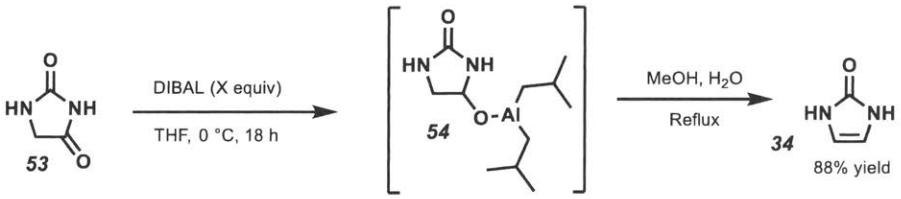

Reduction of Hydantoin Conditions

Entry	DIBAL Equiv.[a]	Conversion	Yield[b]
1	2	13%	9%
2	3.5	63%	55%
3	4.5	100%	88 - 93%
4	$LiAlH_4$ (2 equiv)	100%	Complex mixture
5	$NaBH_4$ (2 equiv)	0%	SM

[a] DIBAL solution was 25 wt% in PhMe. [b] Yield after quenching and condensation with 10% H_2O in MeOH

Table 7. Synthesis of imidazolone **34** through chemoselective reduction of hydantoin.

1.3.5 Investigations into bis-alkylation cyclization

With our successfully synthesized analytical standards and our nitration studies completed, we then set forth with our investigation into the challenging bis-alkylation, cyclization to access the oxazine core of pretomanid. We envisioned basic conditions as a fitting starting point according to the possible mechanistic pathway (Scheme 6). The key reaction would first proceed by adding base to **34** to form an anionic intermediate with resonance structures **55a** and **55b**. From there, *N*- or *O*-alkylation can occur when (±)-epichlorohydrin (**33**) is added. Once **33** is added, it can either undergo epoxide opening or a chloride displacement. Via pathway A, *N*-alkylation will occur with epoxide opening to give alkoxide **56a**. A second equivalent of base would then form oxazine alkoxide product **58** through an epoxide-opening cyclization. Likewise, pathway B is expected to progress in a similar manner starting with *O*-alkylation. Pathways C and D may also occur with direct chloride displacement of **33** to give **57a** or **57b**, respectively.[38] As all possible pathways converge to form alkoxide oxazine **58**, benzyl bromide **19**

could then be added as a trapping reagent to form des-nitro Pretomanid (**31**). However, if the benzylation step proves to be difficult, then **58** would be quenched as oxazine (±)-**32**.

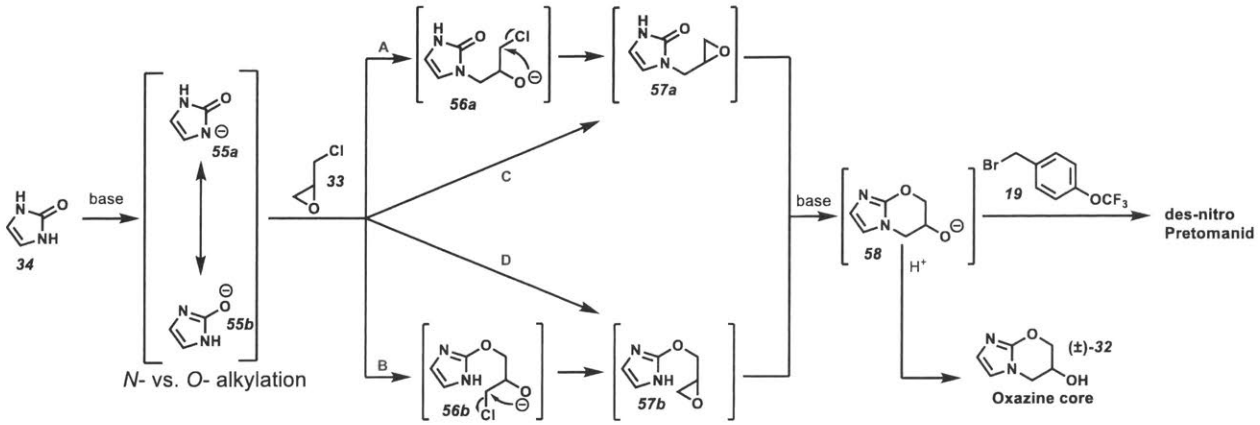

Scheme 6. Epoxide opening (paths A & B) vs. chloride displacement (paths C & D).

In our reaction studies, various bases were studied including carbonates, alkoxides, amines, and sodium hydride (Table 8). Many of these results were found to be complex mixtures. Given the intricacies of the mechanism, different orders of addition were considered such as adding to a solution of imidazolone and base or vice-versa. Multiple temperatures and times were investigated with each entry. For the carbonate series, analogous microwave conditions were also pursued (entry 1). When milder bases such as amines were used, epoxide opening or chloride displacement was observed at elevated temperatures. When stronger bases such as LiHMDS or LDA were used to deprotonate imidazolone, we observed epoxide opening or chloride displacement at low temperatures. We examined less common bases such dimsyl anion but was still met with complex mixtures. [39] These findings lead us to conclude that basic conditions were not likely to undergo the ambitiously proposed transformation. Furthermore, epichlorohydrin is well known to undergo polymerizations and may explain

the many complex mixtures that were observed.[40] As we switched to various Lewis or Brønsted acidic conditions, the results were largely the same in that most of the results were complex mixtures (Table 9).

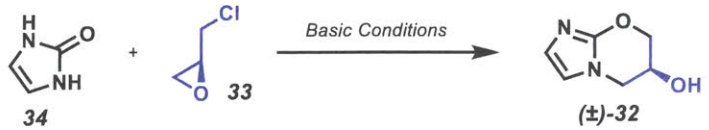

34 + *33* → *(±)-32*

Entry[a]	General Conditions	Solvents	Result
1[b]	X_2CO_3, X = Li, Na, K, Cs	Et_2O, DCM, THF, DMF, DMSO	Complex mixtures
2	XOR bases, X = Na, Li; R = Me, Et, *i*Pr. *t*-Bu	Et_2O, DCM, THF, DMF, DMSO, MeOH, EtOH, *i*PrOH, *t*-BuOH	Complex mixtures; epoxide opening or chloride displacement with alkoxides
3	NaH	Et_2O, DCM, THF, DMF	Complex mixtures
4	NaH with additives: LiI, KI, Et_4NI, TBAI	Et_2O, DCM, THF, DMF, DMSO	Complex mixtures
5	Dimsyl anion	DMSO, THF	Complex mixtures
6	LiHMDS, KHMDS, LDA	Et_2O, DCM, THF, DMF, DMSO	Complex mixtures
7	Amine bases such as Et_3N, DBU, DABCO	Et_2O, DCM, THF, DMF, DMSO	Complex mixtures
8[c]	OMs, OTs, Br derivatives of epichlorohydrin	-	Complex mixtures

[a] Temperature, time, order of addition, and stoichiometry were varied. [b] Conditions were additionally subjected to microwave. [c] Repeated conditions with these variants. OMs generally required higher amounts of base due to its synthesis and use as crude material.

Table 8. Attempted basic conditions for cyclization.

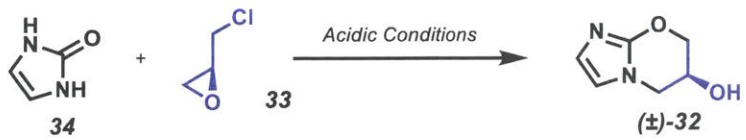

Entry[a]	General Conditions	Solvents	Result
1[b]	CuX or AgX, X = Cl, Br, I, CO_3, OTf, PF_6, BF_4, NO_3	Et_2O, DCM, THF	Complex mixtures
2	HCl in Et_2O	Et_2O, DCM, THF	Complex mixtures
3	TFA, AcOH, H_2SO_4	Et_2O, DCM, THF	Complex mixtures
4	Phosphoric acids[c]	Et_2O, DCM, THF, DMF	Complex mixtures
5	Jacobsen's catalyst[d]	Et_2O, DCM, THF	Complex mixtures
6	$TiCl_4$, $Ti(OiPr)_4$	THF	Complex mixtures

[a] Temperature, time, order of addition, and stoichiometry were varied. [b] Conditions were additionally subjected to microwave. [c] Includes 1,1'-Binaphthyl-2,2'-diyl hydrogenphosphate. [d] N,N'-bis(3,5-di-tert-butylsalicylidene)-1,2-cyclohexanediaminomanganese(III) chloride.

Table 9. Attempted acidic conditions for cyclization.

We concluded that numerous side reactions could be occurring alongside our desired reactivity. Therefore, we reasoned that the best possible solution is to eliminate the need to alkylate imidazolone and have the epoxide present prior to cyclization.

1.3.6 Revised route with appended epoxide

The appended epoxide **60** is a pivotal intermediate that may lead to pretomanid. Therefore, we designed a forward route to access the material expediently and in large quantities to aid with our investigation (Scheme 7). From our cyclization studies, the two similar N-H protons on imidazolone **34** was problematic and having only one present when attaching the epoxide would simplify reactivity. From imidazolone **34**, a monodeprotection will mask one proton followed by subsequent alkylation to provide us **59**. The protecting group would then be ideally removed without affecting the epoxide.

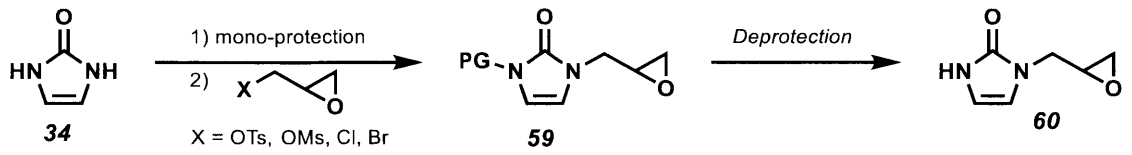

Scheme 7. Anticipated forward route to access appended epoxide **60**.

From Table 10, monoalkylations were met with generally low yields and poor selectivity for the monoalkylated product. This is likely due to the poor solubility of imidazolone **34** and the relatively higher solubility of the monoprotected product. As a result, the monoprotected product becomes more reactive and is thus diprotected. The TMS protecting group was found to be too unstable and resulted in starting material (Table 10, entry 1). When switching to the larger, bulkier TBS group, both mono- and di-protected products **61** and **62** were isolated in 6% and 10%, respectively. When benzyl bromide was used, both mono- and di-products, **63** and **64**, were once again observed in 19% and 16%. A common protecting group for nitrogen was benzoyl chloride and that provided us with **65** and **66** in 8% and 17% yield, respectively. Upon isolation, it was found that dibenzoyl imidazolone **66** was highly crystalline, and thus, allowed us to find recrystallization conditions using DCM and MeOH. Furthermore, removal of the benzoyl group may be milder when compared to removal of a benzyl group or less toxic when removing a silyl due to the use of fluoride.[41]

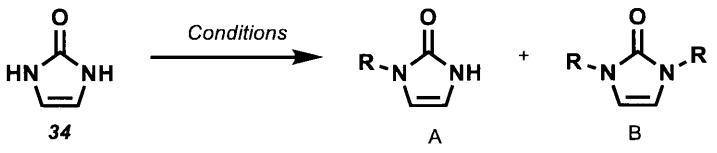

Entry	General Conditions	R	Result	Ratio
1	TMSCl (1 equiv), Et_3N (1.1 equiv), DCM	TMS	SM	NA
2	TBSCl (1 equiv), imidazole (1.1 equiv), DCM	TBS	6% A (**61**), 10% B (**62**)	1:1.7
3	BnBr (1 equiv), K_2CO_3 (1 equiv), DMF	Bn	19% A (**63**), 16% B (**64**)	1:1.2
4	BzCl (1 equiv), TEA (1.1 equiv), DMAP (0.1 equiv), DCM	Bz	8% A (**65**), 17% B (**66**)	1:2

Table 10. Monoprotection conditions of imidazolone (**34**).

With these findings, we revised our strategy for there to be a two-step sequence to access monoprotected imidazolone. While this added an additional step, isolation would be simpler and would thus speed up synthesizing necessary material. From Figure 19, **66** was achieved in 83% at 10 g scale with excess benzoyl chloride and base after recrystallization with methanol and DCM.

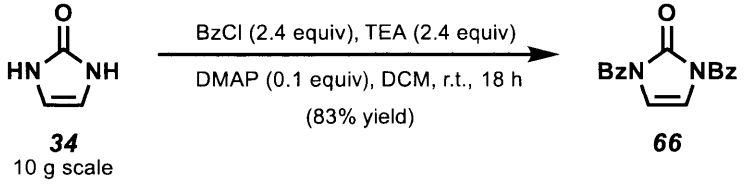

Figure 19. Benzoylation conditions of **34** to access **66**.

The next step was to selectively remove one benzoyl group.[41] From Table 11, we found that tertiary amines were unreactive and provided only starting material (entries 1-4). Hydrazine, commonly used to remove benzoyl groups, resulted in very fast, full deprotection despite lowering the temperature (Table 11, entry 6 & 7). While diethylamine in methanol and DCM resulted in full deprotection, diethylamine in DCM provided our desired benzoylimidazolone **65** in 85% yield at room temperature after 18

hours. Increasing from room temperature to 40 °C to reduce reaction time resulted in a reduced yield of 69% within 3 hours.

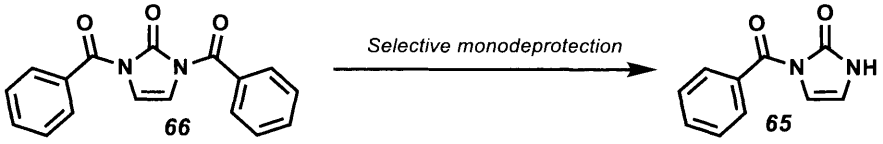

Entry	Conditions	Yield
1	DIPEA (1 equiv), DCM, rt, 18 h	NR
2	DIPEA (1 equiv), MeOH, DCM, rt, 18 h	NR
3	TEA (1 equiv), DCM, rt, 18 h	NR
4	TEA (1 equiv), MeOH, DCM, rt, 18 h	NR
5	NH_2NH_2 (1 equiv), DCM, r.t., <5 min	Full deprotection
6	NH_2NH_2 (1 equiv), DCM, 0° C, <5 min	Full deprotection
7	Et_2NH, MeOH, DCM, r.t., <5 min	Full deprotection
8	Et_2NH, DCM, r.t., 18 h	85% yield
9	Et_2NH, DCM, 40° C, 3 h	69% yield

Table 11. Monobenzoylation conditions of **66** to access **65**.

With benzoyl imidazolone **65** in hand, our next step was to alkylate to give epoxide **67**. The conditions must be selective for deprotonation and not deprotection. From Table 12, epichlorohydrin (**33**) gave a complex mixture, likely through polymerization pathways (entry 1).[40] Methanesulfonyl leaving group was chosen to increase bias towards alkylation over epoxide opening. Using mesylate derivative **68** neat or with a bulky amine base gave no reaction (entries 2 & 3). Use of stronger bases such as LiHMDS resulted in a complex mixture (entry 4). When LDA was used, deprotection product was observed as **70** was isolated as a byproduct in 60% yield (entry 5). Sodium hydride was then used as a base and 10% yield of our desired product was isolated (entry 5). These results could be attributed to the use of mesylate derivative. Since it was unstable to chromatography, it had be used as crude material.

Thus, it could have potentially quenched the bases or caused side reactions from residual acid. Therefore, when we switched to the isolable and pure tosylate **69**, we were able to obtained **67** in 40% yield with sodium hydride in DMF. During this step, *N* vs *O* alkylation was possible, as shown in Scheme 6, *N*-alkylation was confirmed over *O*-alkylation product **71** by HMBC correlation of the methylene and aromatic C-H of imidazolone (Figure 20).

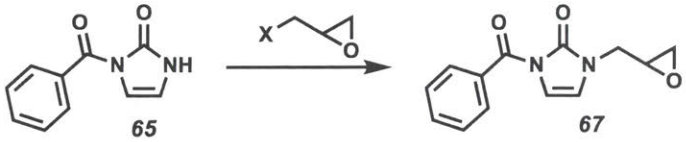

Entry	X	Conditions	Conversion[a]	Yield
1	Cl (**33**)	NaH, DMF, 0 °C	100%	Complex mixture
2	OMs (**68**)	*neat*, up to 3 equiv of epoxide	0%	NR
3	OMs (**68**)	DBU, DCM	0%	NR*
4	OMs (**68**)	LiHMDS, THF, -78 °C	37%	Complex mixture
5	OMs (**68**)	LDA, THF, -78 °C	100%	60% amide byproduct[b]
6	OMs (**68**)	NaH, DMF, 0 °C	77%	10%
7	OTs (**69**)	NaH, DMF, 0 °C	100%	40%

[a] Monitored by TLC. [a] byproduct

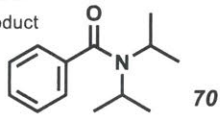

Table 12. Alkylation of **65** to acquire epoxide **67** with various glycidol derivatives under basic conditions.

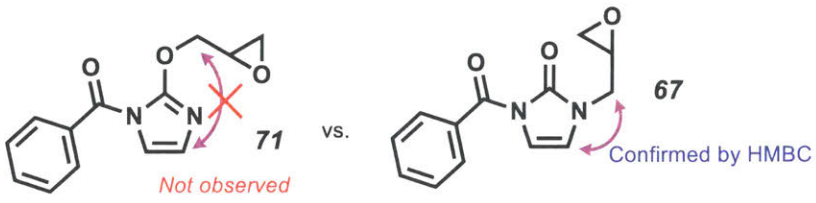

Figure 20. HMBC identification of *O*- vs. *N*-alkylation for **71** vs **67**, respectively.

With benzoyl epoxy imidazolone **67** in hand, we then investigated the possibility of cyclization without removal of the benzoyl group. According to Scheme 8, this

transformation could go through either pathways A or B. In pathway A, cyclization would occur through the *6-endo* epoxide-opening to give intermediate **72**. Then, either through an inter- or intramolecular process, a benzoyl group transfer could occur to give *6-endo* product **73**. Likewise, the 5-exo epoxide opening pathway could occur to give intermediate **74** and then **75**. In general, epoxide-opening cyclizations will favor the *5-exo* product.[42] However, our molecule contains a flat, heterocycle that will cyclize through nucleophilic attack with an sp^2 oxygen. Previous work has shown that templating could play a large role in determining epoxide-opening selectivity.[43] From Table 13, we were unable to promote any cyclization products under microwave conditions up to 140 °C. While there was no reaction observed with aprotic solvents, deprotected byproduct **76** and epoxide opened product **77** were observed for entries 5 and 6, respectively.

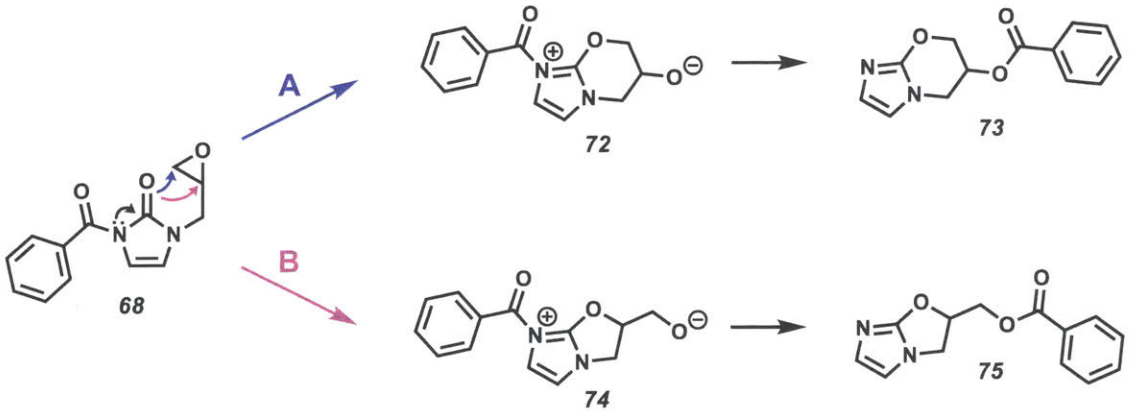

Scheme 8. Oxazine vs oxazole formation and possible benzoyl group transfer to give **73** or **75**, respectively.

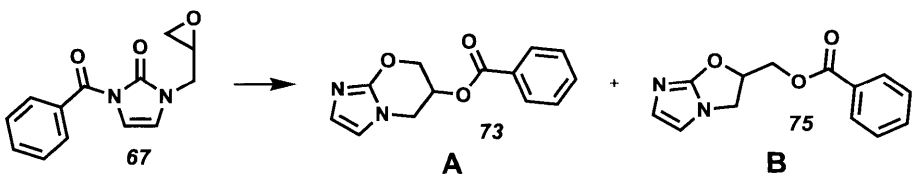

Entry	Solvent	Temperature[a]	Result
1	DCM	r.t. to 140 °C	NR
2	THF	r.t. to 140 °C	NR
3	MeCN	r.t. to 140 °C	NR
4	Dioxane	r.t. to 140 °C	NR
5	HFIP	120 °C	15% ester
6	H_2O	100 °C	13% opened epoxide

[a] Temperatures were studied in 20 °C increments and run for 30 minutes in microwave.

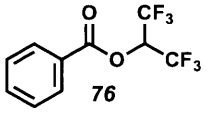

Entry 5 ester byproduct

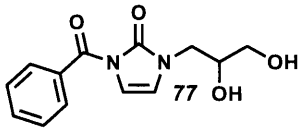

Entry 6 opened epoxide byproduct

Table 13. Attempted cyclization of **67** to form **73** or **75**.

While cyclization of **67** was unsuccessful, we were still on course for our strategy to cyclize appended-epoxide **60**. Therefore, conditions must be explored to remove the benzoyl group without affecting the epoxide. From Table 14, some conditions were revisited that had proven successful in the monodebenzoylation of **66**. Hydrazine was first studied due to its fast reaction rate; however, a complex mixture was observed (entry 1). Less nucleophilic ethylamine was then used and gave full conversion of starting material to give epoxide opened byproduct **78** and ethyl benzamide **79** in 38% and 54% yield, respectively. Our selective monodeprotection conditions provided our desired product **60** in 30% yield. Epoxide-opening had also occurred to give byproduct **80** in 12% yield. These results indicate that both epoxide opening and debenzoylation is occurring. In search for more mild conditions, DMAP in DCM was investigated and no reaction occurred. From an earlier result where using a protic solvents gave ester **76**

(Table 13, entry 5), using a protic solvent such as methanol could possibly improve reaction rate while maintaining mild conditions. Indeed, use of DMAP in a 1:1 mixture of methanol and DCM provided our desired epoxide **60** in 64% yield with full conversion.

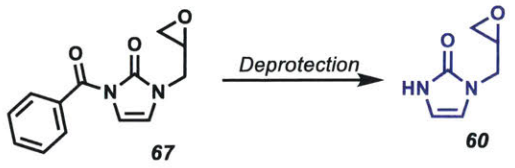

Entry	Conditions	Results
1	NH_2NH_2 (1 equiv), DCM, r.t.	100% conversion, complex mixture
2	$EtNH_2$, DCM, H_2O, 30 min	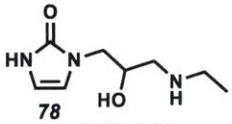 **78** 38% yield 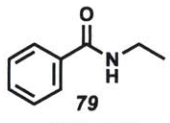 **79** 54% yield
3	Et_2NH, DCM, 4 h, r.t.	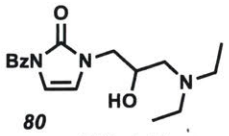 **80** 12% yield 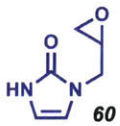 **60** 30% yield 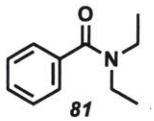 **81** 30% yield 30% SM
4	DMAP, DCM, r.t., 18 h,	No reaction
5	DMAP, MeOH, DCM, r.t., 18 h,	64% yield , 100% conv.

Table 14. Mild debenzoylation conditions of **67**.

Since alkylation is no longer an issue, we reinvestigated our cyclization conditions, shown in Table 15. While most conditions gave complex mixtures, we observed trace amounts of desired (±)-**32** (entries 9 & 10). When TMSOTf was used as a Lewis acid, we were able to isolate 5-exo product **43** in 18% yield. In each condition examined, the starting epoxide material **60** was freshly prepared because it was found to dimerize readily upon removal of solvent via vacuum. If left standing, it would hydrolyze with any moisture present. Importantly, **60** was only soluble in protic solvents

or those that are highly polar and nucleophilic such as DMSO. As a result, these solvents were incompatible with the epoxide. Storage was possible for this material but it had to be kept under inert atmosphere and frozen in benzene, despite its poor solubility.

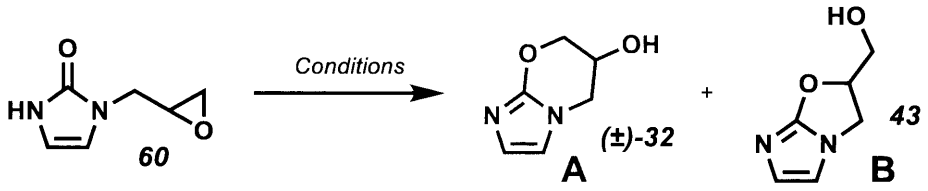

Entry	Reagents	Solvent	Temperature	Result
1	NaH	THF	0 °C	Complex mixture
2	-	H_2O	up to 100 °C	Complex mixture
3	Amines	THF	up to 80 °C	Complex mixture
4	LiHMDS	THF	- 78 °C	Complex mixture
5	Amberlite IRA400, Na_2CO_3	THF	up to 80 °C	Complex mixture
6	Xtal-FluorE	Dioxane	up to 80 °C	Complex mixture
7	TFA	THF	up to 80 °C	Complex mixture
8	CSA	THF	60 °C	trace product
9	$AgPF_6$	THF	40 °C	trace product
10	BF_3•OEt_2, TEA	THF	40 °C	Complex mixture
11	TMSOTf, DCM	DCM	RT	18% B

Table 15. Reinvestigation of cyclization conditions with appended epoxide **60**.

From our investigations thus far, we were encouraged by formation of trace amounts of (±)-**32**. Undeniably, it was possible to form the oxazine core through this strategy. Our next challenge was to overcome the sensitive nature of the terminal epoxide, which appears to be reacting with the already present nucleophilic nitrogen and any impurities. Since our highest yield for the cyclization was the undesired *5-exo*

product, a modified strategy that would bias towards the *6-endo* product while reducing the terminal epoxide's reactivity would be ideal.

1.3.7 Introduction of trimethylsilyl group

In regard to epoxide openings, there are numerous examples where selectivity can be biased towards either the *5-endo* or *6-exo* product through templating[43] or substituent effects.[44] Research in the Jamison group have shown that selectivity for the *6-endo* epoxide opening was possible over the *5-exo* through the use of a trimethylsilyl group that, after directing the regioselectivity of epoxide ring-opening, is lost prior to isolation of product.[45] From Scheme 9, our new targets, *trans*-**82** or *cis*-**83**, would likely resolve many of the current issues such as the sensitivity of having a terminal epoxide, lack of solubility in most organic solvents, and most importantly, selectivity towards the oxazine core over the oxazole core. After cyclization to *trans*-**84** or *cis*-**85**, we would then have the flexibility to remove the TMS group along any point in the remainder of synthesis that would provide us the highest yielding desilylated product.

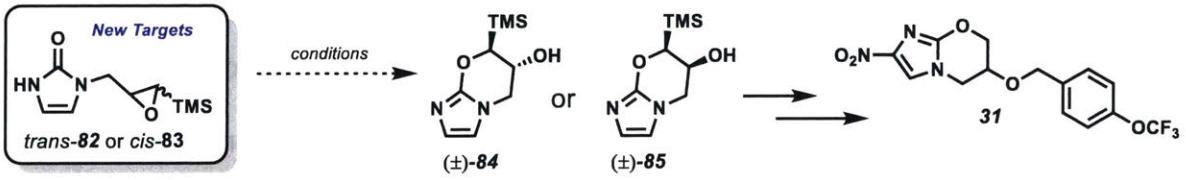

Scheme 9. Revised route with TMS-group to potentially resolve existing issues.

Retrosynthetically, the stereochemistry of the epoxide could be either *cis* or *trans*, depending on yield and selectivity of cyclization (Scheme 10). According to the proposed transition state for cyclization, we anticipated that the *trans*-TMS epoxide would be better suited given that the TMS-group would be equatorial and 1,3-diaxial

interactions would be avoided (Figure 21) Regardless, both isomers would be investigated and be accessed from readily available propargyl alcohol **88.**

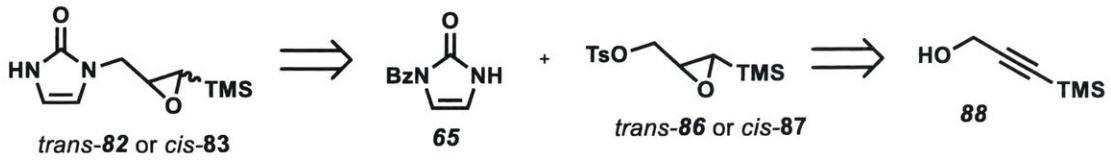

Scheme 10. Retrosynthesis of TMS-epoxy imidazolone **82** and **83**.

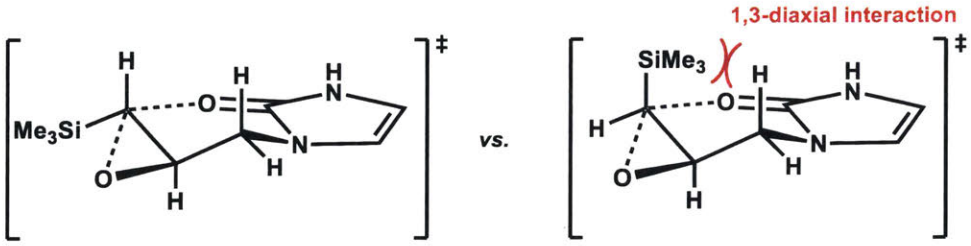

Figure 21. Proposed transition stage for cyclization of *trans* TMS-epoxy imidazolone **82** and *cis* TMS-epoxy imidazolone **83.**

With our new strategy established, our first course of action was the synthesis of *trans* epoxide **82**. The synthesis commenced with silylation of propargyl alcohol **89** to give TMS-propargyl alcohol **88** in 94% yield. Red-Al reduction in ether at 0 °C furnished exclusively *trans* TMS allyl alcohol **90** in 99% yield (Scheme 11). From there, *trans* TMS epoxide **86** could be accessed through two routes (Scheme 12). For route A, tosylation would occur first followed by epoxidation. However, standard tosylation conditions were unsuccessful or resulted in low yield (entries 1-3). With TsCl, there was likely acid present as impurities and caused unwanted side reactions. Switching to strongly basic conditions with butyllithium and Tf_2O gave tosyl allyl alcohol **91** in 51% yield (entry 4). In the following step, epoxidation occurred very sluggishly and conversion was very minimal even after 48 hours. The absence of hydrogen bonding to coordinate epoxidation with mCPBA significantly affected reaction rate.[46] Compared to route A,

route B was much more efficient. From **90**, epoxidation furnished *trans* epoxide **92** in 63% yield at a 10 g scale.††† Then, tosylation with Ts_2O afforded tosyl TMS epoxide **86** in 80% yield at a 6 g scale. With tosyl epoxide **86** in hand, subjecting it to alkylation conditions established earlier (Section 1.3.7, Table 12, entry 7), we were able to obtain to obtain TMS-epoxy imidazolone **93** in 51% yield with full conversion (Figure 22). This higher yield supports our previous rationale that the TMS group reduces side reactivity involving the terminal epoxide in **60**.

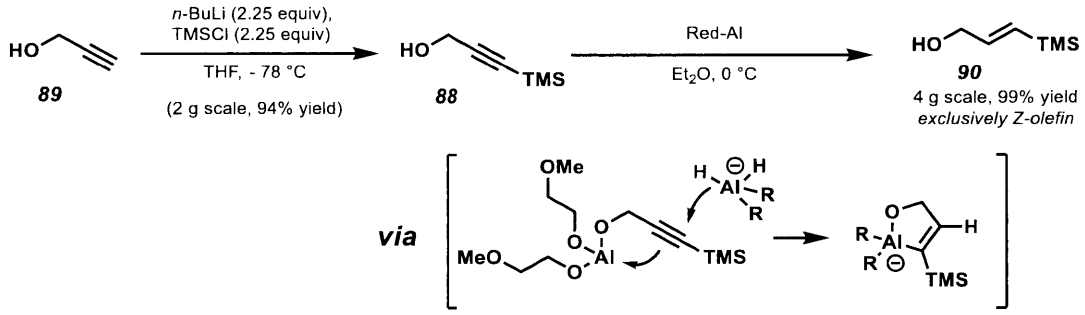

Scheme 11. Synthesis of TMS propargyl alcohol **90** from **89**.

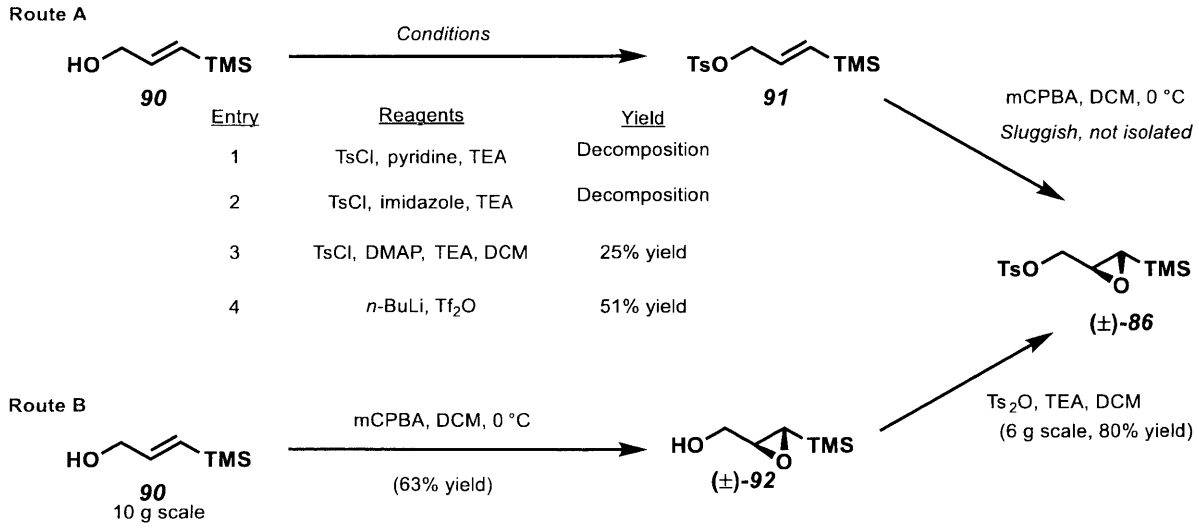

Scheme 12. Two possible routes to access *trans* epoxide **86**.

††† mCPBA was used as the impure commercial grade of <77% by weight.

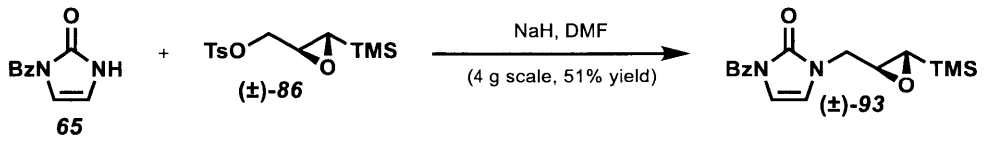

Figure 22. Alkylation conditions to synthesize **93**.

Our next step was to synthesize *cis* epoxide **87**. From TMS propargyl alcohol **88**, a Lindlar's reduction strategy was chosen based on precedence by Compain (Figure 23).[47] From Table 16, almost every possible variable for the reduction was investigated. Overall, over 50 conditions were examined with 27 shown. In general, the results were widely varied ranging from no product to complete *E* selectivity. The best solvent was methanol as it allowed for the highest concentration of dissolved hydrogen gas.[48] At 1% catalyst loadings, there was little to no reactivity unless high pressure and temperature was used (entries 1-12). Since the high pressures required using a Parr bomb reactor, the scale-up would be limited and thus 10% catalyst loadings were used going forward (entries 5-12). Quinoline concentration was important as excess amounts typically reduced conversion. Temperature significantly reduced reaction time; however, isomerization was likely occurring and resulted in reduced selectivity. In each experiment, full conversion was necessary as the starting material **88** and both *E* and *Z* olefins were inseparable. When the scales were varied, the results were difficult to reproduce. As eventual scale-up was necessary, these conditions would result in an exorbitant amount of Lindlar's catalyst. Ultimately, this reaction was not pursued further.

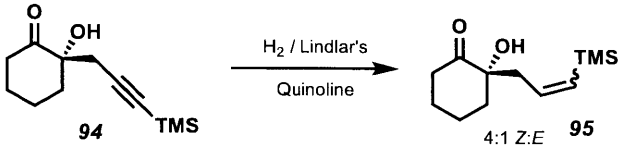

Figure 23. Precedence by Compain for Lindlar's reduction.

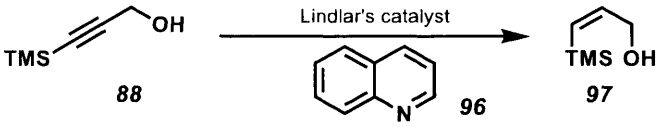

Entry[a]	Solvent	Catalyst loading (mol%)	Concentration (M)	Quinoline Equiv.	T (C)	Pressue (bar)	Time (h)	Ratio (Z:E)[c]	Conv.[d]
1	IPA	1	0.5	3	50	1	60	6:1	7%
2	EtOH	1	0.5	3	50	1	60	6:1	7%
3	MeOH	1	0.5	3	rt	1	60	Z	2%
4	EtOH	1	0.5	3	rt	1	60	Z	2%
5	MeOH	1	0.5	1	rt	5[b]	2	Only Z	6%
6	MeOH	1	0.5	1	rt	15[b]	2	10:1	9%
7	MeOH	1	0.5	1	rt	50[b]	2	7:4	22%
8	MeOH	1	0.5	3	rt	15[b]	2	Only Z	2%
9	MeOH	1	0.5	1	rt	15[b]	24, 48	5:1	85%
10	MeOH	1	0.5	0.5	rt	15[b]	24, 48	1.6:1	89%
11	MeOH	1	0.5	1	rt	25[b]	24, 48	2.13:1	84%
12	MeOH	1	0.5	0.5	rt	25[b]	24, 48	1:1	95%
13	EtOAc	10	0.2	0	rt	1	24	nd	trace
14	EtOAc	10	0.2	1.2	rt	1	24	nd	trace
15	EtOAc	10	0.2	3.1	rt	1	24	nd	trace
16	MeOH	10	0.5	1.2	rt	1	2	nd	40%
17	MeOH	10	0.5	1.2	rt	1	5	20:3	50%
18	MeOH	10	0.5	1.2	rt	1	24	4:1	100%
19	MeOH	10	0.5	1.2	50	1	2	nd	~65%
20	MeOH	10	0.5	1.2	50	1	5	nd	100%
21	MeOH	10	0.5	1.2	50	1	24	3:50	100%
22	MeOH	10	0.5	0	50	1	2	nd	25%
23	MeOH	10	0.5	0	50	1	5	nd	100%
24	MeOH	10	0.5	0	50	1	24	all *E*	100%
25	EtOH	10	0.5	1.2	50	1	2	nd	50%
26	EtOH	10	0.5	1.2	50	1	5	nd	>95%
27	EtOH	10	0.5	1.2	50	1	24	4:5	100%

[a] All reactions were run on 100 mg scale. [b]Parr bomb reactor. [c] determined by ^{1}H NMR. [b] Determined by GC-MS and ^{1}H NMR.

Table 16. Lindlar's reduction conditions studied to access **97** in high selectivity and full conversion.

Our next strategy involved using a modified method by the Jamison group in 2006 (Scheme 13).[49] In that work, TMS propargyl alcohol **88** was used to access both *E*- and *Z*-isomers through a divergent route by using either Vitride or DIBAL, respectively. We reasoned that after DIBAL reduction, quenching with a proton source could give us *Z*-olefin **97**. From Table 17, the DIBAL reduction required an excess amount of 4.5 equivalents to give full conversion over 3.5 equivalents (entries 1-3). Furthermore, there was significant solvent effects where completely opposite selectivity was observed (entry 3 vs. entry 4). While heating to 40 °C allowed for full conversion after 24 h, it was likely also causing decreased selectivity through thermal isomerization (entries 5 & 6). Scaling up resulted in decreased selectivity; however, higher yield was observed (entry 6). Our best conditions were found with ether and hexanes at 4.5 equivalents of DIBAL at room temperature. While the reaction took 5 days to complete, the yield and selectivity was excellent (33:1, *Z*:*E*) to provide synthetically useful amounts of material after aqueous work-up with Rochelle's salt and (entry 7). Of note, we found that the material could be used as the crude mixture for the next reaction, thus, requiring no chromatographic separation.

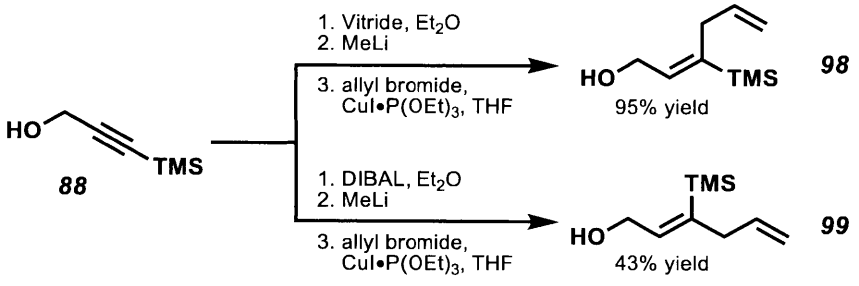

Scheme 13. Precedence by Langille and Jamison, 2006.

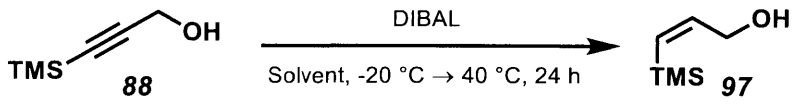

Entry	Solvent	DIBAL Soln[a]	Equiv	Conversion	Yield	Ratio (*Z*:*E*)
1	Et_2O	THF	3.5	27	2%	3:1
2	Et_2O	PhMe	3.5	92	56%	48:1
3	Et_2O	PhMe	4.5	100	53%	12:1
4	PhH	PhMe	4.5	100	61%	3:100
5	Et_2O	Cy	4.5	100	56%	20:1
6	Et_2O	Heptane	4.5	100	56% (88%[b])	50:1 (25:1[b])
7	Et_2O	Hexanes	4.5	100	82%	33:1[c,d]

[a]All solutions are 1 M. [b] 3 g scale. [c] 4.25 g scale. [d] Room temperature, 120 hours.

Table 17. Reduction of **88** with DIBAL.

Our next step was the epoxidation of *Z* olefin **97** followed by alkylation via imidazolone **65**. From Scheme 14, *Z* olefin **97** was epoxidized with 97% pure *m*CPBA to give *cis* epoxide **100** with slightly reduced *cis*/*trans* ratio. Less pure *m*CPBA was found to generally give much lower yields or complex mixtures. Tosylation of **100** provided tosyl epoxide **87** in 86% yield. Next, **87** was then used to alkylate benzoyl imidazolone **65** to give **101** in 12% yield. Overall, the synthesis of *cis*-TMS imidazolone **101** was significantly more challenging the *trans* analogue. It is likely that for **90**, the reduction forced the TMS and methylene in close proximity resulting in severe steric repulsion,[50] which is then carried throughout the synthesis as the epoxide.

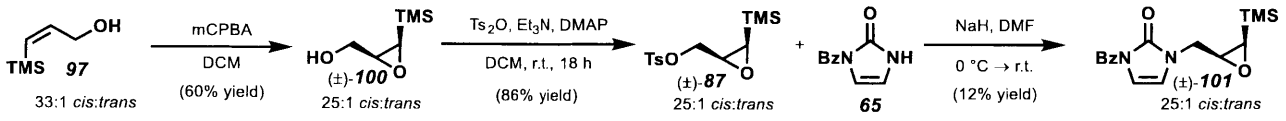

Scheme 14. Synthesis of *cis*-TMS epoxy imidazolone **101**.

With *trans* **93** and *cis* **101** TMS-epoxy imidazolone isomers in hand, our next step was to remove the benzoyl protecting group and examine possible cyclization conditions to access the oxazine core. Afterwards, TMS removal conditions will be examined.

1.3.8 Access to pretomanid via trimethylsilyloxiranes

Our studies towards cyclization of *trans* **93** commenced with our debenzoylation conditions with DMAP in 1:1 methanol and DCM (Figure 24). To our surprise, we isolated three unique products that were identified as the epoxide **82**, our desired oxazine core **84**, and undesired oxazole **102** in 60% with a 5:7:3 ratio. While the epoxide product **82** was straightforward to elucidate given its unique epoxide chemical shifts on ^{1}H NMR, oxazine **84** and oxazole **101** were harder to discern (Figure 25). With regards to splitting patterns on ^{1}H NMR, both would be very similar. As we turn to HMBC analysis, we expected there to be a correlation with the TMS methine doublet (H3) in oxazine **84** with the central carbon (C1). Likewise, there would be a correlation between the methine multiplet (H3) of oxazole **102** with central carbon (C1). However, this was observed in neither case. Upon closer inspection, both products contained a correlation between the methylene (H5 of **84**, H4 of **102**, respectively) and the central carbon (C1 for both **84** and **102**). However, we observed that of the HMBC correlation pairs, one pair contained a weak C-H correlation and a strong C-H correlation while the other pair had both very strong C-H correlations. Upon modeling both products through MM2 calculations, it was found that the methine doublet of oxazine **84** (H3) (Figure 26) and methine multiplet of oxazole **102** (H3) both displayed a nearly 90° dihedral angle with the central carbon (C1 for both) (Figure 27). This aligned well with why we were

unable to observe that HMBC correlation.[51] As for the methylenes, one of the protons of oxazine **84** (H5) was close to 90° with the central carbon (C1) (Figure 26) whereas both methylene protons of oxazole **102** (H4) was nearly 120° (Figure 27). Therefore, this supports that our major product was indeed our desired 6-endo cyclized epoxide. This result allowed for two possibilities: 1) we could bypass the deprotection step completely and 2) achieve our desired oxazine core.

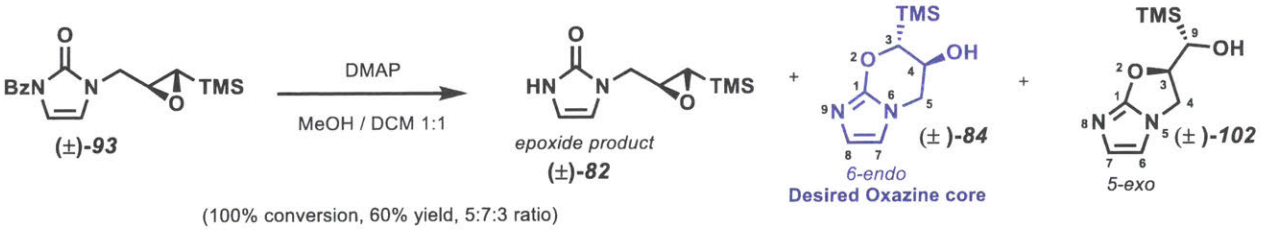

Figure 24. Unexpected cyclized products **84** and **102** from debenzoylation.

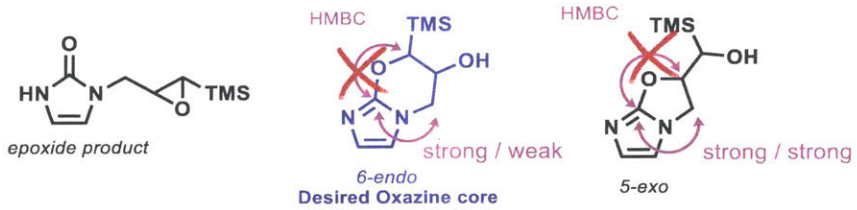

Figure 25. Structure comparison between **82**, **84**, and **102**.

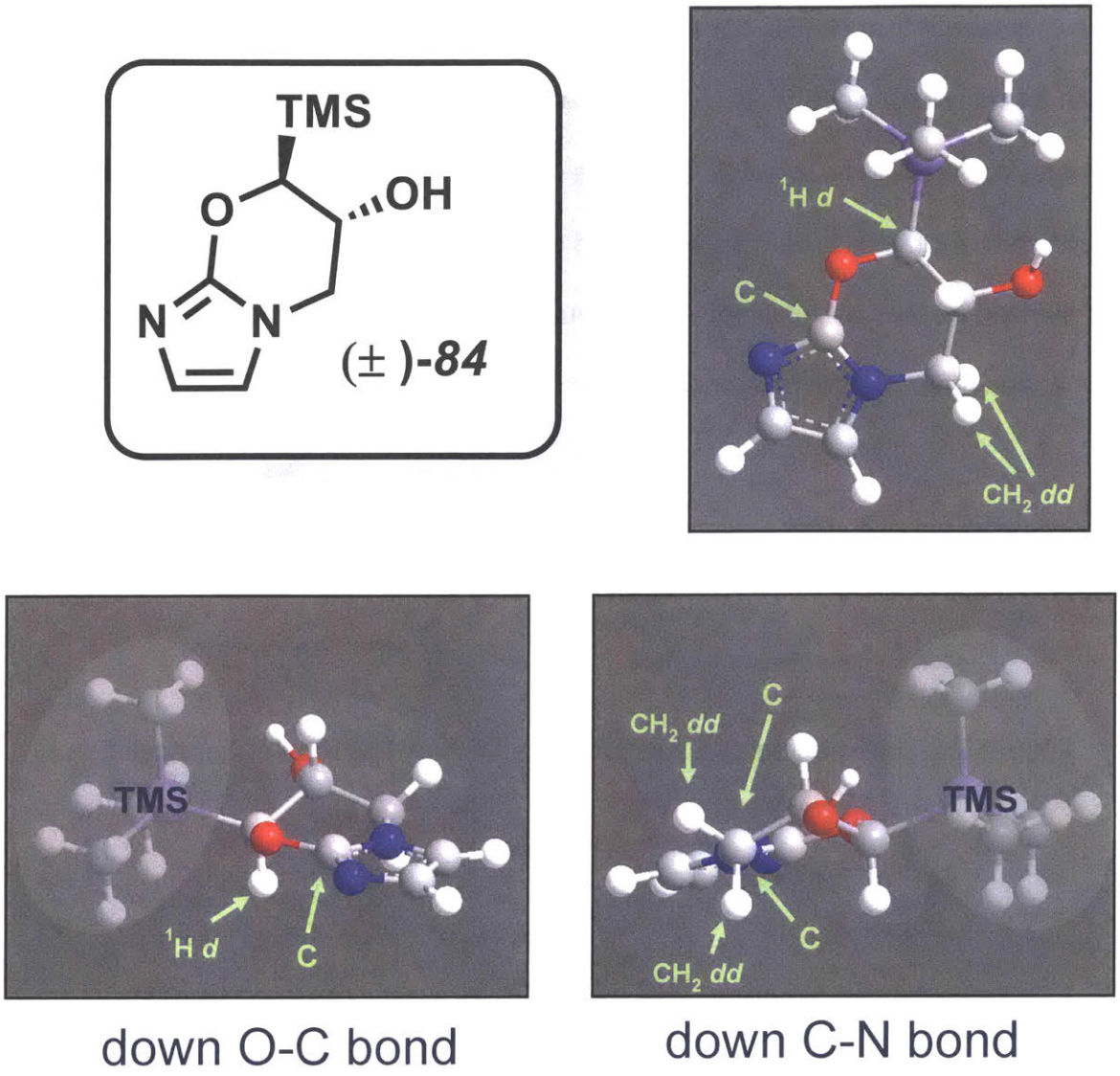

Figure 26. HMBC and MM2 analysis of oxazine **84**. (top right) Full structure view. (bottom right) View down C-N bond with methylene protons shown. (bottom left) view down O-C bond with methine proton shown.

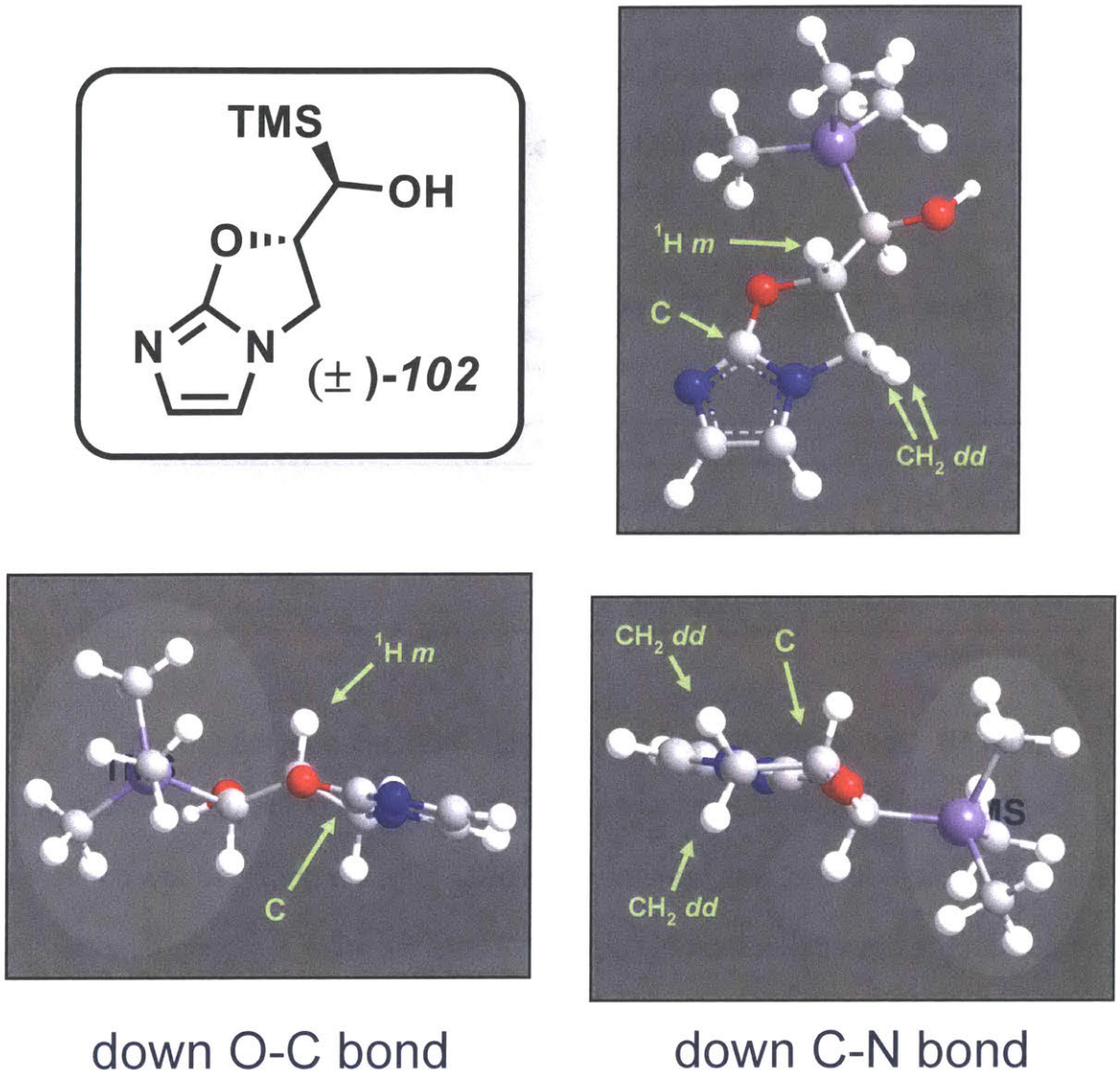

Figure 27. HMBC and MM2 analysis of oxazole **102**. (top right) Full structure view. (bottom right) View down C-N bond with methylene protons shown. (bottom left) view down O-C bond with methine proton shown.

With oxazine **84** as our likely major product, we set our attention to optimizing the conditions for yield and selectivity. From Table 18, we found that varying the temperature and time did little to increase selectivity towards oxazine **84**. When heated to 50 °C in the microwave for 15 minutes, only epoxide **82** and oxazine **84** was obtained

in full conversion at 95% yield and a 3.8:1 selectivity. Prolonging the heating to 1 hour resulted in an overall lower yield, but higher selectivity for the oxazine **84** and oxazole **102** (entry 3). Increasing the temperature higher to 100 °C, we observed only cyclized products **84** and **102** in 65% yield in a 4:5 ratio.

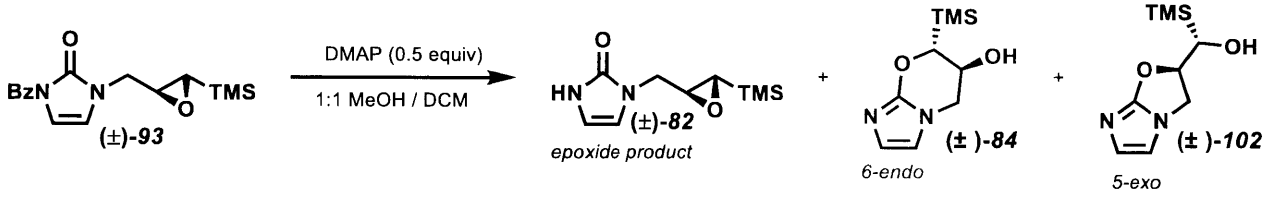

Entry	Temperature (°C)	Time (h)	Conversion	Yield	Ratio (Ep:6-*endo*:5-*exo*)
1	rt	18	100%	60%	5:7:3
2	50*	0.25	100%	95%	3.8:1:0
3	50*	1	100%	74%	1:2:2
4	100*	10 min	100%	65%	4:5

* microwave

Table 18. Optimization based on conditions from unexpected product **84**.

Our next optimization studies investigated the benefits of the protic nature of the solvent, given that methanol was present. With DCM only, we observed low conversion and yields with the epoxide as the only product (Table 19, entry 1). Using a more lipophilic and bulky protic solvents such as IPA resulted in drastically reduced yields of 8% with the epoxide as the only product (entry 2). When we switched to more acidic trifluorethanol (TFE), we observed low yields of 27%; however, only our desired oxazine **84** was formed (entry 3). With hexafluoroisopropanol (HFIP), we observed an increased in yield to 53% of only oxazine **84** after 18 hours at room temperature (entry 4). Switching to microwave heating at 50 °C, we were able to isolate oxazine **84** as the only product in 88-98% yield. We then investigated the stoichiometry of DMAP and found that at 0.1 equivalents of DMAP, we observed a decreased yield of 70% and a 1:7:0

selectivity of epoxide **82** to oxazine **84** to oxazole **102**. To determine if DCM was necessary, HFIP only conditions were performed and similar results (entry 7) were observed to that of entry 5. Importantly, these reactions were easy to perform and do not require any careful handling nor does it required air-free techniques.

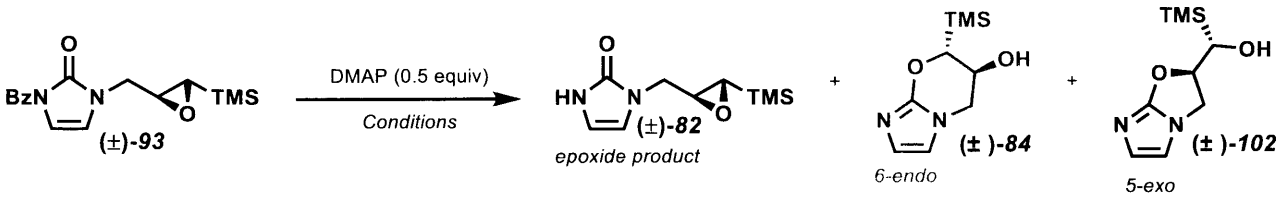

Entry	Solvent	Temperature (°C)	Time (h)	Conversion	Yield	Ratio (Ep:6-*endo*:5-*exo*)
1	DCM only	rt	96	63%	37%	epoxide only
2	1:1 IPA / DCM	rt	48	100%	8%	epoxide only
3	1:1 TFE / DCM	rt	18	100%	27%	*6-endo* only
4	1:1 HFIP / DCM	rt	18	100%	53%	6-*endo* only
5	1:1 HFIP / DCM	50[a]	1	100%	88-98%	6-*endo* only
6	1:1 HFIP / DCM[b]	50[a]	1	100%	70%	1:7:0
7	HFIP only	50[a]	1	100%	88-95%	6-*endo* only

[a] 1 h in microwave. [b] 0.1 equiv DMAP.

Table 19. Investigations under protic conditions to access **84**.

After achieving complete selectivity for our desired TMS-oxazine **84**, the next step was to remove the silyl group to give oxazine (±)-**32**.[45] According to Table 20, TBAF in THF at room temperature gave trace amounts of product (entry 1). However, upon gentle heating, we observed 87% conversion and 28% desilylated product (±)-**32** (entry 2). Importantly, the NMR data from this matches our analytical standard oxazine (±)-**32** that we synthesized earlier in our research program, supporting the formation of the oxazine core. As we increased heating to 60 °C and reduced the reaction time, we observed (±)-**32** in 65% yield (entry 3). Desilylation was then attempted in methanol and DCM for the possibility of telescoping desilylation immediately after cyclization.

However, this resulted in no reaction (entry 4). Basic conditions as reported by Heffron and coworkers were unsuccessful (entries 5 & 6). The reasoning is likely due to the trans relationship between the silyl group and the alcohol as opposed to the *cis* in their system.[45]

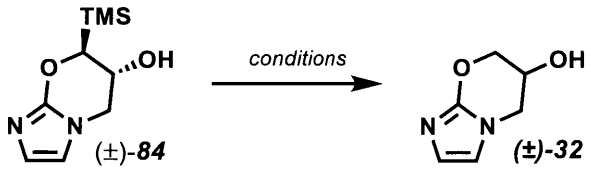

(±)-*84* (±)-*32*

Entry	Reagent	Solvent	Temperature (°C)	Time (h)	Conversion	Yield
1	TBAF	THF	rt	>168	<5%	Trace
2	TBAF	THF	50*	1	87%	28%
3	TBAF	THF	80*	0.5	100%	49%
4	TBAF	1:1 MeOH / DCM	100	1	SM	0%
5	Cs_2CO_3	1:1 MeOH / DCM	50	1	<5	Trace
6	Cs_2CO_3	1:1 HFIP / DCM	100	1	<5	0

Table 20. Investigations into desilylation of **84** to access (±)-**32**. Basic and TBAF conditions were examined.

After the *trans* epoxide system was successfully cyclized and desilylated, we turned our interest towards the analogous *cis* epoxide to investigate its cyclization conditions and how it compares to **93**. Upon subjecting *cis* TMS-epoxy imidazolone **101** to the same conditions its *trans* counterpart, we observed debenzoylated product **106** in 69% yield with *6-exo* **85** in less than 10% yield (Scheme 15). Isolated **83** was then subjected to HFIP under gentle heating for 1 hour and we observed full conversion after 1 hour to give cyclized **85** in 60% yield. Afterwards, TBAF desilylation afforded our oxazine core (±)-**32** in 55% yield.

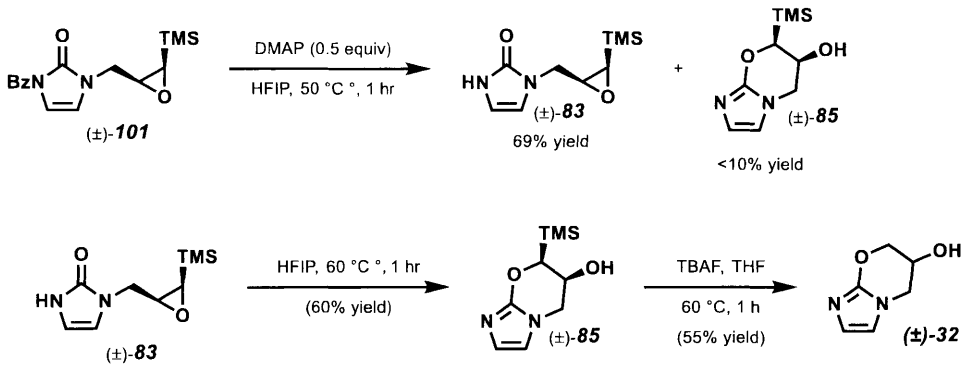

Scheme 15. Synthesis of oxazine (±)-**32** via cis-epoxide **101**.

As we compare the *trans* route against the *cis* route, we conclude that the *trans* route is more practical and expedient. The *cis* variants were in general more unstable to standard conditions and required careful handling and storage. For example, a 4:1 *Z*:*E* mixture of TMS-olefin **95** isomerized to a 1:1 *Z*:*E* mixture after one week. Furthermore, the reactions were often difficult to reproduce due to their reactive nature. Therefore, with each step established and successfully completed, our last efforts will be put towards the enantioselective route to pretomanid.

1.3.9 Enantioselective synthesis of pretomanid

From our successful late-stage nitration to our conditions to exclusively form the *6-endo* oxazine core, we present our final enantioselective route to access pretomanid (Scheme 16). From imidazolone **34**, double benzoylation followed by a selective monobenzoylation gave **65** in 76% yield over two steps. **65** is then alkylated with chiral epoxide **86**,[52] accessed through a Sharpless epoxidation, to give benzoyl TMS-epoxy **93** (79:1 er, >97% ee). From there, **93** is cyclized via epoxide-opening to furnish TMS-oxazine core **84** in 98% yield. Then, desilylation with TBAF allows access to oxazine **32** in 55% yield. After desilylation, benzylation provided des-nitro pretomanid **31** in 64%

yield. Last, our late-stage nitration established pretomanid (**9**) in 58% yield with 98% ee and a 7:1 selectivity over the 5-nitro variant. The longest linear sequence is nine steps from propargyl alcohol **89** or twelve steps total (including hydantoin (**53**) reduction), with a 3.1% overall yield.

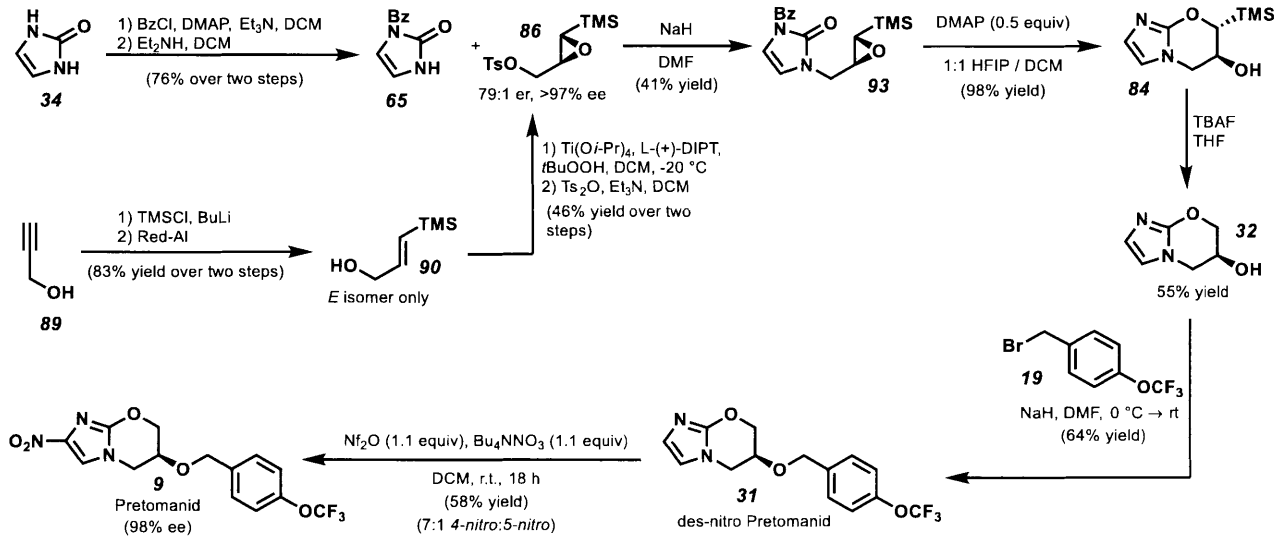

Scheme 16. Enantioselective synthesis of pretomanid (**9**).

1.4 Conclusions and future directions

Pretomanid has emerged as a potential cornerstone anti-TB API and it is critical for us to design a new synthesis that avoids the explosive starting material while advancing chemical knowledge. Our research program was successful in achieving pretomanid through a challenging, highly selective *6-endo* epoxide-opening to access the oxazine core and late-stage nitration thereby avoiding explosive, starting material **15**.

From our initial proposal, we sought to reduce the total step count compared to existing syntheses. Furthermore, we anticipated that we could avoid the use of protecting groups entirely. However, given the complications brought forth by the similar

N-H protons on imidazolone **34**, benzoyl protecting groups were necessary to effect our desired cyclization. Nonetheless, our route offers a new strategy to access potentially new imidazooxazine and possibly imidazooxazole derivatives. To our knowledge, the only existing method to access such structures is through an S_NAr cyclization that requires a leaving group present. For many of our steps, we relied on chromatographic purifications. That said, most of the material were crystalline in nature and this opens opportunity for crystallization purification. For our enantioselective synthesis, the steps were performed at laboratory scales (<1 g). For the Sharpless epoxidation of **90**, a decrease in selectivity (6:1 er) was observed at larger scales (5 g). Therefore, future work could be performed to adapt our route for a larger scale synthesis of pretomanid (**9**).

1.5 Works Cited

[1] *Global Tuberculosis Report 2018. World Health Organization*: Geneva, Switzerland, **2018**.

[2] Pai, M., Pehr, M. A., Dowdy, D., Dheda, K., Divangachi, M., Boehme, C. C., Ginsberg, A., Swaminathan, S., Spigelman, Getahun, H., Menzies, D., Raviglione, M. Tuberculosis. *Nature Reviews* **2016**, doi:10.1038/nrdp.2016.76

[3] A) Simmons, J. D.; Stein, C. M.; Seshadri, C.; Campo, M. Alter, G.; Fortune, S.; Schurr, E.; Wallis, R. S.; Churchyard, G.; Mayanja-Kizza, H.; Boom, W. H.; Hawn, T. R. Immunological mechanisms of human resistance to persistent *Mycobacterium tuberculosis* infection. *Nature Reviews Immunology* **2018, 18**, 575. B) Barry 3rd, C. E.; Boshoff, H. I.; Dartois, V.; Dick, T.; Ehrt, S.; Flynn, J.; Schnappinger, D.; Wilkinseon, R. J.; Young, D. The spectrum of latent tuberculosis: rethinking the biology and intervention strategies. *Nature Reviews* **2009**, *7*, 845. C) Miranda, M. S.; Breiman, A.; Allain, S.; Deknuydt, F.; Altare, F. The tuberculosis granuloma: an unsuccessful host defence mechanism providing a safety shelter for the bacteria? *Clinical and Developmental Immunology* **2012**, 2012, Article ID 139127.

[4] Kaufmann S. H. Fact and fiction in tuberculosis vaccine research: 10 years later. *The Lancet Infectious Diseases* **2011**, *11*, 633.

[5] A) Adams, D. O. The granulomatous inflammatory response. A review. *American Journal of Pathology* **1976**, *84*, no. 1, 164. B) Sandor, M.; Weinstock, J. V.; Wynn, T. A. Granulomas in schistosome and mycobacterial infections: a model of local immune responses. *Trends in Immunology* **2003**, *24*, 44.

[6] Kumar, K.; Kon, O. M. Diagnosis and treatment of tuberculosis: latest developments and future priorities. *Ann. Res. Hosp.* **2017**, *1*:37.

[7] Pai, M.; Behr, M.A.; Dowdy, D.; Dheda, K.; Divangahi, M.; Boehme, C. C.; Ginsberg, A.; Swaminathan, S.; Spigelman, M.; Getahun, H.; Menzies, D.; Raviglione, M. Tuberculosis. *Nature Reviews* **2016**, DOI:10.1038/nrdp.2016.76.

[8] A) Ahsan, M. J.; Ansari, M. Y.; Yasmin, S.; Jadav, S. S.; Kumar, P.; Garg, S. K.; Aseri, A.; Khalilullah, H. Tuberculosis: Current treatment, diagnostics, and newer antitubercular. Agents in clinical trials *Infectious Disorders – Drug Targets* **2015**, *15*, 32. B) Spigelman, M. K. New

tuberculosis therapeutics: A growing pipeline. *The Journal of Infectious Diseases* **2007**, *196*, S28.

[9] The TB Alliance. TB medicine pretomanid enters regulatory review process in the United States. https://www.tballiance.org/news/tb-alliance-and-mylan-announce-global-collaboration-commercialize-investigational-drug (accessed April 29, 2019)

[10] The TB Alliance. TB Alliance and Mylan Announce global collaboration to commercialize investigational drug pretomanid as part of two regimens to treat tuberculosis. https://www.tballiance.org/news/tb-alliance-and-mylan-announce-global-collaboration-commercialize-investigational-drug (accessed April 29, 2019)

[11] Stover, C. K.; Warrener, P.; VanDevanter, D. R.; Sherman, D. R.; Arain, T. M.; Langhorne, M. H.; Anderson, S. W.; Towell, J. A.; Yuan, Y.; McMurray, D. N.; Kreiswirth, B. N.; Barry, C. E.; Baker, W. R. A small-molecule nitroimidazopyran drug candidate for the treatment of tuberculosis. *Nature* **2000**, *405*, 962.

[12] A) Ang, C. W.; Jarrad, A. M.; Cooper, M. A.; Blaskovich, M. A. Nitroimidazoles: molecular fireworks that combat a broad spectrum of infectious diseases. *J. Med. Chem.* **2017**, *60*, 7636.

[13] *The use of delamanid in the treatment of multidrug-resistant tuberculosis in children and adolescents: Interim policy guidance*; World Health Organization: Geneva, Switzerland, 2016.

[14] A) Singh, R.; Manjunatha, U.; Boshoff, H. I. M.; Ha, Y. H.; Niyomrattanakitt, P.; Ledwidge, R.; Dowd, C. S.; Lee, I. Y.; Kim, P.; Zhang, L.; Kang, S.; Keller, T. H.; Jiricek, J.; Barry 3rd, C. E. PA-824 Kills nonreplicating mycobacterium tuberculosis by intracellular NO release. *Science* **2008**, *322*, 1392. B) Manjunatha, U.; Boshoff, H. I. M.; Barry III, C. E. The mechanism of action of PA-824. *Comm. & Int. Bio.* **2009**, 2, 215. C) Stover, C. K.; Warrener, P.; VanDevanter, D. R.; Sherman, D. R.; Arain, T. M.; Langhorne, M. H.; Anderson, S. W.; Towell, J. A.; Yuan, Y.; McMurray, D. N.; Kreiswirth, B. N.; Barry, C. E.; Baker, W. R. A small-molecule nitroimidazopyran drug candidate for the treatment of tuberculosis. *Nature* **2000**, *405*, 962. D) Boshoff, H. I.; Barry III, C. E. Is the mycobacterial cell wall a hopeless drug target for latent tuberculosis? *Drug Discovery Today: Disease Mechanisms* **2006**, *3*, 237.

[15] Baker, W. R.; Shaopei, C.; Keeler, E. L. Nitroimidazole antibacterial compounds and methods of use thereof. Patent WO9701562 (A1), January 16, 1997.

[16] Baker, W. R.; Shaopei, C.; Keeler, E. L. Nitro-[2,1-b]imidazopyran compounds and antibacterial uses thereof. U.S. Patent 6,087,358, July 11, 2000.

[17] A) Urtiew, P. A.; Tarver, C. M.; Simpson, R. L. Shock initiation of 2,4-dinitroimidazole (2,4-DNI). *AIP Conference Proceedings* **1996**, *370*, 887. B) Anniyappan, M.; Sonawane, S.H.; Pawar, S.J.; Sikder, A.K. Thermal decomposition and kinetics of 2,4-dinitroimidazole: An insensitive high explosive. *Thermochimica Acta* **2015**, *614*, 93.

[18] Kim, P.; Zhang, L.; Manjunatha, U. H.; Singh, R.; Patel, S.; Jiricek, J.; Keller, T. H.; Boshoff, H. I.; Barry 3rd, C. E.; Dowd, C. S. Structure-activity relationships of antitubercular nitroimidazoles. 1. Structural Features associated with aerobic and anaerobic activities of 4- and 5-nitroimidazoles. *J. Med. Chem.* **2009**, *52*, 1317.

[19] Orita, A.; Miwa, K.; Uehara, G.; Otera, J. Integration of solventless reaction in a multi-step process: Application to an efficient synthesis of PA-824 *Adv. Synth. Catal.* **2007**, *349*, 2136.

[20] Xueying, L.; Libin, W.; Yue, M.; Weiping, C. Synthesis of Anti-TB Drug Candidate PA-824. Chinese Patent CN104177372, July 31, 2014.

[21] Marsini, M. A.; Reider, P. J.; Sorensen, E. J. A concise and convergent synthesis of PA-824. *J. Org. Chem.* **2010**, *75*, 7479.

[22] Isikgor, F. H.; Becer, C. R. Lignocellulose biomass: A sustainable platform for the production of bio-based chemicals and polymers. *Polym. Chem.* **2015**, DOI: 10.1039/c5py00263j

[23] Ragauskas, A. J.; Williams, C. K.; Davison, B. H.; Britovsek, G.; Cairney, J.; Eckert, C. A.; Frederick Jr., W. J.; Hallet, J. P.; Leak, D. J.; Liotta, C. L.; Mielenz, J. R.; Murphy, R.; Templer, R.; Tschaplinski, T. The path forward for biofuels and biomaterials. *Science* **2006**, *311*, 484.

[24] Hering, K. W.; Chambournier, G.; Endres, G. W.; Fedij, V.; Krell II, T. J.; Mahmoud, H. M. Methods of synthesizing a prostacyclin analog. W.O Patent 2014/089385 A2, June 12, 2014.

[25] Kappe, C. O. Controlled microwave heating in modern organic synthesis. *Angew. Chem. Int. Ed.* **2004**, *43*, 6250.

[26] Lygo, B., Andrews, B. I. Asymmetric phase-transfer catalysis utilizing chiral quaternary ammonium salts: asymmetric alkylation of glycine imines. *Acc. Chem. Res.* **2004**, *37*, 518.

[27] Thompson, A.M,; Bonnet, M.; Lee, H. H.; Franzblau, S. G.; Wan, B.; Wong, G. S.; Cooper, C. B.; Denny, W. A. Antitubercular nitroimidazoles revisited: synthesis and activity of the authentic 3-nitro isomer of pretomanid. *ACS Med. Chem. Lett.* **2017**, *8*, 1275.

[28] Minch, M. J. Orientational dependence of vicinal proton-proton NMR coupling constants: The Karplus relationship. *Concepts in Magnetic Resonance* **1994**, *6*, 41.

[29] Kaburagi, Y.; Kishi, Y. Operationally simple and efficient workup procedure for TBAF-mediated desilylation: application to halichondrin synthesis. *Org. Lett.* **2007**, *9*, 723.

[30] Katritzky, A. R.; Scriven, E. F. V.; Majumder, S.; Akhmedova, R. G.; Akhmedov, N. G.; Vakulenko, A. V. Direct nitration of five membered heterocycles. *Arkivoc* **2005**, 179.

[31] Tian, W.; Grivas, S.; Olsseon, K. Nitration of 5-fluoro-2,I,3-benzoselenadiazoles, and the synthesis of 4-fluoro-3-nitro-, 4- fluoro-6-nitro-, 5-fluoro-3- nitro-o-phenylened amines and 3,4-diamino-2-nitrophenols by subsequent deselenation. *J. Chem. Soc. Perkin Trans. 1* **1993**, *2*, 257.

[32] Rajaraman, S.; Yaqub, U. Process for nitration of N-substituted imidazoles. U.S. Patent 0,045,722, February 21, 2008.

[33] Shackelford, S. A.; Anderson, M. B.; Christie, L. C.; Goetzen, T.; Guzman, M. C.; Hananel, M. A.; Kornreich, W. D.; Li, H.; Pathak, V. P.; Rabinovich, A. K.; Rajapakse, R. J.; Truesdale, L. K.; Tsank, S. M.; Vazir, H. N. Electrophilic tetraalkylammonium nitrate nitration. II. Improved anhydrous aromatic and heteroaromatic mononitration with tetramethylammonium nitrate and triflic anhydride, including selected microwave examples. *J. Org. Chem.* **2003**, *68*, 267.

[34] Walker, M. D.; Andrews, B. L.; Burton, A. J.; Humphreys, L. D.; Kelly, G.; Schilling, M. B.; Scott, P. W. The development of a new manufacturing route to the novel anticonvulsant SB-406725A. *Org. Process. Res. Dev.* **2010**, *14*, 108.

[35] A) Baxter, R. L.; Camp, D. J.; Coutts, A.; Shaw, N. Synthesis and Biological Activity of 9-mercaptodethiobiotin – A Putative Biotin Precursor in *Escherichia coli*. *J. Chem. Soc. Perkin Trans.* **1992**, 255. B) Zav'yalov, S. I.; Radul, O. M.; Gunar, V. I.; Rodionova, N. A. Synthesis of ethyl ester of α-oxodehydrodesthiobiotin. *N. D. Zelinskii Institute of Organic Chemistry, Academy of Sciences of the USSR* **1972**, *10*, 2335. C) Hilbert, G. E. The synthesis of 2-imidazolone-4-carboxylic acid and 2-imidazolone. *J. Am. Chem. Soc.*, **1932**, *54*, 3413.

[36] A) Han, S.; Zard, S. Z. Stabilization of radicals by imides. A modular stereoselective approach to protected functional 1,2-diamines. *Org. Lett.* **2014**, *16*, 5386. B) Antonova, M. M.; Baranov, V. V.; Kravchenko, A. N. Methods for the synthesis of 1-substituted 1H-imidazol-2(3H)-ones. *Chemistry of Heterocyclic* Compounds **2015**, *51*, 395.

[37] A) Whitney, R. A. Cycloaddition reactions of 1,3-diacetylimidazolin-2-one. *Tet. Lett.* **1981**, *22*, 2063. B) Fiala, T.; Sindelar, V. Synthesis of norbornahemicucurbiturils. *Synlett* **2013**, *24*, 2443.

[38] Jacobsen, E. N.; Tokunaga, M.; Larrow, E. Stereoselective Ring Opening Reactions. U.S. Patent 6,262,278, July 17, 2001.

[39] A) Corey, E. J.; Chaykovsky, M. Methylsulfinylcarbanion. *J. Am. Chem. Soc.* **1962**, *84*, 866. B) Corey, E. J.; Chaykovsky, M. Methylsulfinyl Carbanion (CH3-SO-CH2-). Formation and applications to organic synthesis. *J. Am. Chem. Soc.* **1965**, *87*, 1345.

[40] Herzberger, J.; Niederer, K.; Pohlit, H.; Seiwert, J.; Worm, M.; Wurm, F. R.; Frey, H. Polymerization of ethylene oxide, propylene oxide, and other alkylene oxides: synthesis, novel polymer architectures, and bioconjugation. *Chem. Rev.* **2016**, *116*, 2170.

[41] Wuts, P. G. M.; Greene, T. W. *Greene's Protective Groups in Organic Synthesis, Fourth Edition*; John Wiley & Sons, Inc.: New Jersey, 2007.

[42] Na, J. Houk, K. N.; Shevlin, C. G.; Janda, K. D.; Lerner, R. A. The energetic advantage of 5-exo versus 6-endo epoxide openings: a preference overwhelmed by antibody catalysis. *J. Am. Chem. Soc.* **1993**, *115*, 8453.

[43] A) Byers, J. A.; Jamison, T. F. Entropic factors provide unusual reactivity and selectivity in water-promoted epoxide-opening reactions. *Proc. Natl. Acad. Sci.* **2013**, *110*, 16724. B) Mousseau, J. J.; Morten, C. J.; Jamison, T. F. A dioxane template for highly selective epoxy alcohol cyclizations. *Chem. Eur. J.* **2013**, *19*, 10004. C) Underwood, B. S.; Tanuwidjaja, J.; Jamison, T. F. Total syntheses of the squalene-derived halogenated polyethers ent-dioxepandehydrothyrsiferol and armatol A via bromonium- and Lewis acid-nitiated epoxide-opening cascades. *Tetrahedron* **2013**, *69*, 5205. D) Morten, C. J.; Byers, J. A.; Jamison, T. F. Evidence that epoxide-opening cascades romoted by Wawter are stepwise and become faster and more selective after the first cyclization. *J. Am. Chem. Soc.* **2011**, *133*, 1902. E) Morten, C. J.; Byers, J.A.; Van Dyke, A.R.; Vilotijevic, I.; Jamison, T. F. The development of *endo*-selective epoxide-opening cascades in water *Chem. Soc. Rev.* **2009**, *38*, 3175. F) Morten, C. J.; Jamison, T. F. Water overcomes methyl group directing effects in epoxide-opening cascades. *J. Am. Chem. Soc.* **2009**, *131*, 6678. G) Byers, J. A.; Jamison, T. F. On the synergism tetween H_2O and a tetrahydropyran template in the regioselective cyclization of an epoxy alcohol. *J. Am. Chem. Soc.* **2009**, *131*, 6383. H) Vilotijevic, I.; Jamison, T. F. Epoxide-opening cascades promoted by Water. *Science* **2007**, *317*, 1189.

[44] A) Nicolaou, K. C.; Duggan, M. E.; Hwang, C-K.; Somers, P. K. Activation of 6-*endo* over 5-*exo* epoxide openings. Ring-selective formation of tetrahydropyran systems and stereocontrolled synthesis of the ABC ring framework of brevetoxin B. *JCS Chem. Commun.* **1985**, 1359. B) Nicolaou, K. C.; Prasad, C. V. C.; Somers, P. K.; Hwang, C. K. Activation of 6-endo over 5-exo hydroxy epoxide openings. Stereoselective and ring selective synthesis of tetrahydrofuran and tetrahydropyran systems. *J. Am. Chem. Soc.* **1989**, *111*, 5330. C) Mukai, C.; Ikeda, Y.; Sugimoto, Y.; Hanaoka, M. Regioselective and stereospecific formation of 2-ethynyl-3-hydroxytetrahydropyran derivatives via 6-endo ring closure. *Tet. Lett.* **1994**, *35*, 2179. D) Mori, Y.; Yaegashi, K.; Furukawa, H. *J. Am. Chem. Soc.* **1996**, *118*, 8158. E) Morimoto, Y.; Nishikawa, Y.; Ueba, C.; Tanaka, T. Reagent-controlled switching of 5-exo to 6-endo cyclizations in epoxide openings. *Angew. Chemie Int. Ed.* **2006**, *45*, 810.

[45] A) Simpson, G. L.; Heffron, T. P.; Merino, E.; Jamison, T. F. Ladder polyether synthesis *via* epoxide-opening cascades using a disappearing directing Group *J. Am. Chem. Soc.* **2006**, *128*, 1056. B) Heffron, T. P.; Jamison, T. F. $SiMe_3$-based homologation–epoxidation–cyclization strategy for ladder THP synthesis. *Org. Lett.* **2003**, *5*, 2339. C) Heffron, T. P.; Simpson, G. L. ; Merino, E.; Jamison, T. F. Ladder polyether synthesis via epoxide-opening cascades directed by a disappearing trimethylsilyl group. *J. Org. Chem.* **2010**, *75*, 2681.

[46] Hoveyda, A. H.; Evans, D. A.; Fu, G. C. Substrate-directable chemical reactions. *Chem. Rev.* **1993**, *93*, 1307.

[47] A) Compain, P.; Gore, J.; Vatele, J. M. Rearrangement of α-hydroxy imines to α-amino ketones: Mechanistic aspects and synthetic applications *Tetrahedron* **1996**, *52*, 6647.B) Oger, C.; Balas, L.; Durand, T.; Galano, J-M. Are alkyne reductions chemo-, regio-, and stereoselective enough to provide pure (Z)-olefins in polyfunctionalized bioactive molecules? *Chem. Rev.* **2013**, *113*, 1313.

[48] A) Radhakrlshnan, K.; Ramachandran, P. A.; Brahme, P. H.; Chaudhari, R. V. Solubility of hydrogen in methanol, nitrobenzene, and their mixtures. Experimental data and correlation. *J. Chem. Eng. Data 1983*, 28, 1. B) Trinh, T. H. K.; de Hemptinne, J. C.; Lugo, R.; Ferrando, N.; Passarello, J. P. Hydrogen solubility in hydrocarbon and oxygenated organic compounds. *J. Chem. Eng. Data* **2016**, *61*, 19.

[49] Langille, N. F.; Jamison, T. F. trans-Hydroalumination/Alkylation: One-pot synthesis of trisubstituted allylic alcohols *Org. Lett.* **2006**, *17*, 3761.

[50] Eric V. Anslyn and Dennis A. Dougherty *Modern Physical Organic Chemistry*; University Science Books, 2006.

[51] Simpson, J. H. Organic structure determination using 2-D NMR spectroscopy. A problem-based approach. 2nd ed.; Elsevier: San Diego, 2012.

[52] A) Enantiomeric ratio was determined by Mosher ester analysis and HPLC trace analysis. B) Kobayashi, Y.; Ito, T.; Yamakawa, I.; Urabe, H.; Sato, F. Remarkable efficiency in the catalytic epoxidation of (*E*)-3-trimethylsilyl-2-propen-1-ol. *Synlett* **1991**, *811.* C) Raubo, P.; Wicha, J. Synthesis of optically active 2,3-0-isopropylidene-l-(trimethylsilyl)glyceraldehyde and other derivatives of (a-hydroxyacyl)silane. *J. Org. Chem.* **1994**, 16, 59. D) Hoye, T. R.; Jeffrey, C. S.; Shao, F. Mosher ester analysis for the determination of absolute configuration of stereogenic (chiral) carbinol carbons. *Nature Protocols* **2007**, *2*, 2457.

Chapter One

Enantioselective Synthesis of Pretomanid –

Experimental Section

General Information

Reactions were performed under an inert argon atmosphere unless otherwise stated. Commercially available chemicals were purchased from either Sigma-Aldrich Chemical Company (Milwaukee, WI), Alfa Aesar (Ward Hill, MA), Acros Organics (Pittsburgh, PA), or TCI America (Portland, OR). Anhydrous tetrahydrofuran (THF), dimethylformamide (DMF), dichloromethane, dichloroethane, dimethyl sulfoxide (DMSO), triethylamine, toluene, and acetonitrile were purified via an SG Water USA solvent column system (Nashua, NH) before use. All reactions were monitored with thin-layer chromatography (TLC), which was performed using EMD 60-F254 silica glass plates and visualized with a UV lamp (254 nm). Microwave conditions were performed with Biotage Initiator+ using microwave reaction vials with cap with septum and magnetic bars purchased from Biotage. All microwave reactions were run under normal absorption with 45 second pre-stirring. Products were purified on SNAP Ultra columns utilizing the Biotage® IsoleraTM flash purification system.

NMR spectra were obtained in $CDCl_3$, MeOD, or DMSO-d_6 purchased from Cambridge Isotope Laboratories and used as received. Norell 5 mm NMR tubes with standard septa caps were used. ^1H NMR Spectra were obtained on Bruker Avance 400 (400 MHz for ^1H, 100 MHz for ^{13}C), JEOL 500 MHz (500 MHz for ^1H, 126 MHz ^{13}C), and Bruker AVANCE 600 MHz (600 MHz for ^1H, 151 MHz for ^{13}C) equipped with TXI Cryoprobe. ^{13}C spectra were obtained with ^1H decoupling. ^1H chemical shifts are reported in parts per million relative to TMS (δ = 0.00 ppm) and were referenced to the residual solvent peak. The following designations are used to describe multiplicities: s (singlet), b (broad singlet), d (doublet), t (triplet), q (quartet), dd (doublet of doublets), dt

(doublet of triplets), m (multiplet). Unless otherwise noted, NMR spectra were collected at room temperature (23–27 °C). High-resolution mass-spectrometry (HRMS) data were acquired on a Bruker Daltronics APEXIV 4.7 Tesla FT-ICR Mass Spectrometer (DART and ESI), a JEOL Accutof 4G LC-Plus system outfitted with an ionSense DART ionization source (DART), or an Agilent 6545 Q-TOF LC/MS (ESI). HPLC trace data were obtained with Agilent Technology 1290 Infinity II with Chiralcel OD-H column. Optical rotation was obtained using an Anton Paar Polarimeter MCP 500.

Section 1.3.2 – Experimental Information

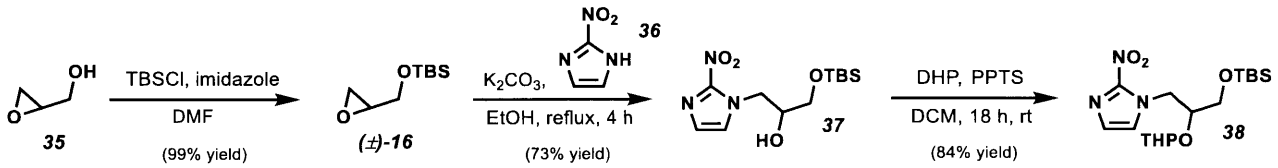

tert-butyldimethyl(oxiran-2-ylmethoxy)silane (16): Synthesized according to a reported procedure.[1] Glycidol (**35**) (10.0 g, 8.95 mL, 135 mmol) was added dropwise to a stirred solution of imidazole (26.45 g, 176 mmol) and TBSCl (14.7 g, 216 mmol) in DMF (80 mL) at 0 °C. The reaction was allowed to warm to rt and stirred for 30 min. The reaction was quenched with 250 mL of sat. NH_4Cl solution and 250 mL of DI water. The reaction mixture was extracted 5 times with 150 mL hexanes, and the combined organics were washed with 500 mL of brine and dried over Na_2SO_4. The crude was purified with column chromatography with 10% EtOAc in hexanes to give (±)-**16** (25.2 g, 134 mmol, 99% yield) as a clear oil. Spectral data were in agreement with the literature.[1]

1-((tert-butyldimethylsilyl)oxy)-3-(2-nitro-1H-imidazol-1-yl)propan-2-ol (37): Synthesized according to a reported procedure.[2] To a mixture of **36** (5.00 g, 44.2 mmol) and K_2CO_3 (0.856 g, 6.19 mmol) in EtOH (53.1 mL) was added (±)-**16** (12.5 g, 13.9 mL, 66.3 mmol). The solution was heated at 85 °C for 5 h. The solvent was removed under reduced pressure and DCM (50 mL) was added. The precipitates were filtered off and the filtrated was concentrated under reduced pressure. The crude mixture was purified

---

[1] Hering, K. W.; Chambournier, G.; Endres, G. W.; Fedij, V.; Krell II, T. J.; Mahmoud, H. M. Methods of Synthesizing a Prostacyclin analog. W.O Patent 2014/089385 A2, June 12, 2014.
[2] Singh, R.; Manjunatha, U.; Boshoff, H. I. M.; Ha, Y. H.; Niyomrattanakitt, P.; Ledwidge, R.; Dowd, C. S.; Lee, I. Y.; Kim, P.; Zhang, L.; Kang, S.; Keller, T. H.; Jiricek, J.; Barry 3rd, C. E. PA-824 Kills Nonreplicating Mycobacterium tuberculosis by Intracellular NO Release. *Science* **2008**, *322*, 1392.

via column chromatography to give **37** (5.84 g, 19.4 mmol, 73% yield) as a yellow orange solid. Spectral data were in agreement with the literature.[1]

^{1}H NMR (500 MHz, Chloroform-*d*) δ 7.19 (s, 1H), 7.12 (s, 1H), 4.66 (dd, *J* = 13.8, 3.1 Hz, 1H), 4.34 (dd, *J* = 13.8, 8.3 Hz, 1H), 4.07 – 3.98 (m, 1H), 3.74 (dd, *J* = 10.3, 4.2 Hz, 1H), 3.59 (dd, *J* = 10.2, 5.1 Hz, 1H), 0.90 (d, *J* = 3.1 Hz, 9H), 0.08 (d, *J* = 2.1 Hz, 6H).

^{13}C NMR (126 MHz, Chloroform-*d*) δ 128.19, 127.35, 70.55, 64.18, 52.50, 25.90, 25.72, 18.33, -3.50, -5.38.

1-(3-((tert-butyldimethylsilyl)oxy)-2-((tetrahydro-2H-pyran-2-yl)oxy)propyl)-2-nitro-1H-imidazole (38): Synthesized according to a reported procedure.[2] To a mixture of **37** (5.00 g, 16.6 mmol) and PPTS (6.25 g, 24.9 mmol) in DCM (50 mL) was added DHP (2.79 g, 3.03 mL, 33.2 mmol). The mixture was stirred overnight and quenched with 125 mL saturated $NaHCO_3$ solution. The organic layer was collected and the aqueous layer was extracted twice with 70 mL DCM. The combined organics were washed with 200 mL brine and dried over Na_2SO_4. The solvent was removed under reduced pressure and purified via column chromatography to give both diastereomers of **38** (5.39 g, 14.0 mmol, 84% yield) as a yellow oil. Spectral data were in agreement with the literature.2

^{1}H NMR (500 MHz, Chloroform-*d*) δ 7.13 - 7.09 (m, 2H), 5.09 - 3.45 (m, 5H), 1.98 - 1.24 (m, 9H), 0.90 (s, 9H), 0.08 (s, 6H).

^{13}C NMR (126 MHz, Chloroform-*d*) δ 127.82, 127.65, 127.12, 100.27, 96.97, 63.23, 63.06, 62.52, 61.82, 51.30, 50.56, 30.68, 30.48, 25.93, 25.88, 25.73, 25.22, 25.10, 19.75, 19.50, 18.30, -3.51, -5.37.

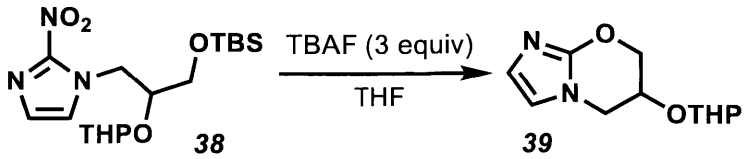

6-((tetrahydro-2H-pyran-2-yl)oxy)-6,7-dihydro-5H-imidazo[2,1-b][1,3]oxazine (39): Synthesized according to a modified reported procedure.[2] Tetrabutylammonium fluoride (TBAF, 1 M in THF, 3 mL, 3 mmol) was added to a stirred solution of **38** (390 mg, 1 mmol, 1 equiv) in 4 mL THF in a microwave vial. The reaction heated to 130 °C for 5 min and allowed to cool before removing vial cap. Reaction was quenched with 10 mL saturated NaHCO3 and extracted with 15 mL DCM twice. The combined organic extracts were washed with 15 mL brine, collected, dried over Na_2SO_4, and concentrated under reduced pressure. The dark brown oily crude was purified by chromatography with 5-10% MeOH in DCM to obtain both diastereomers of **39** (176 mg, 0.79 mmol, 78% yield) as a light brown oil. Spectral data were in agreement with the literature.[2]

^{1}H NMR (500 MHz, Chloroform-*d*) δ 6.66 (d, J = 2.1 Hz, 1H), 6.49 (d, J = 2.1 Hz, 1H), 4.84 - 3.42 (m, 5H), 2.02 - 1.46 (m, 9H).

^{13}C NMR (126 MHz, Chloroform-*d*) δ 149.39, 149.21, 124.64, 124.56, 114.19, 114.09, 98.21, 97.81, 69.45, 67.06, 65.80, 65.25, 62.89, 62.52, 47.79, 46.23, 30.55, 30.51, 25.26, 19.29, 18.99.

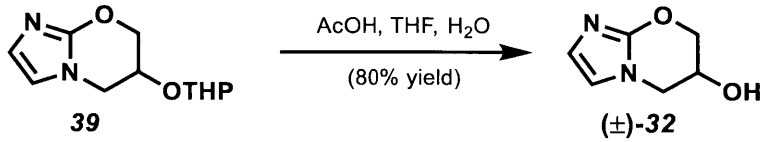

6,7-dihydro-5H-imidazo[2,1-b][1,3]oxazin-6-ol ((±)-32): Synthesized according to a modified reported procedure.[2] To a solution of 66 mL AcOH, 33 mL THF, and 15 mL

H_2O opened to air, **39** (3.3 g, 14.7 mmol) was added and stirred overnight at 60 °C. The reaction was then concentrated under reduced pressure. Trituration of the crude oil with DCM gave (±)-**32** (1.65 g, 11.8 mmol, 80% yield) as an off-white solid. Spectral data were in agreement with the literature.[2]

^{1}H NMR (500 MHz, Methanol-*d4*) δ 6.63 (d, J = 1.6 Hz, 1H), 6.54 (d, J = 1.6 Hz, 1H), 4.30 (d, J = 2.8 Hz, 2H), 4.25 (d, J = 3.0 Hz, 1H), 4.13 (dd, J = 12.9, 3.8 Hz, 1H), 3.90 (d, J = 2.8 Hz, 1H).

^{13}C NMR (126 MHz, Methanol-*d4*) δ 149.29, 122.19, 114.60, 70.22, 60.53, 48.28.

gCOSY and HMBC *(See Spectral Data section)*

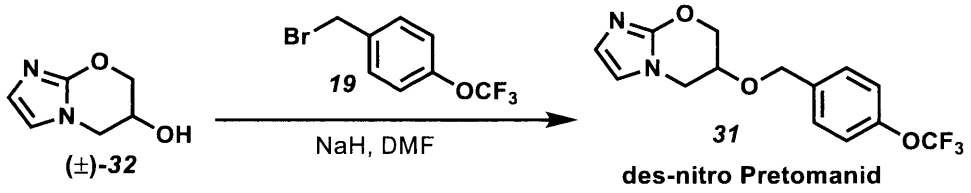

6-((4-(trifluoromethoxy)benzyl)oxy)-6,7-dihydro-5H-imidazo[2,1-b][1,3]oxazine (31): Synthesized according to a modified reported procedure.[2] To a solution of NaH (95% pure, 1.07 mg, 4.46 mmol) in DMF (0.2 M, 15 mL) at 0 °C, (±)-**32** (500.0 mg, 3.57 mmol) in 3 mL DMF was added dropwise. The reaction mixture was stirred for 1 h or until bubbling ceased. **19** (0.628 mL, 1.00 g, 3.92 mmol) was then added dropwise at 0 °C and the reaction was stirred for 5 h at rt. The reaction was quenched with 1 mL MeOH, diluted with 20 mL of sat. ammonium chloride, and extracted 4 times with 20 mL DCM. The combined organics were then washed with 40 mL brine, dried over Na_2SO_4, and concentrated. Crude was purified with column chromatography with 5% MeOH in

DCM to give **31** (803 mg, 2.56 mmol) as a white solid. Spectral data were in agreement with the literature.[2]

^{1}H NMR (600 MHz, Chloroform-*d*) δ 7.35 (d, J = 8.5 Hz, 1H), 7.23 – 7.19 (m, 1H), 6.69 (d, J = 1.7 Hz, 1H), 6.49 (d, J = 1.6 Hz, 1H), 4.71 (d, J = 12.0 Hz, 1H), 4.62 (d, J = 12.0 Hz, 1H), 4.46 (ddd, J = 11.8, 4.6, 1.9 Hz, 1H), 4.29 (dd, J = 11.9, 1.9 Hz, 1H), 4.11 (dd, J = 12.1, 4.2 Hz, 1H), 4.08 – 3.96 (m, 1H).

^{13}C NMR (151 MHz, Chloroform-*d*) δ 148.99, 135.76, 129.00, 124.74, 121.29, 121.17, 119.58, 114.06, 77.24, 77.03, 76.81, 70.18, 67.66, 66.93, 46.63.

HRMS (ESI, *m/z*) $[M+H]^+$ Calculated for $C_{14}H_{14}F_3N_2O_3^+$: 315.0951; found 315.0946.

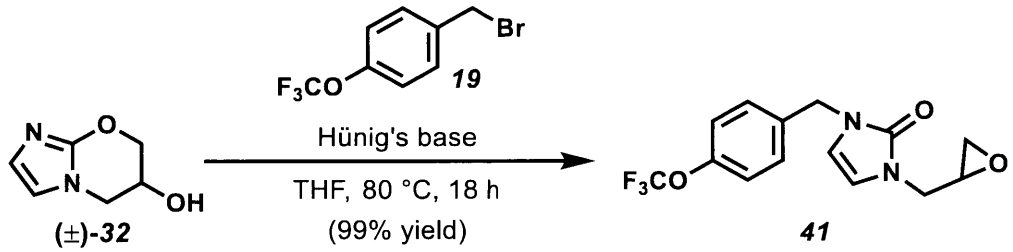

1-(oxiran-2-ylmethyl)-3-(4-(trifluoromethoxy)benzyl)-1,3-dihydro-2H-imidazol-2-one (41): To a stirred solution of (±)-**32** (30.0 mg, 0.214 mmol) and diisopropylethylamine (45 μL, 33.20 mg, 0.257 mmol) in 2.14 mL THF at rt, **19** (81.9 mg, 52 μL, 0.321 mg) was added and refluxed at 80 °C overnight. The reaction was quenched with 3 mL sat. $KHCO_3$ solution, extracted twice with 5 mL DCM, and dried over Na_2SO_4. The crude mixture was concentrated under reduced pressure and purified with column chromatography to give **41** (67 mg, 0.214 mmol) as a white solid.

^{1}H NMR (500 MHz, Methanol-d_4) δ 7.34 (d, J = 8.4 Hz, 2H), 7.22 (d, J = 8.3 Hz, 2H), 6.54 (d, J = 3.0 Hz, 1H), 6.46 (d, J = 3.0 Hz, 1H), 4.82 (s, 2H),4.00 (dd, J = 7.7, 5.0 Hz,

1H), 3.86 (dd, *J* = 14.1, 4.2 Hz, 1H), 3.67 (dd, *J* = 14.0, 7.5 Hz, 1H), 3.45 (dd, *J* = 10.7, 4.6 Hz, 1H), 3.37 (dd, *J* = 10.7, 5.4 Hz, 1H).

^{13}C NMR (126 MHz, Methanol-*d*$_4$) δ 153.31, 148.62, 136.51, 129.05, 121.01, 112.55, 110.61, 69.31, 48.51, 48.17, 45.99, 34.70.

^{19}F NMR (471 MHz, Methanol-*d*$_4$) δ -59.47.

HSQC and HMBC (See Spectral Data section)

HRMS (ESI, *m/z*) $[M+H]^+$ Calculated for $C_{14}H_{14}F_3N_2O_3^+$: 315.0951; Found 315.0947.

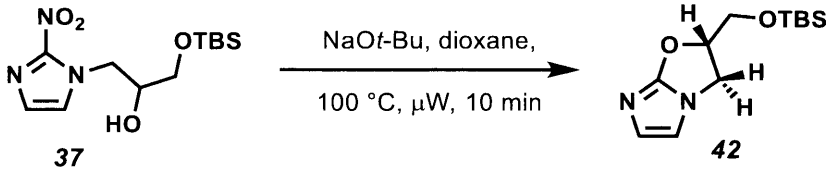

(S)-2-(((tert-butyldimethylsilyl)oxy)methyl)-2,3-dihydroimidazo[2,1-b]oxazole (42): To a solution of 6.4 mL dioxane with **37** (200 mg, 0.664 mmol) in a microwave vial, NaO*t*-Bu (70.15 mg, 0.365 mL, 0.73 mmol) was added. The reaction was heated to 100 °C in the microwave for 10 min. The reaction was concentrated under reduced pressure and purified via flash chromatography with 5% MeOH in DCM to give **42** (119 mg, 0.468 mmol) as a white solid.

^{1}H NMR (500 MHz, Chloroform-*d*) δ 6.63 (s, 1H), 6.54 (m, 1H), 5.21 (m, 1H), 4.15 – 4.03 (m, 2H), 3.96 – 3.83 (m, 2H), 0.83 (s, 9H), 0.07 (s, 3H), 0.03 (s, 3H).

^{13}C NMR (126 MHz, Chloroform-*d*) δ 160.03, 129.43, 110.47, 86.12, 63.46, 44.92, 25.76, 18.26, -5.37.

HMBC (See Spectral Data section)

HRMS (ESI, *m/z*) $[M+H]^+$ Calculated for $C_{12}H_{23}N_2O_2Si^+$: 255.1523; Found 255.1520.

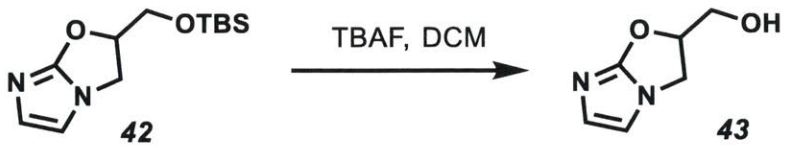

(2,3-dihydroimidazo[2,1-b]oxazol-2-yl)methanol (42): To a stirred solution of **42** (96 mg, 0.377 mmol), TBAF (108.5 mg, 0.415 mmol, 415μL, 1 M in THF) was added slowly at rt. The reaction was stirred for 30 min or until full conversion by TLC. The reaction mixture was then concentrated and purified via column chromatography (10% MeOH in DCM) to give **43** (45 mg, 0.321 mmol, 85% yield) as a white solid. Spectral data are in agreement with literature.[3]

^{1}H NMR (600 MHz, Methanol-*d4*) δ 6.72 (d, J = 1.8 Hz, 1H), 6.56 (d, J = 1.8 Hz, 1H), 5.38 – 5.31 (m, 1H), 4.24 (t, J = 9.1 Hz, 1H), 4.06 (dd, J = 9.5, 6.9 Hz, 1H), 3.92 (dd, J = 12.8, 3.4 Hz, 1H), 3.76 (dd, J = 12.7, 4.3 Hz, 1H).

^{13}C NMR (151 MHz, Methanol-*d4*) δ 159.77, 127.19, 110.97, 87.80, 61.72, 48.46, 48.04, 44.19.

HRMS (ESI, *m/z*) $[M+H]^+$ Calculated for $C_6H_9N_2O_2^+$: 141.0659; Found 141.0659.

Section 1.3.3 – Experimental Information

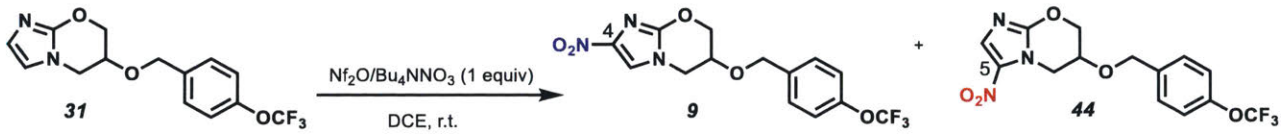

[3] Suehiro, M.; Yang, G.; Torchon, G.; Ackerstaff, E.; Humm, J.; Koutcher, J.; Ouerfelli,O. Radiosynthesis of the tumor hypoxia marker [^{18}F]TFMISO via O-[^{18}F]trifluoroethylation reveals a striking difference between trifluoroethyl tosylate and iodide in regiochemical reactivity toward oxygen nucleophiles. *Bioorg. Med. Chem.* **2011**, 19, 2287–2297.

2-nitro-6-((4-(trifluoromethoxy)benzyl)oxy)-6,7-dihydro-5H-imidazo[2,1-b][1,3]oxazine ((±)-Pretomanid) (9) and 3-nitro-6-((4-(trifluoromethoxy)benzyl)oxy)-6,7-dihydro-5H-imidazo[2,1-b][1,3]oxazine (44): In a glovebox, tetrabutylammonium nitrate (10.7 mg, 0.035 mmol) was measured into a sealed vialed. The sealed vial was taken out and connected with an Argon line. Nf_2O (20.3 mg, 10.7 μL, 0.035 mmol) in DCM (0.16 mL) was added slowly, and the reaction was stirred at rt for 1.5 h. **31** (10 mg, 0.032 mmol) in DCM (0.16 mL) was added slowly and the reaction was stirred overnight at rt. The mixture was quenched with 1 mL 5% $NaHCO_3$ and extracted three times with 2 mL DCM. The combined organics were dried over Na_2SO_4, and purified with column chromatography (5 to 10% methanol in DCM) to give **9** (5.3 mg, 0.015 mmol) as a white solid and **44** (0.8mg, 0.008 mmol) as a white solid. Spectral data are in agreement with literature.[1]

2-nitro-6-((4-(trifluoromethoxy)benzyl)oxy)-6,7-dihydro-5H-imidazo[2,1-b][1,3]oxazine (Pretomanid) (9):

^{1}H NMR (600 MHz, Methanol-*d4*) δ 7.77 (s, 1H), 7.45 (d, J = 8.6 Hz, 2H), 7.26 (d, J = 8.1 Hz, 2H), 4.79 – 4.69 (m, 3H), 4.50 (d, J = 12.1 Hz, 1H), 4.37 – 4.21 (m, 3H).

^{13}C NMR (151 MHz, Methanol-*d4*) δ 148.68, 147.75, 142.50, 136.86, 128.99, 121.35, 120.68, 116.30, 69.37, 67.94, 66.98, 46.80.

[1] Thompson, A.M,; Bonnet, M.; Lee, H. H.; Franzblau, S. G.; Wan, B.; Wong, G. S.; Cooper, C. B.; Denny, W. A. Antitubercular nitroimidazoles revisited: synthesis and activity of the authentic 3-nitro isomer of pretomanid. *ACS Med. Chem. Lett.* **2017**, *8*, 1275.

^{1}H NMR (600 MHz, Chloroform-*d*) δ 7.43 (s, 1H), 7.37 d, J = 8.5 Hz, 2H), 7.24 (d, J = 8.5 Hz, 2H). 4.75 (d, J = 11.9 Hz, 1H), 4.71 – 4.62 (m, 2H), 4.43 – 4.36 (m, 1H), 4.19 – 4.14 (m, 3H).

^{13}C NMR (151 MHz, Chloroform-*d*) δ 149.20, 145.63, 144.94, 135.06, 129.13, 121.28, 119.64, 114.85, 70.27, 67.06, 66.55, 47.61.

^{1}H NMR (600 MHz, DMSO-*d6*) δ 8.04 (s, 1H), 7.45 (d, J = 8.6 Hz, 2H), 7.38 – 7.31 (m, 2H), 4.75 – 4.61 (m, 3H), 4.48 (d, J = 11.9 Hz, 1H), 4.32 – 4.22 (m, 3H).

^{13}C NMR (151 MHz, DMSO-*d6*) δ 148.20, 147.57, 142.56, 137.78, 129.88, 121.44, 118.48, 79.65, 69.19, 68.30, 67.04, 47.22.

HRMS (ESI, *m/z*) [M+H]$^+$ Calculated for $C_{14}H_{13}F_3N_3O_5^+$: 360.0802; Found 360.0797.

Section 1.3.4 – Experimental Information

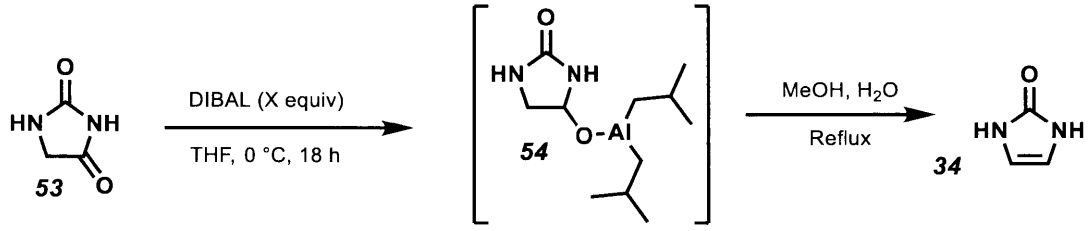

1,3-dihydro-2H-imidazol-2-one (34): To a dried flask under argon containing **53** (10 g, 99.92 mmol) and 30 mL THF at 0 °C, DIBAL (25 wt% in toluene, 1.5 M, 300 mL, 63.95 g, 460 mmol) was added dropwise over 30 min and stirred over night at r.t. Reaction was cooled down to 0 °C and SLOWLY quenched with 500 mL 9:1 MeOH:H_2O solution.

> ***Caution:*** *Stirring is very important! Make sure to have a large stir bar that can sweep most of the bottom of the flask and a stir plate with a strong magnet.*

Caution: *Upon addition of the quench, bubbling is rigorous. The mixture will solidify as a gel indicating that the most of the DIBAL has been consumed. The gel will return to liquid state after standing for a few hours or upon slowly adding more MeOH:H_2O solution. It is safe to break apart the gel with a spatula at that point, if necessary.*

The mixture was stirred further for 6 hours at rt. A condenser was attached and the reaction mixture was heated to 100 °C and refluxed overnight. Mixture was then filtered and the unwanted precipitate was washed with MeOH. The solvents were removed under reduced pressure to give **34** (7.82 g, 93.01 mmol) as a white solid. Spectral data are in agreement with literature.[2]

^{1}H NMR (500 MHz, DMSO-*d6*) δ 9.67 (s, 2H), 6.20 (s, 2H).

^{13}C NMR (500 MHz, DMSO-*d6*) δ 155.52, 109.07.

^{1}H NMR (500 MHz, Methanol-*d4*) δ 9.93 (s, 2H), 6.32 (s, 2H).

^{13}C NMR (126 MHz, Methanol-*d4*) δ 155.63, 109.18.

Section 1.3.6 – Experimental Information

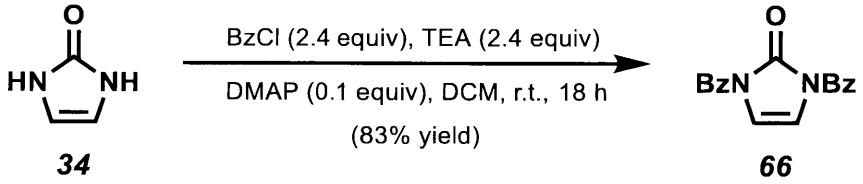

1,3-dibenzoyl-1,3-dihydro -2H-imidazol-2-one (66): To a dried flask containing **34** (10 g, 118.9 mmol) and DMAP (1.45 g, 11.9 mmol) in 48 mL DCM, TEA (14.44 g, 19.9 mL,

[2] Fiala, T.; Sindelar, V. Synthesis of norbornahemicucurbiturils. *Synlett* **2013**, *24*, 2443.

142.72 mmol) was slowly added dropwise followed by dropwise addition of benzoyl chloride (35.11 g, 29.0 mL, 249.8 mmol). Reaction was quenched with 50 mL sat. aq. KHCO3, and the extracted organic layer was washed three times with 50 mL brine. The organic layer dried over Na_2SO_4 and the solvent was removed under reduced pressure. The dried crude was dissolved in a minimal amount of DCM and chilled MeOH was added. The precipitate was filtered and collected. After two crystallizations, **66** (28.9 g, 98.9 mmol, 83% yield) was obtained as a light, white solid.

^{1}H NMR (500 MHz, Chloroform-*d*) δ 7.74 (d, J = 7.7 Hz, 4H), 7.54 (t, J = 14.9 Hz, 7 Hz, 2H), 7.42 (t, J = 7.8 Hz, 4H), 7.10 (s, 2H).

^{13}C NMR (126 MHz, Chloroform-*d*) δ 167.03, 148.50, 133.33, 131.97, 129.74, 128.26, 112.07.

HRMS (ESI, *m/z*) $[M+H]^+$ Calculated for $C_3H_5N_2O^+$: 293.0921; Found 293.0914.

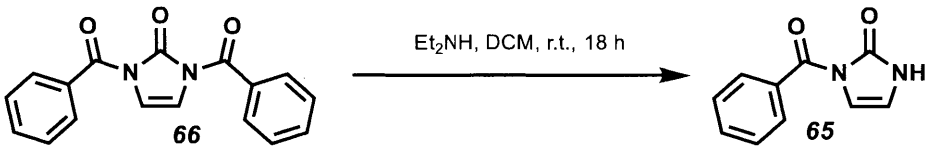

1-benzoyl-1,3-dihydro-2H-imidazol-2-one (65): To a solution of **66** (10 g, 34.21 mmol) in 171 mL of DCM at rt, diethylamine (2.5 g, 3.54 mL, 34.21 mmol) was added dropwise and stirred overnight. The reaction was quenched with 100 mL DI water and extracted twice with 100 mL DCM. The combined organics were washed with 100 mL brine. The organic layer was dried over Na_2SO_4, concentrated under reduced pressure, and purified via column chromatography with 50% EtOAc in Hexanes to give **65** (4.46 g, 23.70 mmol) as a white solid.

^{1}H NMR (500 MHz, Chloroform-*d*) δ 10.16 (s, 1H), 7.77 (d, J = 7.4 Hz, 2H), 7.57 (t, J = 7.4 Hz, 1H), 7.45 (t, J = 7.7 Hz, 2H), 6.74 (d, J = 5.1 Hz, 1H), 6.27 (d, J = 2.4 Hz, 1H).

^{13}C NMR (126 MHz, Chloroform-*d*) δ 167.49, 153.33, 133.00, 132.68, 130.04, 129.77, 128.46, 128.42, 128.24, 112.06, 109.77, 77.46, 77.20, 76.95.

HRMS (ESI, *m/z*) $[M+H]^+$ Calculated for $C_{10}H_9N_2O_2^+$: 189.0659; found 189.0657.

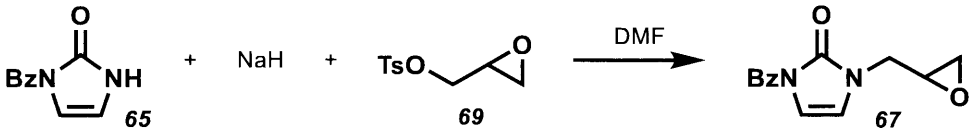

1-benzoyl-3-(oxiran-2-ylmethyl)-1,3-dihydro-2H-imidazol-2-one (67): To a solution of NaH (153.03 mg, 95% pure) in 20 mL of DMF at 0 °C, **65** (1 g, 5.31 mmol) in 3.5 mL of DMF was added slowly. The reaction was stirred for 1.5 h or until bubbling ceased. **69** (1.46 g, 6.38 mmol) in 3.5 mL of DMF was then added at 0 °C and reaction was stirred overnight at rt. The reaction was quenched with 50 mL 5% LiCl aqueous solution, and extracted three times with 30 mL of EtOAc. The combined organics were washed twice with 50 mL brine and dried over Na_2SO_4. The crude mixture was concentrated under reduced pressure and purified via column chromatography with 25% - 50% EtoAc in hexanes to give **67** (656 mg, 41% yield) as a vicious, clear oil.

^{1}H NMR (500 MHz, Chloroform-*d*) δ 7.74 (d, J = 7.5 Hz, 2H), 7.56 (t, J = 7.4 Hz, 1H), 7.44 (t, J = 7.7 Hz, 1H), 6.92 (d, J = 3.4 Hz, 1H), 6.47 (d, J = 3.3 Hz, 1H), 4.06 (dd, J = 15.0, 2.8 Hz, 1H), 3.43 (dd, J = 14.9, 6.3 Hz, 1H), 3.18 (m, 1H), 2.82 (t, J = 4.3 Hz, 1H), 2.57 (dd, J = 4.6, 2.6 Hz, 1H).

^{13}C NMR (126 MHz, Chloroform-*d*) δ 167.48, 151.07, 132.87, 132.59, 129.79, 129.59, 128.04, 115.06, 108.48, 77.42, 77.17, 76.91, 50.16, 45.02, 44.98.

HRMS (ESI, *m/z*) $[M+Na]^+$ Calculated for $C_{13}H_{12}N_2NaO_3^+$: 267.0740; Found 267.0736.

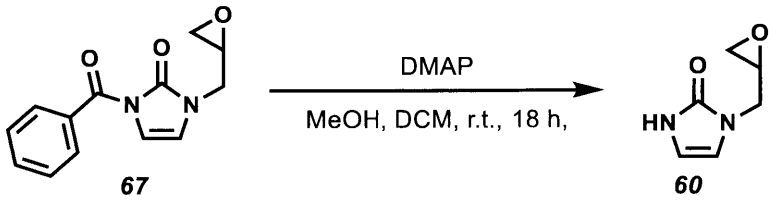

67 ***60***

1-(oxiran-2-ylmethyl)-1,3-dihydro-2H-imidazol-2-one (60): To a solution of **67** (200 mg, 0.818 mmol) in 4 mL DCM, DMAP (50 mg, 0.409 mmol) in 4 mL MeOH was added dropwise and stirred overnight. The reaction was concentrated under reduced pressure and purified with column chromatography with 10% MeOH in DCM to give **60** (72 mg, 0.52 mmol, 64% yield) as a viscous, clear oil.

^{1}H NMR (500 MHz, Chloroform-d) δ 10.43 (broad, 1 H), 6.29 (t, J = 2.3 Hz, 2H), 4.06 (dd, J = 14.9, 2.8 Hz, 1H), 3.58 (dd, J = 15.0, 5.8 Hz, 1H), 3.19 (dq, J = 6.2, 2.9 Hz, 1H), 2.81 (t, J = 4.3 Hz, 1H), 2.55 (dd, J = 4.7, 2.6 Hz, 1H).

^{13}C NMR (126 MHz, Chloroform-*d*) δ 154.75, 112.23, 108.48, 50.60, 44.89, 44.43.

^{1}H NMR (500 MHz, Methanol-*d*$_4$) δ 6.44 (d, J = 3.0 Hz, 1H), 6.37 (d, J = 3.0 Hz, 1H), 3.96 (dd, J = 14.9, 3.3 Hz, 1H), 3.57 (dd, J = 14.9, 5.8 Hz, 1H), 3.15 (td, J = 6.0, 2.9 Hz, 1H), 2.77 (t, J = 4.4 Hz, 1H), 2.53 (dd, J = 4.8, 2.5 Hz, 1H).

^{13}C NMR (126 MHz, Methanol-*d*$_4$) δ 154.20, 112.61, 108.08, 49.88, 44.32, 44.25.

Section 1.3.7 – Experimental Information

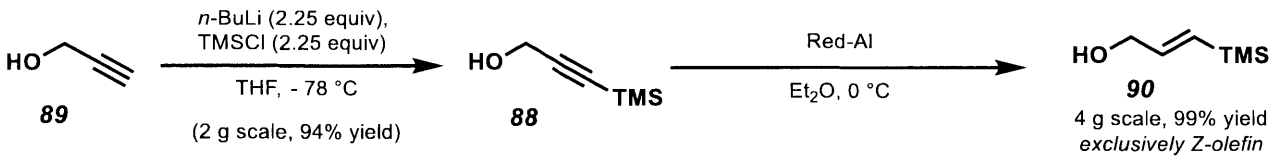

3-(trimethylsilyl)prop-2-yn-1-ol (88): Synthesized according to literature procedure.[3] To a solution of **91** (2.00 g, 2.06 mL, 35.7 mmol) in THF (71.0 mL) at -78 °C was added *n*-BuLi (5.14 g, 21.1 mL, 2.5 M solution, 80.3 mmol) dropwise. After addition was complete, the reaction was allowed to slowly warm to rt and stirred for 1.5 h. The reaction was then cooled back down to -78 °C and TMSCl (8.72 g, 10.2 mL, 80.3 mmol) was added dropwise. After addition was complete, the reaction was allowed to slowly warm to rt and stirred overnight. The reaction was quenched with 100 mL of 1 M HCl solution and diluted with 100 mL Et_2O. The layers were separated and the aqueous layer was extracted 3 more times with 100 mL Et_2O. The combined organics were washed with 300 mL brine and dried over Na_2SO_4. The resultant crude mixture was concentrated under reduced pressure and purified via column chromatography to give **89** (4.3 g, 33.5 mmol, 94% yield) as a pale yellow oil. Spectral data are in agreement with literature.[3]

(E)-3-(trimethylsilyl)prop-2-en-1-ol (90): Synthesized according to literature procedure.[4] To a solution of **88** (4.00 g, 4.57 mL, 31.2 mmol) in Et_2O (62.4 mL) at 0 °C was added Red-Al (10.61 g, 20.3 mL, 3.07 M, 62.4 mmol). The reaction was allowed to

[3] Langille, N. F.; Jamison, T. F. trans-Hydroalumination/Alkylation: One-Pot Synthesis of Trisubstituted Allylic Alcohols *Org. Lett.* **2006**, *17*, 3761.

[4] A) Arai, S.; Hori, H.; Amako, Y. Nishida, A. A new protocol for nickel-catalysed regio- and stereoselective hydrocyanation of allenes. *Chem. Comm.* **2015**, *51*, 7493. B) Kacprzynski, M. A.; Kazane, S. A.; May, T. L.; Hoveyda, A. H. Cu-catalyzed asymmetric conjugate additions of dialkyl- and diarylzinc reagents to acyclic β-silyl-α,β-unsaturated ketones. Synthesis of allylsilanes in high diastereo- and enantiomeric purity. *Org. Lett.* **2007**, *9*, 3187.

warm to rt and stirred for 6 h. The reaction was quenched with 4 mL H_2O and 8 mL H_2SO_4 (3.6 M) at 0 °C. The reaction was diluted with 100 mL Et_2O and 100 mL H_2O. The layers were separated and the aqueous layer was extracted 3 more times with 100 mL Et_2O. The combined organic layer was washed with 300 mL brine and dried over Na_2SO_4. The crude mixture was concentrated under reduced pressure to give **90** (4.05 g, 31.2 mmol, 99% yield) as a pale yellow oil and used without further purification. Spectral data are in agreement with literature.[4]

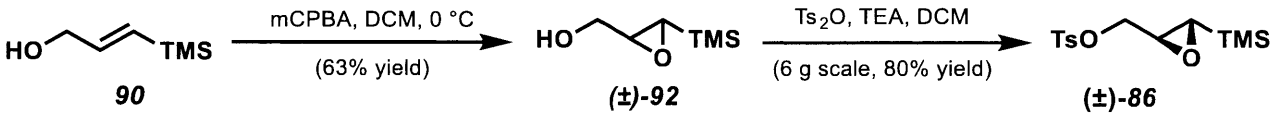

90 ***(±)-92*** ***(±)-86***

***(trans*-3-(trimethylsilyl)oxiran-2-yl)methanol (92):** To a solution of (±)-**92** (2 g, 15.35 mmol) in 61 mL DCM at 0 °C, *m*CPBA (3.18 g, <77% wt) was added slowly. The reaction was allowed to warm to rt and stirred overnight. The reaction cooled down to 0 °C and quenched slowly with 20 mL of sat. $Na_2S_2O_8$ solution and allowed to stir for 30 min. 40 mL sat. $NaHCO_3$ was added and the aqueous layer was extracted three times with 40 mL of DCM. The combined organics were washed twice with 50 mL sat. $NaHCO_3$, dried over Na_2SO_4, and concentrated under reduced pressure. The crude was purified by column chromatography with 50-80% EtOAc in hexanes to give (±)-**92** (1.41 g, 9.64 mmol, (63% yield) as a clear, viscous oil.

^{1}H NMR (500 MHz, Chloroform-*d*) δ 3.91 (dd, J = 12.4, 2.4 Hz, 1H), 3.48 (dd, J = 12.7, 5.1 Hz, 1H), 2.97 (m, 1H), 2.20 (d, J = 3.6 Hz, 1H), 0.01 (s, 9H).

^{13}C NMR (126 MHz, Chloroform-*d*) δ 63.51, 56.14, 48.39, -3.60.

HRMS (ESI, *m/z*) $[M+H]^+$ Calculated for $C_6H_{15}O_2Si^+$: 147.0836; Found 147.0815.

(*trans* 3-(trimethylsilyl)oxiran-2-yl)methyl 4-methylbenzenesulfonate ((±)-86): To a solution of Ts_2O (278.9 mg, 0.854 mmol) in DCM (3.4 mL), (±)-**92** (100 mg, 0.683 mmol) in 3.4 mL DCM was added at 0 °C. Et_3N (86.5 mg, 0.119 mL, 0.854 mmol) mas added dropwise at °C and the reaction was allowed to warm to rt and stirred overnight. The reaction was then quenched with 7 mL sat. $NaHCO_3$ and extracted twice with 7 mL DCM. The combined organics was washed with 14 mL brine, dried over Na_2SO_4, and concentrated under reduced pressure. The crude was purified with column chromatography to give (±)-**86** (166 mg, 0.552 mmol, 81% yield) as an off-white semi-solid.

^{1}H NMR (500 MHz, Chloroform-*d*) δ 7.79 (d, J = 7.8 Hz, 2H), 7.34 (d, J = 8.0 Hz, 2H), 4.26 (dd, J = 11.2, 3.3 Hz, 1H), 3.89 (dd, J = 10.9, 6.3 Hz, 1H), 3.03 (dd, J = 6.3, 3.3 Hz, 1H), 2.43 (s, 3H), 2.04 (d, J = 4.0 Hz, 1H), 0.03 (d, J = 1.1 Hz, 9H).

^{13}C NMR (126 MHz, Chloroform-*d*) δ 145.10, 132.90, 129.99, 128.06, 72.37, 52.53, 49.08, 21.75, -3.69.

HRMS (ESI, *m/z*) $[M+H]^+$ Calculated for $C_{13}H_{21}O_4SSi^+$: 301.0924; Found 301.0919.

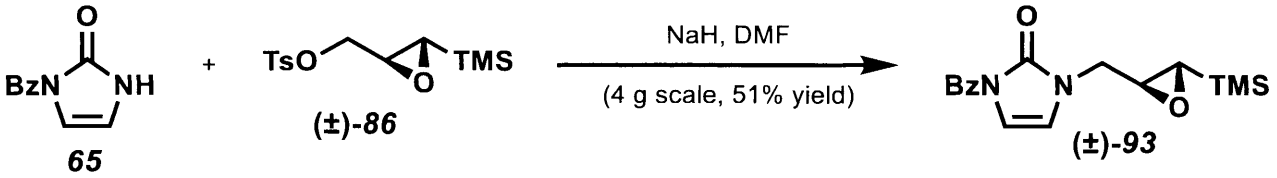

1-benzoyl-3-(*trans*-(3-(trimethylsilyl)oxiran-2-yl)methyl)-1,3-dihydro-2H-imidazol-2-one((±)-93): Procedure was performed according to synthesis of **67**. To a solution of NaH (561 mg, 95% pure) in 56 mL of DMF at 0 °C, **65** (4 g, 21.3 mmol) in 25 mL of

DMF was added slowly. After addition was complete, the reaction was stirred for 1.5 h or until bubbling ceased. (±)-**86** (7.02 g, 6.38 mmol) in 25 mL of DMF was then added at 0 °C and reaction was stirred overnight at rt. The reaction was quenched with 200 mL 5% LiCl aqueous solution, and extracted three times with 100 mL of EtOAc. The combined organics were washed twice with 200 mL brine and dried over Na_2SO_4. The crude mixture was concentrated under reduced pressure and purified via column chromatography with 25% - 50% EtOAc in hexanes to give **(±)-93** (3.42 g, 10.8 mmol, 51% yield) as a viscous, clear oil.

^{1}H NMR (500 MHz, Chloroform-*d*) δ 7.75 (d, J = 7.5 Hz, 2H), 7.56 (t, J = 14.2 Hz, 7.5 Hz, 1H), 7.45 (t, J = 16 Hz, 7.8 Hz, 2H), 6.92 (d, J = 3.3 Hz, 1H), 6.49 (d, J = 3.2 Hz, 1H), 4.19 (dd, J = 14.6, 2.5 Hz, 1H), 3.27 (dd, J = 14.6, 6.9 Hz, 1H), 3.02 (dt, J = 6.2, 3.0 Hz, 1H), 2.09 (d, J = 3.6 Hz, 1H), 0.05 (s, 9H)

^{13}C NMR (126 MHz, Chloroform-*d*) δ 167.53, 151.01, 132.82, 132.66, 129.58, 128.02, 115.07, 108.45, 54.04, 49.41, 46.74, -3.62.

HMBC, HSQC (See Spectral Data Section)

HRMS (ESI, *m/z*) $[M+H]^+$ Calculated for $C_{16}H_{21}N_2O_3Si^+$: 317.1316; Found 317.1312.

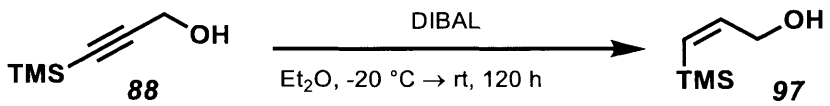

(Z)-3-(trimethylsilyl)prop-2-en-1-ol (97): To a solution of **88** (4.25 g, 4.91 mL, 33.14 mmol) in 66 mL Et_2O, DIBAL (1 M in hexanes, 14.14 g, 99.42 mL, 99.42 mmol) was added dropwise at 0 °C, allowed to warm rt, and stirred for 120 h. The reaction was cooled down to 0 °C and quenched with 5 mL MeOH. 50 mL of sat. Rochelle's salt was

added and stirred for 30 min, and extracted twice with 40 mL Et_2O. The combined organics were washed with 60 mL brine, dried over Na_2SO_4, and concentrated under reduced pressure. Purification by chromatography provided **97** (3.53 g, 27.06 mmol, 82% yield) as a clear oil, in 33:1 *Z*:*E* ratio.

^{1}H NMR (600 MHz, Chloroform-*d*) δ 6.47 (dt, J = 14.3, 6.4 Hz, 1H), 5.74 (dt, J = 14.3, 1.3 Hz, 1H), 4.23 (ddd, J = 6.7, 5.7, 1.3 Hz, 2H), 0.15 (s, 9H).

^{13}C NMR (151 MHz, Chloroform-*d*) δ 146.33, 132.47, 63.25, -1.76.

HRMS (DART, *m/z*) $[M-H]^-$ Calculated for $C_6H_{13}OSi^-$: 129.0741; Found 129.0738.

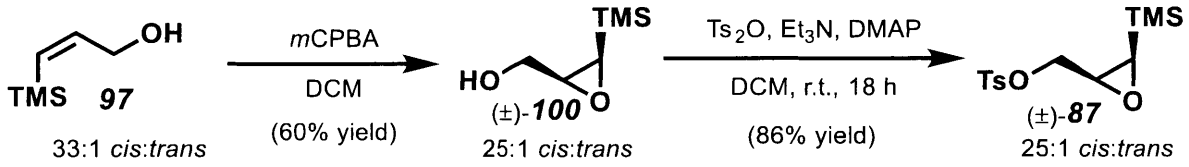

(±)-(*cis*-3-(trimethylsilyl)oxiran-2-yl)methanol (100): Procedure was performed similarly to the synthesis of(±)-**92**. Purified *m*CPBA (see below) was prepared using a modified literature procedure.[5] To a solution of **97** (1.00 g, 7.68 mmol) in 38.4 mL DCM at 0 °C, *m*CPBA (1.66 g) was added slowly. The reaction was allowed to warm to rt and stirred overnight. The reaction cooled down to 0 °C and quenched slowly with 25 mL of sat. $Na_2S_2O_8$ solution and allowed to stir for 30 min. 25 mL sat. $NaHCO_3$ was added and the aqueous layer was extracted three times with 40 mL of DCM. The combined organics were washed twice with 70 mL sat. $NaHCO_3$, dried over Na_2SO_4, and concentrated under reduced pressure. The crude was purified by column

[5] Horn, A.; Kazmaier, U. Purified *m*CPBA, a useful reagent for the oxidation of aldehydes. *Eur. J. Org. Chem.* **2018**, *20*, 2531.

chromatography with 50-80% EtOAc in hexanes to give (±)-**100** (0.676 g, 4.58 mmol, 63% yield) as a clear oil.

***m*CPBA purification:** In a 1 L volumetric flask, NaOH (0.1 N, 410 mL) and KH_2PO_4 (0.2 M, 250 mL) was mixed. The flask was filled up to 1 L with distilled water and the pH was adjusted to give 7.5 pH buffer solution. Commercial *m*CPBA (<77% wt, 15 g) was dissolved in 200 mL Et_2O and washed four times with 200 mL 7.5 pH buffer solution and once with 200 mL saturated $KHCO_3$. The organic layer was dried over Na_2SO_4 and the solvent was *carefully and gently* removed under reduced pressure to give *m*CPBA (10.2, 97% purity) as a dry, white solid. The peracid was stored under argon at 4 °C.

^{1}H NMR (500 MHz, Chloroform-*d*) δ 3.86 (ddd, *J* = 12.1, 7.6, 3.0 Hz, 1H), 3.49 (ddd, *J* = 12.0, 7.2, 4.5 Hz, 1H), 3.35 (ddd, *J* = 7.6, 5.3, 3.0 Hz, 1H), 2.31 (d, *J* = 5.4 Hz, 1H), 0.12 (s, 9H).

^{13}C NMR (126 MHz, Chloroform-*d*) δ 63.65, 57.77, 49.95, -1.63.

HRMS (ESI, *m/z*) $[M+H]^+$ Calculated for $NaC_6H_{14}O_2Si^+$: 169.0655; Found 169.0656.

(±)-(*cis*-3-(trimethylsilyl)oxiran-2-yl)methyl 4-methylbenzenesulfonate (87): Procedure was performed similarly to the synthesis of **86**. To a solution of Ts_2O (368 mg, 1.13 mmol), DMAP (12.5 mg, 0.103 mmol), and Et_3N (114 mg, 0.160 mL, 1.13 mmol) in DCM (3.00 mL), (±)-**100** (150.0 mg, 1.03 mmol) in 3.00 mL DCM was added at 0 °C. Et_3N (86.5 mg, 0.119 mL, 0.854 mmol) mas added dropwise at °C and the reaction was allowed to warm to rt and stirred overnight. The reaction was then quenched with 5 mL sat. $NaHCO_3$ and extracted twice with 5 mL DCM. The combined organics were washed with 10 mL brine, dried over Na_2SO_4, and concentrated under

reduced pressure. The crude was purified with column chromatography to give (±)-**87** (265 mg, 0.882 mmol, 86% yield) as an off-white semi-solid.

^{1}H NMR (500 MHz, Chloroform-*d*) δ 7.80 (d, J = 8.4 Hz, 2H), 7.35 (d, J = 8.1 Hz, 2H), 4.21 (dd, J = 11.0, 3.8 Hz, 1H), 3.90 (dd, J = 11.1, 7.3 Hz, 1H), 3.35 (ddd, J = 7.3, 5.3, 3.7 Hz, 1H), 2.44 (s, 3H) 2.26 (d, J = 5.3 Hz, 1H), 0.06 (s, 9H).

^{13}C NMR (126 MHz, Chloroform-*d*) δ 145.18, 132.83, 130.00, 128.12, 70.75, 49.56, 21.76, -1.92.

HRMS (ESI, *m/z*) $[M+H]^+$ Calculated for $C_{13}H_{21}O_4SSi^+$: 301.0924; Found 301.0919.

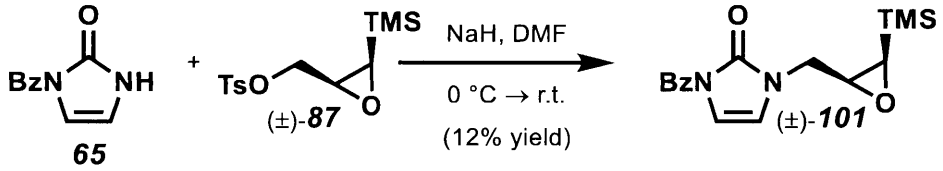

1-benzoyl-3-((cis-3-(trimethylsilyl)oxiran-2-yl)methyl)-1,3-dihydro-2H-imidazol-2-one (101): Procedure was performed according to synthesis of **67**. To a solution of NaH (14.0 mg, 0.583 mmol, 95% pure) in 1.70 mL of DMF at 0 °C, **65** (100.0 mg, 0.531 mmol) in 1.00 mL of DMF was added slowly. After addition was complete, the reaction was stirred for 1.5 h or until bubbling ceased. (±)-**87** (175.6 g, 0.584 mmol) in 1 mL of DMF was then added at 0 °C and reaction was stirred overnight at rt. The reaction was quenched with 10 mL 5% LiCl aqueous solution, and extracted three times with 8 mL of EtOAc. The combined organics were washed twice with 20 mL brine and dried over Na_2SO_4. The crude mixture was concentrated under reduced pressure and purified via column chromatography with 25% - 50% EtoAc in hexanes to give (±)-**101** (19.9 mg, 0.063 mmol, 12% yield) as a viscous, clear oil.

^{1}H NMR (500 MHz, Chloroform-d) δ 7.76 (dd, J = 8.3, 1.3 Hz, 2H), 7.64 – 7.52 (m, 1H), 7.45 (t, J = 7.8 Hz, 2H), 6.95 (d, J = 3.4 Hz, 1H), 6.55 (d, J = 3.4 Hz, 1H), 4.30 (dd, J = 14.5, 2.0 Hz, 1H), 3.33 (ddd, J = 9.0, 5.3, 2.1 Hz, 1H), 3.02 (dd, J = 14.5, 9.1 Hz, 1H), 2.33 (d, J = 5.3 Hz, 1H), 0.17 (s, 9H).

^{13}C NMR (126 MHz, Chloroform-d) δ 167.55, 151.00, 132.86, 132.66, 129.61, 128.04, 114.56, 108.69, 77.37, 77.11, 76.86, 55.63, 49.48, 45.32, -1.66.

HRMS (ESI, *m/z*) [M+H]$^+$ Calculated for $C_{16}H_{21}N_2O_3Si^+$: 317.1316; Found 317.1316.

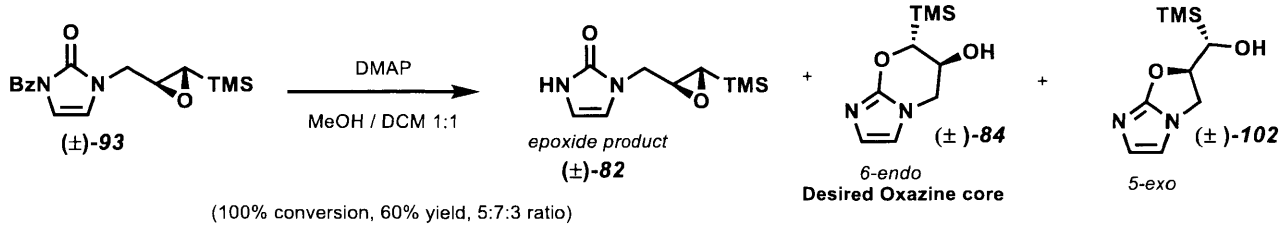

1-(*trans*-(3-(trimethylsilyl)oxiran-2-yl)methyl)-1,3-dihydro-2H-imidazol-2-one (82), 7-(trimethylsilyl)-6,7-dihydro-5H-imidazo[2,1-b][1,3]oxazin-6-ol (84), and (2,3-dihydroimidazo[2,1-b]oxazol-2-yl)(trimethylsilyl)methanol (102): The procedure was performed similarly to the synthesis of **60**. To a solution of **93** (344 mg, 1.09 mmol) in DCM (2.70 mL), DMAP (66.4 mg, 0.544 mmol) in MeOH (2.70 mL) was added and the reaction was stirred over night at rt. The reaction mixture was concentrated under reduced pressure and purified via column chromatography (5% to 10% MeOH in DCM) to give **84** (45.8 mg, 0.215 mmol, 19.8% yield) as a clear oil, **84** (64.4 mg, 0.303 mmol, 27.9% yield) as a white solid, and **102** (27.7 mg, 0.130 mmol, 12.0% yield) as a white solid.

1-(trans-(3-(trimethylsilyl)oxiran-2-yl)methyl)-1,3-dihydro-2H-imidazol-2-one (82) spectral data:

^{1}H NMR (500 MHz, Methanol-*d*$_4$) δ 6.44 (d, *J* = 2.9 Hz, 1H), 6.37 (d, *J* = 3.0 Hz, 1H), 3.99 (dd, *J* = 14.6, 3.2 Hz, 1H), 3.55 (dd, *J* = 14.7, 6.0 Hz, 1H), 3.03 (dt, *J* = 6.4, 3.4 Hz, 1H), 2.09 (d, *J* = 3.5 Hz, 1H), 0.03 (s, 9H).

^{13}C NMR (126 MHz, Methanol-*d*$_4$) δ 154.14, 112.63, 108.09, 53.91, 49.08, 45.74, -5.10.

HRMS (ESI, *m/z*) $[M+H]^+$ Calculated for $C_9H_{17}N_2O_2Si^+$: 213.1054; Found 213.1051.

7-(trimethylsilyl)-6,7-dihydro-5H-imidazo[2,1-b][1,3]oxazin-6-ol (84) spectra data:

^{1}H NMR (500 MHz, Methanol-*d*$_4$) δ 6.61 (d, *J* = 1.6 Hz, 1H), 6.54 (s, 1H), 4.25 (q, *J* = 5.3 Hz, 1H), 4.06 (dd, *J* = 5.5, 3.3 Hz, 2H), 3.80 (dd, *J* = 12.2, 5.4 Hz, 1H), 0.10 (s, 9H).

^{13}C NMR (126 MHz Methanol-*d*$_4$) δ 150.06, 122.27, 114.22, 77.23, 62.58, 53.51, 48.71, -4.79.

HMBC, HSQC, gCOSY (See Spectral Data Section)

HRMS (ESI, *m/z*) $[M+H]^+$ Calculated for $C_9H_{17}N_2O_2Si^+$: 213.1054; Found 213.1052.

(2,3-dihydroimidazo[2,1-b]oxazol-2-yl)(trimethylsilyl)methanol (102) spectral data

^{1}H NMR (500 MHz, Methanol-*d*$_4$) δ 6.44 (d, *J* = 3.3 Hz, 1H), 6.35 (d, *J* = 2.8 Hz, 1H), 3.89 – 3.79 (m, 2H), 3.70 (dd, *J* = 14.1, 6.5 Hz, 1H), 3.04 (d, *J* = 8.5 Hz, 1H), 0.07 (s, 9H).

^{13}C NMR (126 MHz, Methanol-*d*$_4$) δ 154.74, 130.74, 113.99, 107.52, 72.61, 65.73, -4.03.

HMBC, HSQC, gCOSY (See Spectral Data Section)

HRMS (ESI, *m/z*) $[M+H]^+$ Calculated for $C_9H_{17}N_2O_2Si^+$: 213.1054; Found 213.1052.

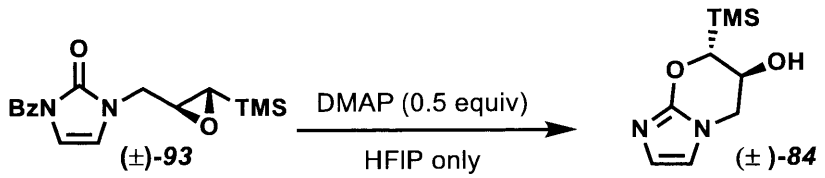

7-(trimethylsilyl)-6,7-dihydro-5H-imidazo[2,1-b][1,3]oxazin-6-ol (84): The procedure was performed similarly to the synthesis of **60**. A solution of **93** (500.0 mg, 1.58 mmol) and DMAP (96.5 mg, 0.790 mmol) in HFIP (8 mL) was prepared in a microwave vial opened to air. The reaction mixture was microwaved at 50 °C for 1 h under normal absorption. After completion of microwave, the reaction mixture was concentrated under reduced pressure and purified via column chromatography to give **84** (333 mg, 1.57 mmol, 99% yield) as a white solid. Spectral data are in agreement with previously synthesized **84**.

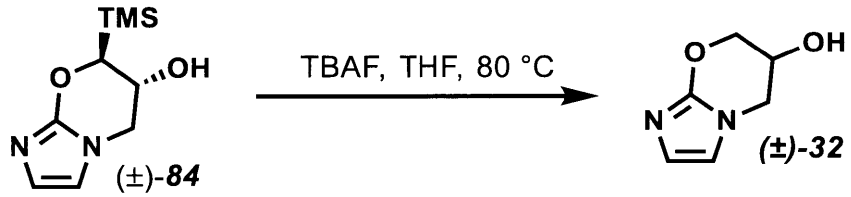

6,7-dihydro-5H-imidazo[2,1-b][1,3]oxazin-6-ol ((±)-32): To a solution of (±)-**84** (10 mg, 0.047 mmol) in 0.235 mL THF in a sealed microwave vial, TBAF (1 M in THF, 13.55 mg, 0.052 mmol) was added and microwaved at 80 °C for 1 h. The reaction was quenched with methanol (1 mL), concentrated, and purified with column chromatography to give (±)-**32** (3.3 mg, 0.015 mmol, 49% yield) as a white solid. Spectral data were in agreement with previously synthesized (±)-**32**.

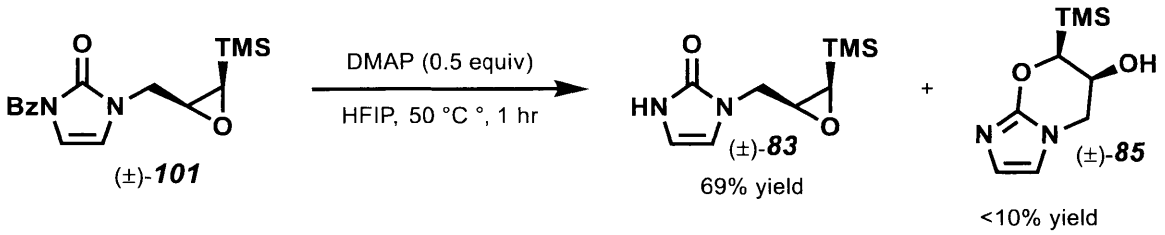

1-(*cis*-3-(trimethylsilyl)oxiran-2-yl)methyl)-1,3-dihydro-2H-imidazol-2-one (83): Procedure was performed similarly to the synthesis of (±)-**84**. A solution of **101** (40.0 mg, 0.126 mmol) and DMAP (7.72 mg, 0.063 mmol) in HFIP (0.630 mL) was prepared in a microwave vial opened to air. The reaction mixture was microwaved at 50 °C for 1 h under normal absorption. After completion of microwave, the reaction mixture was concentrated under reduced pressure and purified via column chromatography to give **83** (18.6 mg, 0.088 mmol, 69% yield) as a white solid.

^{1}H NMR (500 MHz, Chloroform-*d*) δ 9.30 (s, 1H), 6.40 (t, J = 2.5 Hz, 1H), 6.30 (t, J = 2.6 Hz, 1H), 4.35 (dd, J = 14.6, 2.1 Hz, 1H), 3.34 (ddd, J = 9.1, 5.3, 2.2 Hz, 1H), 3.09 (dd, J = 14.5, 8.8 Hz, 1H), 2.32 (d, J = 5.3 Hz, 1H), 0.18 (s, 9H).

^{13}C NMR (126 MHz, Chloroform-*d*) δ 154.28, 111.91, 108.20, 77.36, 77.10, 76.85, 56.18, 49.46, 45.00, -1.65.

gCOSY, HMBC (See Spectral Data Section)

HRMS (ESI, *m/z*) [M+H]$^+$ Calculated for $C_9H_{17}N_2O_2Si^+$: 213.1054; Found 213.1051.

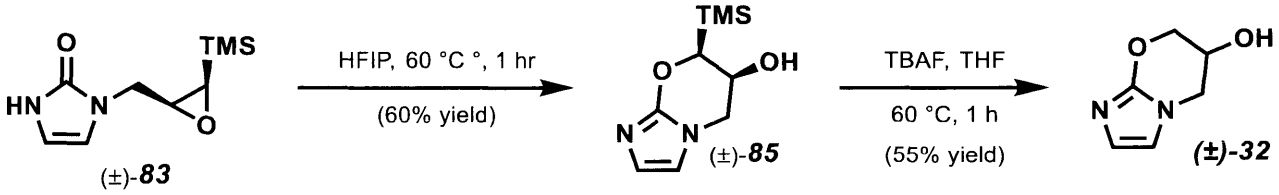

(±)-7-(trimethylsilyl)-6,7-dihydro-5H-imidazo[2,1-b][1,3]oxazin-6-ol (85): A solution of **83** (18.6 mg, 0.088 mmol) in HFIP (0.44 mL) was prepared in a microwave vial opened to air. The reaction mixture was microwaved at 50 °C for 1 h under normal absorption. After completion of microwave, the reaction mixture was concentrated under reduced pressure and purified via column chromatography to give **85** (11.2 mg, 0.053 mmol, 60% yield) as a white solid.

1H NMR (500 MHz, Chloroform-*d*) δ 6.44 (d, J = 1.8 Hz, 1H), 6.31 (d, J = 1.8 Hz, 1H), 4.22 (d, J = 4.0 Hz, 1H), 4.01 (dd, J = 12.4, 4.1 Hz, 1H), 3.97 – 3.87 (m, 2H), 0.25 (s, 9H).

13C NMR (126 MHz, Chloroform-*d* D) δ 150.14, 123.41, 114.20, 76.18, 63.40, 51.41, -2.95.

gCOSY, HMBC (See Spectral Data section)

HRMS (ESI, *m/z*) [M+H]$^+$ Calculated for $C_9H_{17}N_2O_2Si^+$: 213.1054; Found 213.1053.

6,7-dihydro-5H-imidazo[2,1-b][1,3]oxazin-6-ol ((±)-32): To a solution of 106 (3.0 mg, 0.014 mmol) in 0.071 mL THF in a sealed microwave vial, TBAF (1 M in THF, 3.69 mg, 0.014 mL, 0.014 mmol) was added and microwaved at 80 °C for 1 h. The reaction was quenched with methanol (1 mL), concentrated, and purified with column chromatography to give (±)-**32** (1.1 mg, 0.008 mmol, 55% yield) as a white solid. Spectral data are in agreement with previously synthesized(±)-**32**.

Section 1.3.9 – Experimental information

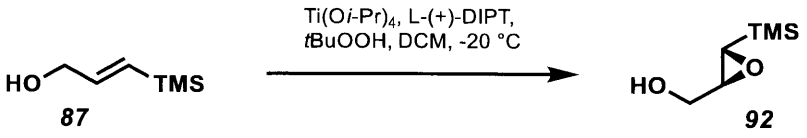

((2S,3S)-3-(trimethylsilyl)oxiran-2-yl)methanol (92): Synthesized according to a reported procedure.[6] To a solution of molecular sieves (**4** Å, 200 mg, 20% wt of alcohol) in DCM (2.2 mL) at -20°C, Ti(O*i*Pr)$_4$ (437 mg, 0.455 mL, 1.54 mmol) was added dropwise followed by L-(+)-DIPT (288 mg, 0.257 mL, 1.23 mmol) and **87** (1.00 g, 1.18 mL, 7.68 mmol). The reaction was stirred for 30 min and *t*BuOOH (1.38 g, 3.07 mL, 15.4 mmol) was added dropwise. The reaction was stirred for 4 days at -20 °C and then poured over a mixture of $FeSO_4 \cdot 7H_2O$ (2.5 g), tartaric acid (50 mg), 20 mL H_2O, and 20 mL Et_2O at 0 °C. The resultant mixture was stirred rigorously at °C and filtered through celite with Et_2O. The reaction mixture was diluted with 10 mL brine and extracted thrice with 20 mL Et_2O. The combined organics were dried over Na_2SO_4 and purified via column chromatography to give **92** (901 mg, 6.16 mmol, 80% yield) as a clear oil. Spectral data are in agreement with previously synthesized **92**.

HPLC Trace data: Obtained using Chiralcel OD-H column with a gradient of 1-30% IPA/Hexane, 230 nm.

*Racemate **92**:*

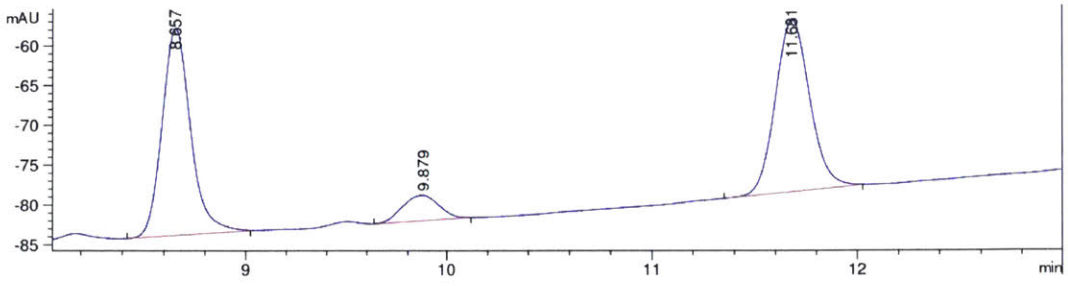

[6] Raubo, P.; Wicha, J. Synthesis of Optically Active 2,3-0-Isopropylidene-l-(trimethylsilyl)glyceraldehyde and Other Derivatives of (a-Hydroxyacyl)silane *J. Org. Chem.* **1995**, *59*, 4356.

#	[min]	Width [min]	Area [mAU*S]	Height [mAU]	Area %
1	8.657	0.1418	250.52213	26.01938	8.2970
2	11.681	0.1498	251.97198	21.64161	8.3450

*Product **92**:*

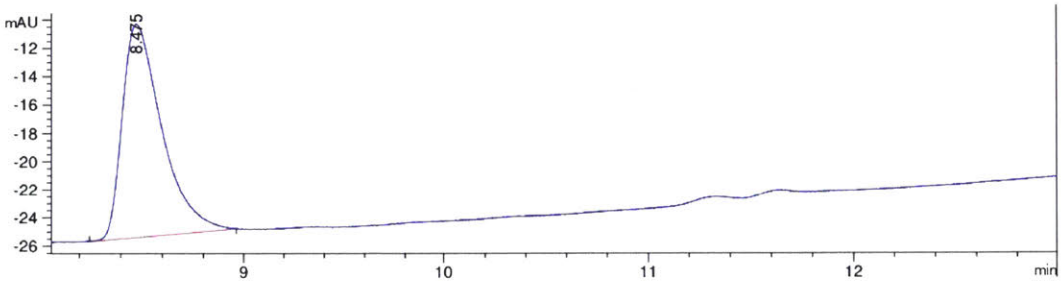

#	[min]	Width [min]	Area [mAU*S]	Height [mAU]	Area %
1	8.475	0.1596	200.87062	15.10533	60.2922
2	-	-	-	-	-

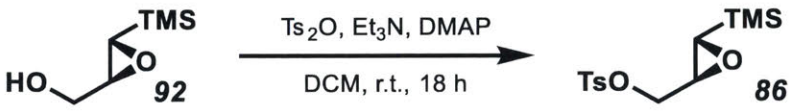

((2S,3S)-3-(trimethylsilyl)oxiran-2-yl)methyl 4-methylbenzenesulfonate (86):

Synthesized according to the synthesis of (±)-**86**. To a solution of Ts_2O (245 mg, 0.752 mmol) in DCM (3.4 mL), **92** (100 mg, 0.683 mmol) in 3.4 mL DCM was added at 0 °C. Et_3N (76.1 mg, 0.105 mL, 0.752 mmol) was added dropwise at °C and the reaction was allowed to warm to rt and stirred overnight. The reaction was then quenched with 7 mL sat. $NaHCO_3$ and extracted twice with 7 mL DCM. The combined organics was washed

with 14 mL brine, dried over Na_2SO_4, and concentrated under reduced pressure. The crude was purified with column chromatography to give **86** (123 mg, 0.409 mmol, 60% yield) as an off-white semi-solid. Spectral data are in agreement with previously synthesized (±)-**86**.

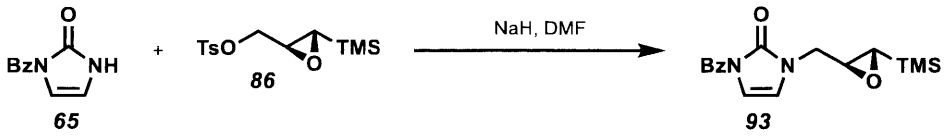

1-benzoyl-3-(((2S,3S)-3-(trimethylsilyl)oxiran-2-yl)methyl)-1,3-dihydro-2H-imidazol-2-one (93): Synthesized according to the synthesis of (±)-**93**. To a solution of NaH (9.82 mg, 95% pure) in 1.9 mL of DMF at 0 °C, **65** (70.0 g, 0.372 mmol) in 1 mL of DMF was added slowly. After addition was complete, the reaction was stirred for 1.5 h or until bubbling ceased. **86** (123 mg, .409 mmol) in 1 mL of DMF was then added at 0 °C and reaction was stirred overnight at rt. The reaction was quenched with 3 mL 5% LiCl aqueous solution, and extracted three times with 3 mL of EtOAc. The combined organics were washed twice with 5 mL brine and dried over Na_2SO_4. The crude mixture was concentrated under reduced pressure and purified via column chromatography with 25% - 50% EtoAc in hexanes to give **93** (48.7 mg, 0.153 mmol, 41% yield) as a viscous, clear oil. Spectral data are in agreement with previously synthesized (±)-**93**.

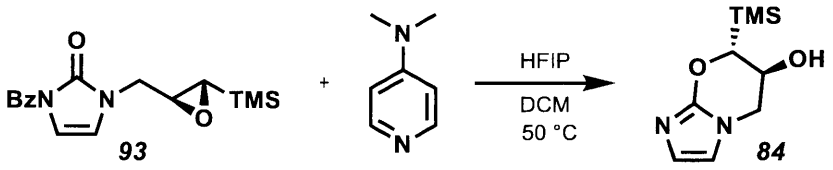

(6S,7R)-7-(trimethylsilyl)-6,7-dihydro-5H-imidazo[2,1-b][1,3]oxazin-6-ol (84): Synthesized according to the synthesis of (±)-**84**. A solution of **93** (48.7 mg, 0.153

mmol) and DMAP (9.4 mg, 0.077 mmol) in HFIP (0.38 mL) and DCM (0.38 mL) was prepared in a microwave vial opened to air. The reaction mixture was microwaved at 50 °C for 1 h under normal absorption. After completion of microwave, the reaction mixture was concentrated under reduced pressure and purified via column chromatography to give **84** (31.9 mg, 0.150 mmol, 98% yield) as a white solid. Spectral data are in agreement with previously synthesized (±)-**84**.

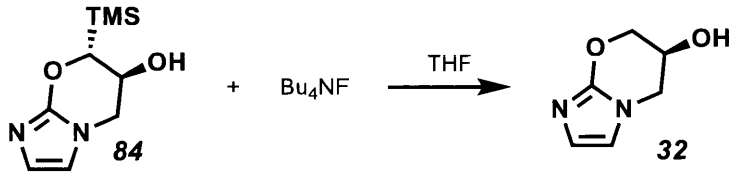

(S)-6,7-dihydro-5H-imidazo[2,1-b][1,3]oxazin-6-ol (32): Synthesized according to the synthesis of (±)-**32**. To a solution of **84** (31.9 mg, 0.150 mmol) in 0.750 mL THF in a sealed microwave vial, TBAF (1 M in THF, 39.3 mg, 0.150 mmol) was added and microwaved at 80 °C for 1 h. The reaction was quenched with methanol (0.5 mL), concentrated, and purified with column chromatography to give **32** (11.6 mg, 0.083 mmol, 55% yield) as a white solid. Spectral data were in agreement with previously synthesized (±)-**32**.

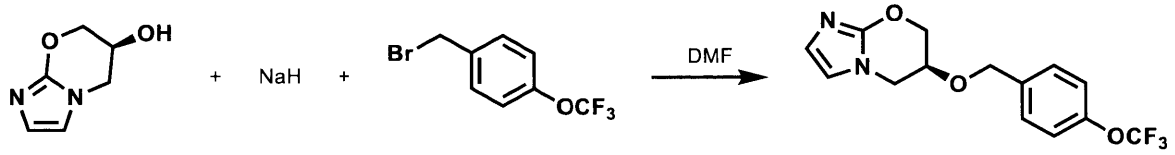

(S)-6-((4-(trifluoromethoxy)benzyl)oxy)-6,7-dihydro-5H-imidazo[2,1-b][1,3]oxazine (31): Synthesized according to the synthesis of (±)-**31**. To a solution of NaH (2.19 mg, 4.46 mmol, 95% pure) in DMF (0.200 mL) at 0 °C, **32** (11.6 mg, 0.083 mmol) in DMF (0.20 mL) was added dropwise. The reaction mixture was stirred for 1 h or until bubbling

ceased. **19** (0.23 mg, 0.038 mL, 0.091 mmol) was then added dropwise at 0 °C and the reaction was stirred for 5 h at rt. The reaction was quenched with 0.10 mL MeOH, diluted with 1 mL of sat. ammonium chloride, and extracted 4 times with 2 mL DCM. The combined organics were then washed with 4 mL brine, dried over Na_2SO_4, and concentrated. Crude was purified with column chromatography with 5% MeOH in DCM to give **31** (16.6 mg, 0.053 mmol, 64% yield) as a white solid. Spectral data were in agreement with previously synthesized (±)-**31**.

Pretomanid (9): Synthesized according to the synthesis of **(±)-9.** In a glovebox, tetrabutylammonium nitrate (13.9 mg, 0.046 mmol) was measured into a sealed microwave vial. The sealed vial was taken out and connected with an argon line. Nf_2O (26.5 mg, 14 μL, 0.046 mmol) in DCE (0.23 mL) was added slowly, and the reaction was stirred at rt for 1.5 h. **31** (14.3 mg, 0.046 mmol) in DCM (0.23 mL) was added slowly and the reaction was stirred overnight at rt. The mixture was quenched with 1 mL 5% $NaHCO_3$ and extracted three times with 2 mL DCM. The combined organics were dried over Na_2SO_4, and purified with column chromatography (5 to 10% methanol in DCM) to give **9** (8.3 mg, 0.023 mmol, 51% yield) as a white solid and **45** (1.2 mg, 0.003 mmol, 7.3% yield) as a white solid. Spectral data are in agreement with previously synthesized material. Analytical standard pretomanid (**9**): α_D^{20} = -36.4 (*c* = 1.00, MeOH); Found α_D^{20} = -35.6 (*c* = 1.00, MeOH).

Chapter One

Enantioselective Synthesis of Pretomanid –

Spectral Data

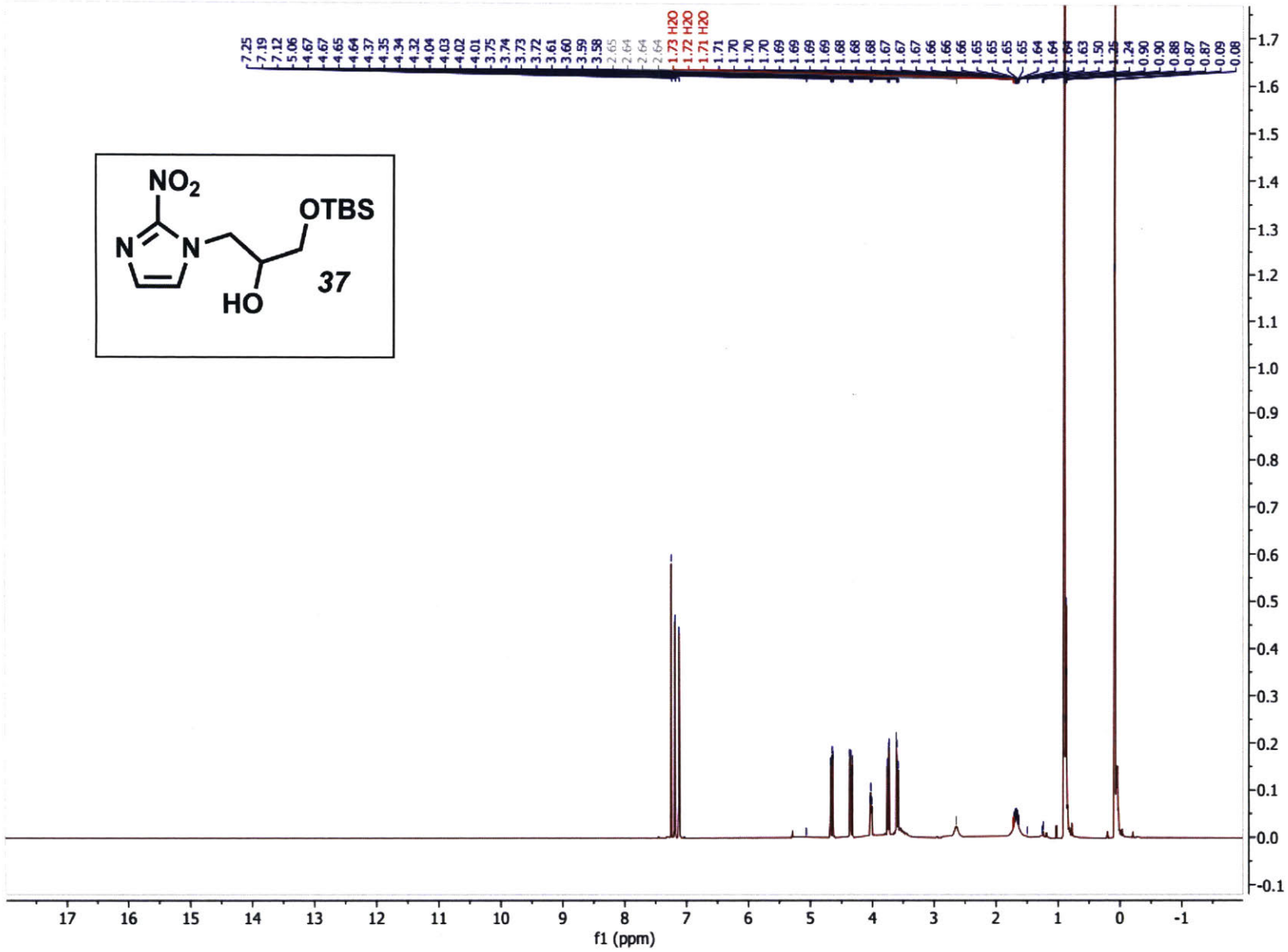
NO2
OTBS
N
N
HO
37
f1 (ppm)

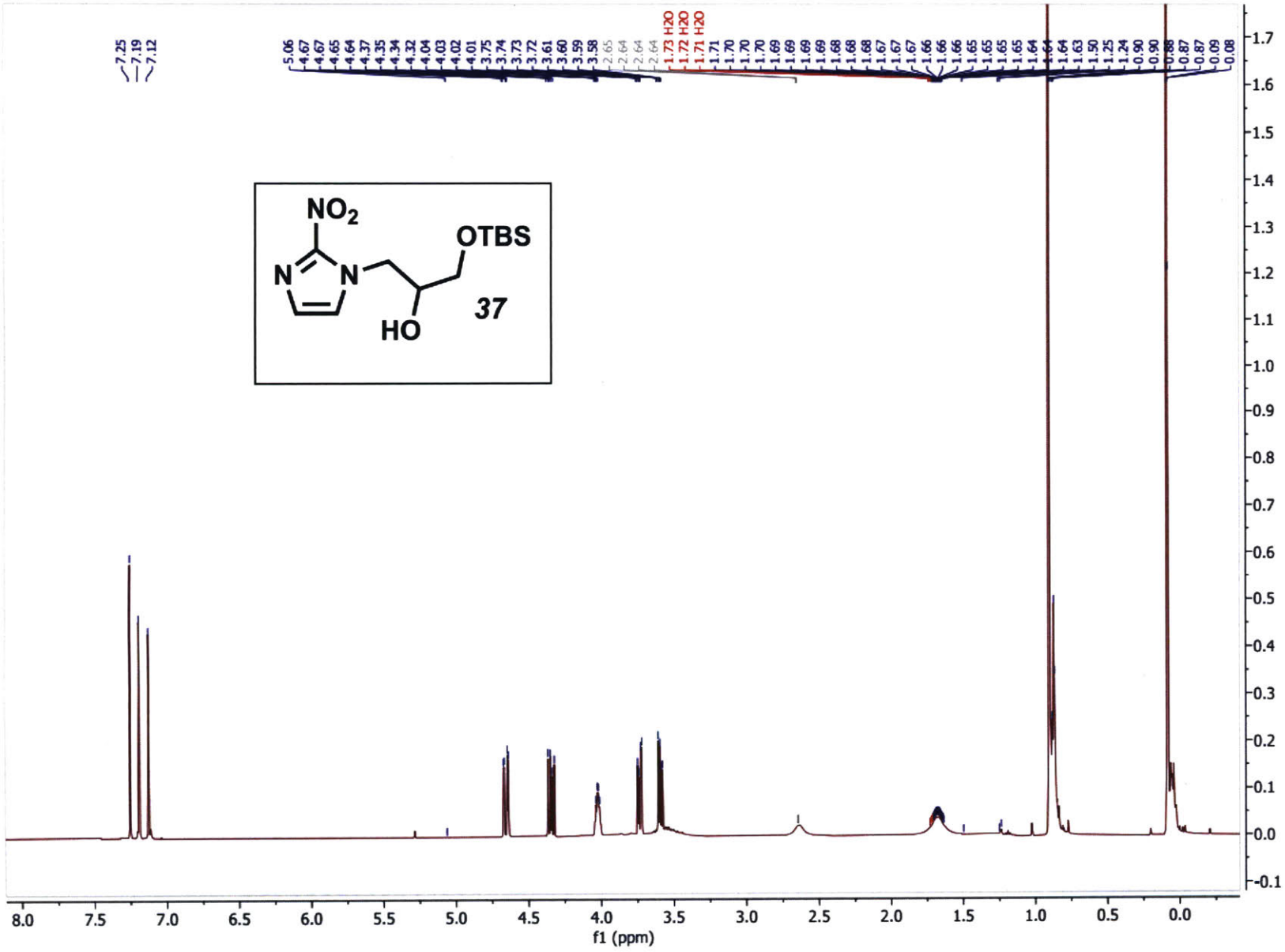
NO2
OTBS
N
N
HO
37
f1 (ppm)

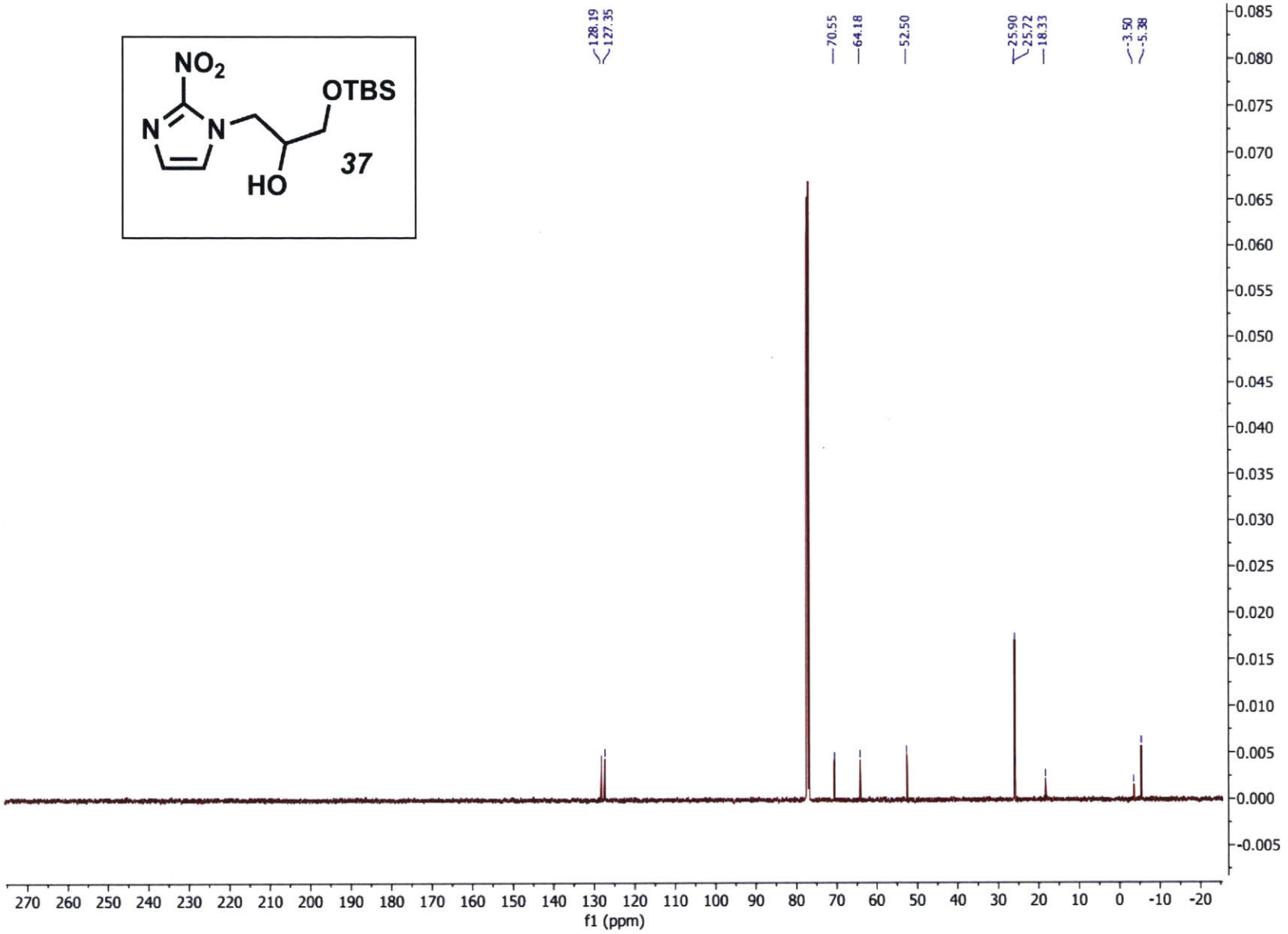
NO2
OTBS
N
N
HO
37
128.19
127.35
70.55
64.18
52.50
25.90
25.72
18.33
-3.50
-5.38
f1 (ppm)

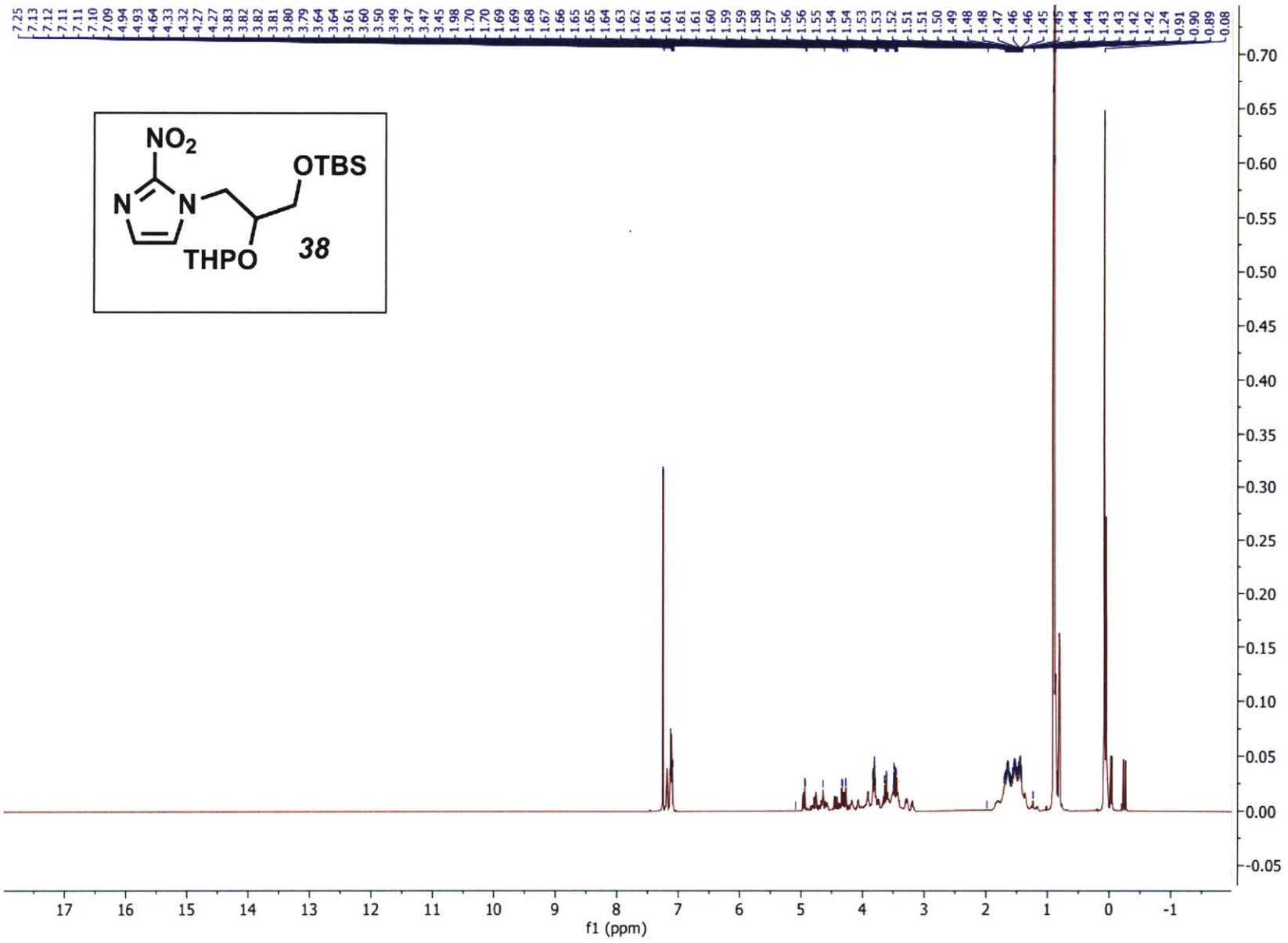
NO2
OTBS
N
N
THPO
38
f1 (ppm)

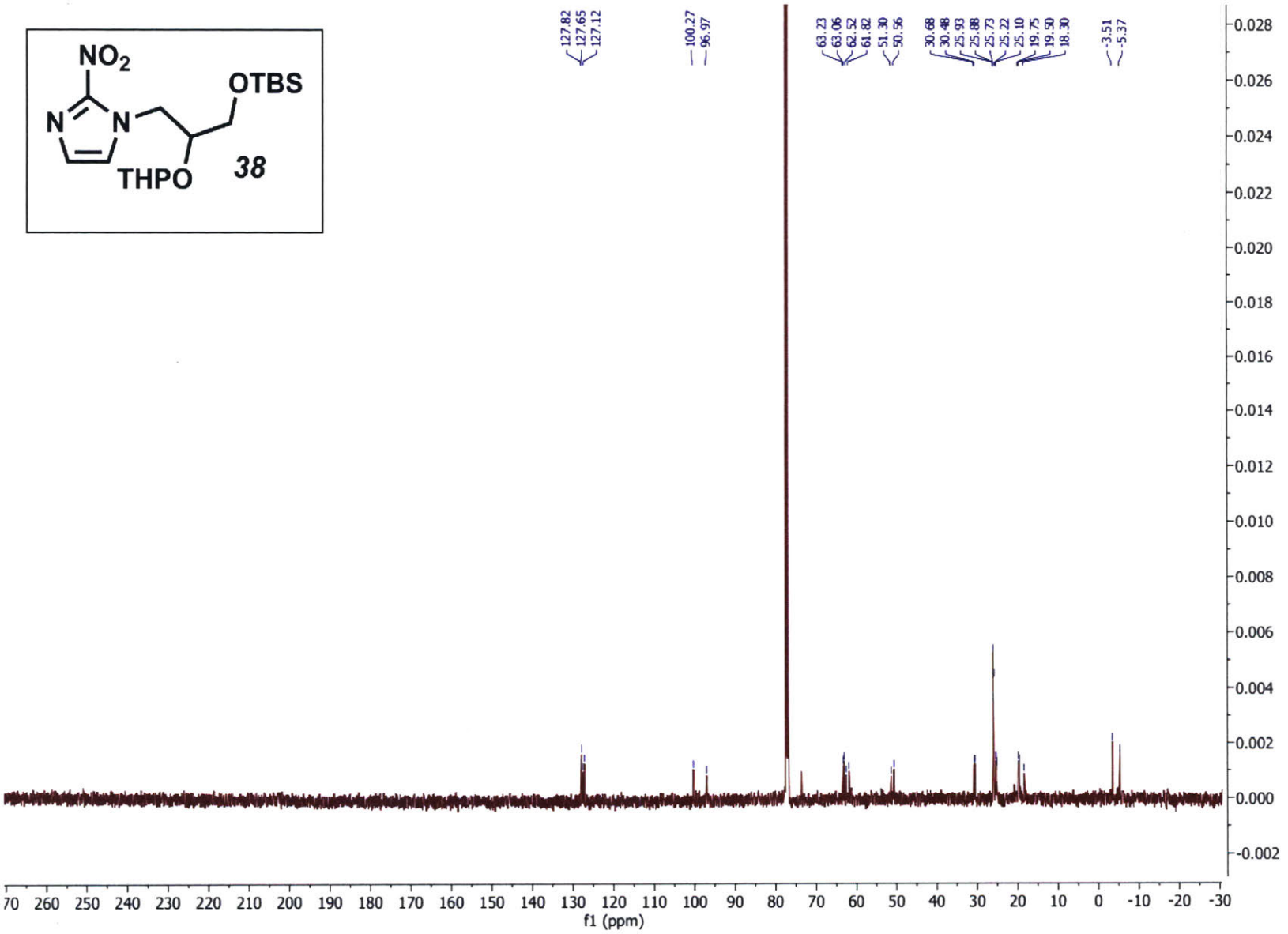
NO2
OTBS
N
N
THPO
38
127.82
127.65
127.12
100.27
96.97
63.23
63.06
62.52
61.82
51.30
50.96
30.68
30.48
25.93
25.88
25.73
25.22
25.10
19.75
19.50
18.30
-3.51
-5.37
f1 (ppm)

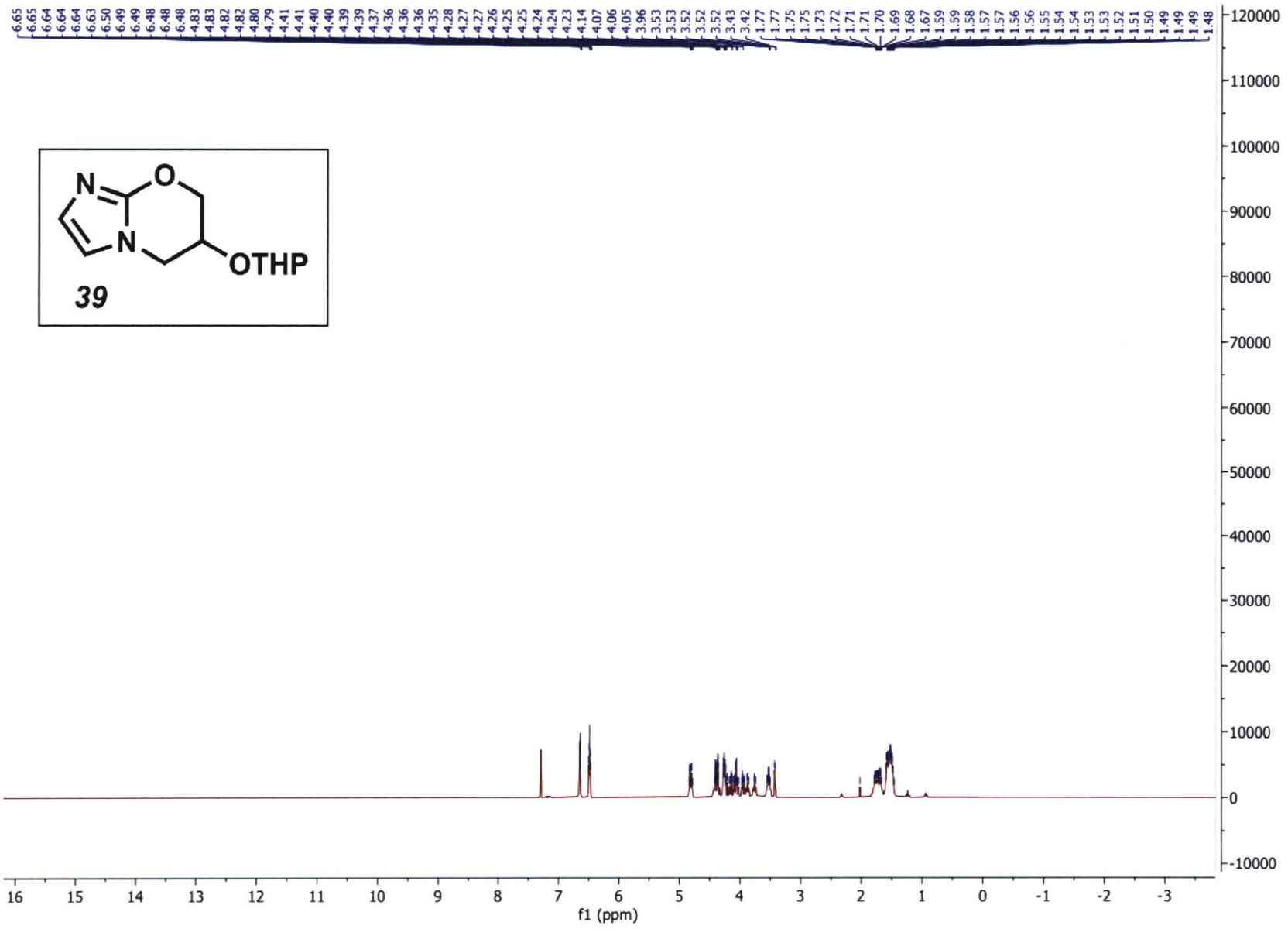
N
O
N
OTHP
39
f1 (ppm)

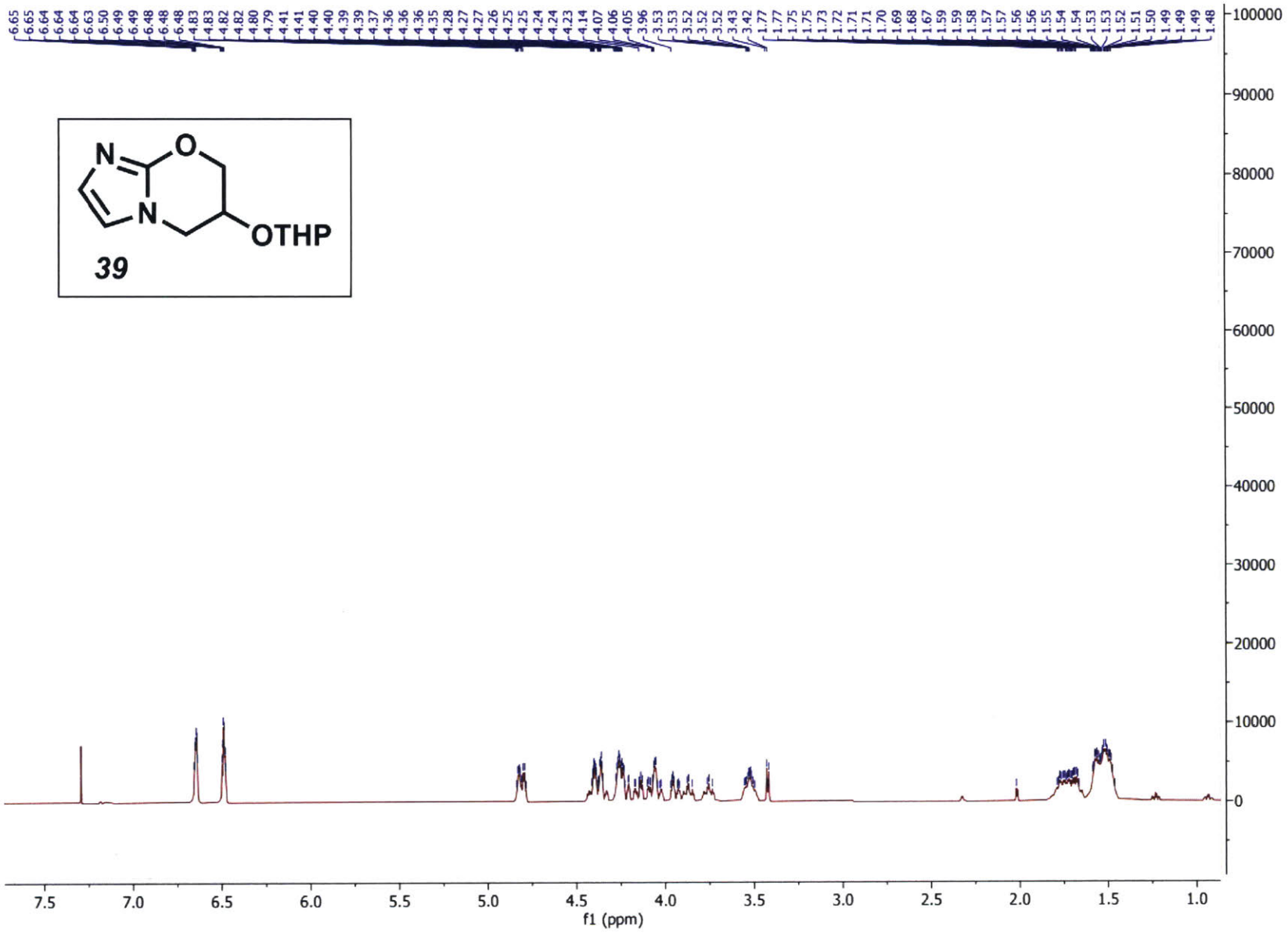
6.65 6.65 6.64 6.64 6.64 6.63 6.50 6.49 6.49 6.48 6.48 6.48 4.83 4.83 4.82 4.82 4.80 4.79 4.41 4.41 4.40 4.40 4.39 4.39 4.37 4.36 4.36 4.35 4.28 4.27 4.27 4.26 4.25 4.25 4.24 4.24 4.23 4.14 4.07 4.06 4.05 3.96 3.53 3.53 3.52 3.52 3.52 3.43 3.42 1.77 1.77 1.75 1.75 1.73 1.72 1.71 1.71 1.70 1.69 1.68 1.67 1.59 1.59 1.58 1.57 1.57 1.56 1.56 1.55 1.54 1.54 1.53 1.53 1.52 1.51 1.50 1.49 1.49 1.49 1.48
N
O
N
OTHP
39
100000
90000
80000
70000
60000
50000
40000
30000
20000
10000
0
7.5
7.0
6.5
6.0
5.5
5.0
4.5
4.0
3.5
3.0
2.5
2.0
1.5
1.0
f1 (ppm)

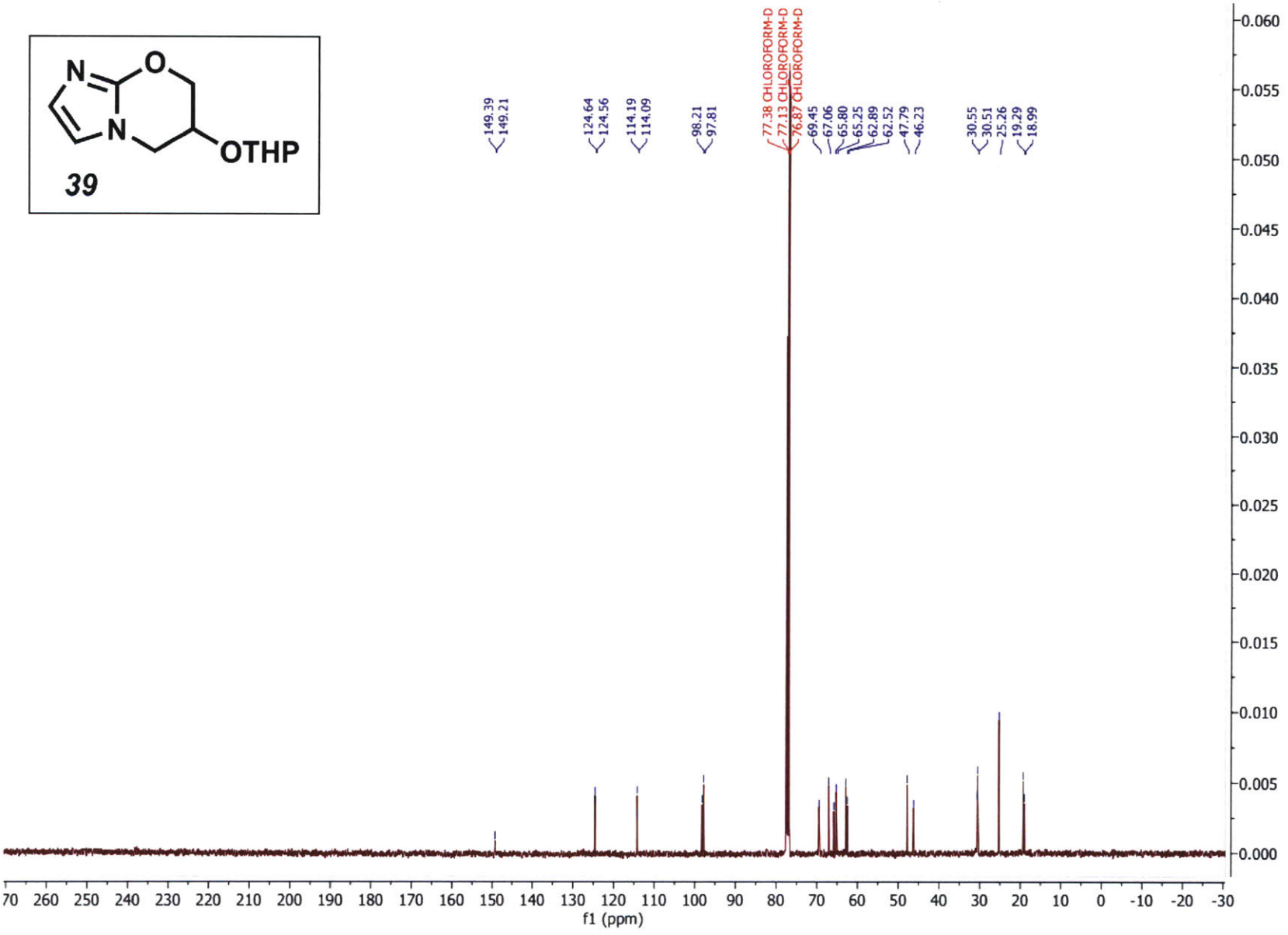
N
O
N
OTHP
39
149.39
149.21
124.64
124.56
114.19
114.09
98.21
97.81
77.38 CHLOROFORM-D
77.13 CHLOROFORM-D
76.87 CHLOROFORM-D
69.45
67.06
65.80
65.25
62.89
62.52
47.79
46.23
30.55
30.51
25.26
19.29
18.99
0.060
0.055
0.050
0.045
0.040
0.035
0.030
0.025
0.020
0.015
0.010
0.005
0.000
70 260 250 240 230 220 210 200 190 180 170 160 150 140 130 120 110 100 90 80 70 60 50 40 30 20 10 0 -10 -20 -30
f1 (ppm)

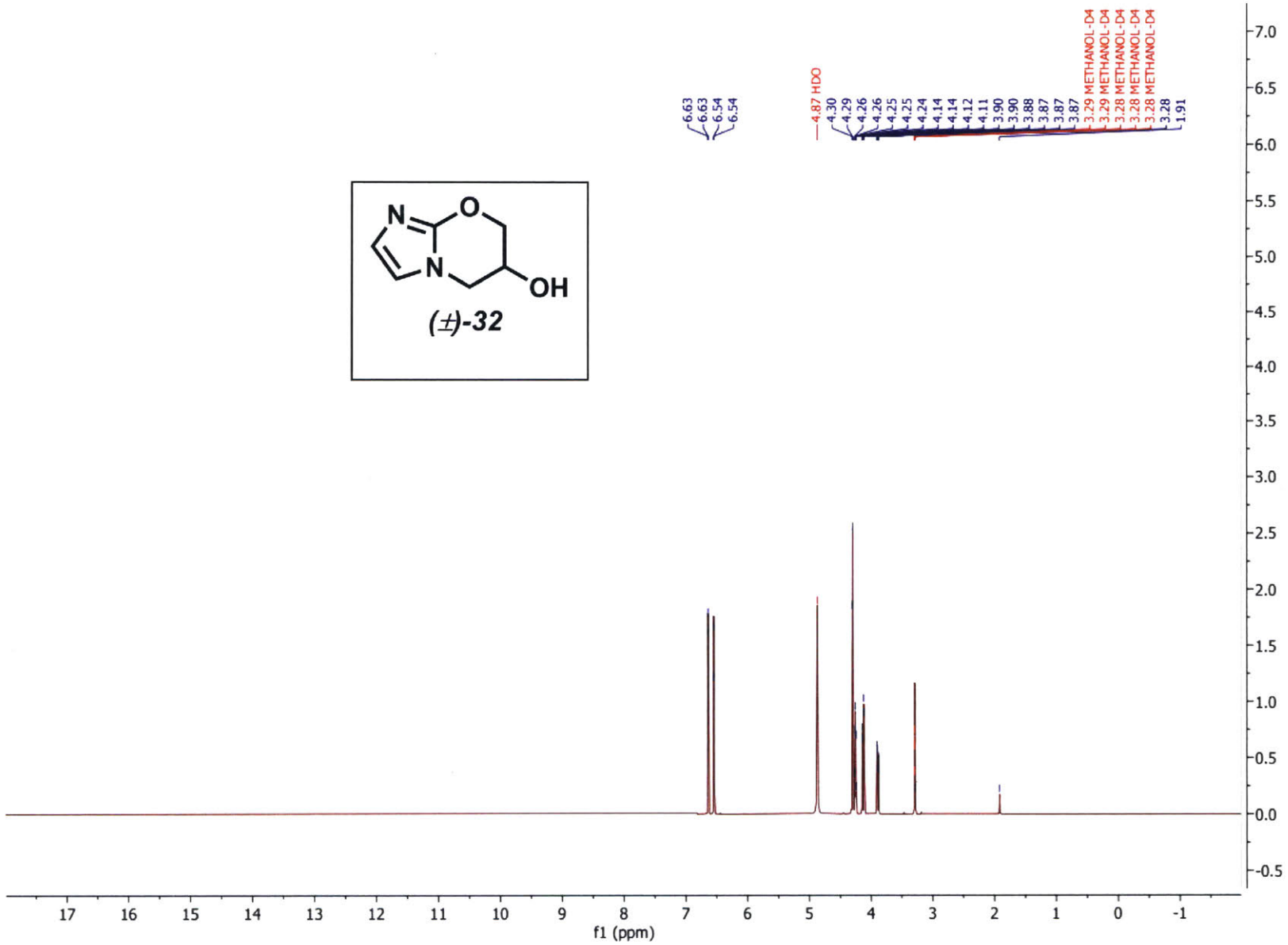
6.63
6.63
6.54
6.54
4.87 HDO
4.30
4.29
4.26
4.26
4.25
4.25
4.24
4.14
4.14
4.12
4.11
3.90
3.90
3.88
3.87
3.87
3.87
3.29 METHANOL-D4
3.29 METHANOL-D4
3.28 METHANOL-D4
3.28 METHANOL-D4
3.28 METHANOL-D4
3.28
1.91
N
O
N
OH
(±)-32
f1 (ppm)

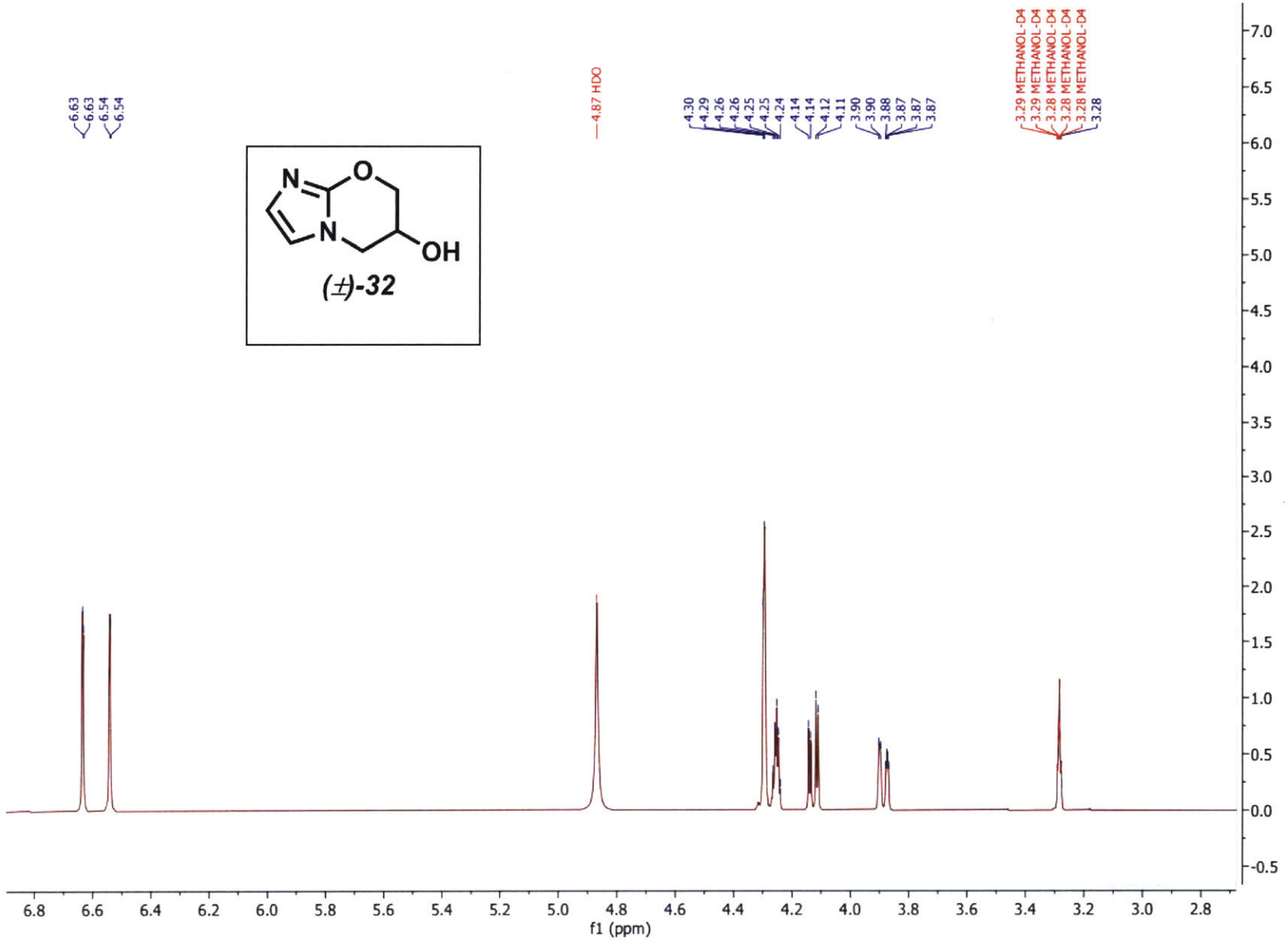
6.63
6.63
6.54
6.54
4.87 HDO
4.30
4.29
4.26
4.26
4.25
4.25
4.24
4.14
4.14
4.12
4.11
3.90
3.90
3.88
3.87
3.87
3.87
3.29 METHANOL-D4
3.29 METHANOL-D4
3.28 METHANOL-D4
3.28 METHANOL-D4
3.28 METHANOL-D4
3.28
N
O
N
OH
(±)-32
f1 (ppm)

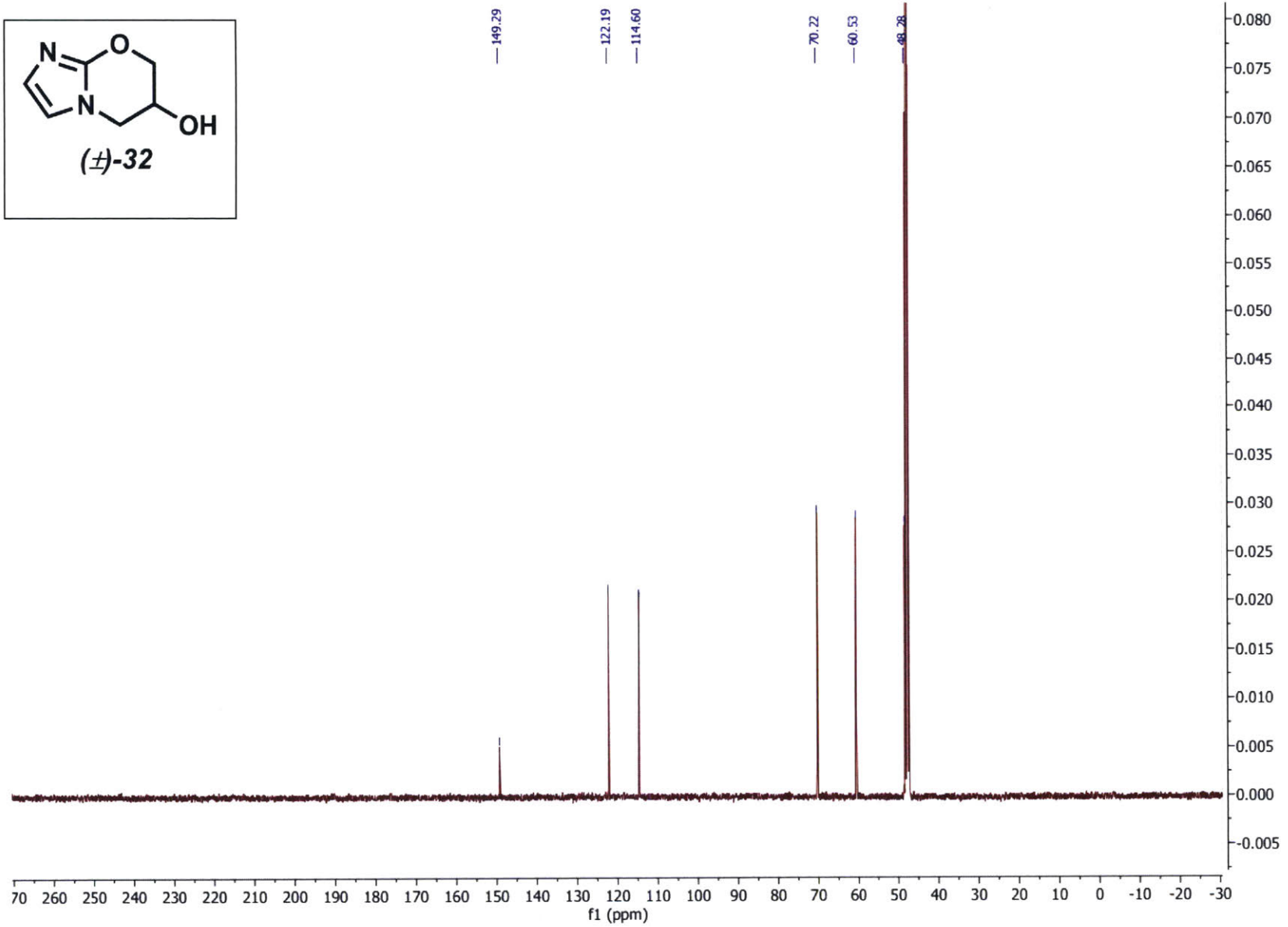
N
O
N
OH
(±)-32
149.29
122.19
114.60
70.22
60.53
68.28
0.080
0.075
0.070
0.065
0.060
0.055
0.050
0.045
0.040
0.035
0.030
0.025
0.020
0.015
0.010
0.005
0.000
-0.005
70 260 250 240 230 220 210 200 190 180 170 160 150 140 130 120 110 100 90 80 70 60 50 40 30 20 10 0 -10 -20 -30
f1 (ppm)

N
O
N
OH
(±)-32
gCOSY
f2 (ppm)
f1 (ppm)

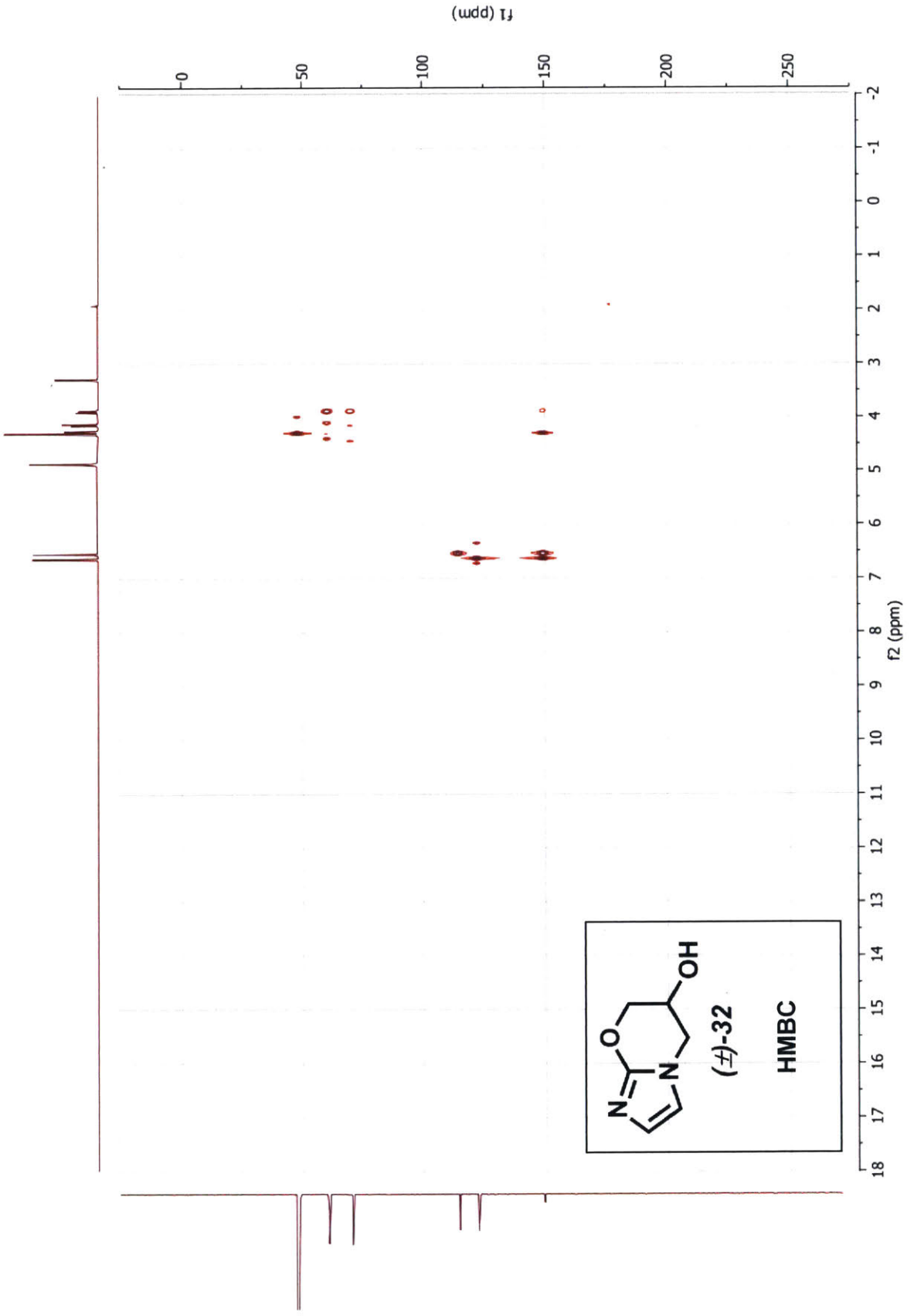
f1 (ppm)
0
50
100
150
200
250
f2 (ppm)
-2
-1
0
1
2
3
4
5
6
7
8
9
10
11
12
13
14
15
16
17
18
OH
O
N
N
(±)-32
HMBC

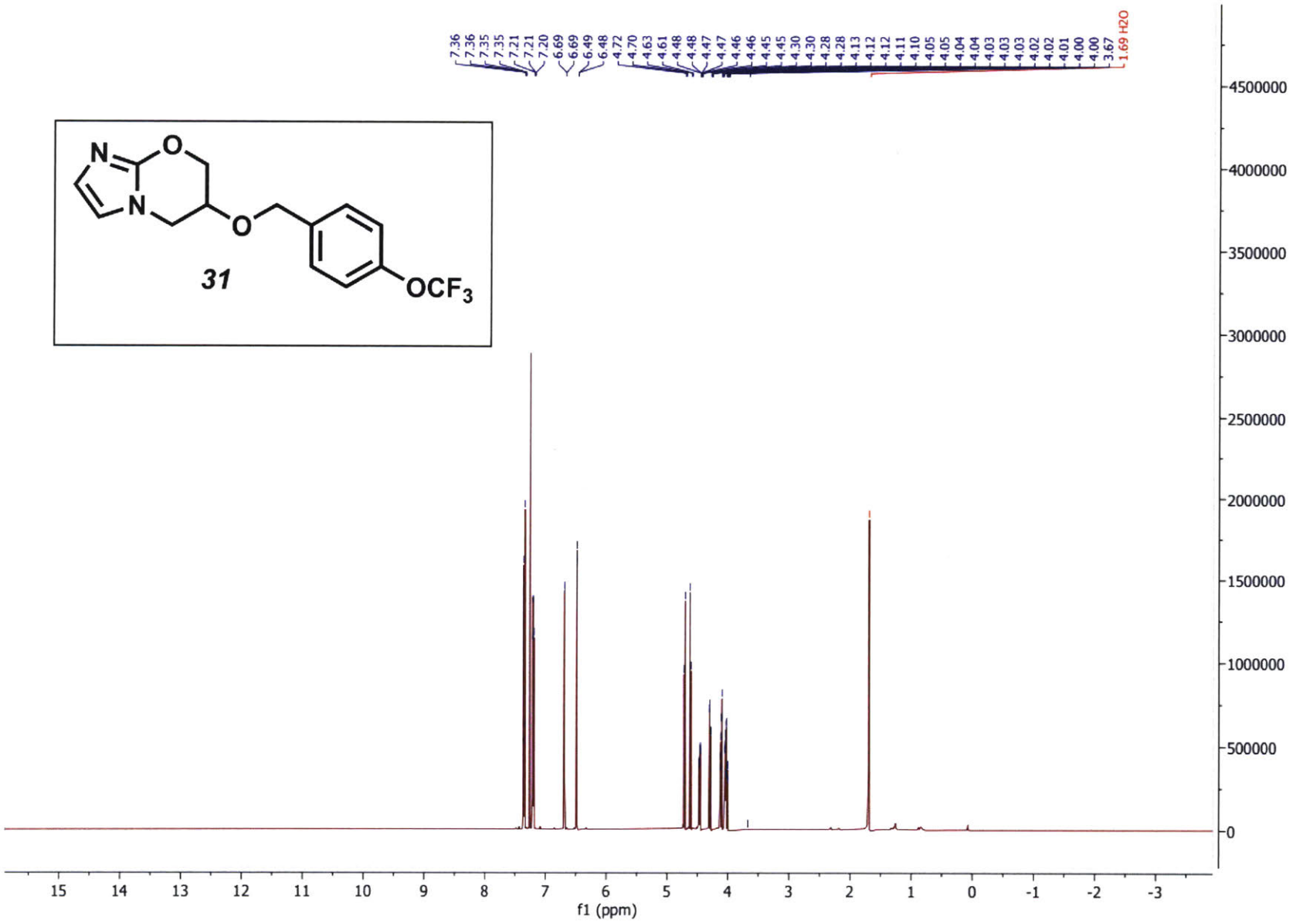
7.36
7.36
7.35
7.35
7.21
7.21
7.20
6.69
6.69
6.49
6.48
4.72
4.70
4.63
4.61
4.48
4.48
4.47
4.47
4.46
4.46
4.45
4.45
4.30
4.30
4.28
4.28
4.13
4.12
4.12
4.11
4.10
4.05
4.05
4.04
4.04
4.03
4.03
4.03
4.02
4.02
4.01
4.00
4.00
3.67
1.69 H2O
N
O
N
O
31
OCF3
4500000
4000000
3500000
3000000
2500000
2000000
1500000
1000000
500000
0
15
14
13
12
11
10
9
8
7
6
5
4
3
2
1
0
-1
-2
-3
f1 (ppm)

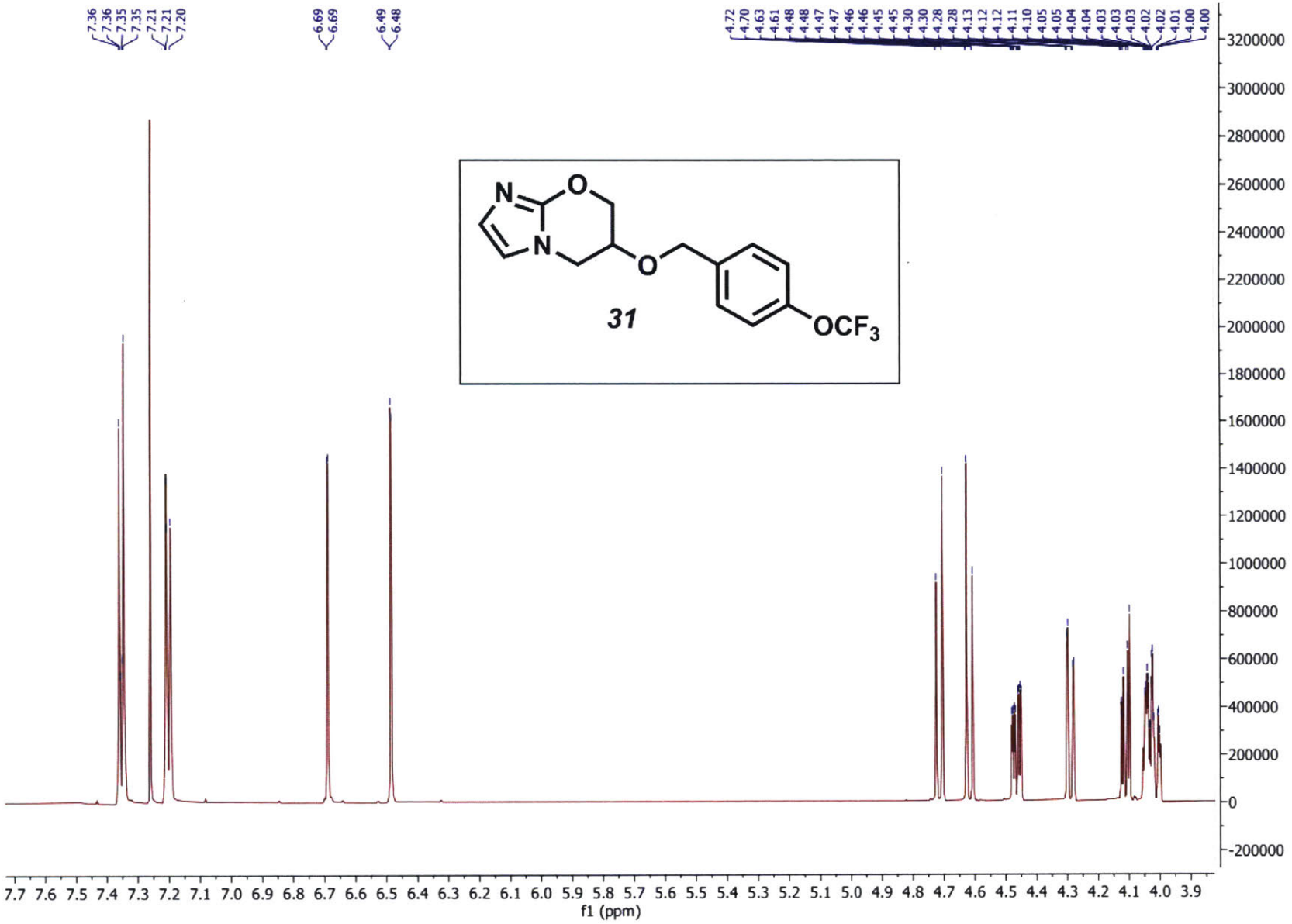
7.36
7.36
7.35
7.35
7.21
7.21
7.20
6.69
6.69
6.49
6.48
4.72
4.70
4.63
4.61
4.48
4.48
4.47
4.47
4.46
4.46
4.45
4.45
4.30
4.30
4.28
4.28
4.13
4.12
4.12
4.11
4.10
4.05
4.05
4.04
4.04
4.03
4.03
4.03
4.02
4.02
4.01
4.00
4.00
N
O
N
O
31
OCF3
3200000
3000000
2800000
2600000
2400000
2200000
2000000
1800000
1600000
1400000
1200000
1000000
800000
600000
400000
200000
0
-200000
7.7 7.6 7.5 7.4 7.3 7.2 7.1 7.0 6.9 6.8 6.7 6.6 6.5 6.4 6.3 6.2 6.1 6.0 5.9 5.8 5.7 5.6 5.5 5.4 5.3 5.2 5.1 5.0 4.9 4.8 4.7 4.6 4.5 4.4 4.3 4.2 4.1 4.0 3.9
f1 (ppm)

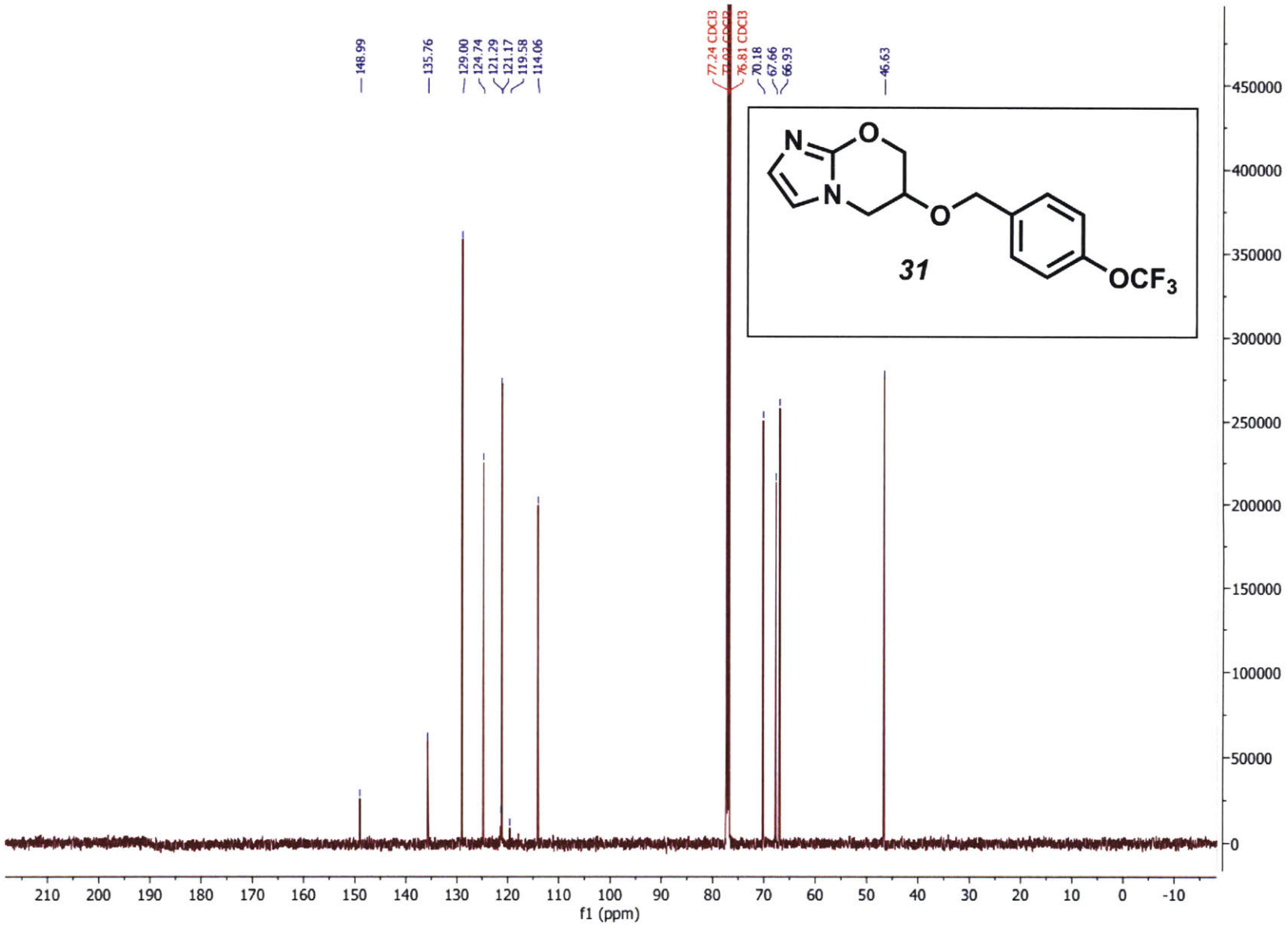
148.99
135.76
129.00
124.74
121.29
121.17
119.58
114.06
77.24 CDCl3
76.81 CDCl3
70.18
67.66
66.93
46.63
31
OCF3
450000
400000
350000
300000
250000
200000
150000
100000
50000
0
210 200 190 180 170 160 150 140 130 120 110 100 90 80 70 60 50 40 30 20 10 0 -10
f1 (ppm)

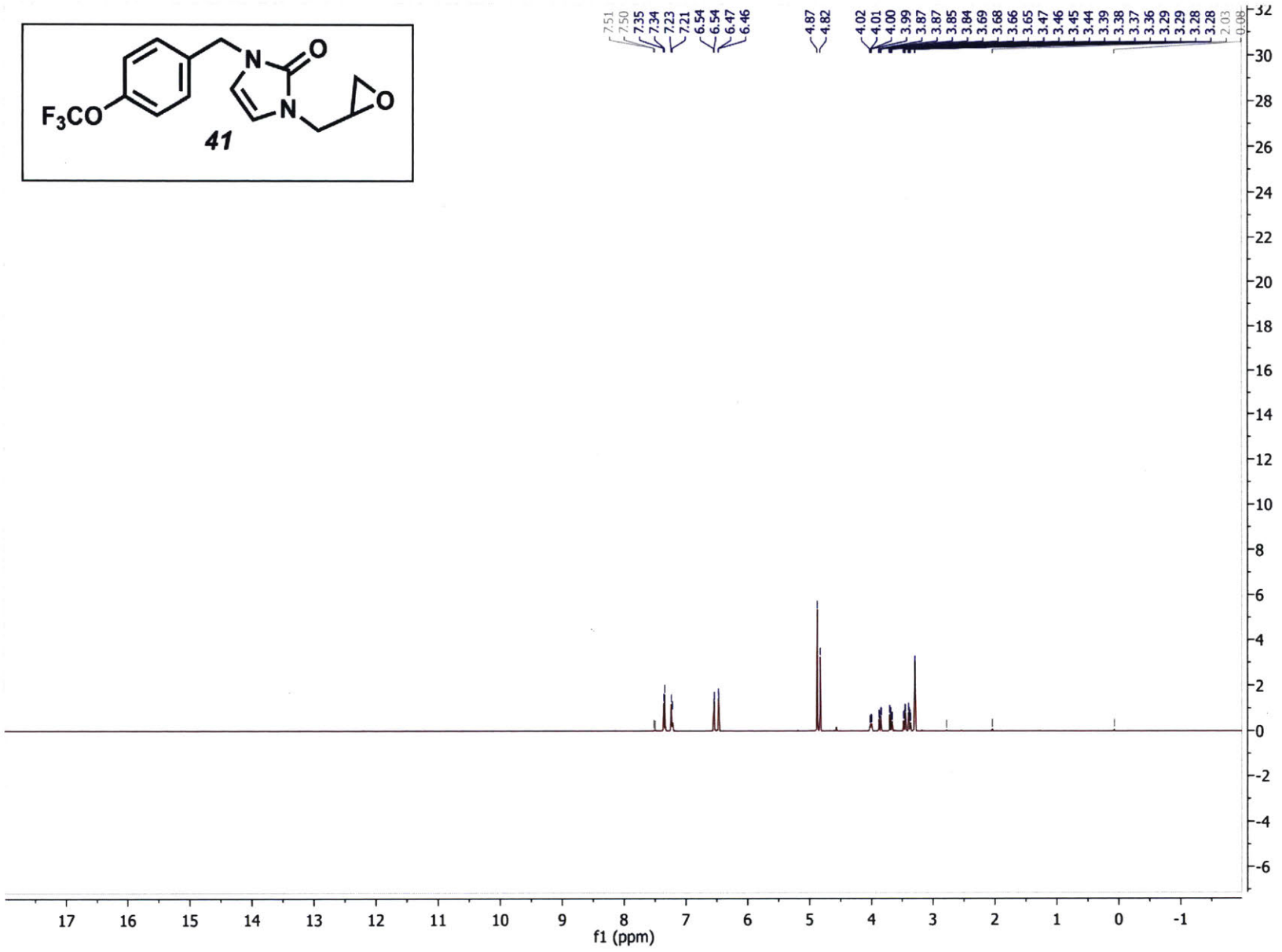
F3CO
41
7.51
7.50
7.35
7.34
7.23
7.21
6.54
6.54
6.47
6.46
4.87
4.82
4.02
4.01
4.00
3.99
3.87
3.87
3.85
3.84
3.69
3.68
3.66
3.65
3.47
3.46
3.45
3.44
3.39
3.38
3.37
3.36
3.29
3.29
3.28
3.28
2.03
0.08
f1 (ppm)

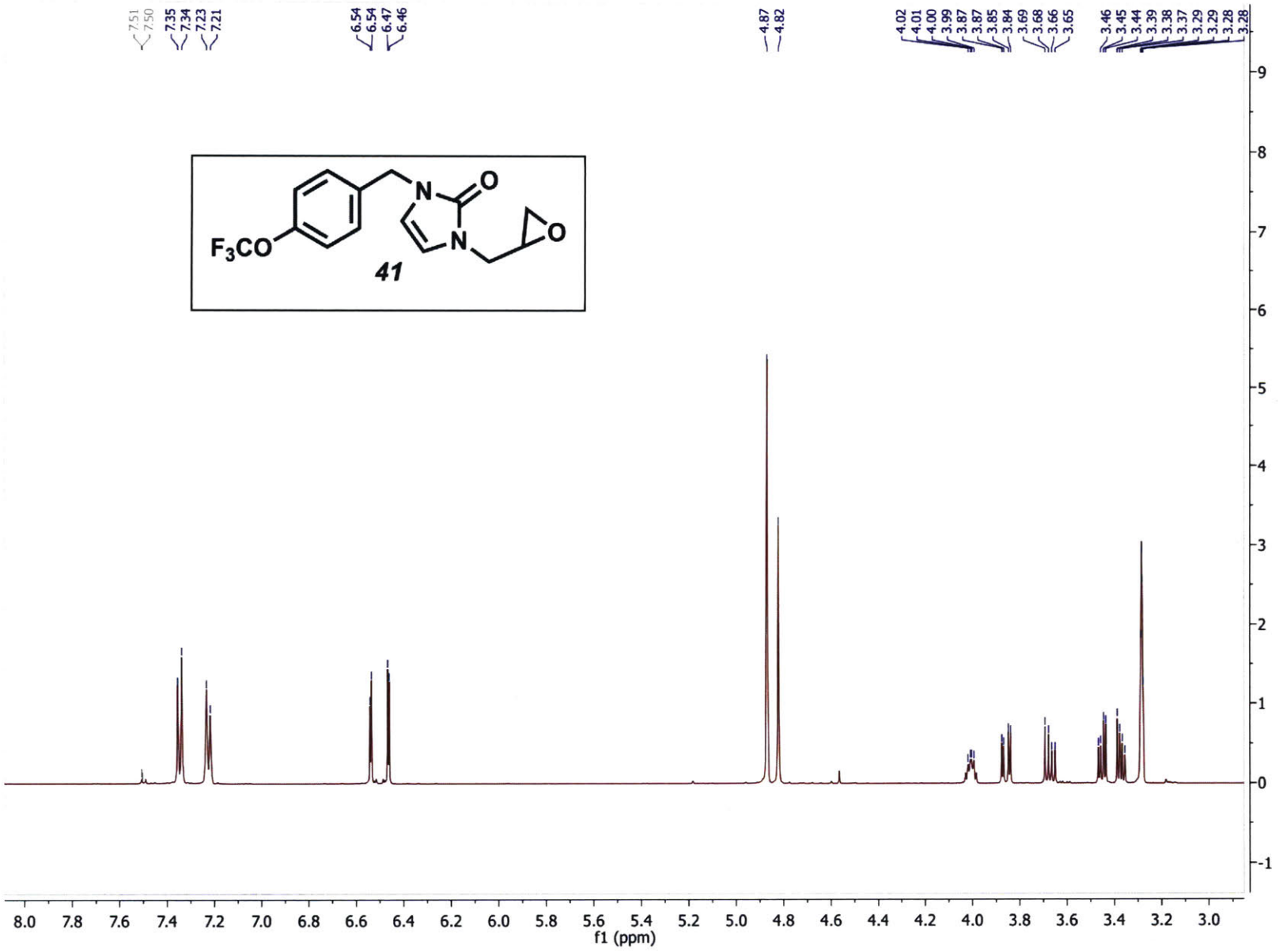
7.51
7.50
7.35
7.34
7.23
7.21
6.54
6.54
6.47
6.46
4.87
4.82
4.02
4.01
4.00
3.99
3.87
3.87
3.85
3.84
3.69
3.68
3.66
3.65
3.46
3.45
3.44
3.39
3.38
3.37
3.29
3.29
3.28
3.28
F3CO
N
O
N
O
41
f1 (ppm)

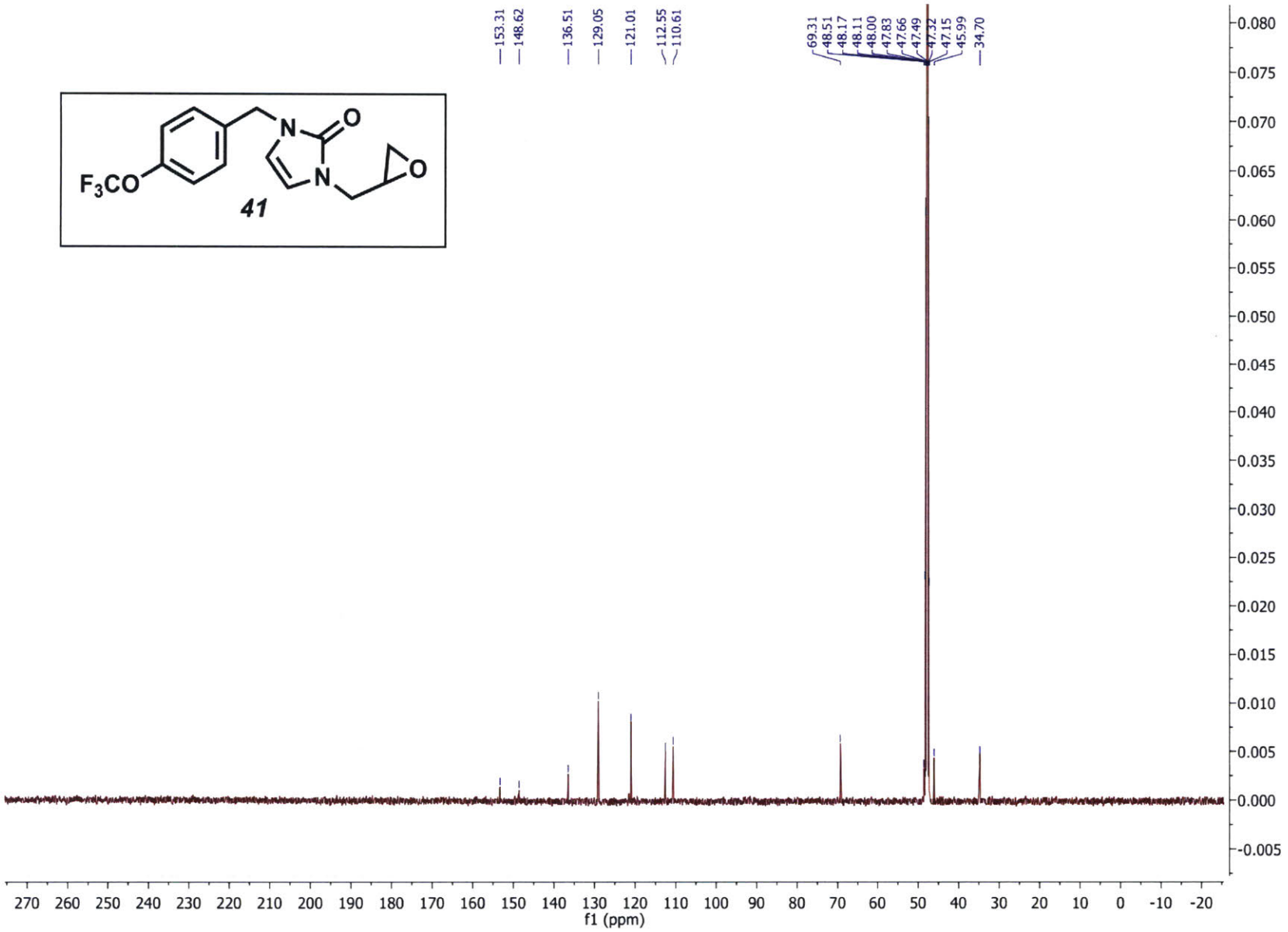
153.31
148.62
136.51
129.05
121.01
112.55
110.61
69.31
48.51
48.17
48.11
48.00
47.83
47.66
47.49
47.32
47.15
45.99
34.70
F3CO
N
O
N
O
41
f1 (ppm)

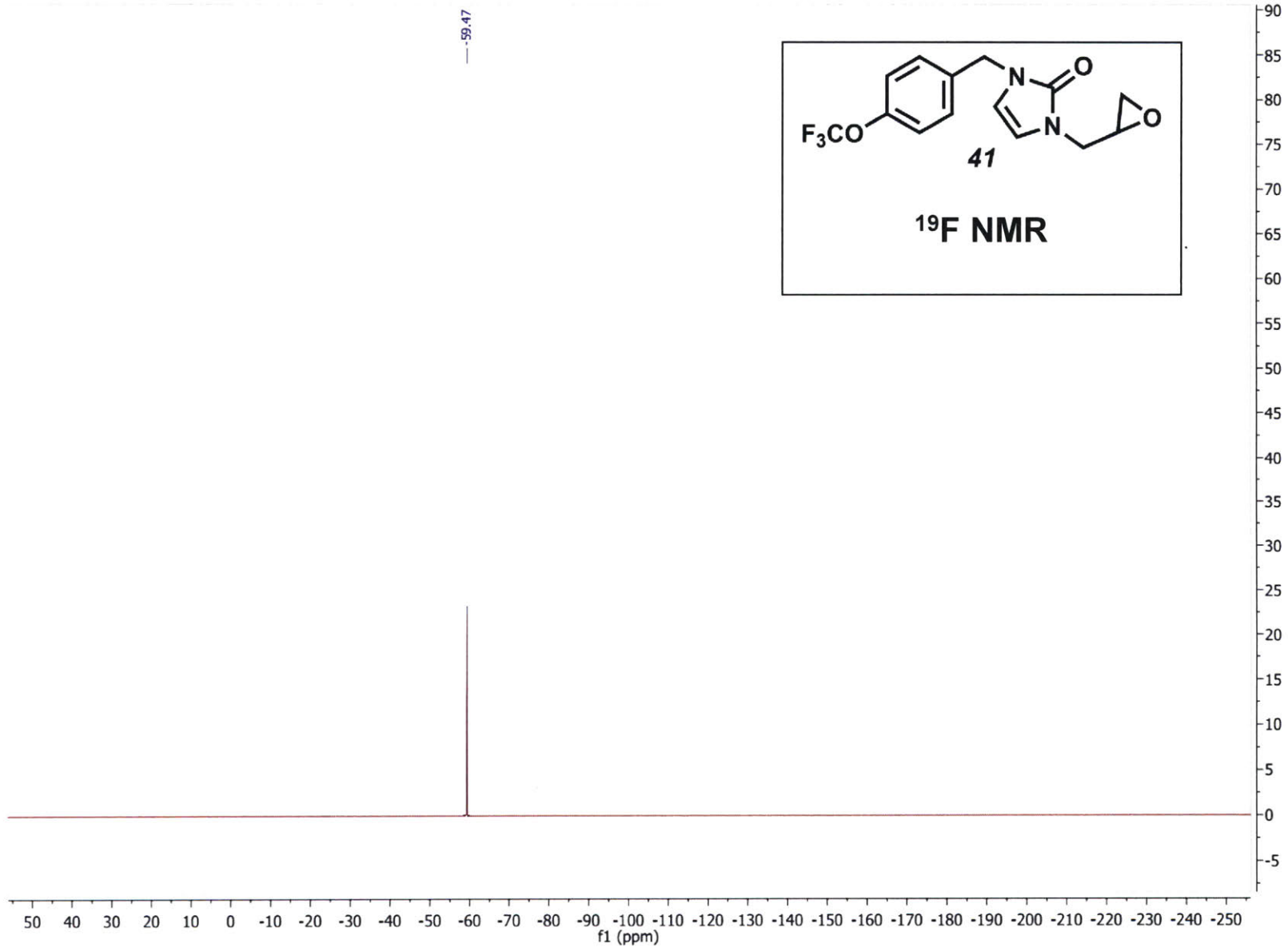
-59.47
F3CO
N
O
N
O
41
19F NMR
90
85
80
75
70
65
60
55
50
45
40
35
30
25
20
15
10
5
0
-5
50 40 30 20 10 0 -10 -20 -30 -40 -50 -60 -70 -80 -90 -100 -110 -120 -130 -140 -150 -160 -170 -180 -190 -200 -210 -220 -230 -240 -250
f1 (ppm)

F3CO
N
O
N
O
41
HSQC
18
17
16
15
14
13
12
11
10
9
8
7
6
5
4
3
2
1
0
-1
f2 (ppm)
0
50
100
150
200
250
f1 (ppm)

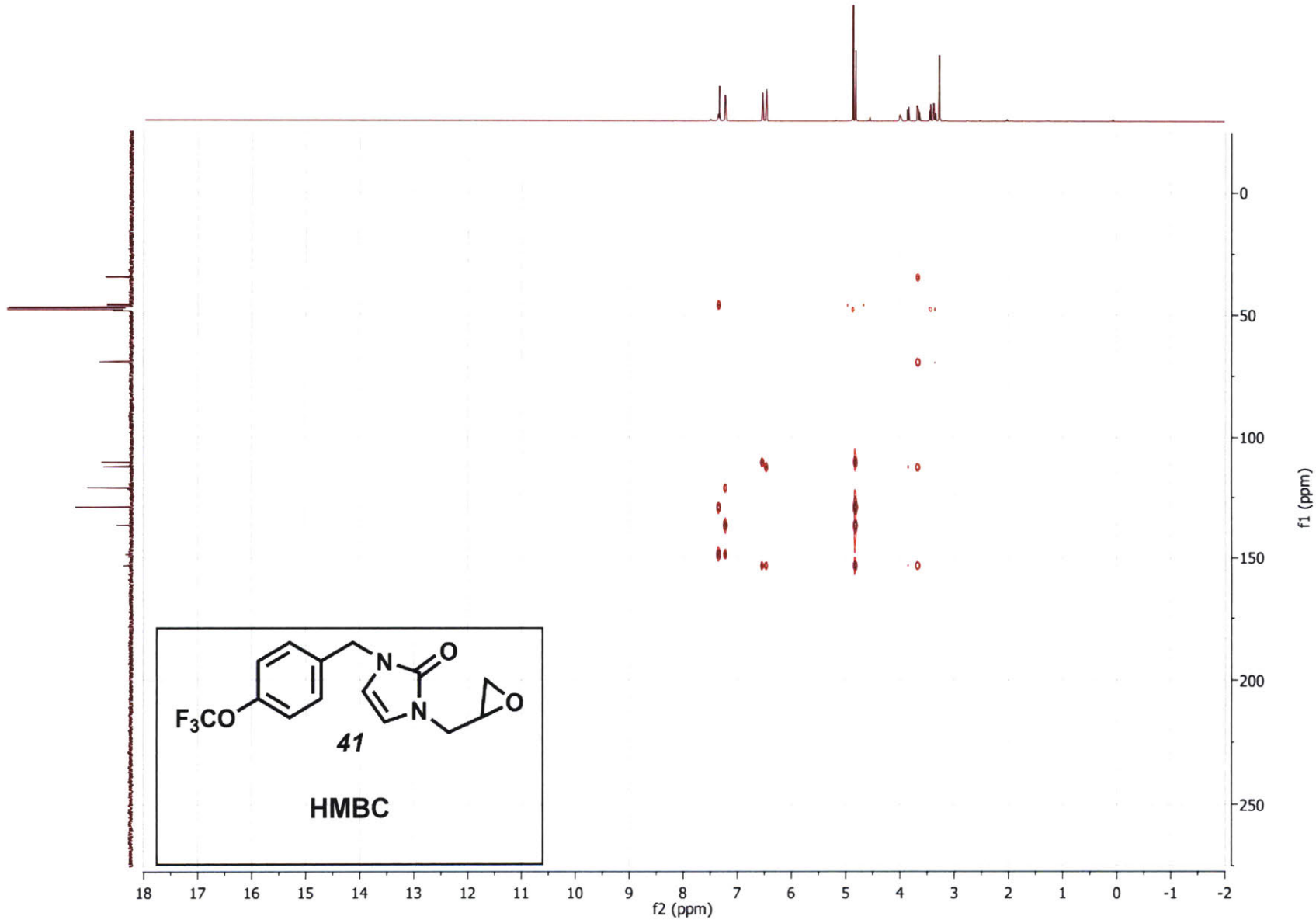
F3CO
N
O
N
O
41
HMBC
18 17 16 15 14 13 12 11 10 9 8 7 6 5 4 3 2 1 0 -1 -2
f2 (ppm)
0 50 100 150 200 250
f1 (ppm)

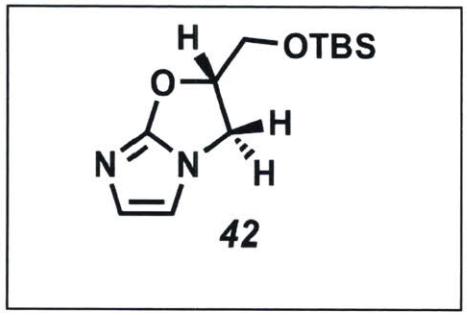
H
OTBS
O
H
N
N
H

42

7.25
6.63
6.54
6.54
5.29
5.22
5.21
4.13
4.12
4.10
4.07
4.06
4.05
4.04
3.94
3.93
3.92
3.91
3.87
3.86
3.85
3.84
1.65
0.83
0.07
0.03
f1 (ppm)

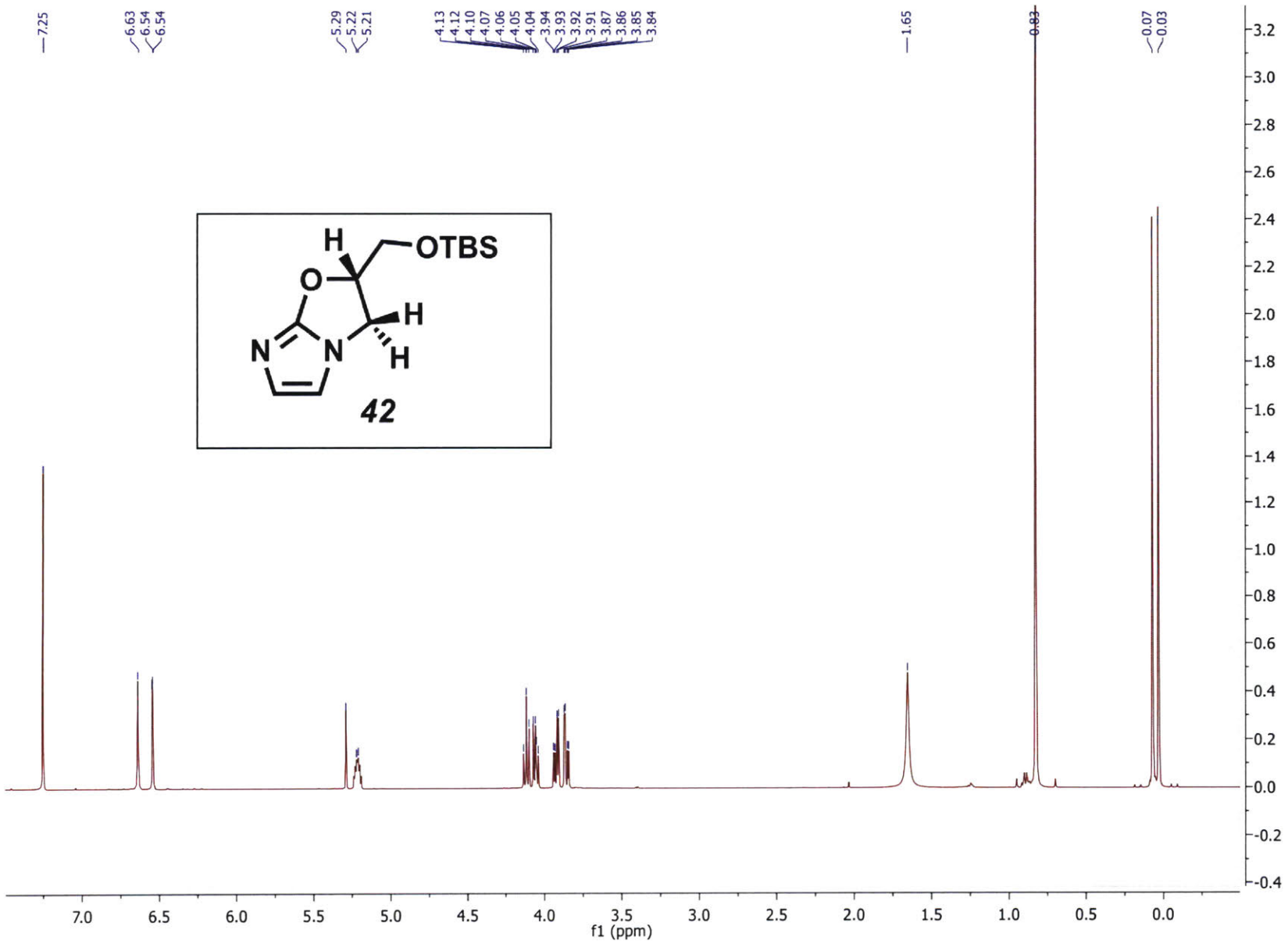
7.25
6.63
6.54
6.54
5.29
5.22
5.21
4.13
4.12
4.10
4.07
4.06
4.05
4.04
3.94
3.93
3.92
3.91
3.87
3.86
3.85
3.84
1.65
0.83
0.07
0.03
H
OTBS
O
H
N
N
H
42
f1 (ppm)

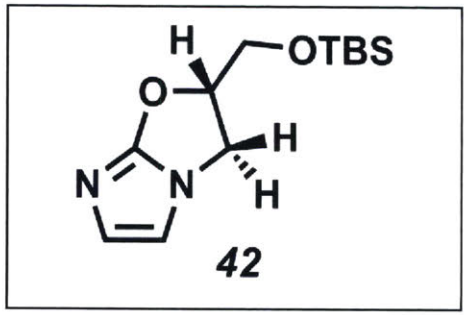
H
OTBS
O
N
N
H
H

42

160.03
129.43
110.47
86.12
77.36 CHLOROFORM-D
77.11 CHLOROFORM-D
76.85 CHLOROFORM-D
63.46
44.92
25.76
18.26
-5.37
0.060
0.055
0.050
0.045
0.040
0.035
0.030
0.025
0.020
0.015
0.010
0.005
0.000
-0.005
270 260 250 240 230 220 210 200 190 180 170 160 150 140 130 120 110 100 90 80 70 60 50 40 30 20 10 0 -10 -20
f1 (ppm)

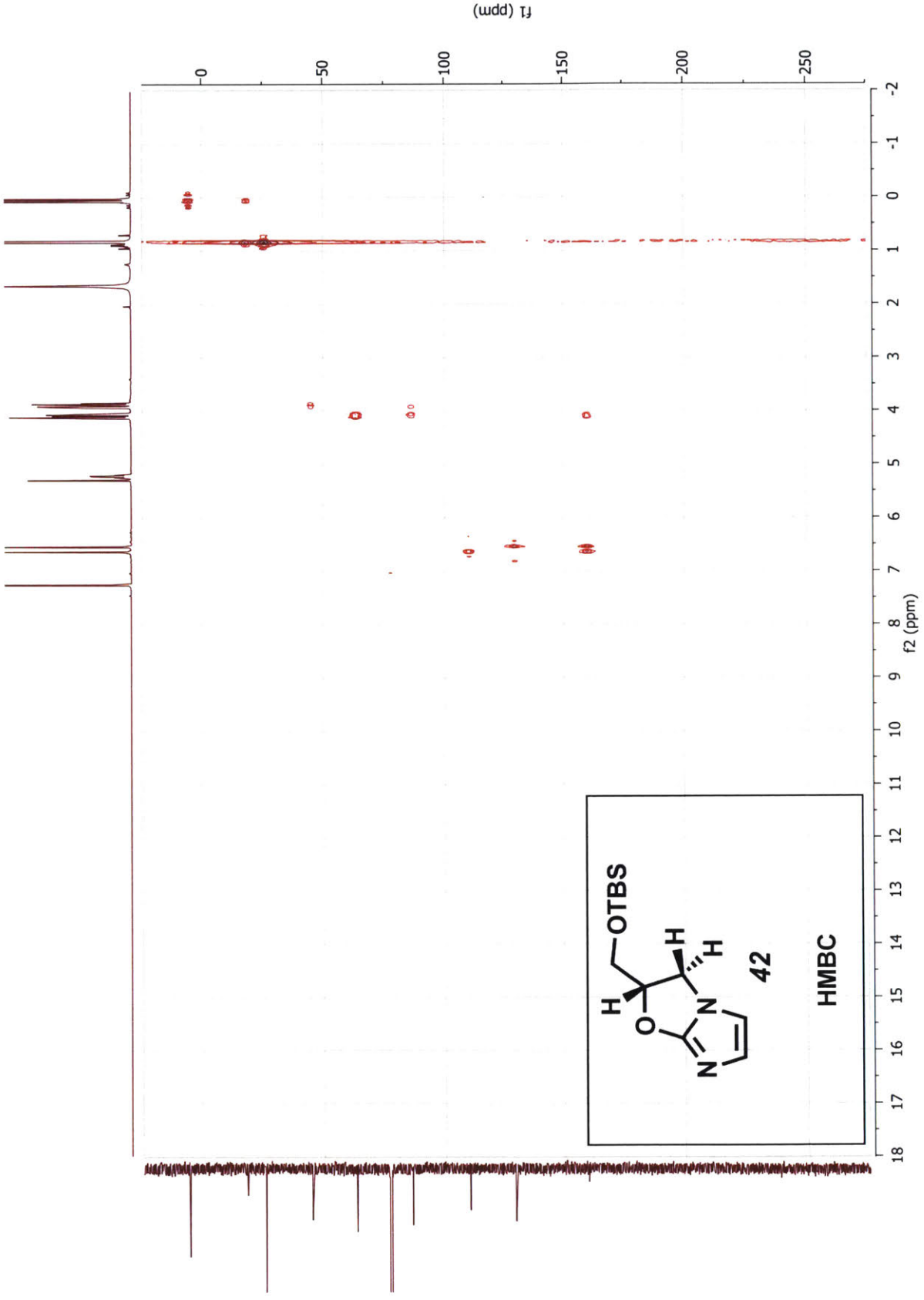
f1 (ppm)
0
50
100
150
200
250
f2 (ppm)
-2
-1
0
1
2
3
4
5
6
7
8
9
10
11
12
13
14
15
16
17
18
OTBS
H
H
H
O
N
N
42
HMBC

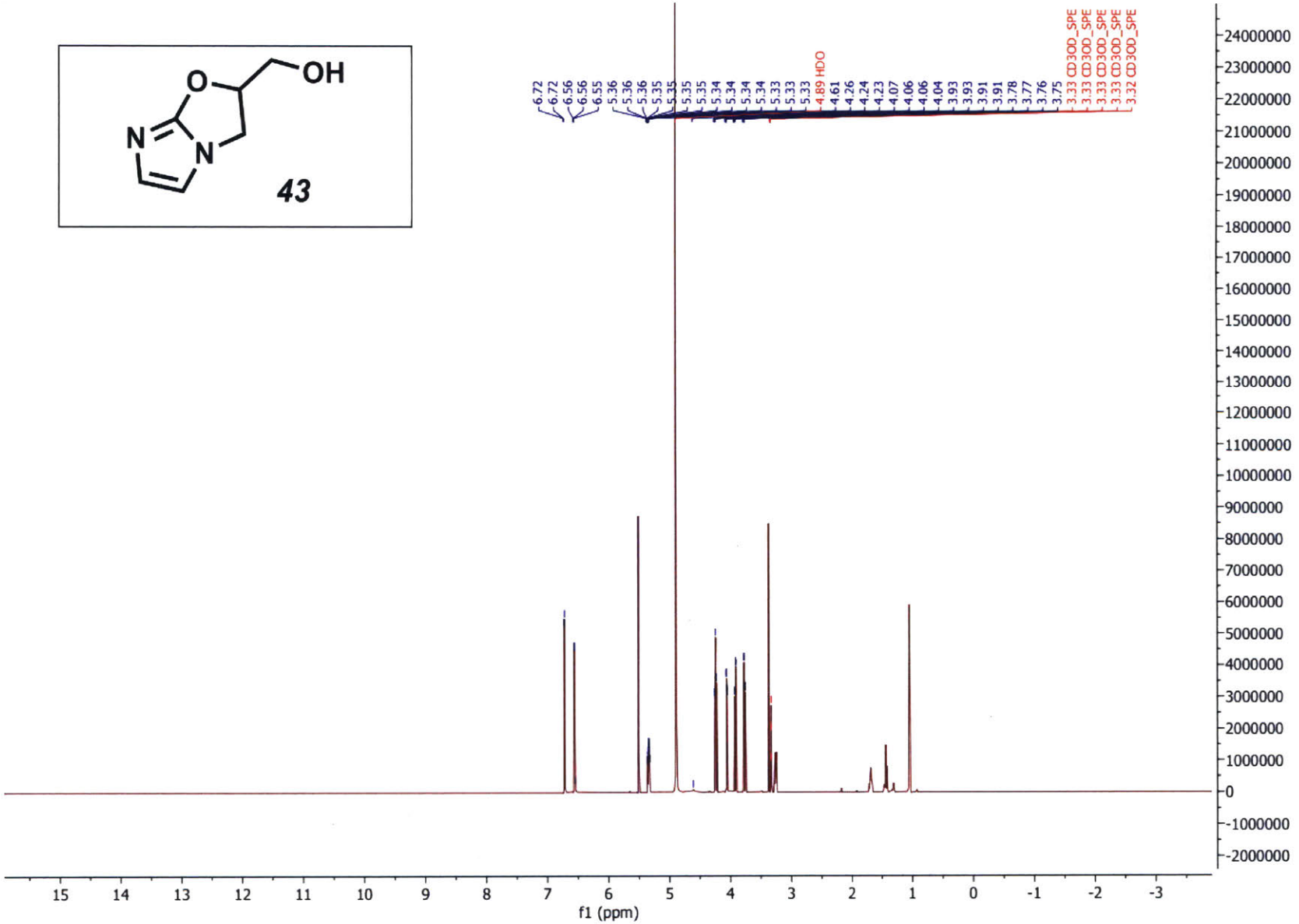
OH
O
N
N
43
6.72
6.72
6.56
6.56
6.55
5.36
5.36
5.35
5.35
5.35
5.35
5.34
5.34
5.34
5.33
5.33
4.89 HDO
4.61
4.26
4.24
4.23
4.07
4.06
4.06
4.04
3.93
3.93
3.91
3.91
3.78
3.77
3.76
3.75
3.33 CD3OD_SPE
3.33 CD3OD_SPE
3.33 CD3OD_SPE
3.33 CD3OD_SPE
3.33 CD3OD_SPE
3.32 CD3OD_SPE
f1 (ppm)

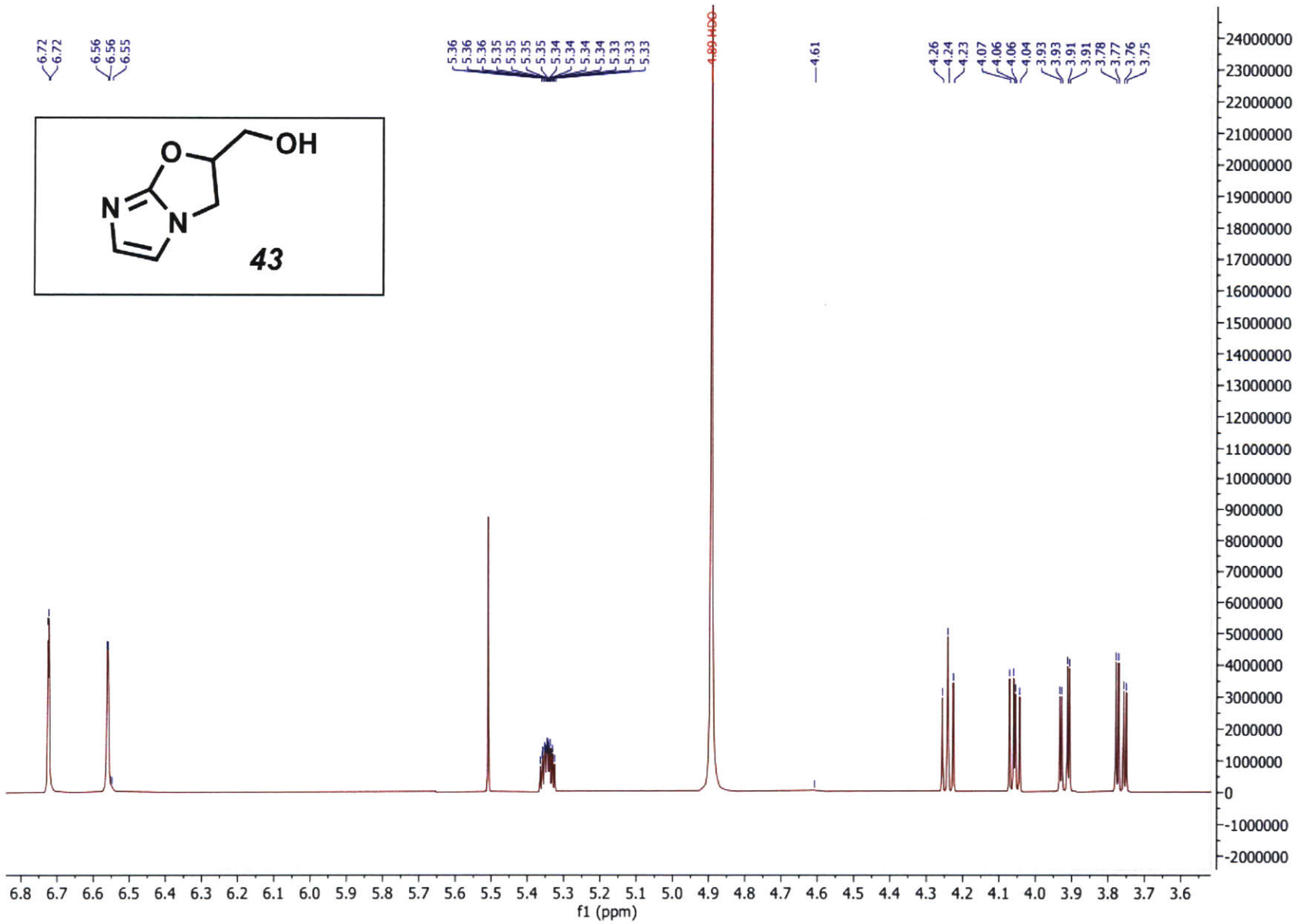
6.72
6.72
6.56
6.56
6.55
5.36
5.36
5.36
5.35
5.35
5.35
5.34
5.34
5.34
5.34
5.33
5.33
5.33
4.89 HDO
4.61
4.26
4.24
4.23
4.07
4.06
4.06
4.04
3.93
3.93
3.91
3.91
3.78
3.77
3.76
3.75
OH
O
N
N
43
f1 (ppm)

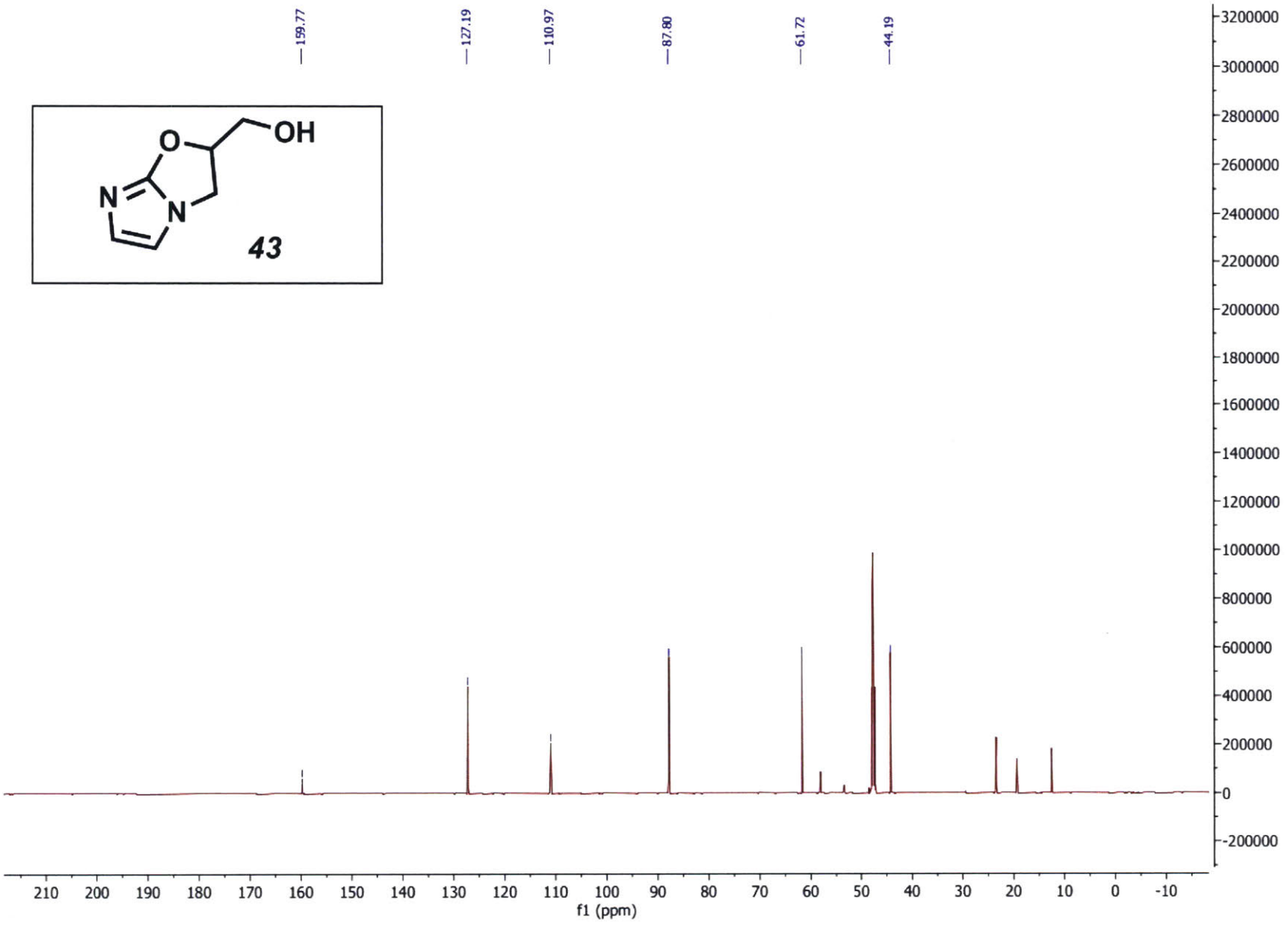
159.77
127.19
110.97
87.80
61.72
44.19
OH
O
N
N
43
3200000
3000000
2800000
2600000
2400000
2200000
2000000
1800000
1600000
1400000
1200000
1000000
800000
600000
400000
200000
0
-200000
210 200 190 180 170 160 150 140 130 120 110 100 90 80 70 60 50 40 30 20 10 0 -10
f1 (ppm)

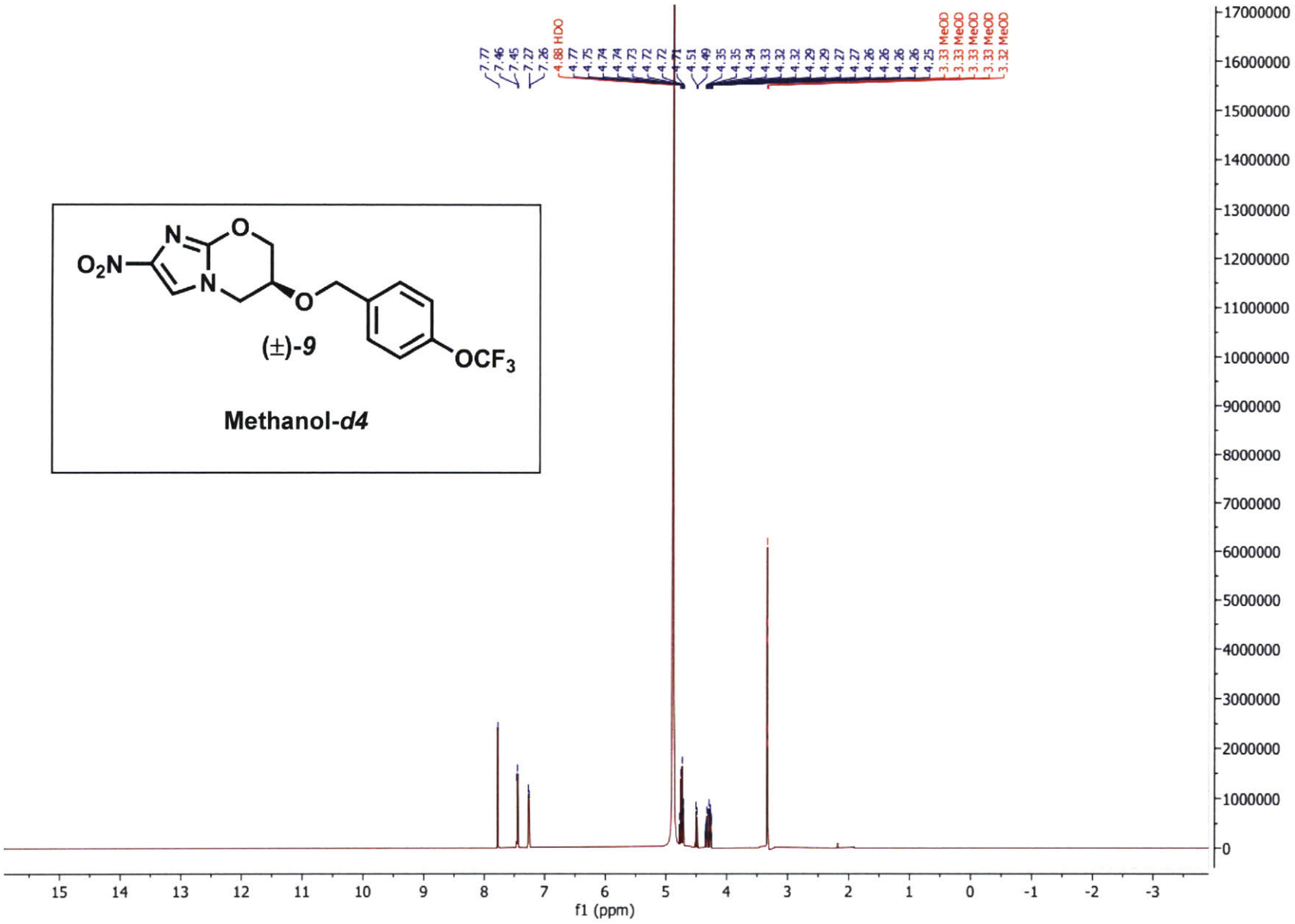
(±)-9
Methanol-d4
f1 (ppm)

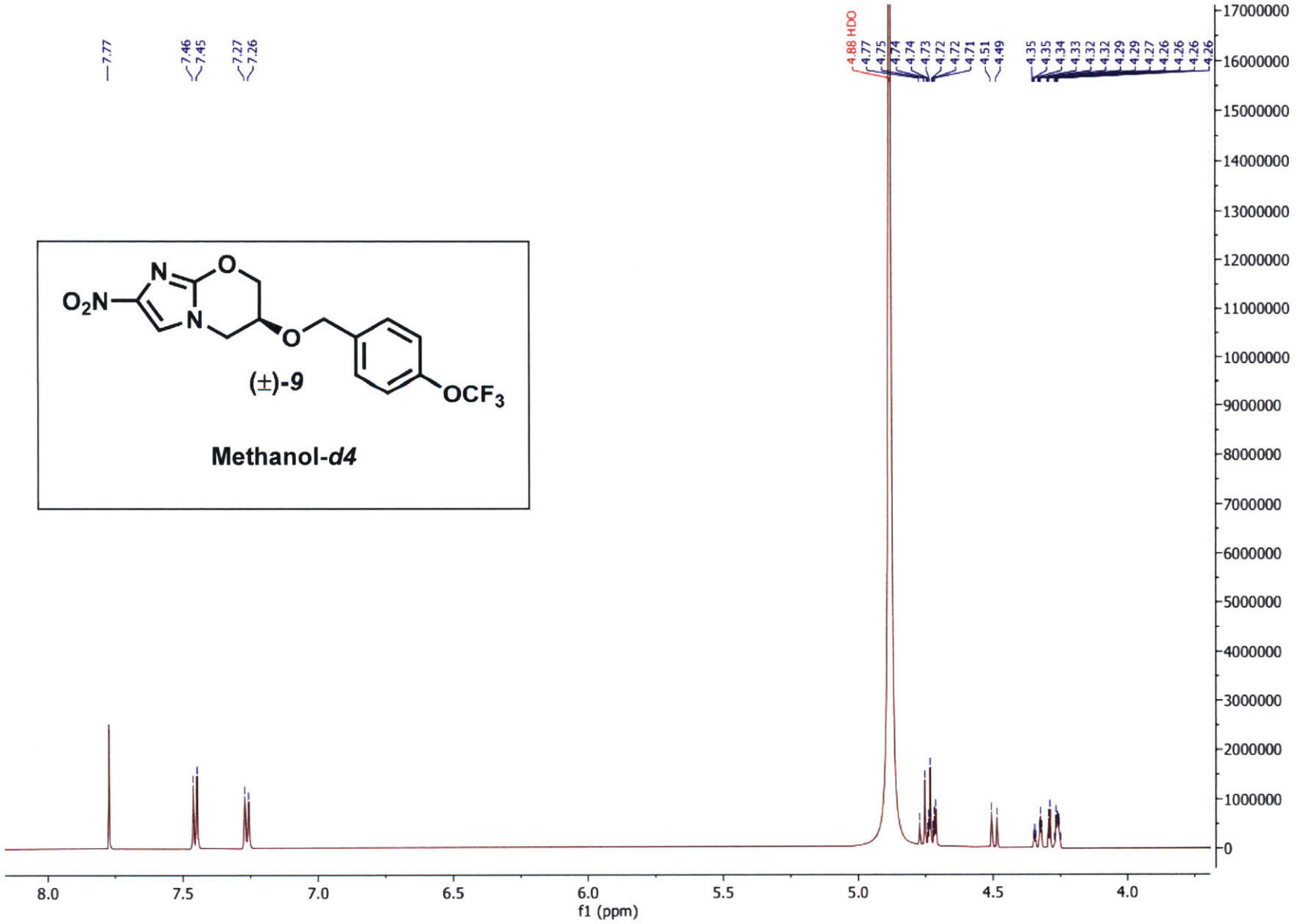
7.77
7.46
7.45
7.27
7.26
4.88 HDO
4.77
4.75
4.74
4.74
4.73
4.72
4.72
4.71
4.51
4.49
4.35
4.35
4.34
4.33
4.32
4.29
4.29
4.27
4.26
4.26
4.26
O2N
N
O
N
O
(±)-9
OCF3
Methanol-d4
17000000
16000000
15000000
14000000
13000000
12000000
11000000
10000000
9000000
8000000
7000000
6000000
5000000
4000000
3000000
2000000
1000000
0
8.0
7.5
7.0
6.5
6.0
5.5
5.0
4.5
4.0
f1 (ppm)

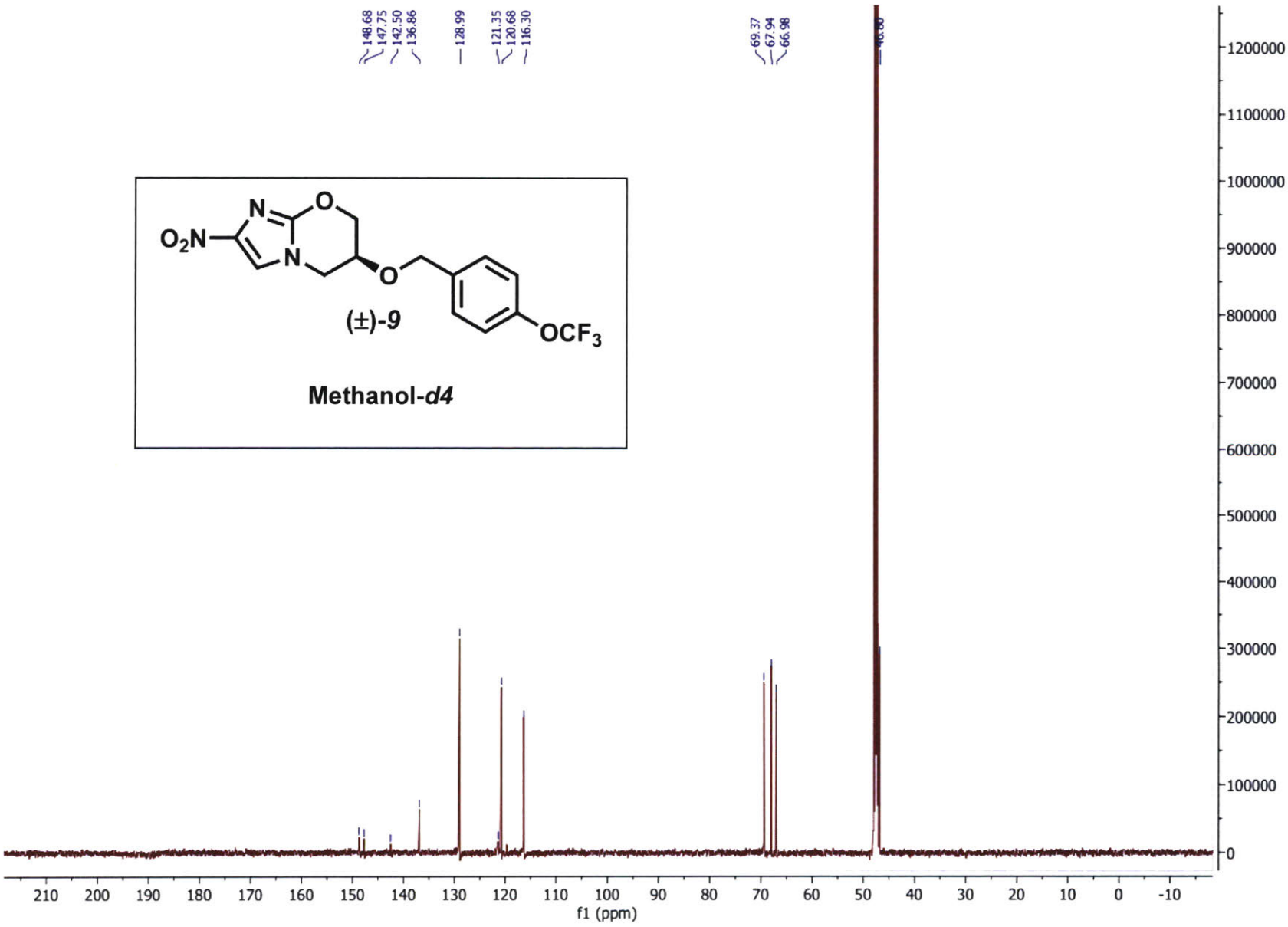
148.68
147.75
142.50
136.86
128.99
121.35
120.68
116.30
69.37
67.94
66.98
(±)-9
Methanol-d4
f1 (ppm)

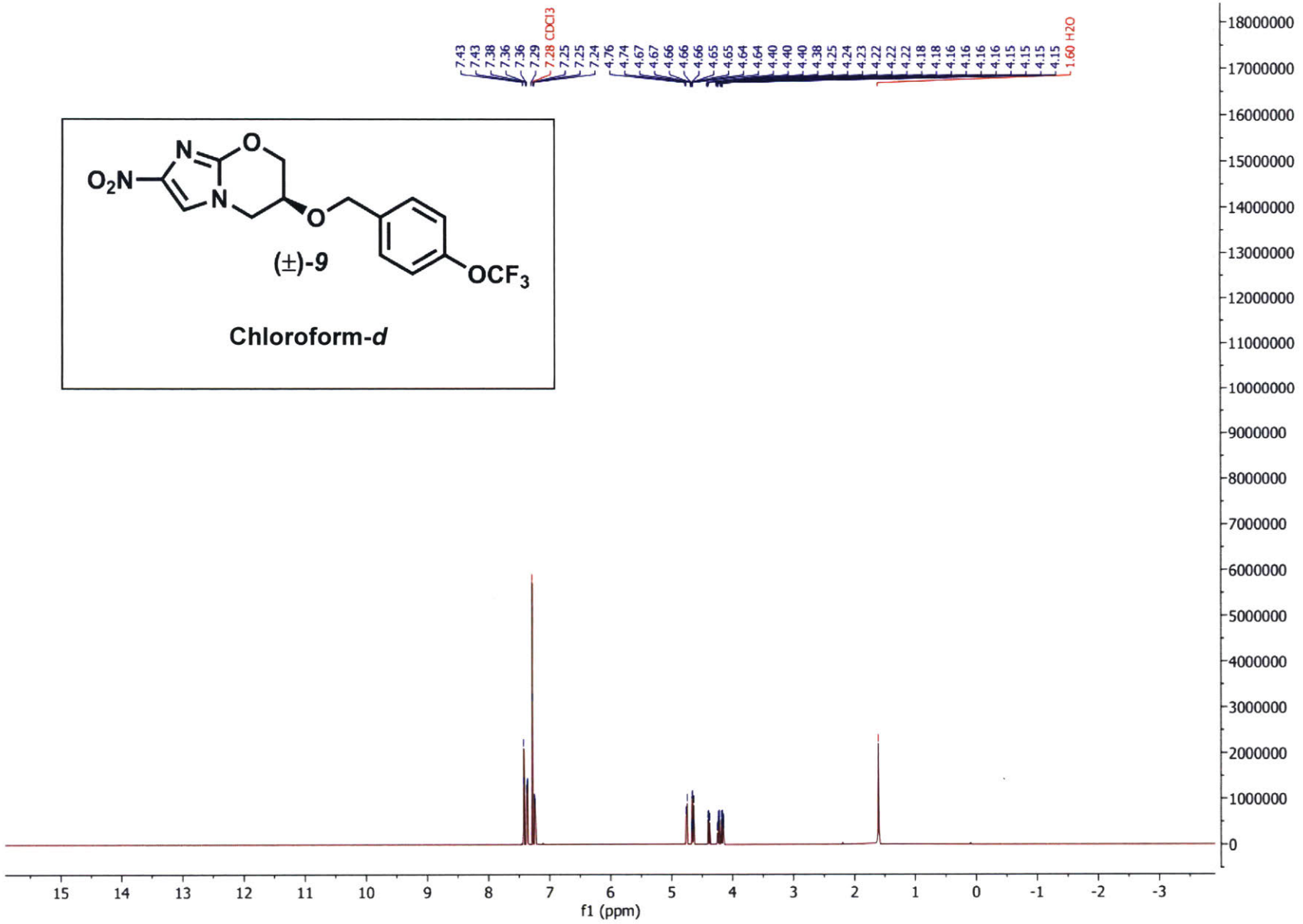
7.43
7.43
7.38
7.36
7.36
7.29
7.28 CDCl3
7.25
7.25
7.24
4.76
4.74
4.67
4.67
4.66
4.66
4.66
4.65
4.65
4.64
4.64
4.40
4.40
4.40
4.38
4.25
4.24
4.23
4.22
4.22
4.22
4.18
4.18
4.16
4.16
4.16
4.16
4.15
4.15
4.15
1.60 H2O
O2N
N
O
N
O
(±)-9
OCF3
Chloroform-d
18000000
17000000
16000000
15000000
14000000
13000000
12000000
11000000
10000000
9000000
8000000
7000000
6000000
5000000
4000000
3000000
2000000
1000000
0
15
14
13
12
11
10
9
8
7
6
5
4
3
2
1
0
-1
-2
-3
f1 (ppm)

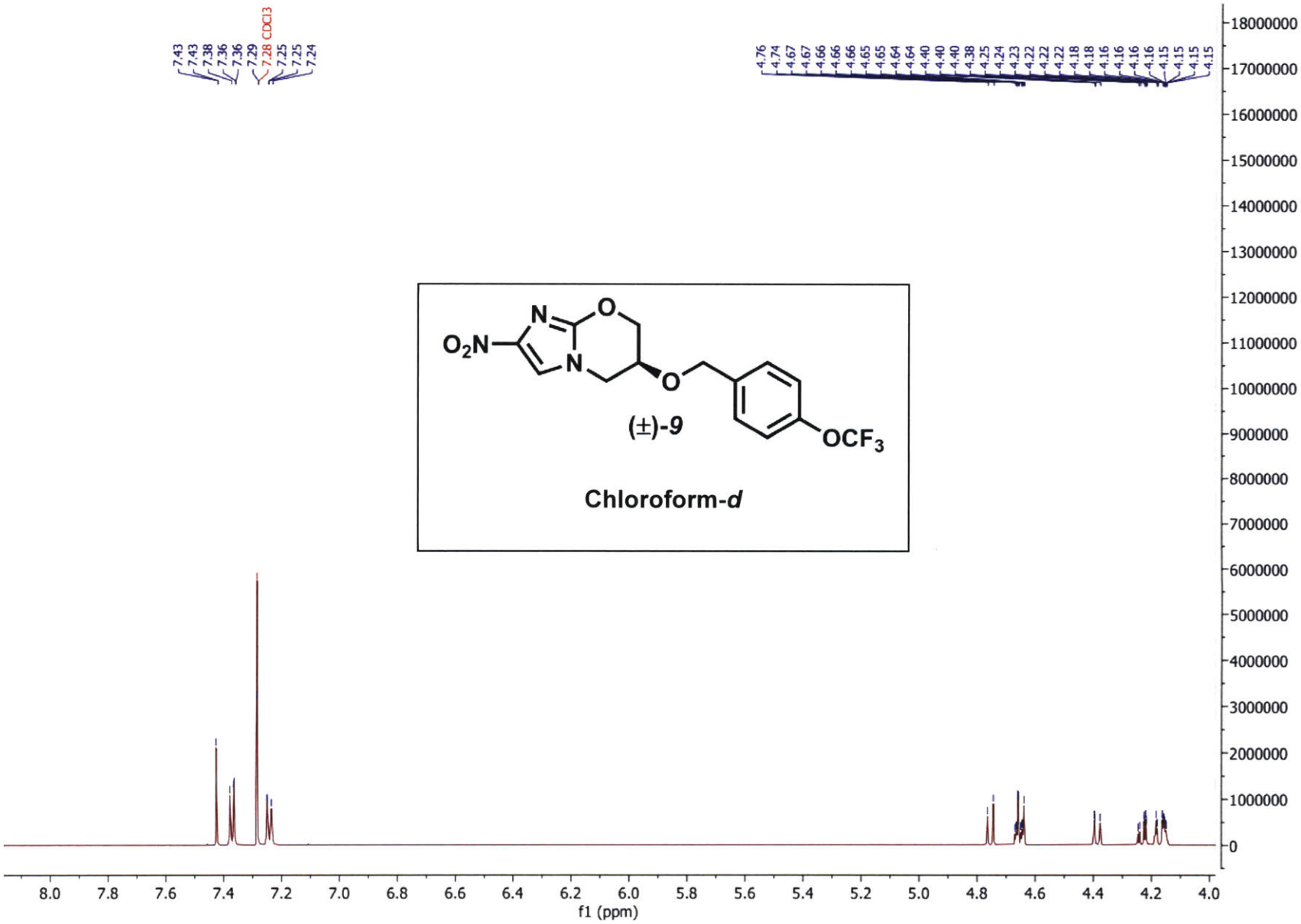
7.43
7.43
7.38
7.36
7.36
7.29
7.28 CDCl3
7.25
7.25
7.24
4.76
4.74
4.67
4.67
4.66
4.66
4.66
4.65
4.65
4.64
4.64
4.40
4.40
4.40
4.38
4.25
4.24
4.23
4.22
4.22
4.22
4.18
4.18
4.16
4.16
4.16
4.16
4.15
4.15
4.15
4.15
18000000
17000000
16000000
15000000
14000000
13000000
12000000
11000000
10000000
9000000
8000000
7000000
6000000
5000000
4000000
3000000
2000000
1000000
0
8.0
7.8
7.6
7.4
7.2
7.0
6.8
6.6
6.4
6.2
6.0
5.8
5.6
5.4
5.2
5.0
4.8
4.6
4.4
4.2
4.0
f1 (ppm)
O2N
N
O
N
O
O
OCF3
(±)-9
Chloroform-d

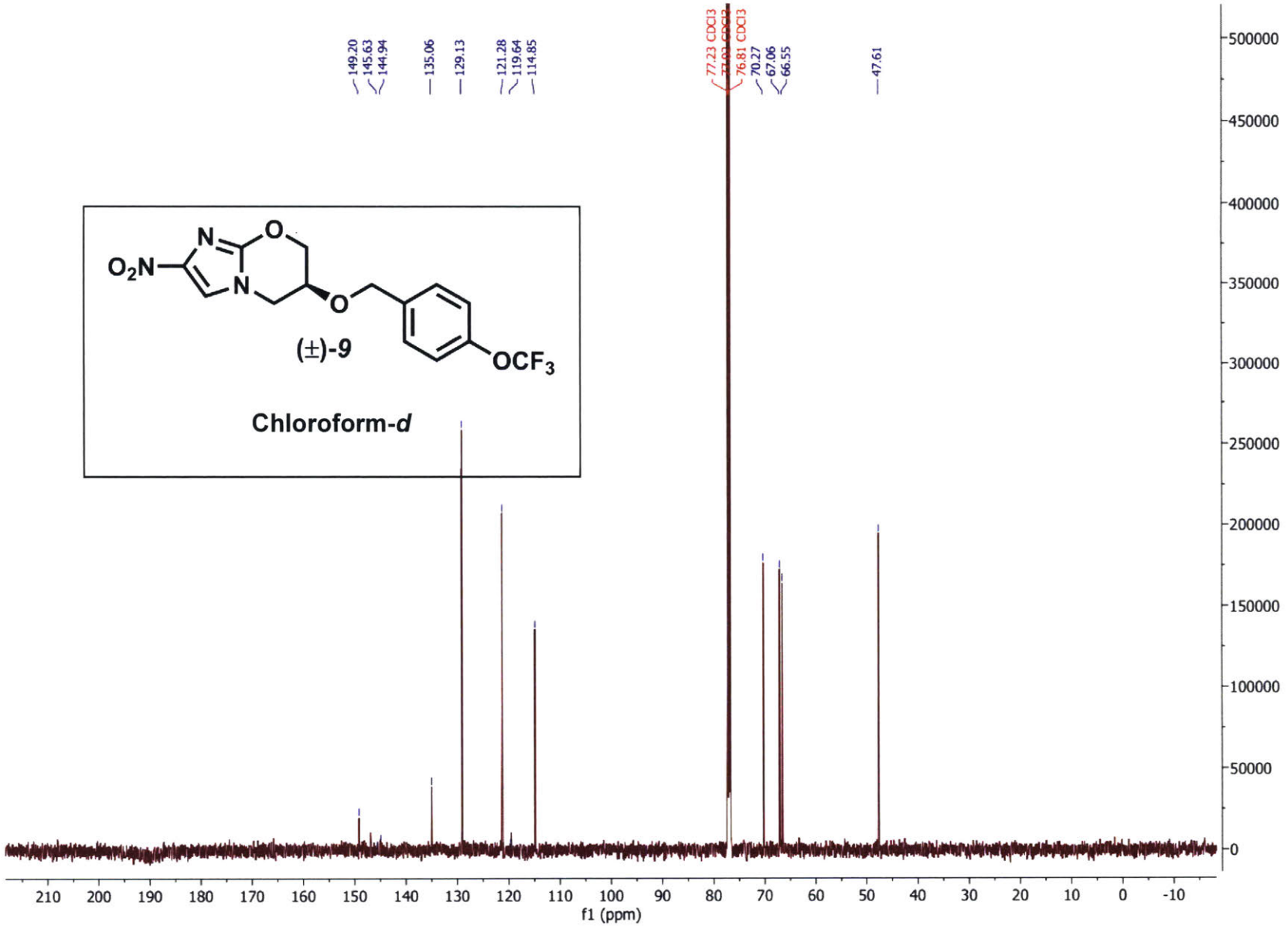
149.20
145.63
144.94
135.06
129.13
121.28
119.64
114.85
77.23 CDCl3
76.81 CDCl3
70.27
67.06
66.55
47.61
(±)-9
Chloroform-d
f1 (ppm)

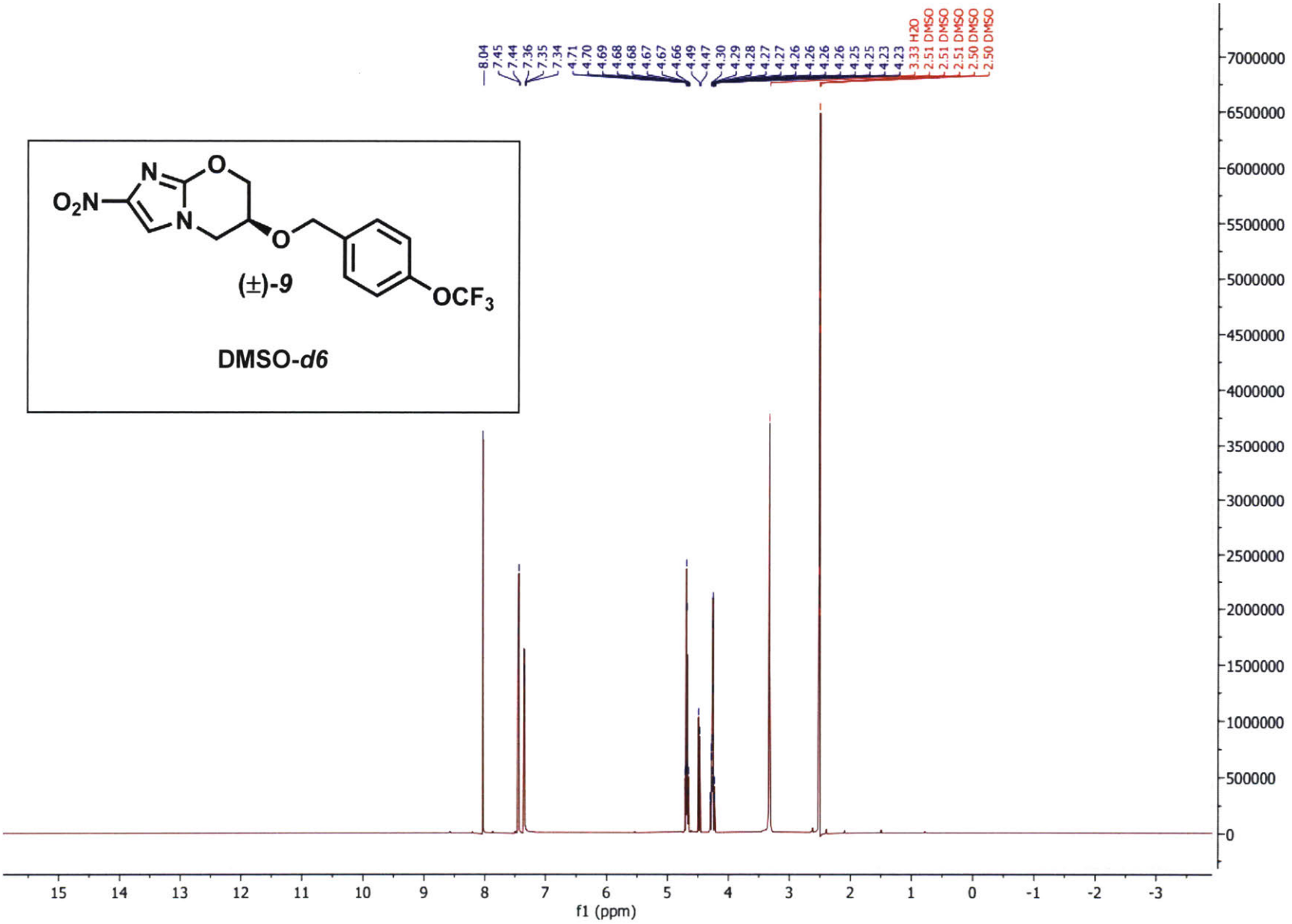
8.04
7.45
7.44
7.36
7.35
7.34
4.71
4.70
4.69
4.68
4.68
4.67
4.67
4.66
4.49
4.47
4.30
4.29
4.28
4.27
4.27
4.26
4.26
4.26
4.26
4.25
4.25
4.23
4.23
3.33 H2O
2.51 DMSO
2.51 DMSO
2.51 DMSO
2.50 DMSO
2.50 DMSO
(±)-9
DMSO-d6
f1 (ppm)

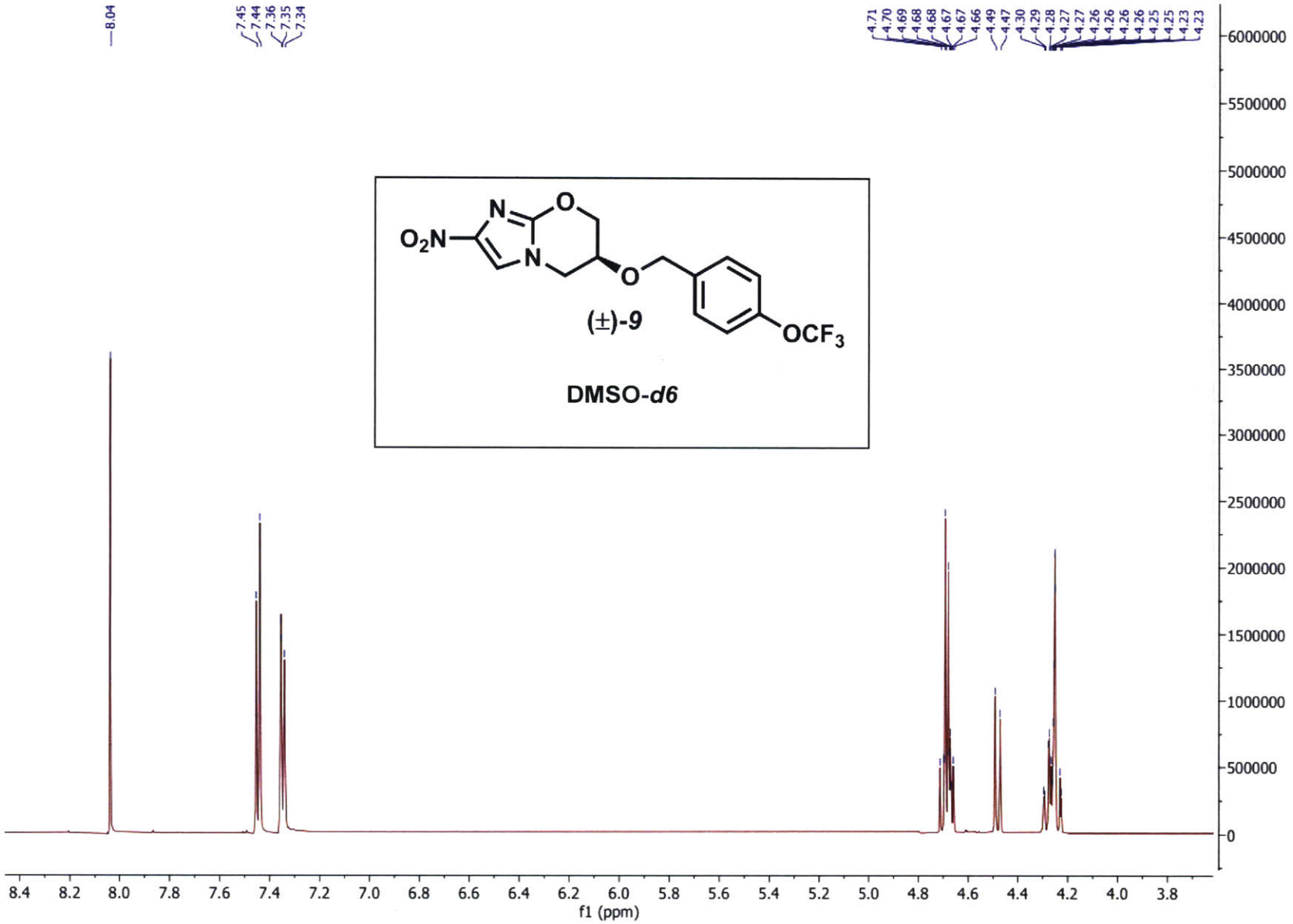
8.04
7.45
7.44
7.36
7.35
7.34
4.71
4.70
4.69
4.68
4.68
4.67
4.67
4.66
4.49
4.47
4.30
4.29
4.28
4.27
4.27
4.26
4.26
4.26
4.25
4.25
4.23
4.23
O2N
N
O
N
O
OCF3
(±)-9
DMSO-d6
6000000
5500000
5000000
4500000
4000000
3500000
3000000
2500000
2000000
1500000
1000000
500000
0
8.4
8.2
8.0
7.8
7.6
7.4
7.2
7.0
6.8
6.6
6.4
6.2
6.0
5.8
5.6
5.4
5.2
5.0
4.8
4.6
4.4
4.2
4.0
3.8
f1 (ppm)

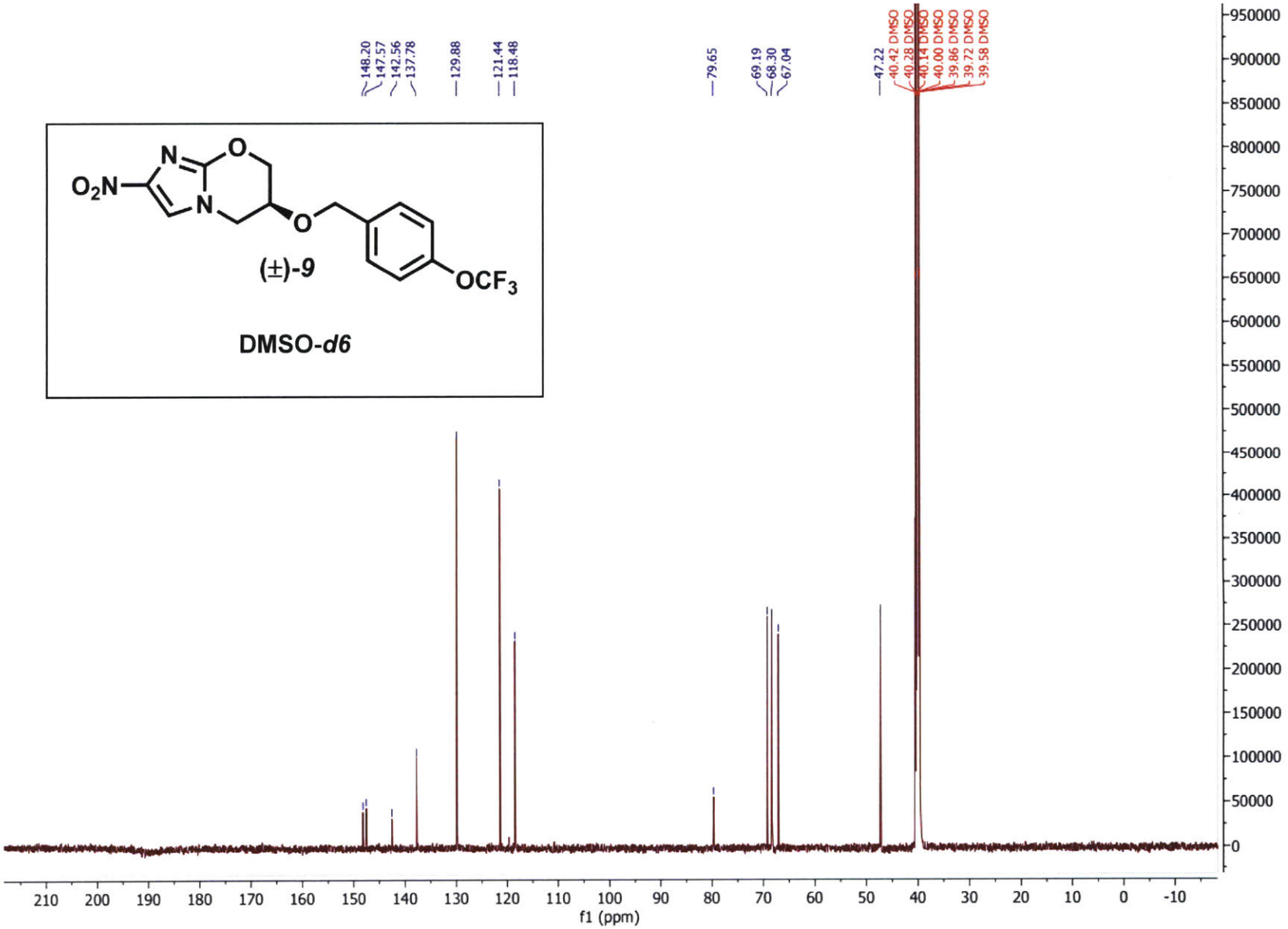
148.20
147.57
142.56
137.78
129.88
121.44
118.48
79.65
69.19
68.30
67.04
47.22
40.42 DMSO
40.28 DMSO
40.14 DMSO
40.00 DMSO
39.86 DMSO
39.72 DMSO
39.58 DMSO
O2N
N
O
N
O
(±)-9
OCF3
DMSO-d6
f1 (ppm)

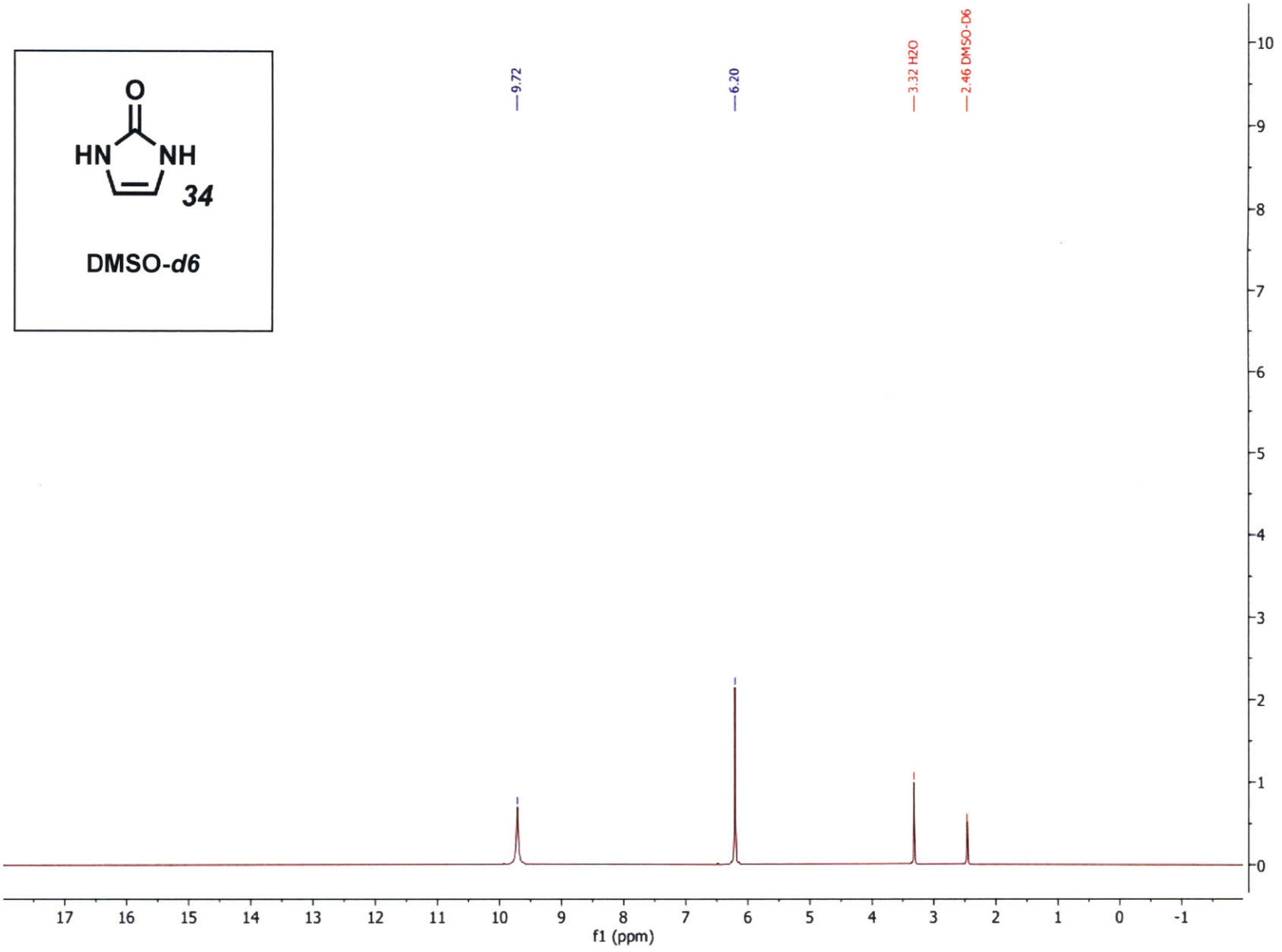
O
HN
NH
34
DMSO-d6
9.72
6.20
3.32 H2O
2.46 DMSO-D6
f1 (ppm)

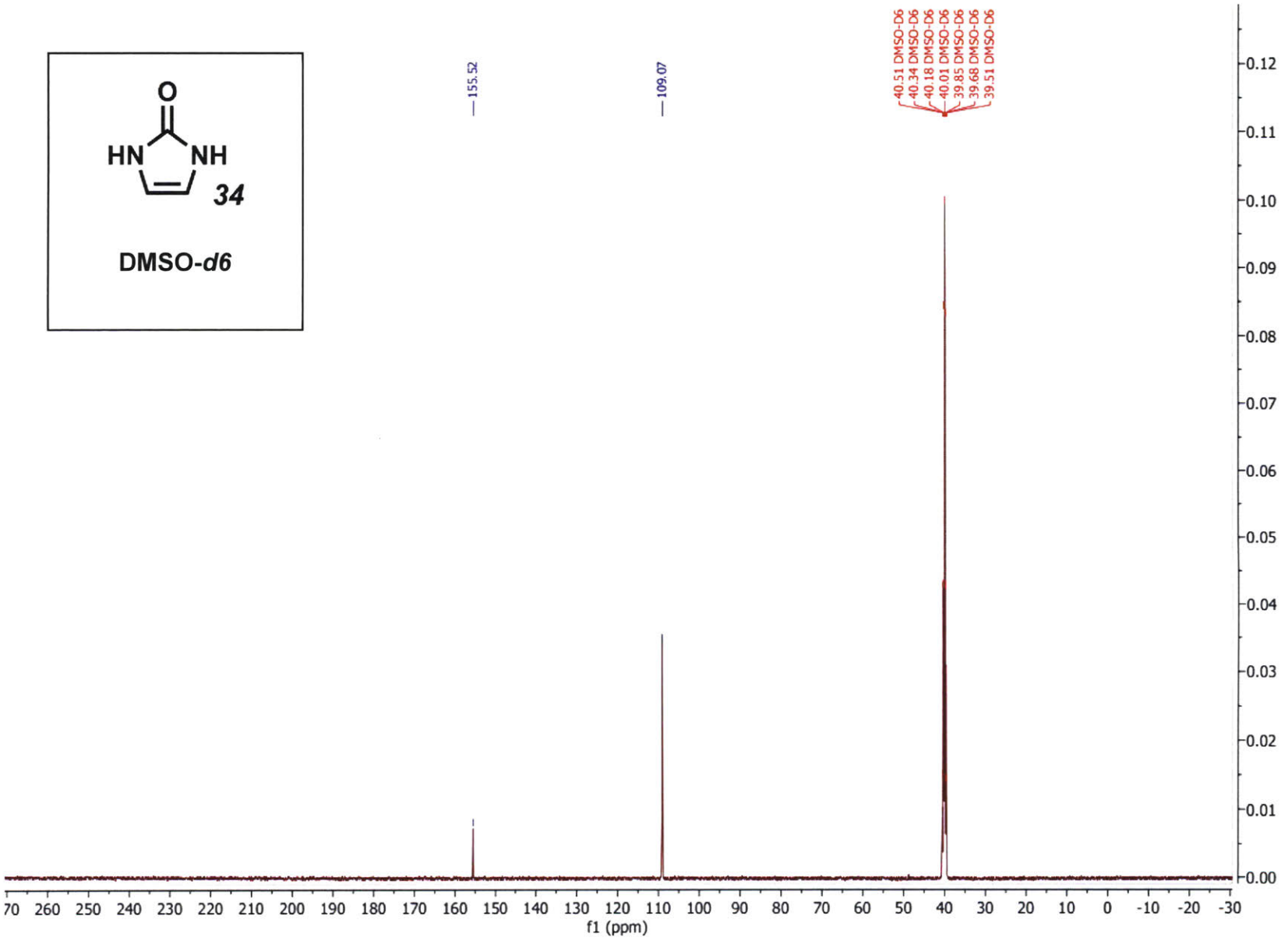
O
HN
NH
34
DMSO-d6
155.52
109.07
40.51 DMSO-D6
40.34 DMSO-D6
40.18 DMSO-D6
40.01 DMSO-D6
39.85 DMSO-D6
39.68 DMSO-D6
39.51 DMSO-D6
0.12
0.11
0.10
0.09
0.08
0.07
0.06
0.05
0.04
0.03
0.02
0.01
0.00
70 260 250 240 230 220 210 200 190 180 170 160 150 140 130 120 110 100 90 80 70 60 50 40 30 20 10 0 -10 -20 -30
f1 (ppm)

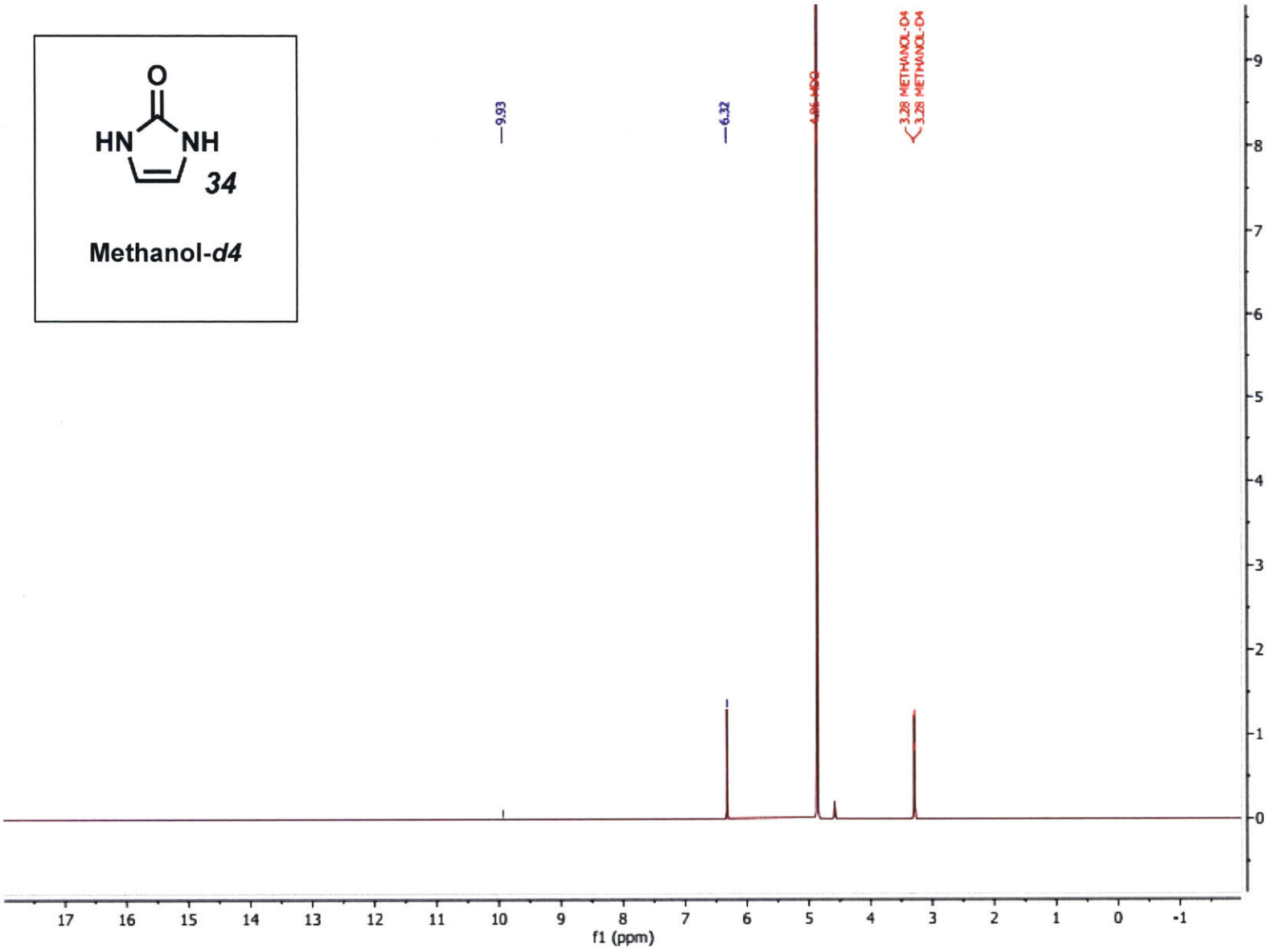
O
HN
NH
34
Methanol-d4
9.93
6.32
4.86 HDO
3.28 METHANOL-D4
3.28 METHANOL-D4
f1 (ppm)

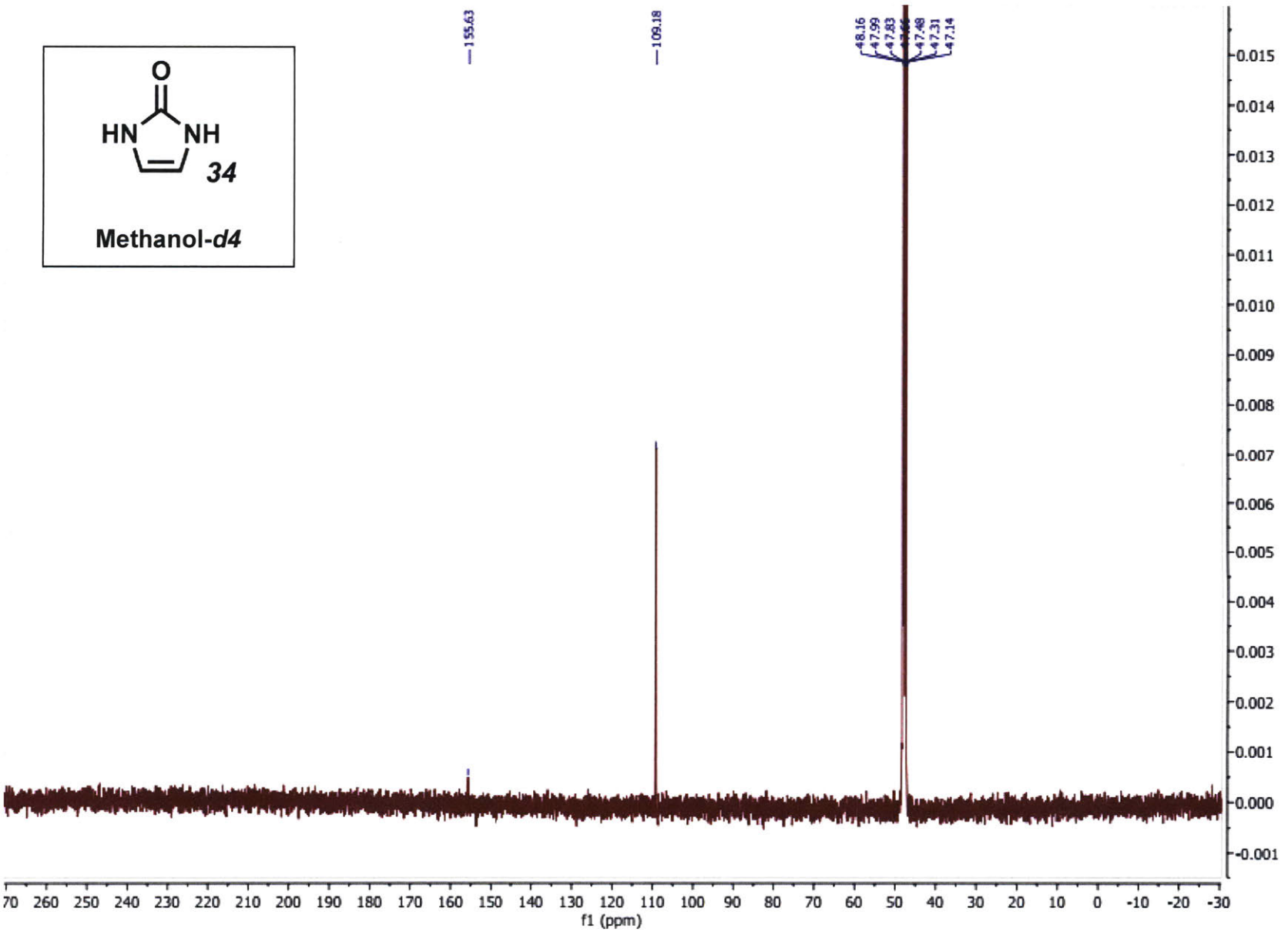
O
HN
NH
34
Methanol-d4
155.63
109.18
48.16
47.99
47.83
47.48
47.31
47.14
0.015
0.014
0.013
0.012
0.011
0.010
0.009
0.008
0.007
0.006
0.005
0.004
0.003
0.002
0.001
0.000
-0.001
70 260 250 240 230 220 210 200 190 180 170 160 150 140 130 120 110 100 90 80 70 60 50 40 30 20 10 0 -10 -20 -30
f1 (ppm)

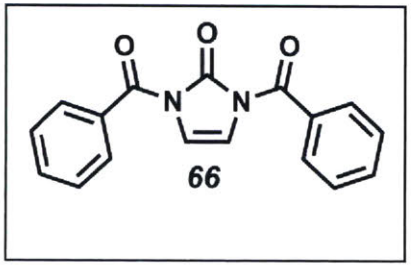
O
O
O
N
N
66

7.75
7.73
7.73
7.56
7.56
7.56
7.54
7.53
7.53
7.53
7.44
7.42
7.41
7.40
7.10
7.0
6.5
6.0
5.5
5.0
4.5
4.0
3.5
3.0
2.5
2.0
1.5
1.0
0.5
0.0
-0.5
17
16
15
14
13
12
11
10
9
8
7
6
5
4
3
2
1
0
-1
f1 (ppm)

7.75
7.73
7.73
7.56
7.56
7.56
7.54
7.53
7.53
7.53
7.44
7.42
7.41
7.40
7.10
O
O
O
N
N
66
5.5
5.0
4.5
4.0
3.5
3.0
2.5
2.0
1.5
1.0
0.5
0.0
-0.5
8.0
7.9
7.8
7.7
7.6
7.5
7.4
7.3
7.2
7.1
7.0
6.9
6.8
6.7
f1 (ppm)

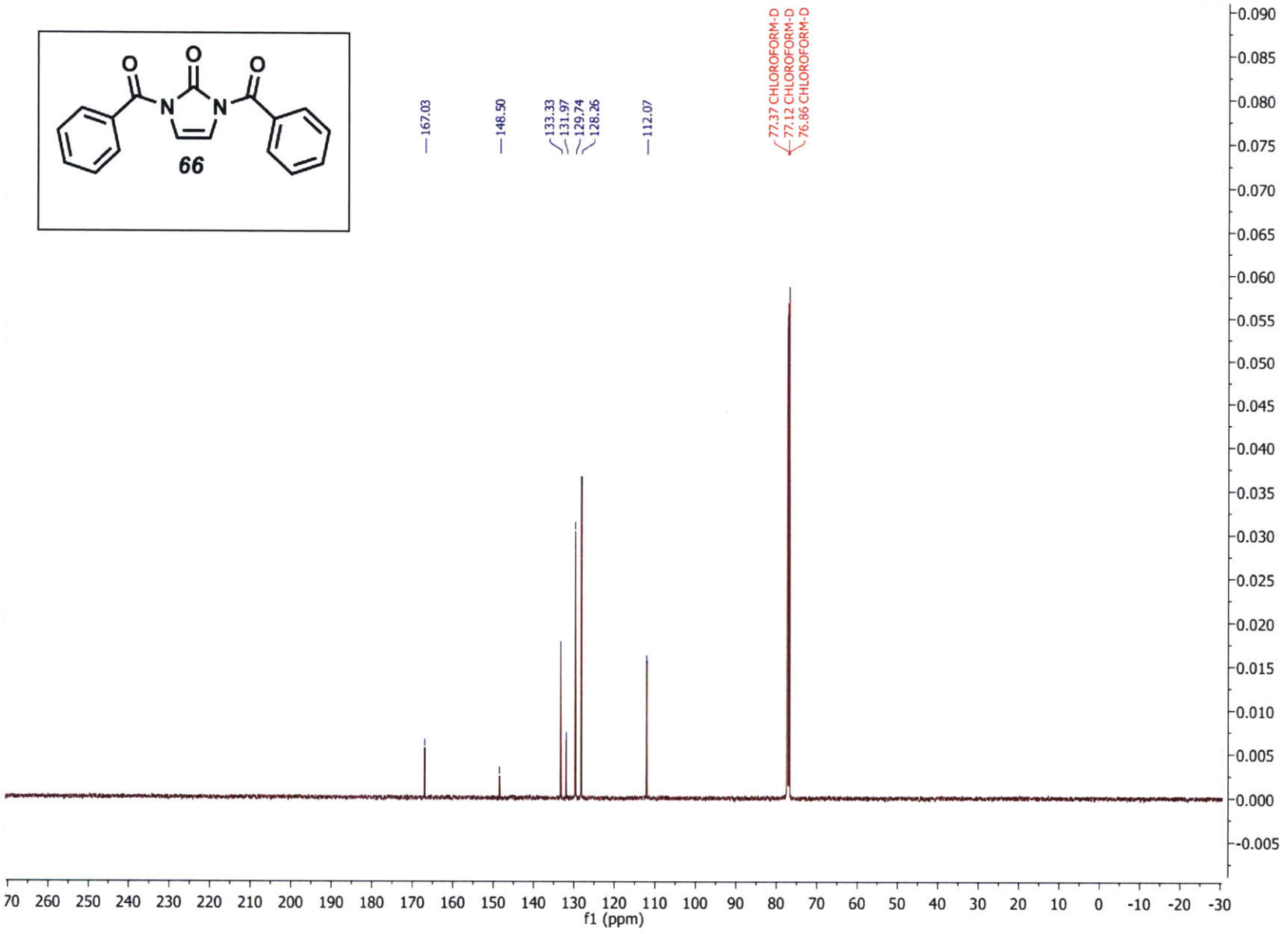
66
167.03
148.50
133.33
131.97
129.74
128.26
112.07
77.37 CHLOROFORM-D
77.12 CHLOROFORM-D
76.86 CHLOROFORM-D
f1 (ppm)

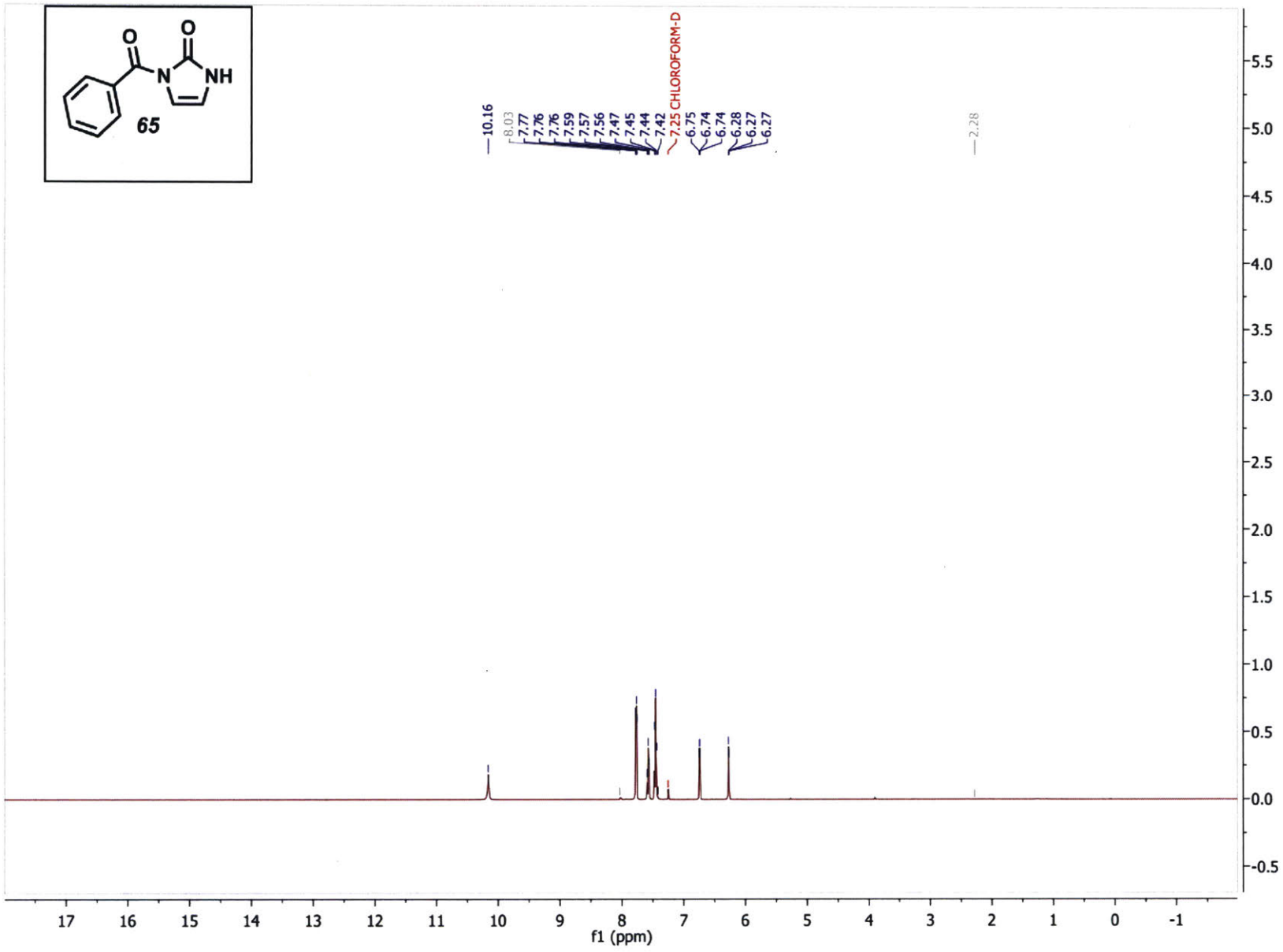
O
O
N
NH
65
10.16
8.03
7.77
7.76
7.76
7.59
7.57
7.56
7.47
7.45
7.44
7.42
7.25 CHLOROFORM-D
6.75
6.74
6.74
6.28
6.27
6.27
2.28
5.5
5.0
4.5
4.0
3.5
3.0
2.5
2.0
1.5
1.0
0.5
0.0
-0.5
17
16
15
14
13
12
11
10
9
8
7
6
5
4
3
2
1
0
-1
f1 (ppm)

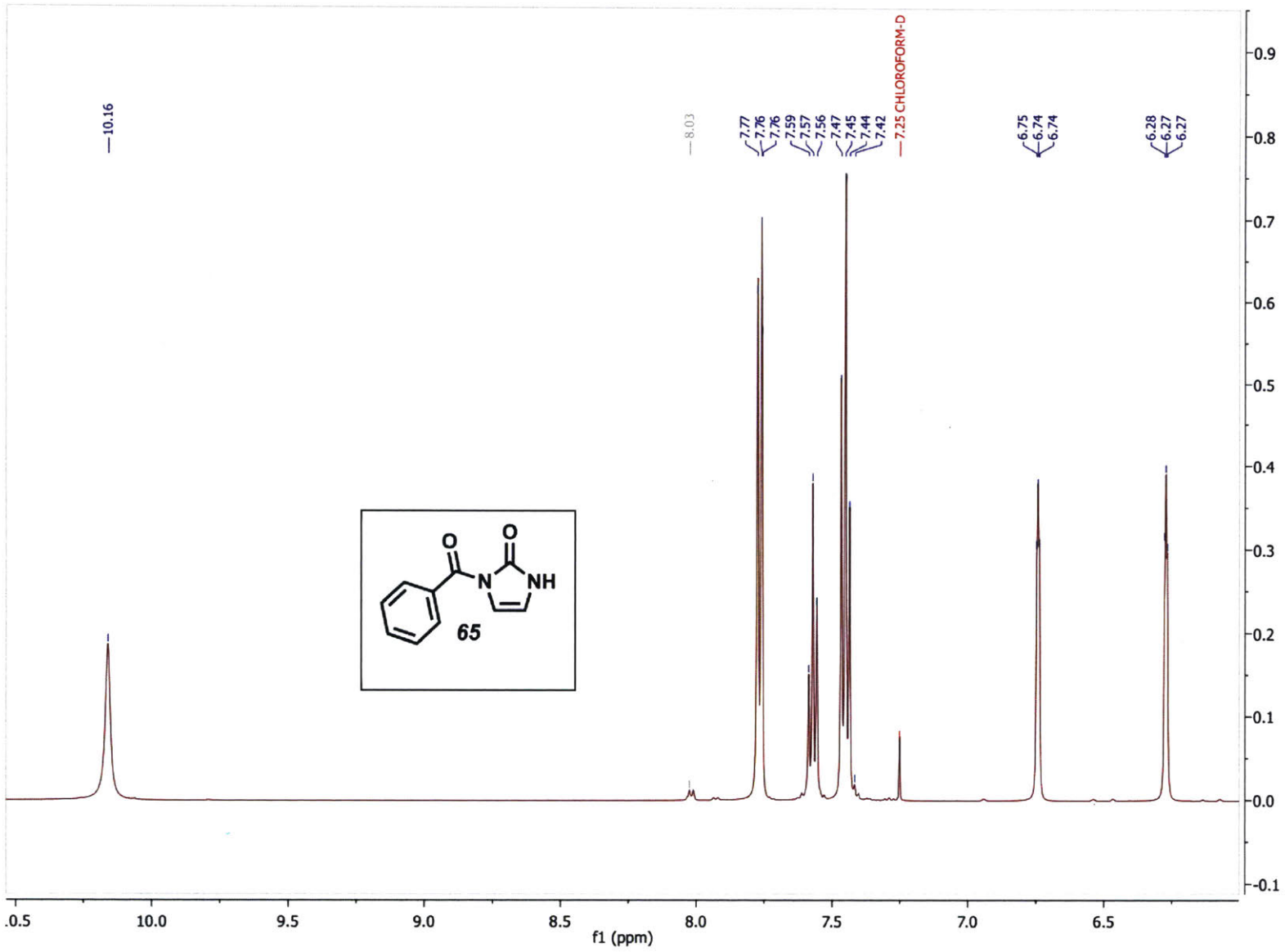
10.16
8.03
7.77
7.76
7.76
7.59
7.57
7.56
7.47
7.45
7.44
7.42
7.25 CHLOROFORM-D
6.75
6.74
6.74
6.28
6.27
6.27
O
O
N
NH
65
f1 (ppm)

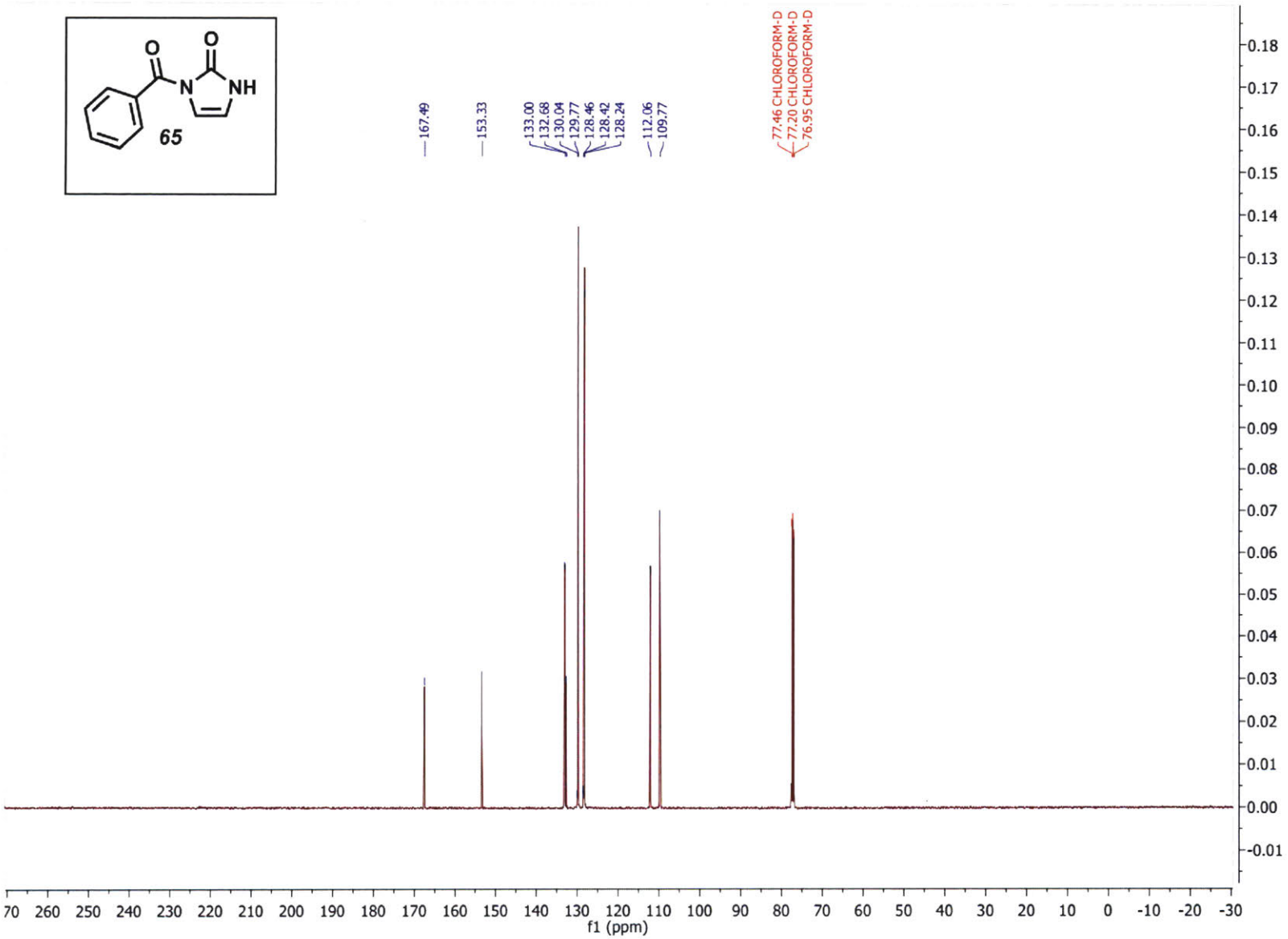
O
O
N
NH
65
167.49
153.33
133.00
132.68
130.04
129.77
128.46
128.42
128.24
112.06
109.77
77.46 CHLOROFORM-D
77.20 CHLOROFORM-D
76.95 CHLOROFORM-D
0.18
0.17
0.16
0.15
0.14
0.13
0.12
0.11
0.10
0.09
0.08
0.07
0.06
0.05
0.04
0.03
0.02
0.01
0.00
-0.01
70 260 250 240 230 220 210 200 190 180 170 160 150 140 130 120 110 100 90 80 70 60 50 40 30 20 10 0 -10 -20 -30
f1 (ppm)

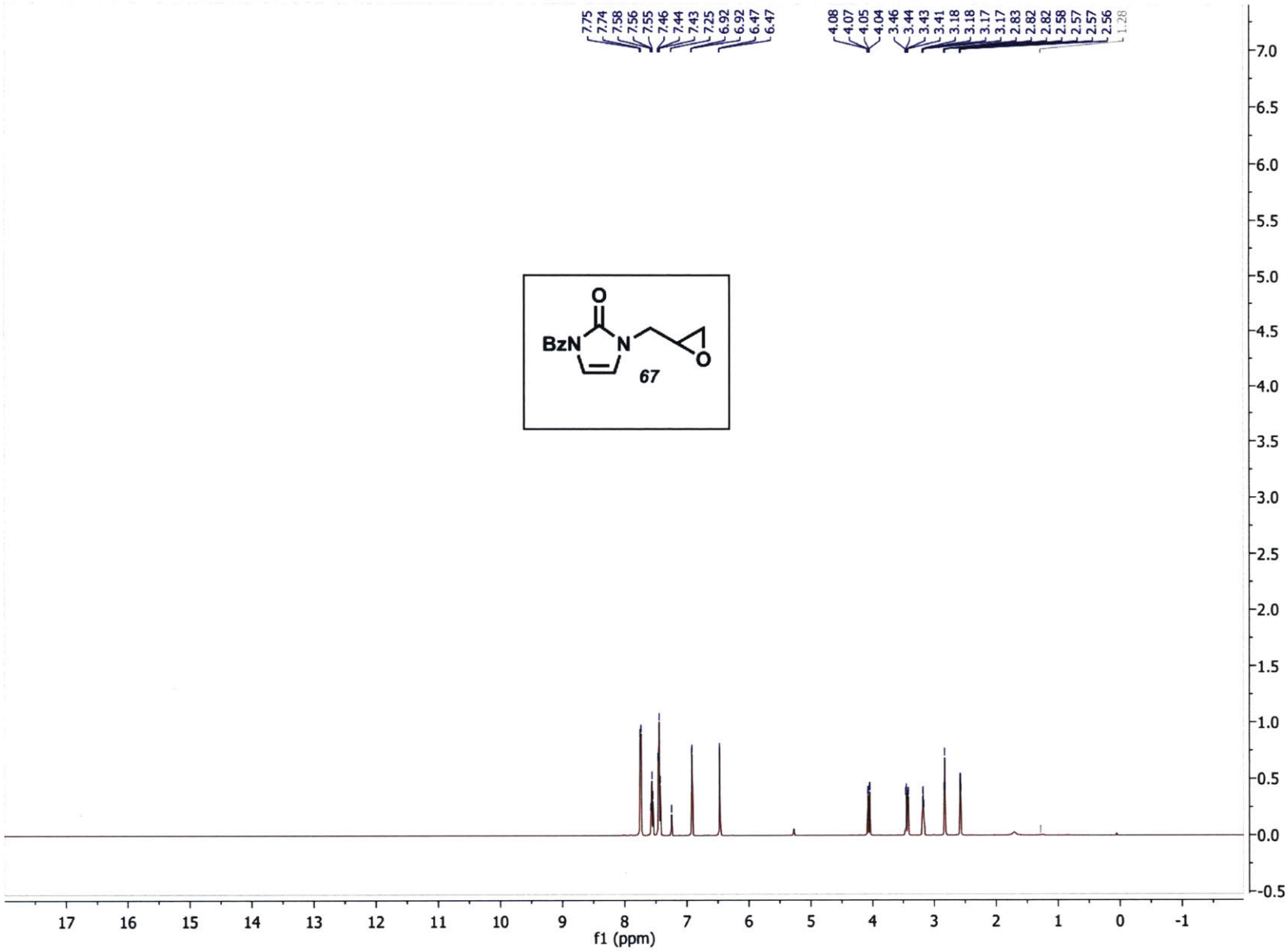
7.75
7.74
7.58
7.56
7.55
7.46
7.44
7.43
7.25
6.92
6.47
6.47
4.08
4.07
4.05
4.04
3.46
3.44
3.43
3.41
3.18
3.18
3.17
3.17
2.83
2.82
2.82
2.58
2.57
2.57
2.56
1.28
BzN
N
O
O
67
f1 (ppm)

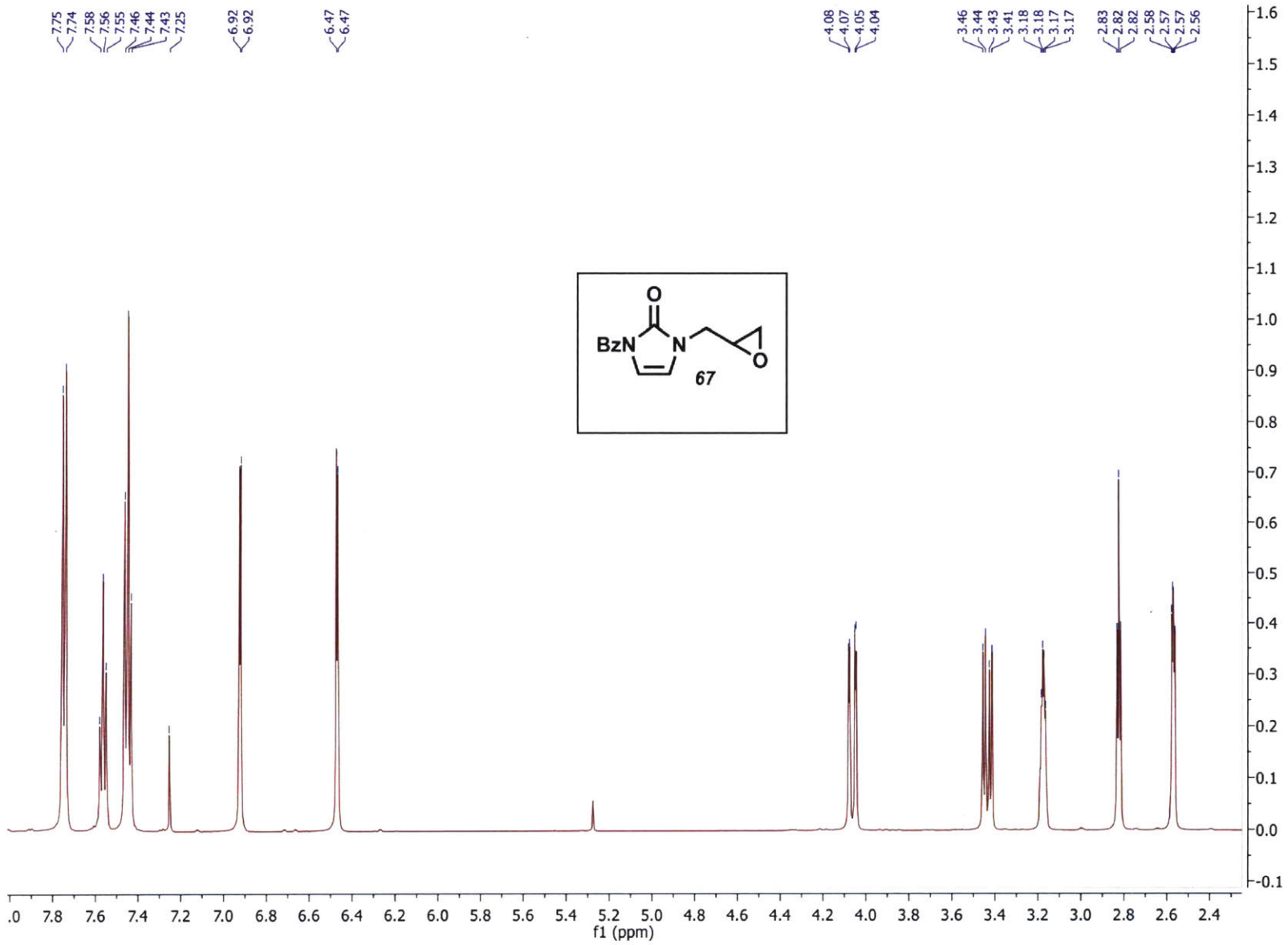
7.75
7.74
7.58
7.56
7.55
7.46
7.44
7.43
7.25
6.92
6.92
6.47
6.47
4.08
4.07
4.05
4.04
3.46
3.44
3.43
3.41
3.18
3.18
3.17
3.17
2.83
2.82
2.82
2.58
2.57
2.57
2.56
BzN
O
N
O
67
f1 (ppm)

BzN
N
O
O
67
167.48
151.07
132.87
132.59
129.79
129.59
128.04
115.06
108.48
77.42 CHLOROFORM-D
77.17 CHLOROFORM-D
76.91 CHLOROFORM-D
50.16
45.02
44.98
f1 (ppm)

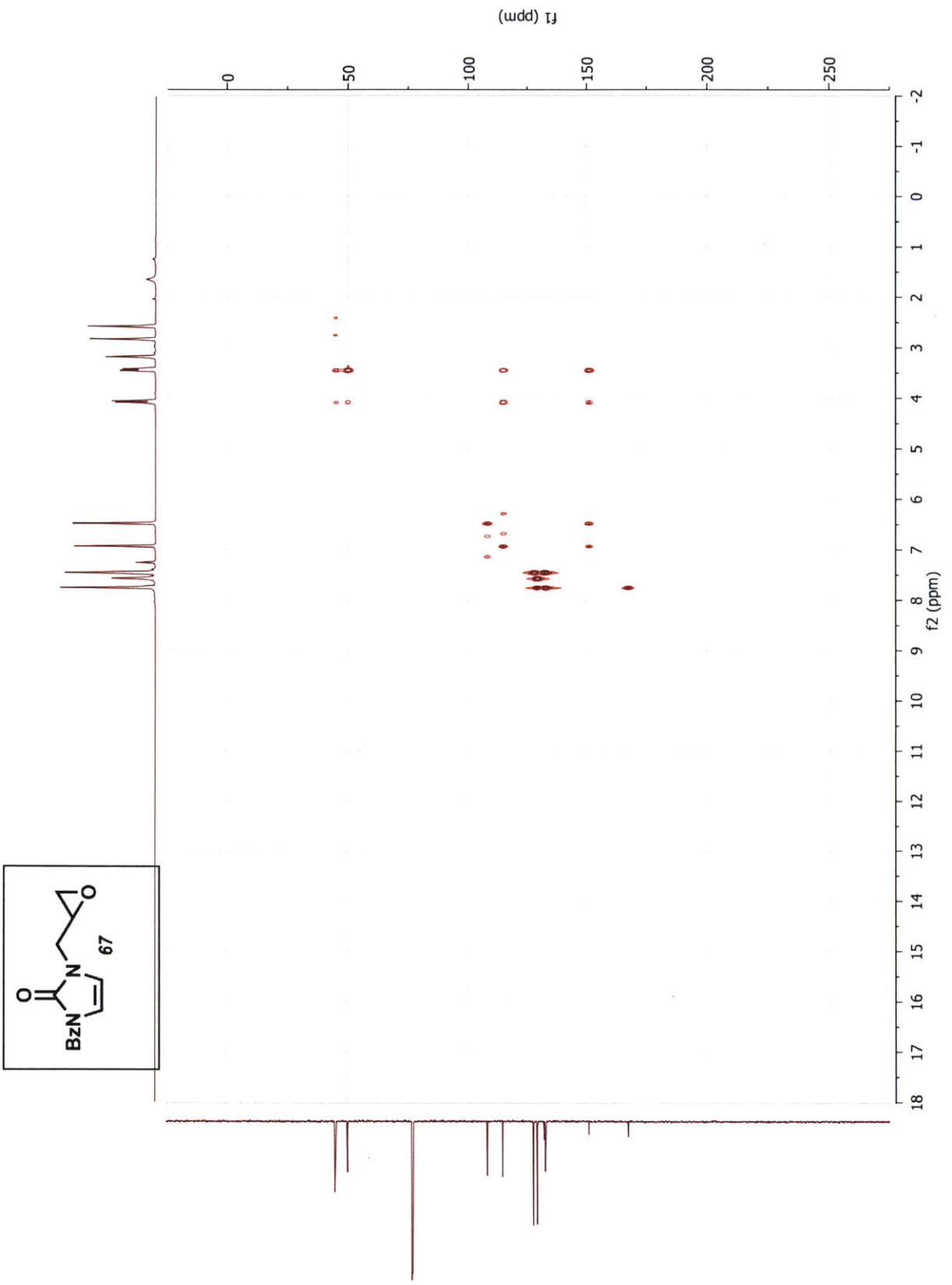
f1 (ppm)
f2 (ppm)
BzN
67

O
O
HN
N
60
10.43
7.25 CHLOROFORM-D
6.30
6.29
6.29
6.28
6.28
4.08
4.08
4.05
4.05
3.60
3.59
3.57
3.56
3.21
3.20
3.20
3.19
3.18
3.18
2.82
2.81
2.80
2.56
2.55
2.55
2.55
1.79 HDO
1.24
1.23
f1 (ppm)

10.43
7.25 CHLOROFORM-D
6.30
6.29
6.29
6.28
6.28
4.08
4.08
4.05
4.05
3.60
3.59
3.57
3.56
3.21
3.20
3.20
3.19
3.18
3.18
2.82
2.81
2.80
2.56
2.55
2.55
2.55
1.79 HDO
HN
N
O
O
60
f1 (ppm)

154.75
112.23
108.48
77.37 CHLOROFORM-D
77.11 CHLOROFORM-D
76.86 CHLOROFORM-D
50.60
44.89
44.43
O
O
HN
N
60
f1 (ppm)

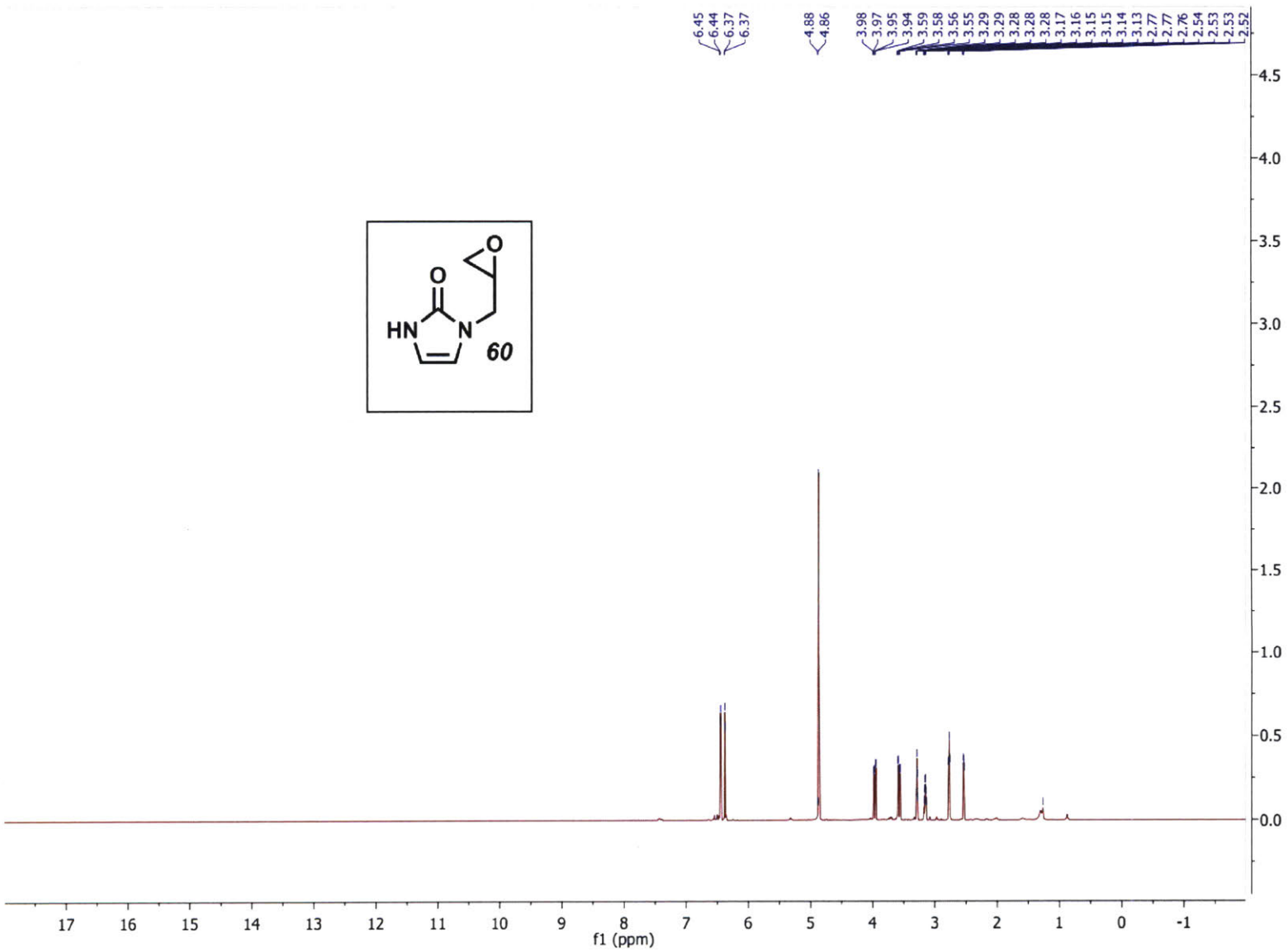
6.45
6.44
6.37
6.37
4.88
4.86
3.98
3.97
3.95
3.94
3.59
3.58
3.56
3.55
3.29
3.29
3.28
3.28
3.28
3.17
3.16
3.15
3.15
3.14
3.13
2.77
2.77
2.76
2.54
2.53
2.53
2.52
HN
N
O
O
60
4.5
4.0
3.5
3.0
2.5
2.0
1.5
1.0
0.5
0.0
17
16
15
14
13
12
11
10
9
8
7
6
5
4
3
2
1
0
-1
f1 (ppm)

6.45
6.44
6.37
6.37
4.88
4.86
3.98
3.97
3.95
3.94
3.59
3.58
3.56
3.55
3.29
3.28
3.28
3.28
3.17
3.16
3.15
3.15
3.14
3.13
2.77
2.77
2.76
2.54
2.53
2.53
2.52
1.26
HN
N
O
O
60
f1 (ppm)

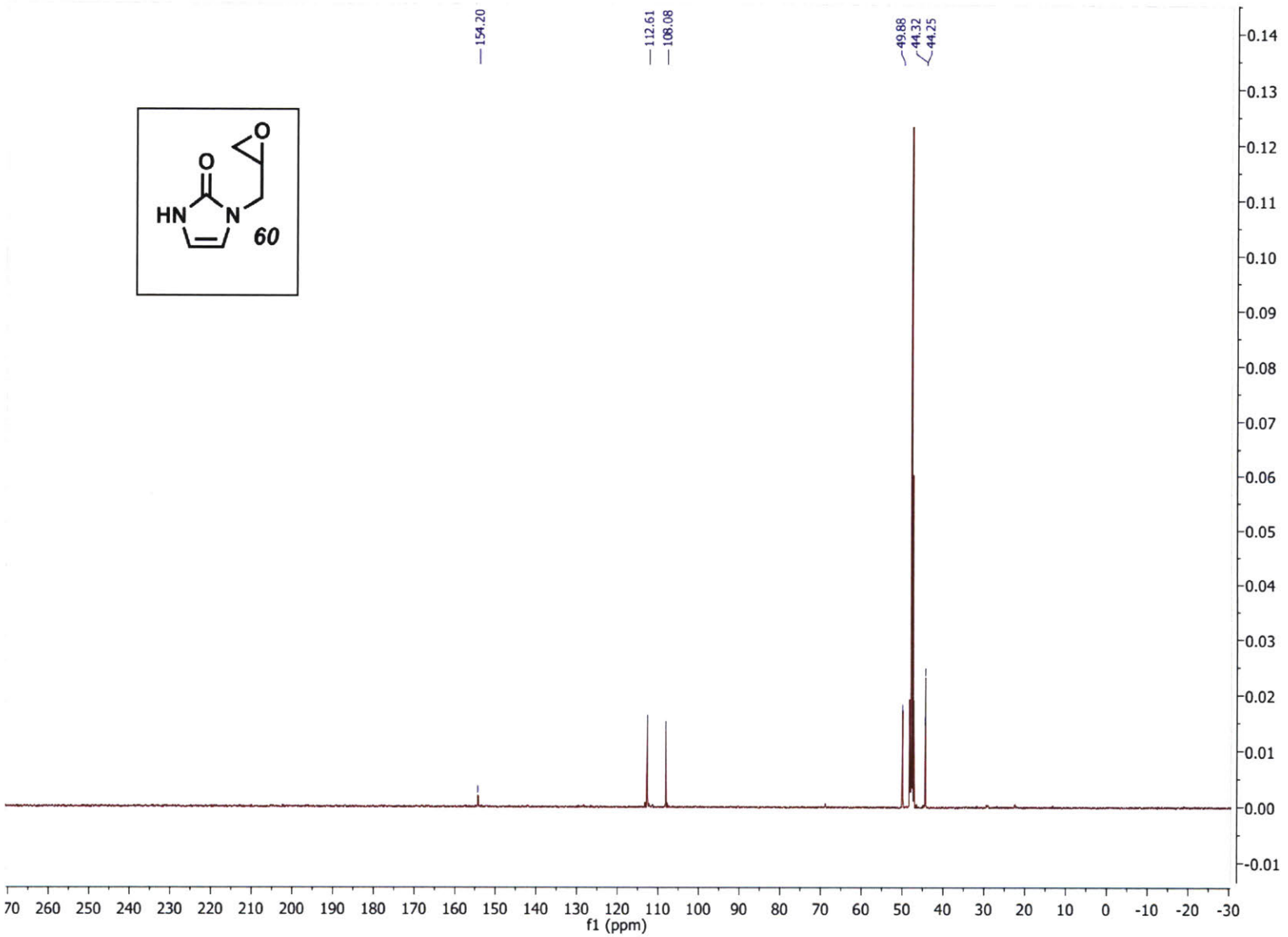
154.20
112.61
108.08
49.88
44.32
44.25
O
O
HN
N
60
0.14
0.13
0.12
0.11
0.10
0.09
0.08
0.07
0.06
0.05
0.04
0.03
0.02
0.01
0.00
-0.01
70 260 250 240 230 220 210 200 190 180 170 160 150 140 130 120 110 100 90 80 70 60 50 40 30 20 10 0 -10 -20 -30
f1 (ppm)

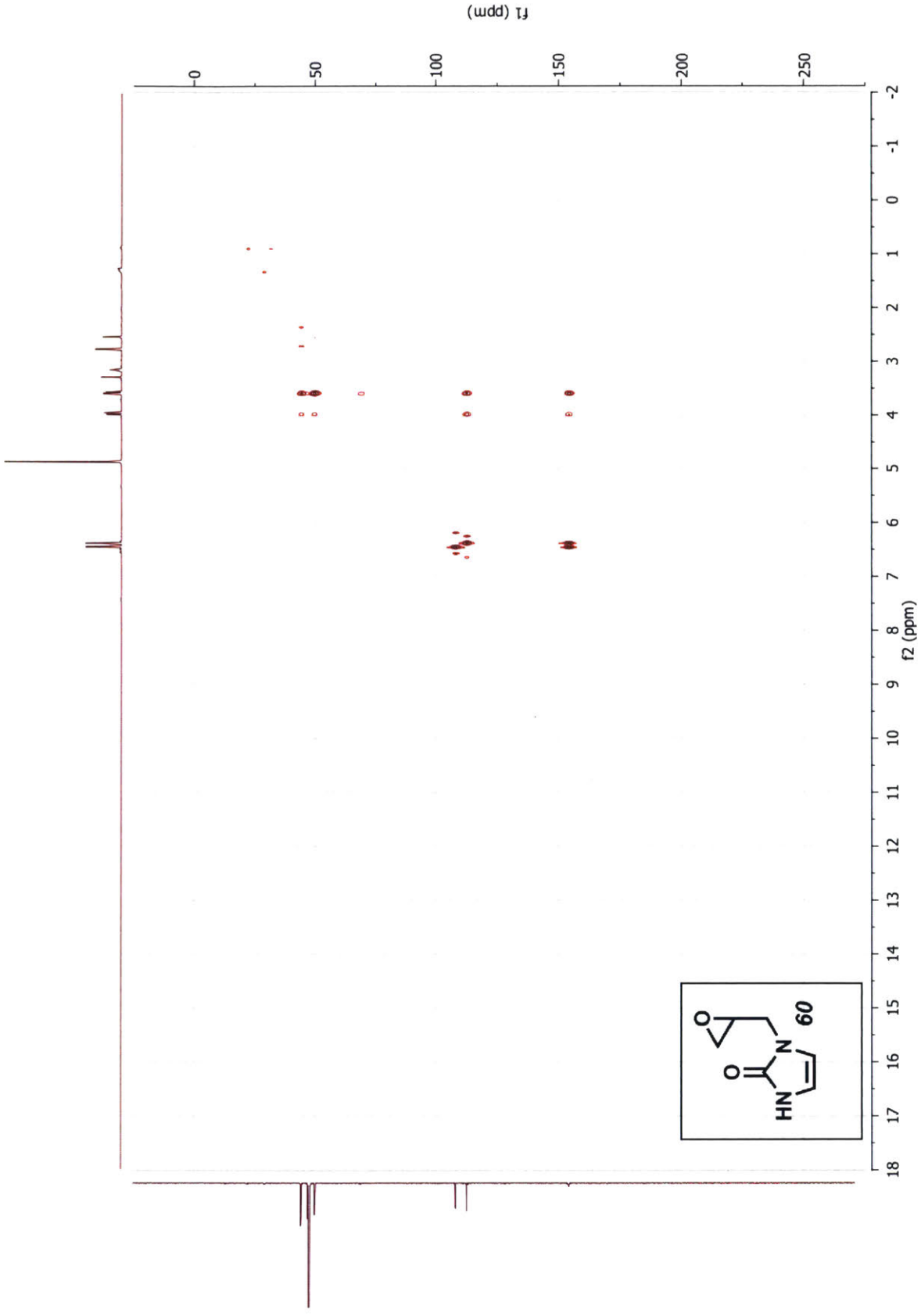
f1 (ppm)
0
50
100
150
200
250
f2 (ppm)
-2
-1
0
1
2
3
4
5
6
7
8
9
10
11
12
13
14
15
16
17
18
O
N
O
HN
60

HO
TMS
O
(±)-92
7.92
7.91
7.90
7.85
7.85
7.84
7.84
7.50
7.35
7.34
7.32
7.25 CHLOROFORM-D
4.92
4.90
3.92
3.92
3.90
3.89
3.50
3.49
3.47
3.46
2.98
2.97
2.97
2.97
2.20
2.19
0.11
0.07
0.01
0.01
0.00
1.00
1.03
0.95
0.91
f1 (ppm)

3.92
3.92
3.90
3.89
3.50
3.49
3.47
3.46
2.98
2.97
2.97
2.97
2.20
2.19
0.11
0.07
0.01
0.01
0.00
HO
TMS
O
(±)-92
1.00
1.03
0.95
0.91
4.0
3.5
3.0
2.5
2.0
1.5
1.0
0.5
0.0
f1 (ppm)
2.8
2.6
2.4
2.2
2.0
1.8
1.6
1.4
1.2
1.0
0.8
0.6
0.4
0.2
0.0
-0.2

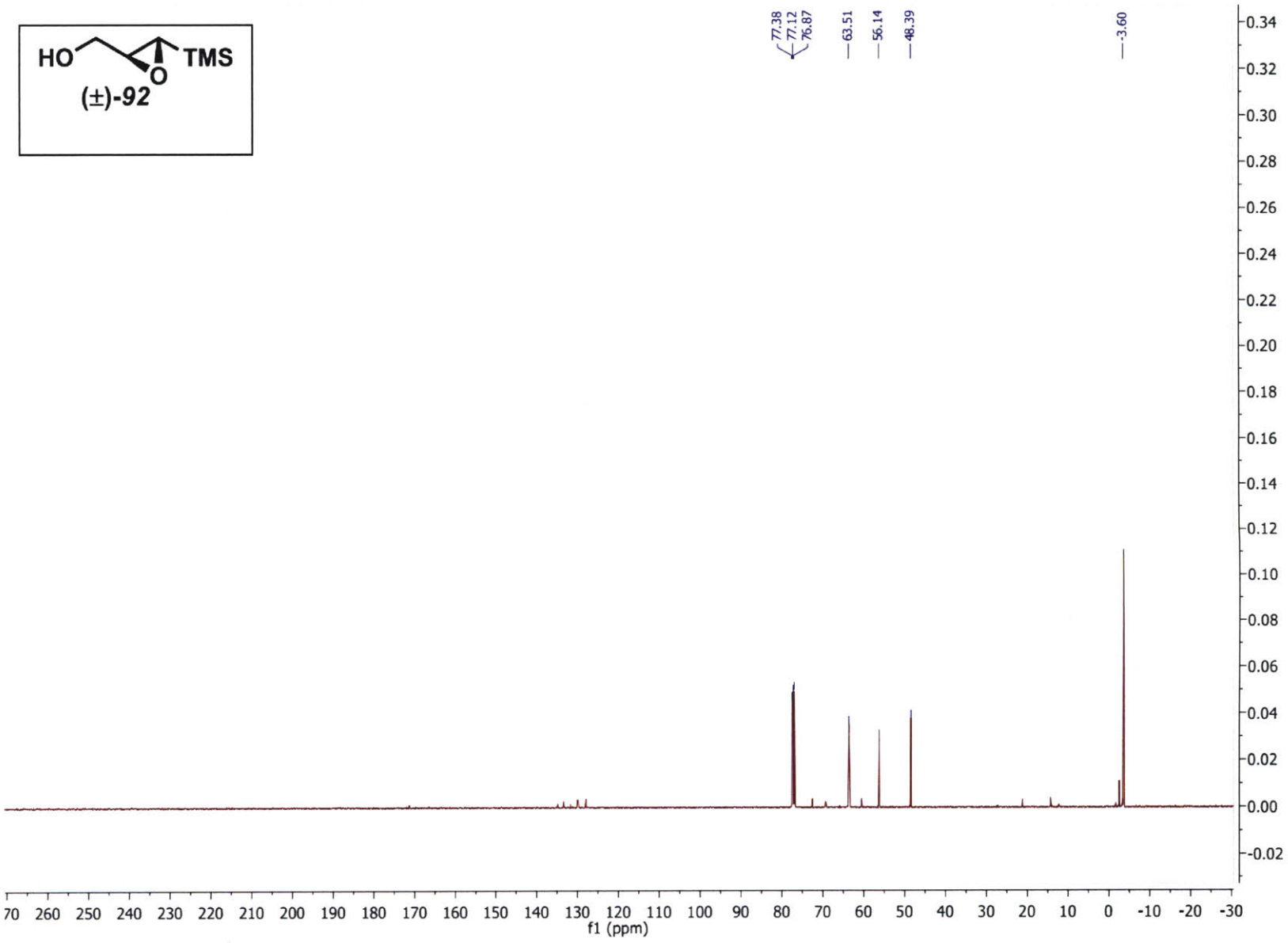
HO
TMS
O
(±)-92
77.38
77.12
76.87
63.51
56.14
48.39
-3.60
f1 (ppm)

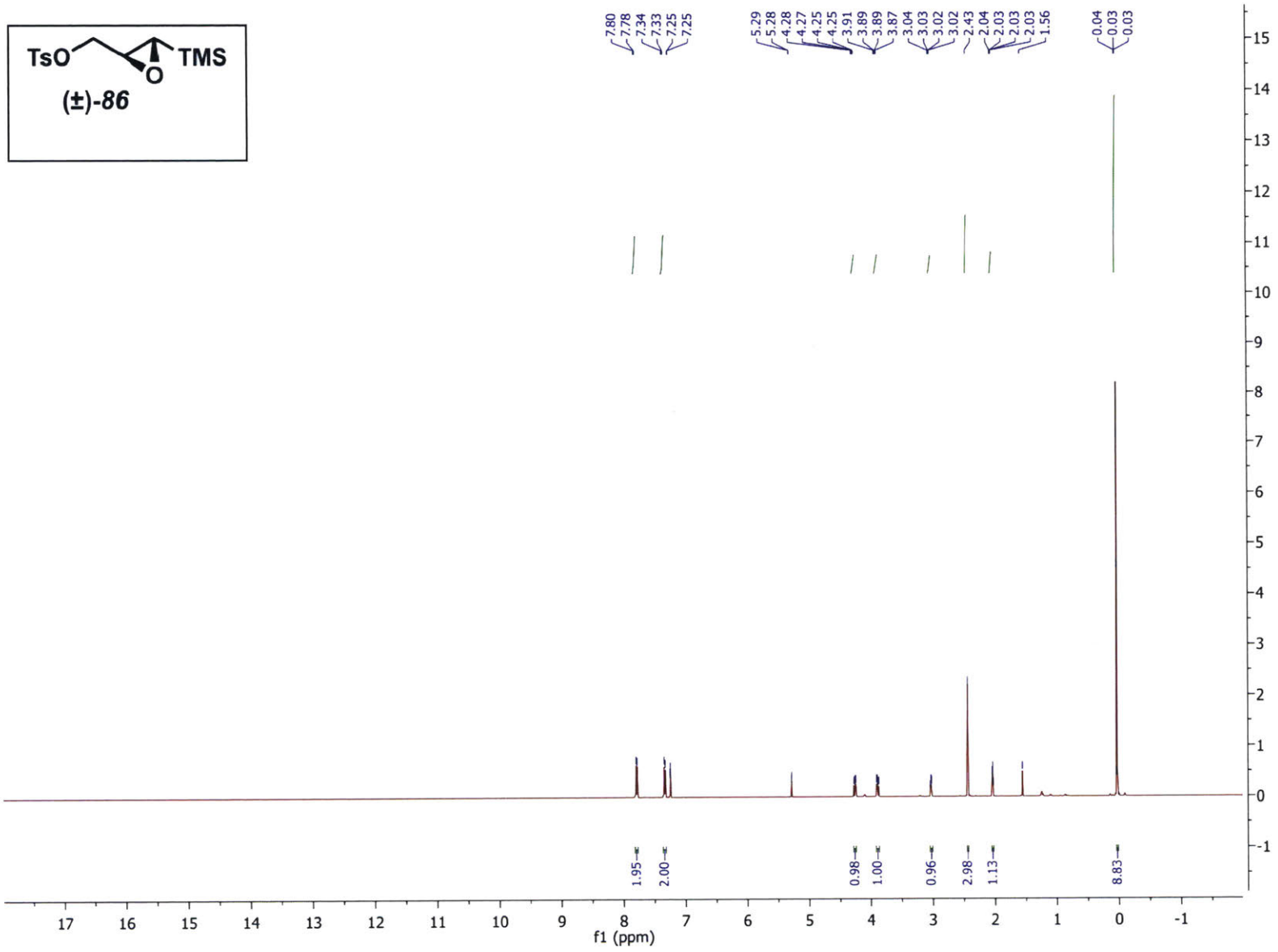
TsO
TMS
O
(±)-86
7.80
7.78
7.34
7.33
7.25
7.25
5.29
5.28
4.28
4.27
4.25
4.25
3.91
3.89
3.89
3.87
3.04
3.03
3.02
3.02
2.43
2.04
2.03
2.03
2.03
1.56
0.04
0.03
0.03
1.95
2.00
0.98
1.00
0.96
2.98
1.13
8.83
f1 (ppm)

7.80
7.78
7.34
7.33
7.25
7.25
5.29
5.28
4.28
4.27
4.25
4.25
3.91
3.89
3.89
3.87
3.04
3.03
3.02
3.02
2.43
2.04
2.03
2.03
2.03
1.56
0.04
0.03
0.03
TsO
TMS
O
(±)-86
1.95
2.00
0.98
1.00
0.96
2.98
1.13
8.83
f1 (ppm)

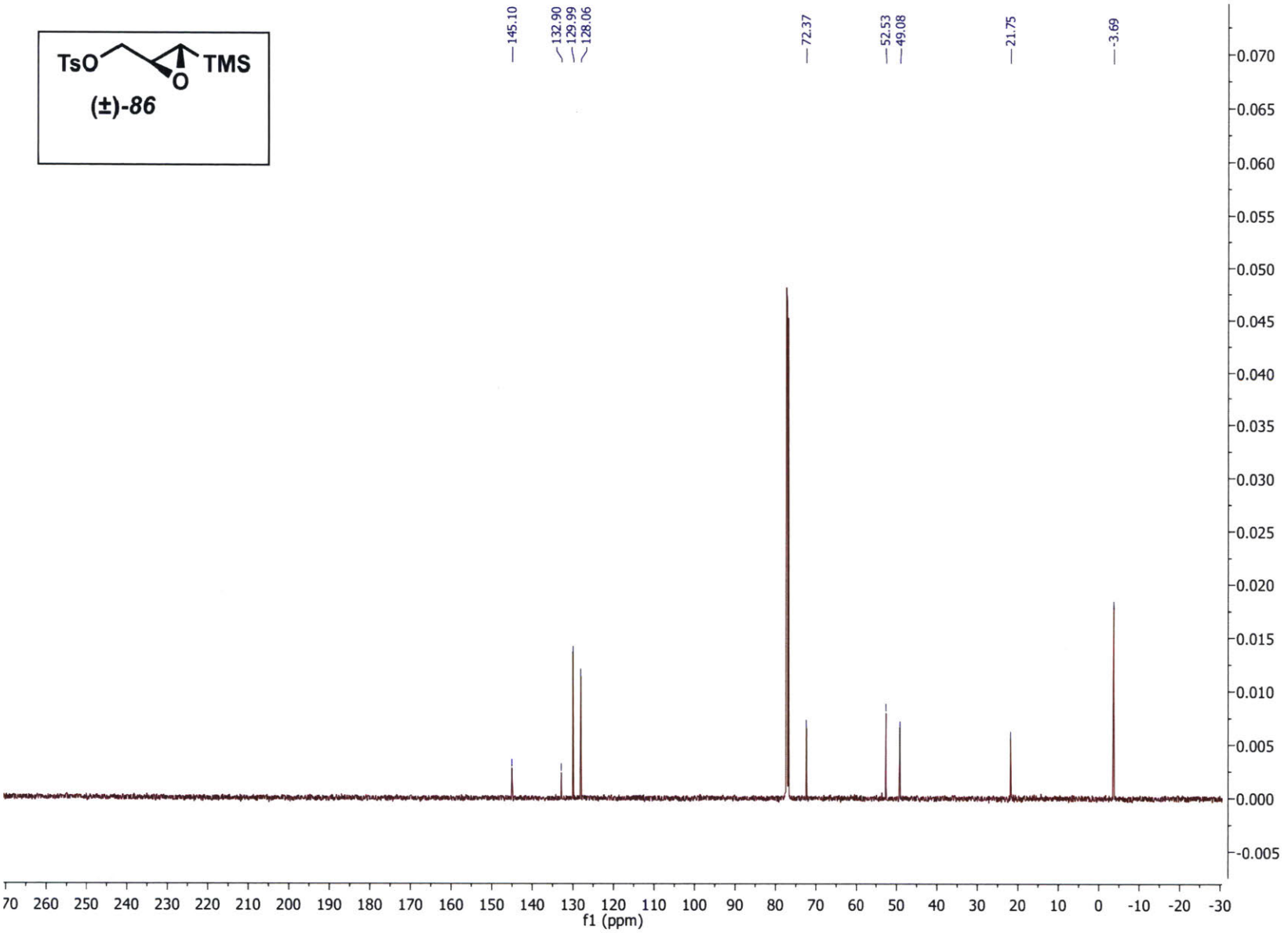
TsO
TMS
O
(±)-86
145.10
132.90
129.99
128.06
72.37
52.53
49.08
21.75
-3.69
f1 (ppm)

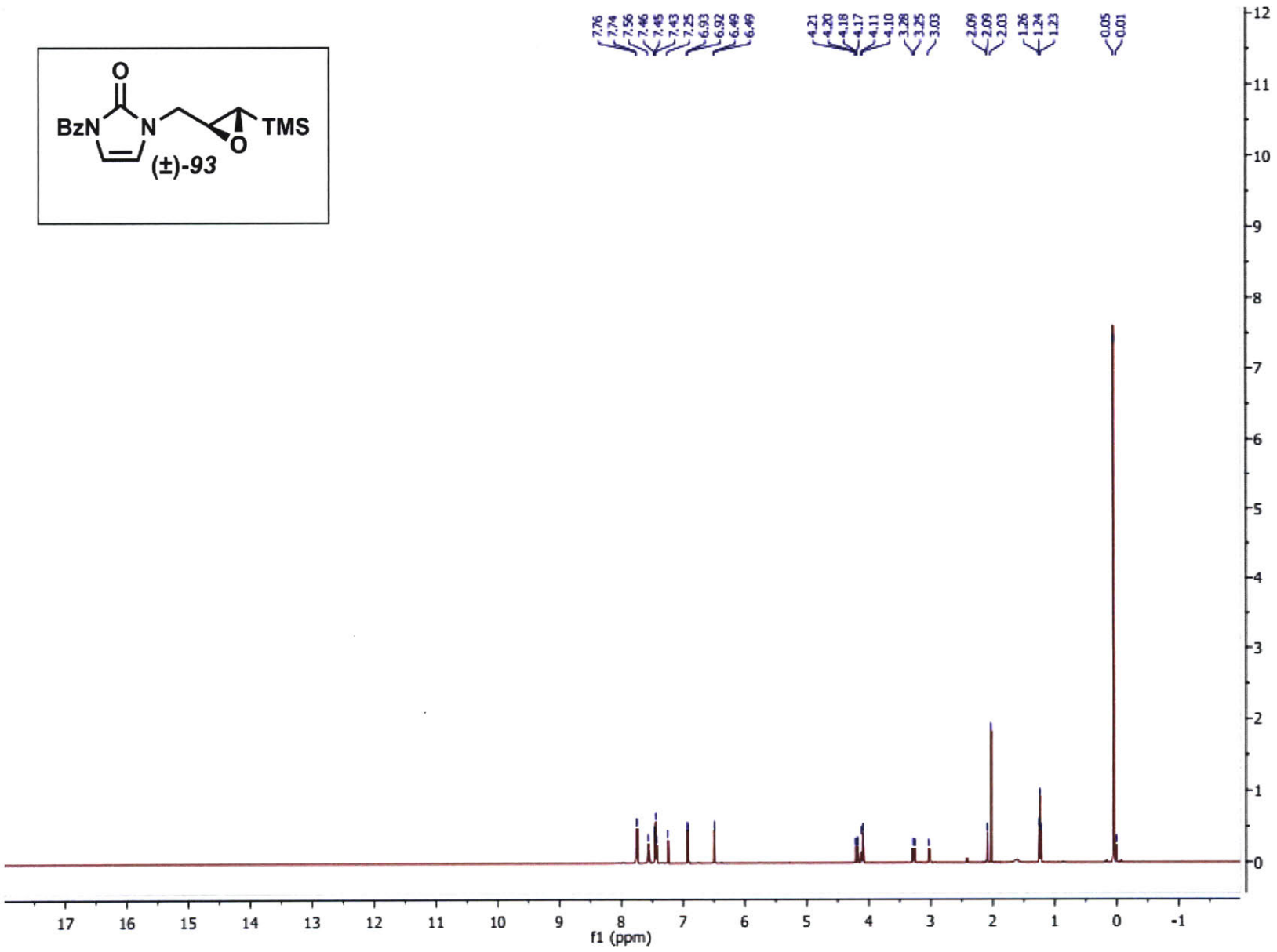
BzN
N
O
O
TMS
(±)-93
7.76
7.74
7.56
7.46
7.45
7.43
7.25
6.93
6.92
6.49
6.49
4.21
4.20
4.18
4.17
4.11
4.10
3.28
3.25
3.03
2.09
2.09
2.03
1.26
1.24
1.23
0.05
0.01
f1 (ppm)

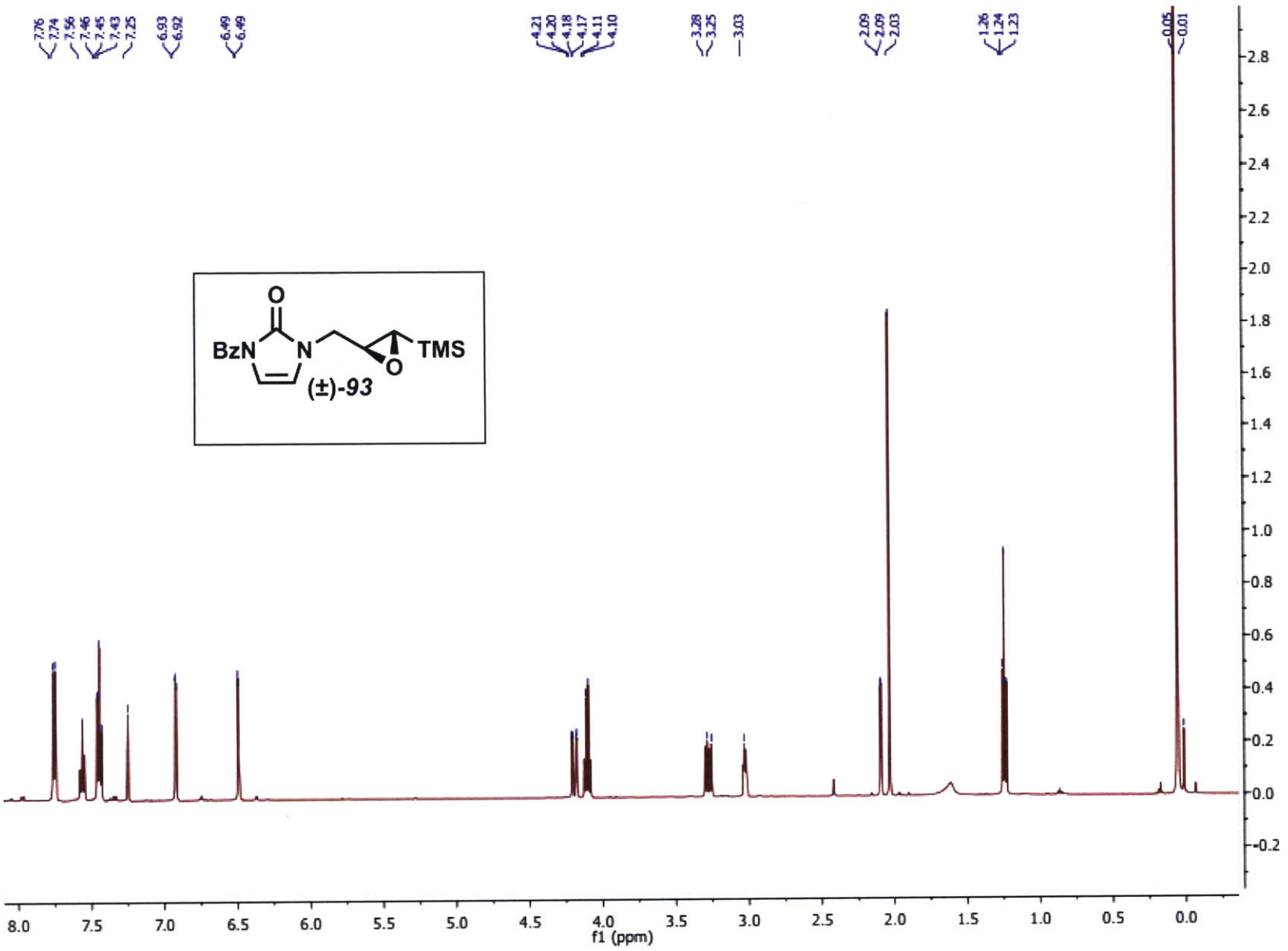
7.76
7.74
7.56
7.46
7.45
7.43
7.25
6.93
6.92
6.49
6.49
4.21
4.20
4.18
4.17
4.11
4.10
3.28
3.25
3.03
2.09
2.09
2.03
1.26
1.24
1.23
0.05
0.01
BzN
N
O
O
TMS
(±)-93
f1 (ppm)

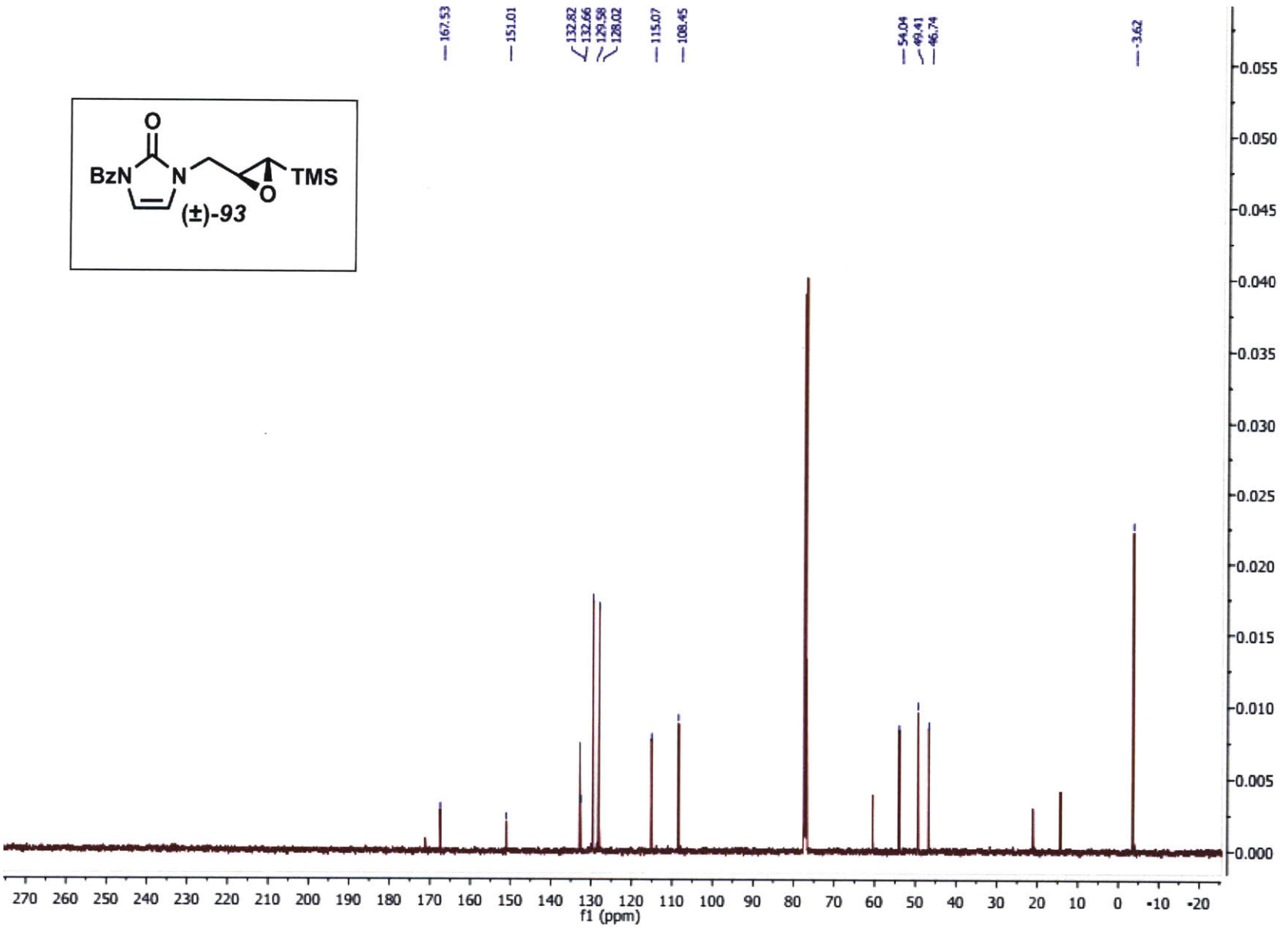
167.53
151.01
132.82
132.66
129.58
128.02
115.07
108.45
54.04
49.41
46.74
-3.62
BzN
N
O
TMS
(±)-93
f1 (ppm)

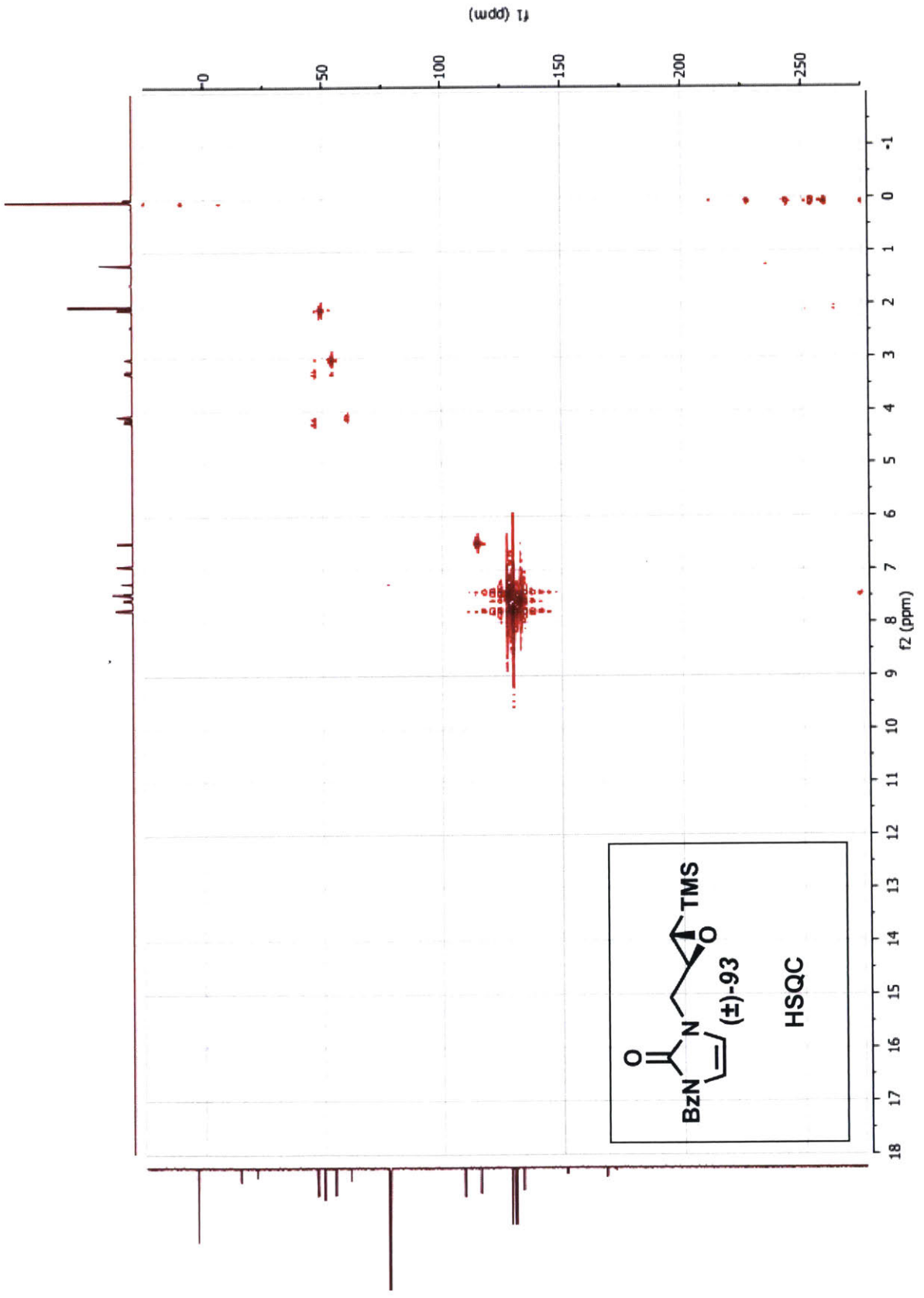
f1 (ppm)
0
50
100
150
200
250
f2 (ppm)
-1
0
1
2
3
4
5
6
7
8
9
10
11
12
13
14
15
16
17
18
BzN
O
N
(±)-93
O
TMS
HSQC

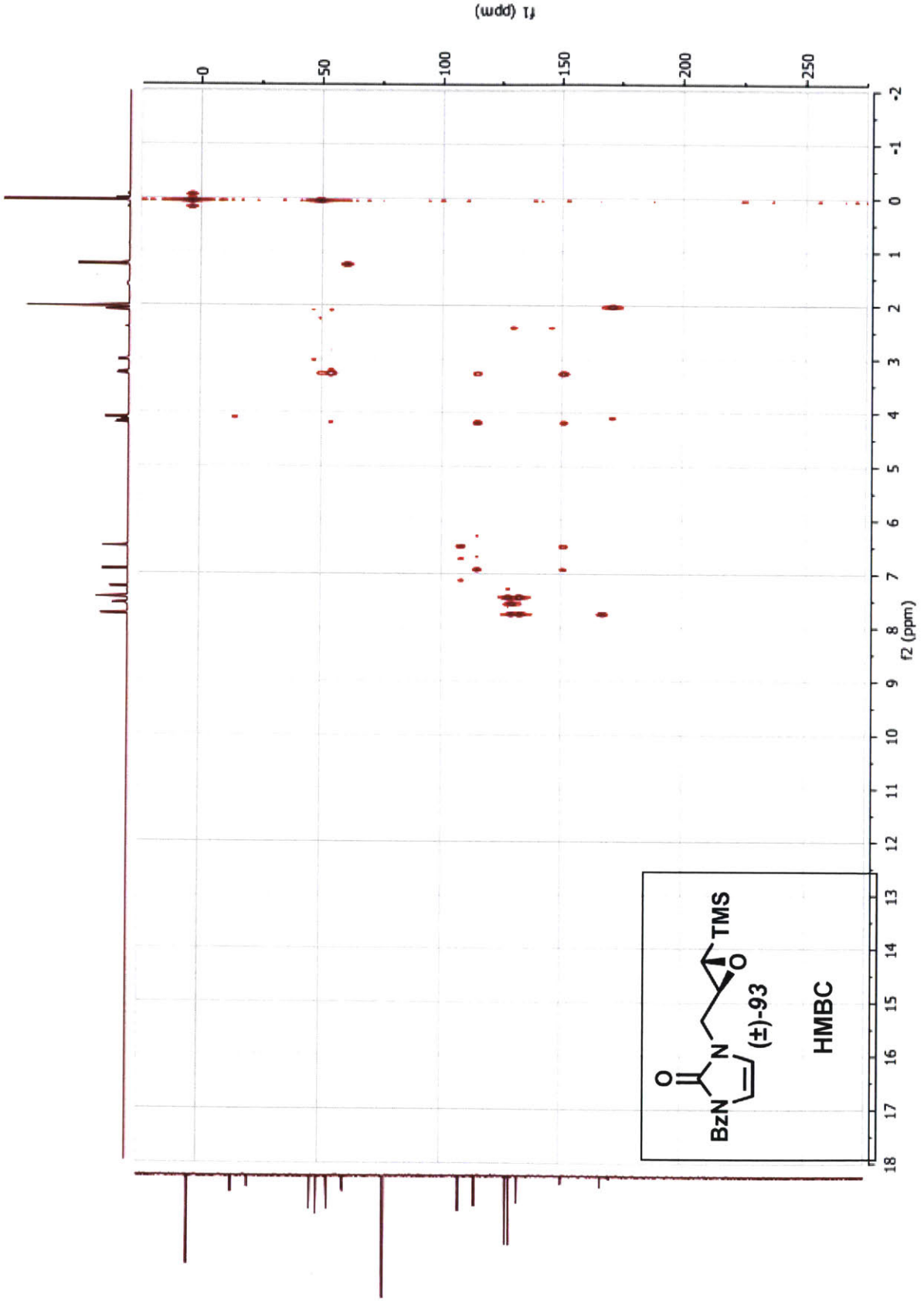
f1 (ppm)
0
50
100
150
200
250
f2 (ppm)
-2
-1
0
1
2
3
4
5
6
7
8
9
10
11
12
13
14
15
16
17
18
BzN
O
N
TMS
O
(±)-93
HMBC

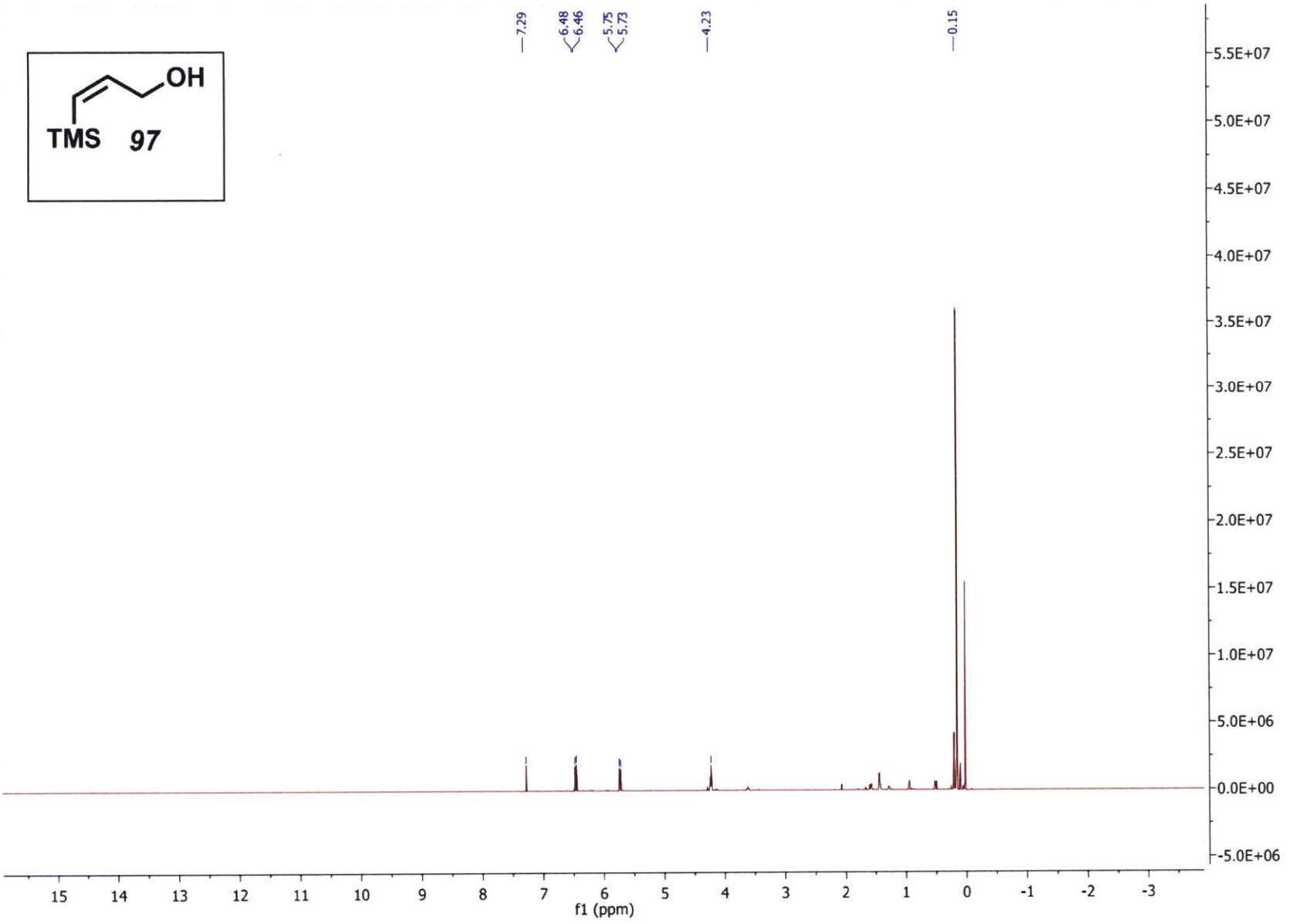
OH
TMS 97
7.29
6.48
6.46
5.75
5.73
4.23
0.15
5.5E+07
5.0E+07
4.5E+07
4.0E+07
3.5E+07
3.0E+07
2.5E+07
2.0E+07
1.5E+07
1.0E+07
5.0E+06
0.0E+00
-5.0E+06
15 14 13 12 11 10 9 8 7 6 5 4 3 2 1 0 -1 -2 -3
f1 (ppm)

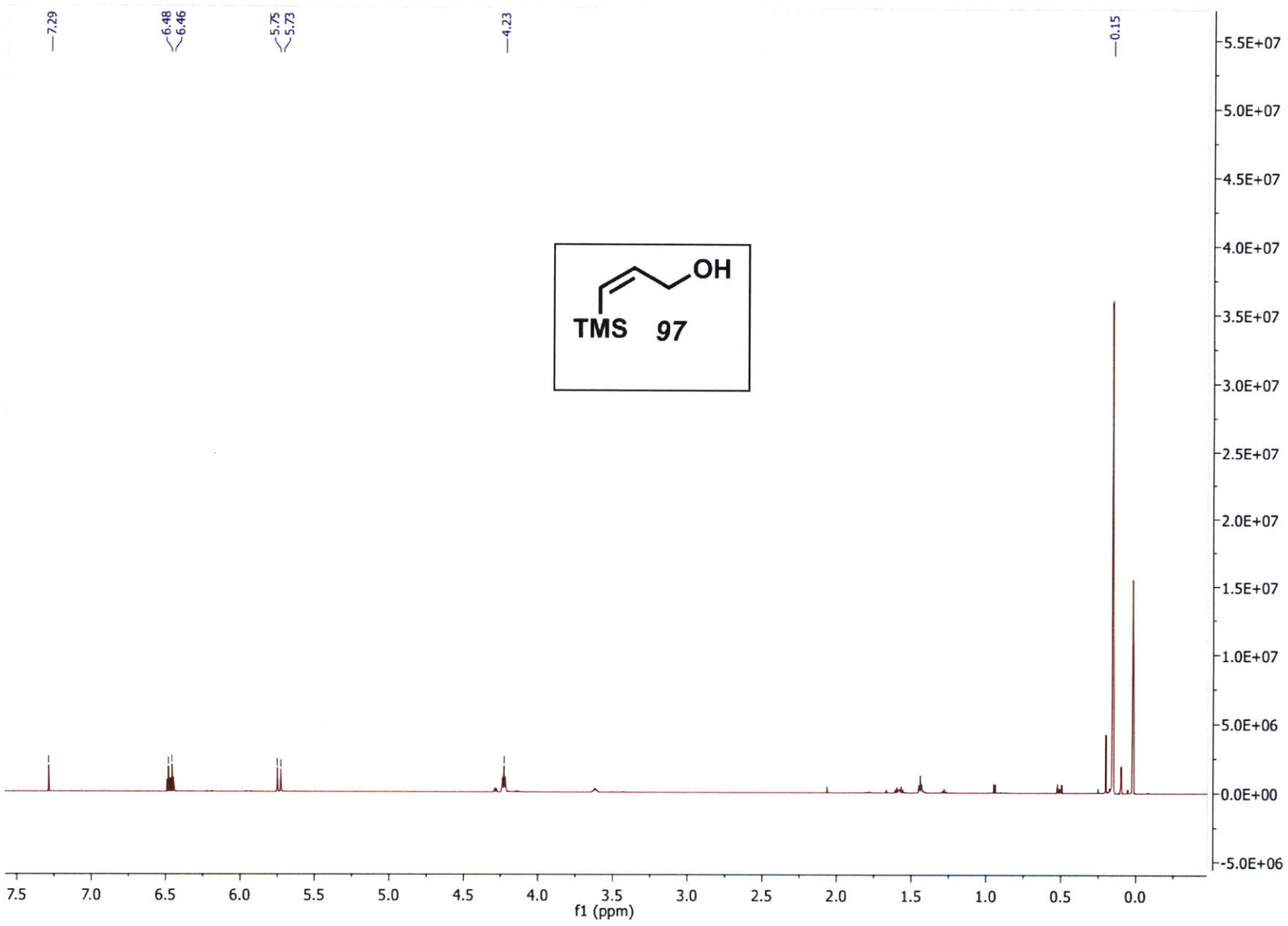
7.29
6.48
6.46
5.75
5.73
4.23
0.15
OH
TMS
97
5.5E+07
5.0E+07
4.5E+07
4.0E+07
3.5E+07
3.0E+07
2.5E+07
2.0E+07
1.5E+07
1.0E+07
5.0E+06
0.0E+00
-5.0E+06
7.5
7.0
6.5
6.0
5.5
5.0
4.5
4.0
3.5
3.0
2.5
2.0
1.5
1.0
0.5
0.0
f1 (ppm)

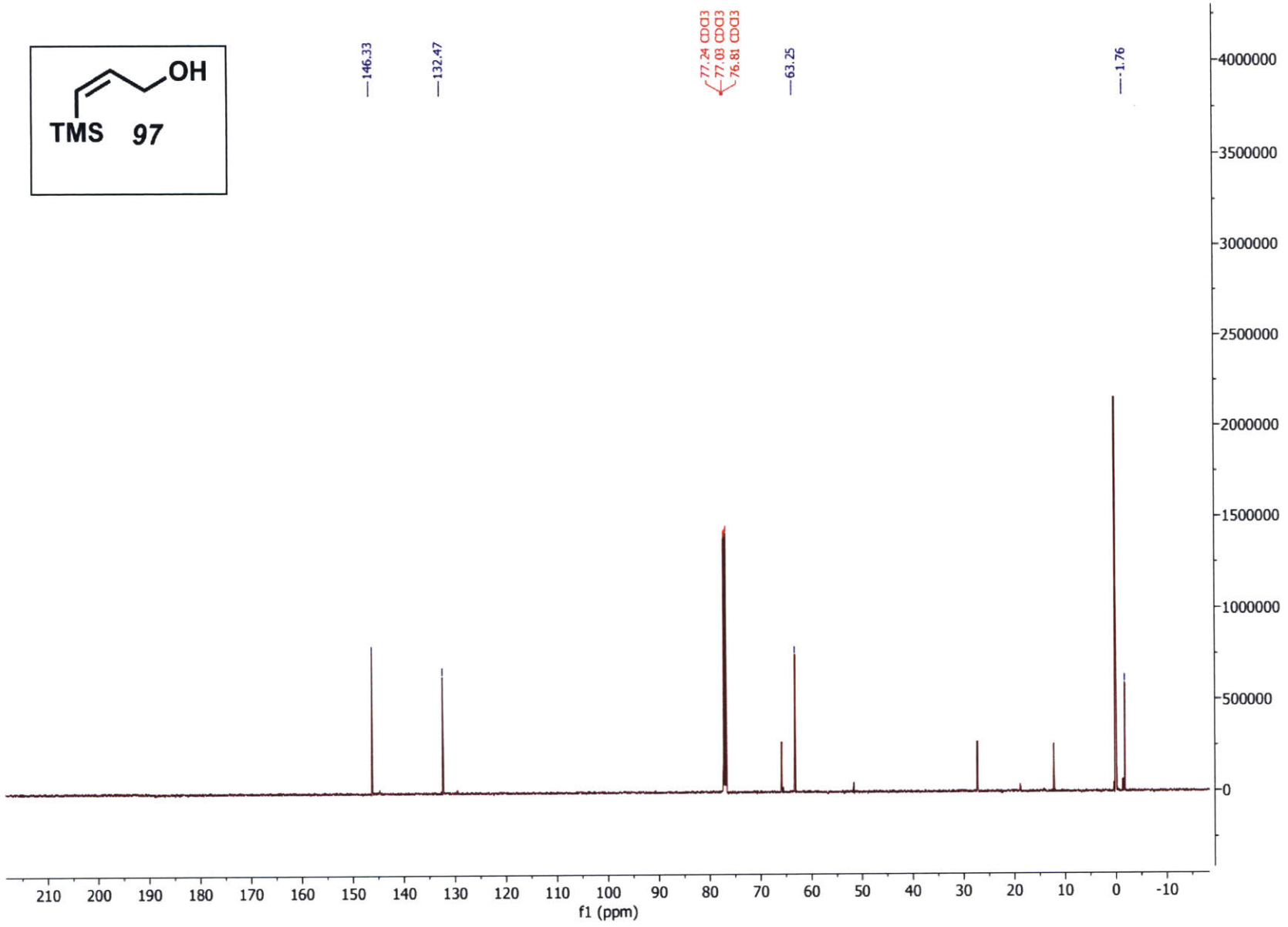
OH
TMS
97
146.33
132.47
77.24 CDCl3
77.03 CDCl3
76.81 CDCl3
63.25
-1.76
4000000
3500000
3000000
2500000
2000000
1500000
1000000
500000
0
210 200 190 180 170 160 150 140 130 120 110 100 90 80 70 60 50 40 30 20 10 0 -10
f1 (ppm)

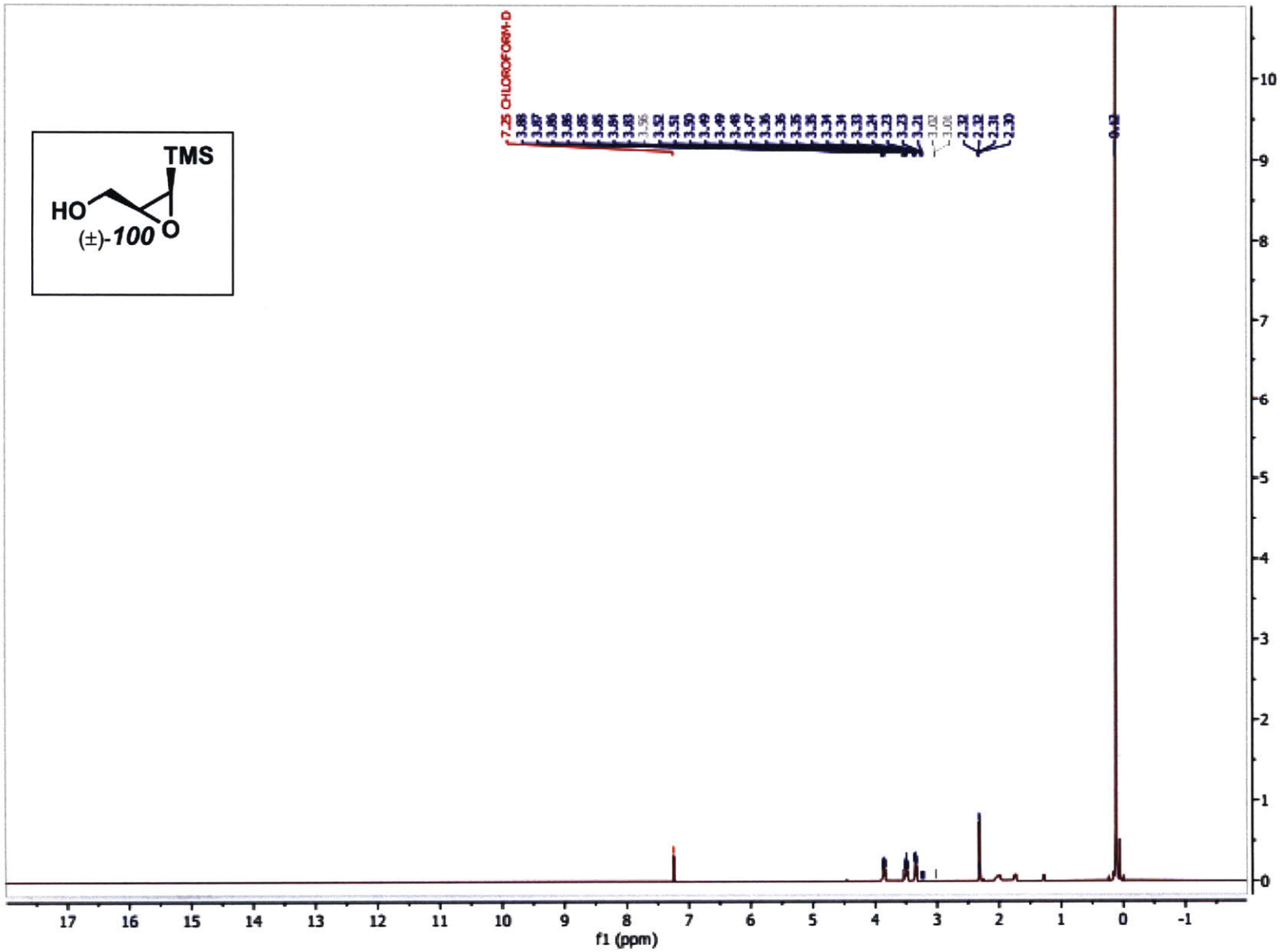
TMS
HO
(±)-100
O
7.25 CHLOROFORM-D
0.00
f1 (ppm)

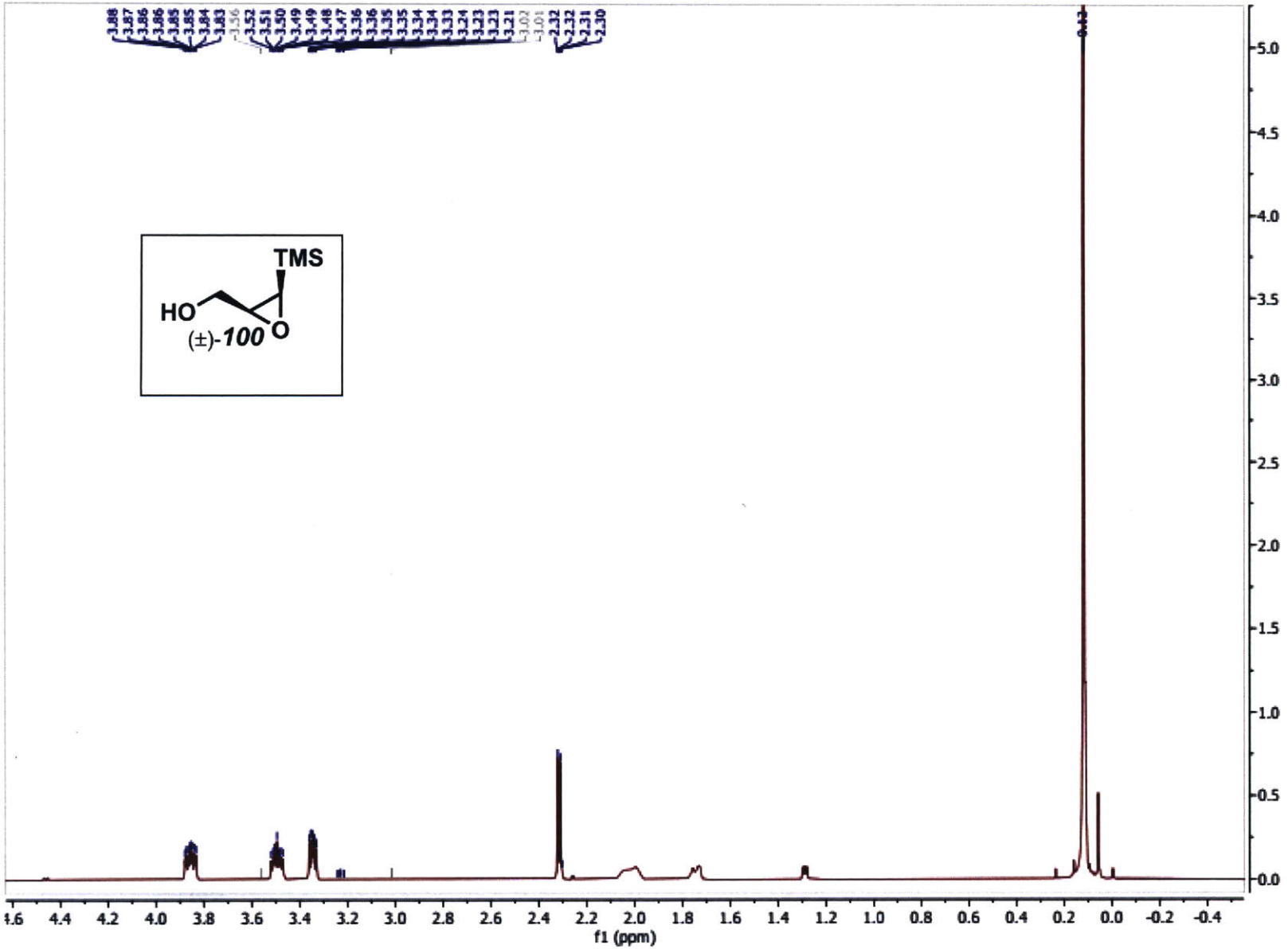
TMS
HO
(±)-100
O
f1 (ppm)

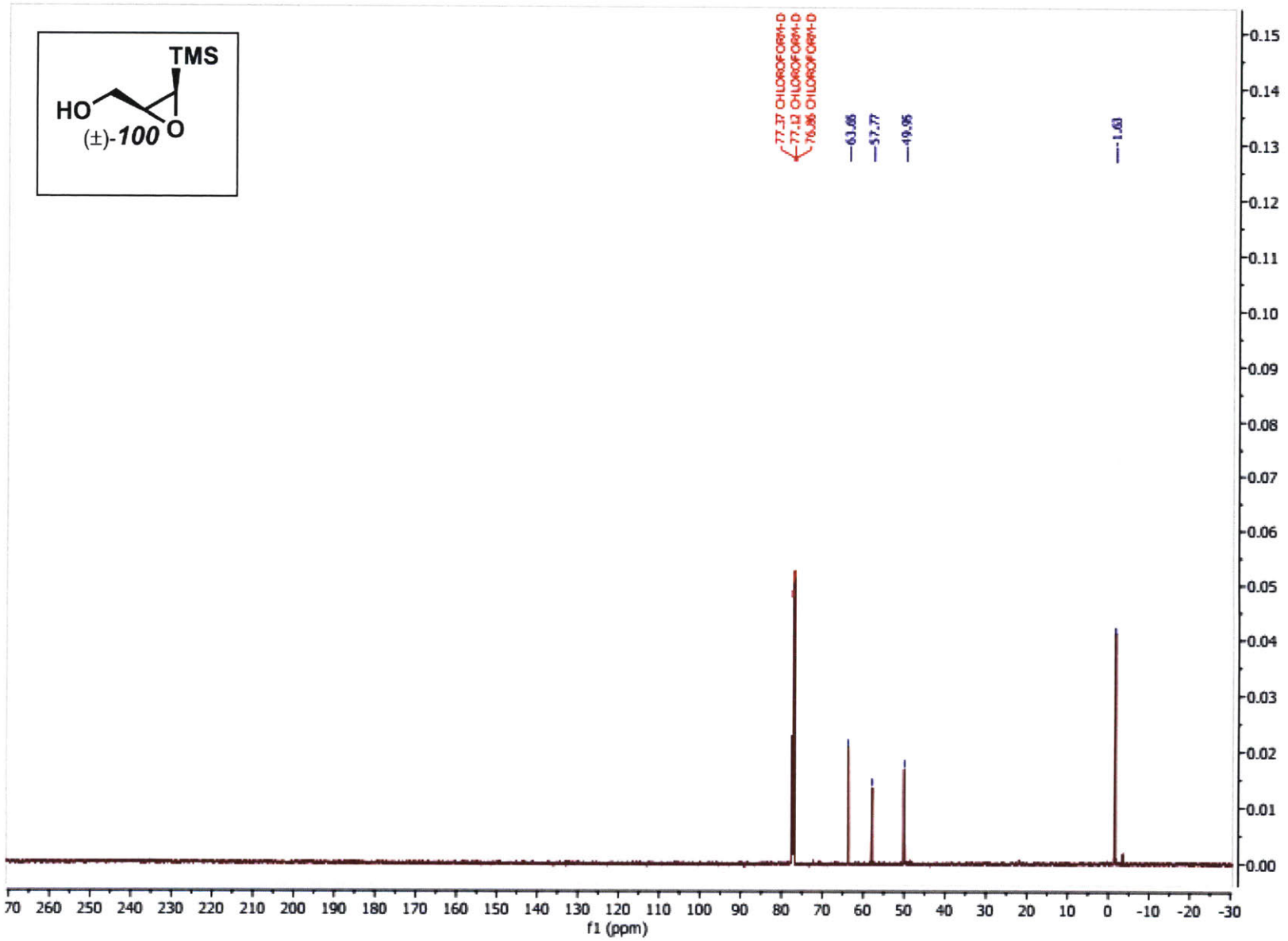
TMS
HO
(±)-100
O
77.37 CHLOROFORM-D
77.12 CHLOROFORM-D
76.86 CHLOROFORM-D
63.65
57.77
49.95
1.63
f1 (ppm)

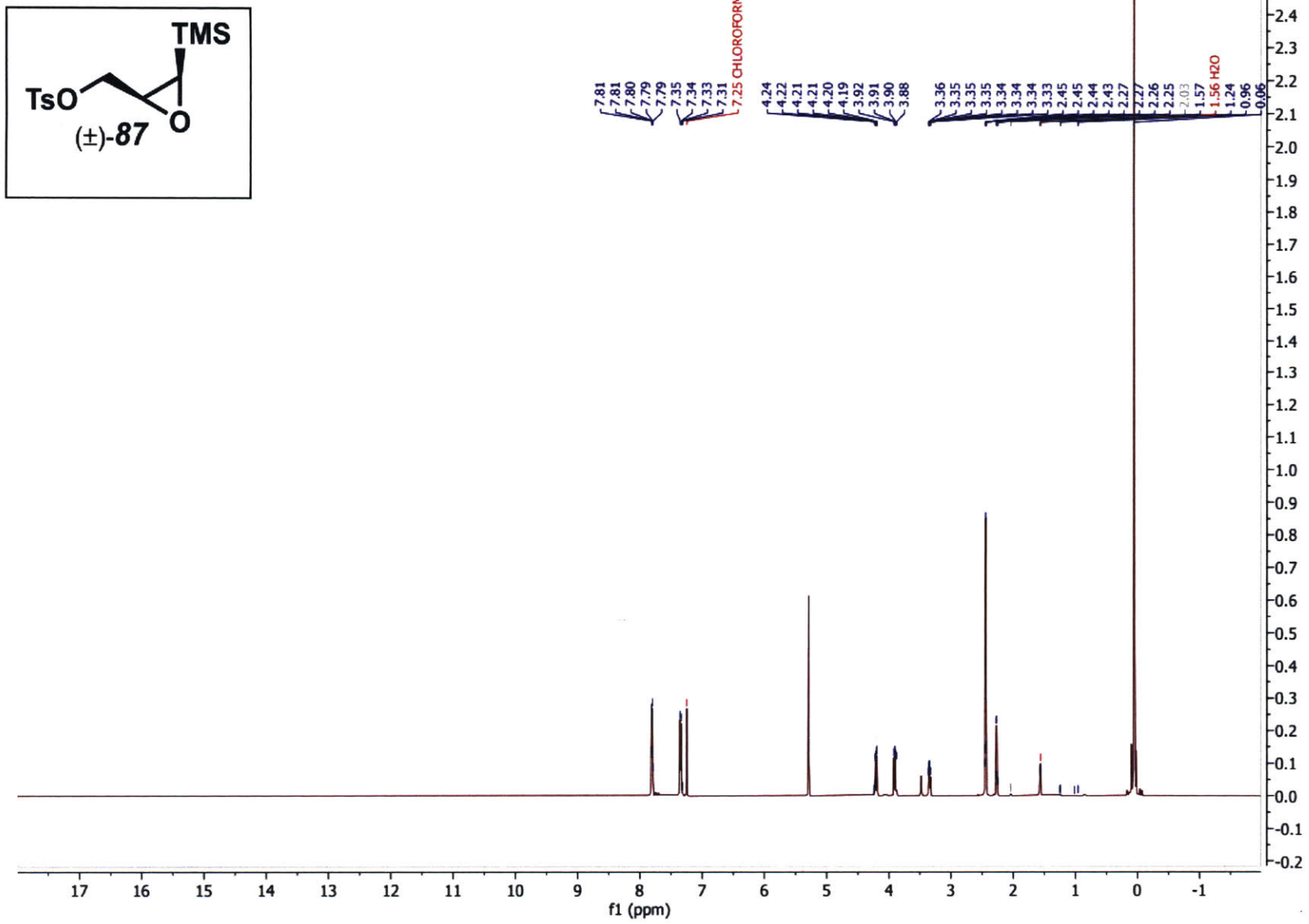
TMS
TsO
O
(±)-87
7.81
7.81
7.80
7.79
7.79
7.35
7.34
7.33
7.31
7.25 CHLOROFORM-D
4.24
4.22
4.21
4.21
4.20
4.19
3.92
3.91
3.90
3.88
3.36
3.35
3.35
3.35
3.34
3.34
3.34
3.33
2.45
2.45
2.44
2.43
2.27
2.27
2.26
2.25
2.03
1.57
1.56 H2O
1.24
0.96
0.06
f1 (ppm)

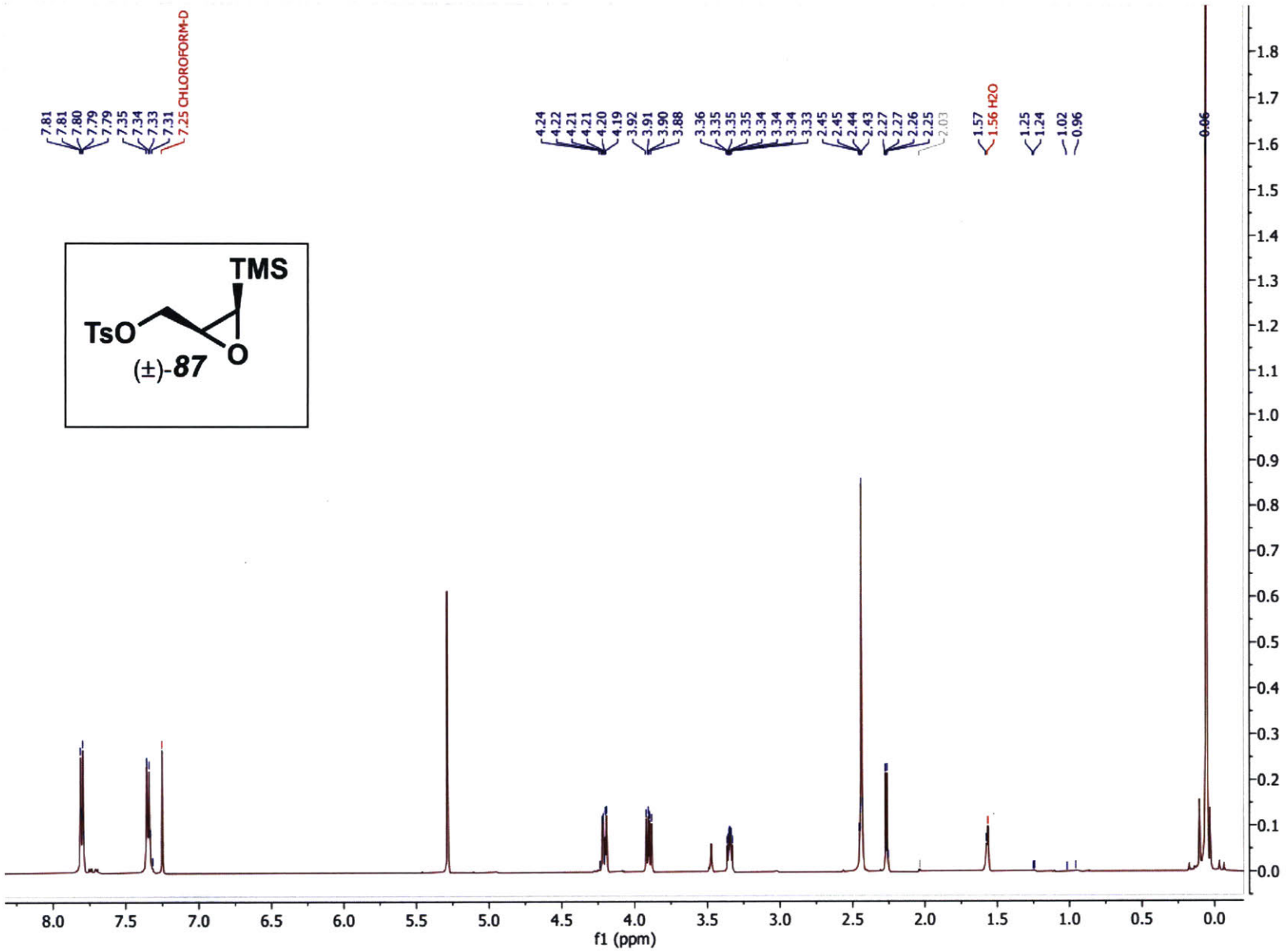
7.81
7.81
7.80
7.79
7.79
7.35
7.34
7.33
7.31
7.25 CHLOROFORM-D
4.24
4.22
4.21
4.21
4.20
4.19
3.92
3.91
3.90
3.88
3.36
3.35
3.35
3.35
3.34
3.34
3.34
3.33
2.45
2.45
2.44
2.43
2.27
2.27
2.26
2.25
2.03
1.57
1.56 H2O
1.25
1.24
1.02
0.96
0.00
TMS
TsO
O
(±)-87
f1 (ppm)

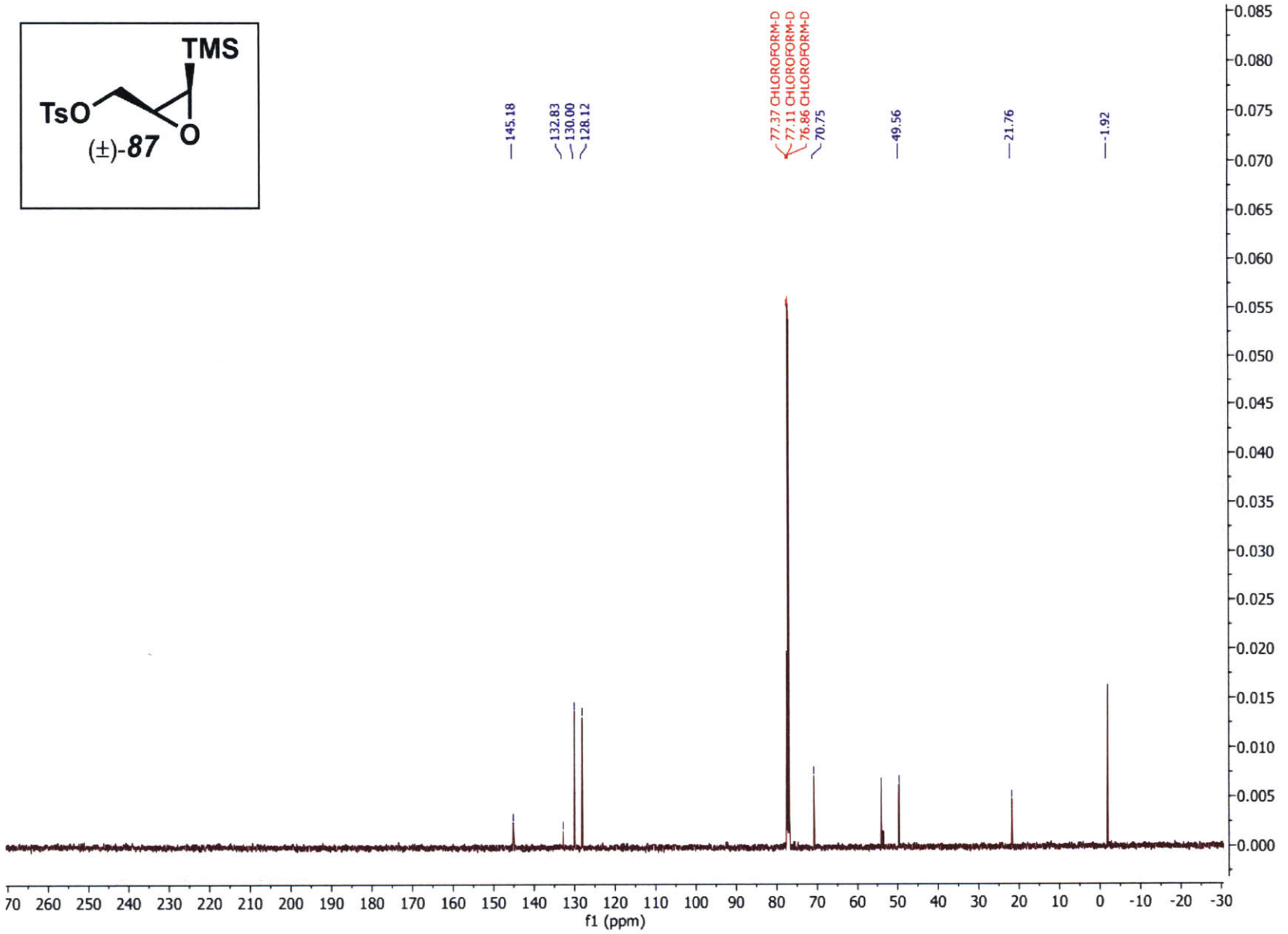
TMS
TsO
O
(±)-87
145.18
132.83
130.00
128.12
77.37 CHLOROFORM-D
77.11 CHLOROFORM-D
76.86 CHLOROFORM-D
70.75
49.56
21.76
-1.92
f1 (ppm)

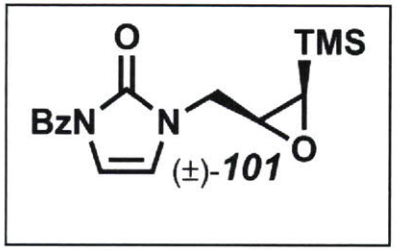
O
TMS
BzN
N
O
(±)-101

7.77
7.77
7.76
7.76
7.75
7.75
7.75
7.58
7.57
7.57
7.56
7.55
7.55
7.55
7.47
7.46
7.45
7.44
7.44
7.25 CHLOROFORM-D
6.96
6.95
6.56
6.55
4.32
4.31
4.29
4.28
3.35
3.34
3.34
3.33
3.33
3.33
3.32
3.32
3.32
3.05
3.04
3.03
3.02
3.00
2.33
2.32
2.31
1.57 H2O
0.17
6.0
5.5
5.0
4.5
4.0
3.5
3.0
2.5
2.0
1.5
1.0
0.5
0.0
17
16
15
14
13
12
11
10
9
8
7
6
5
4
3
2
1
0
-1
f1 (ppm)

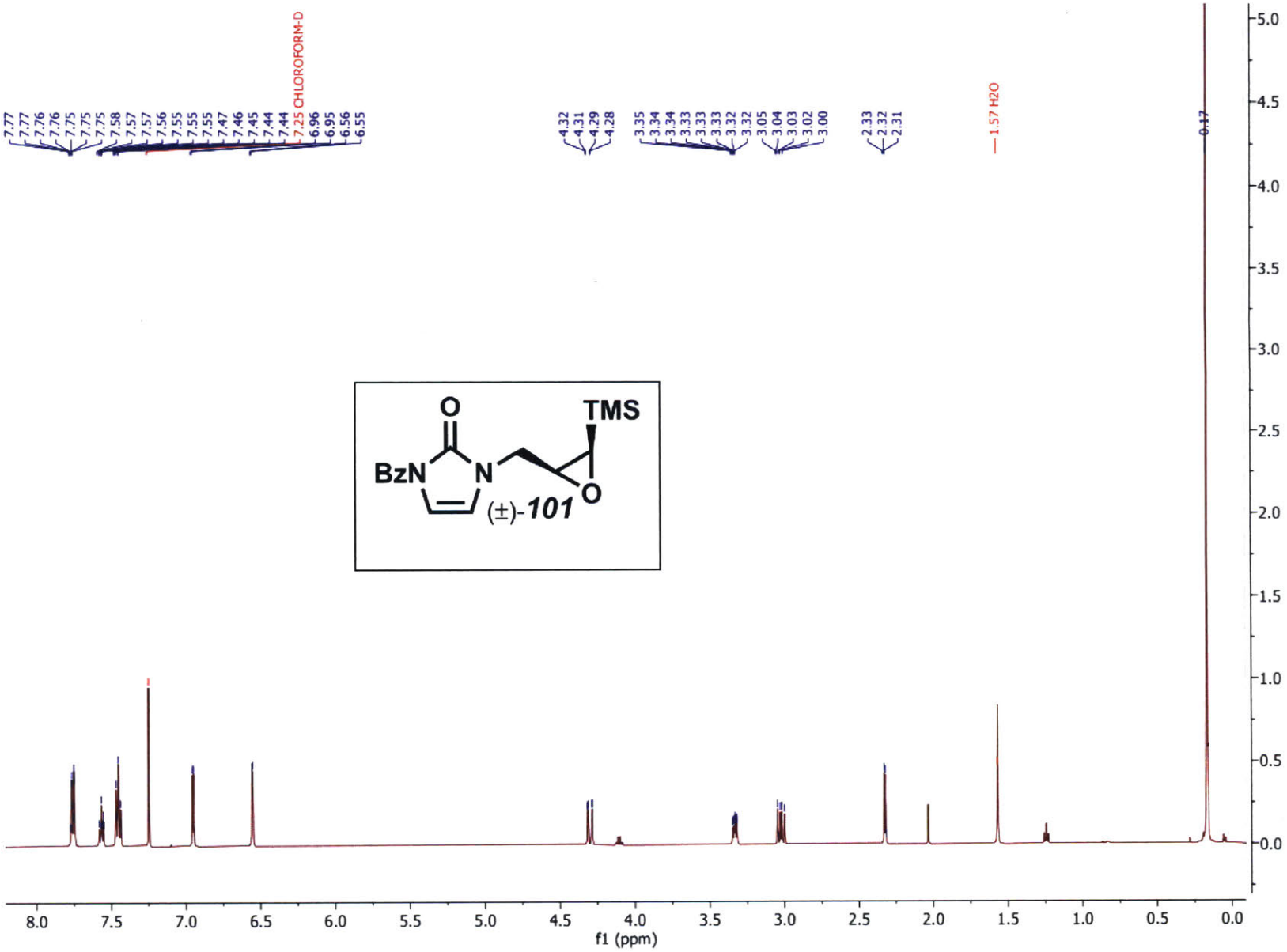
7.77
7.77
7.76
7.76
7.75
7.75
7.75
7.58
7.57
7.57
7.56
7.55
7.55
7.55
7.47
7.46
7.45
7.44
7.44
7.25 CHLOROFORM-D
6.96
6.95
6.56
6.55
4.32
4.31
4.29
4.28
3.35
3.34
3.34
3.33
3.33
3.33
3.32
3.32
3.05
3.04
3.03
3.02
3.00
2.33
2.32
2.31
1.57 H2O
0.17
O
TMS
BzN
N
O
(±)-101
8.0
7.5
7.0
6.5
6.0
5.5
5.0
4.5
4.0
3.5
3.0
2.5
2.0
1.5
1.0
0.5
0.0
f1 (ppm)

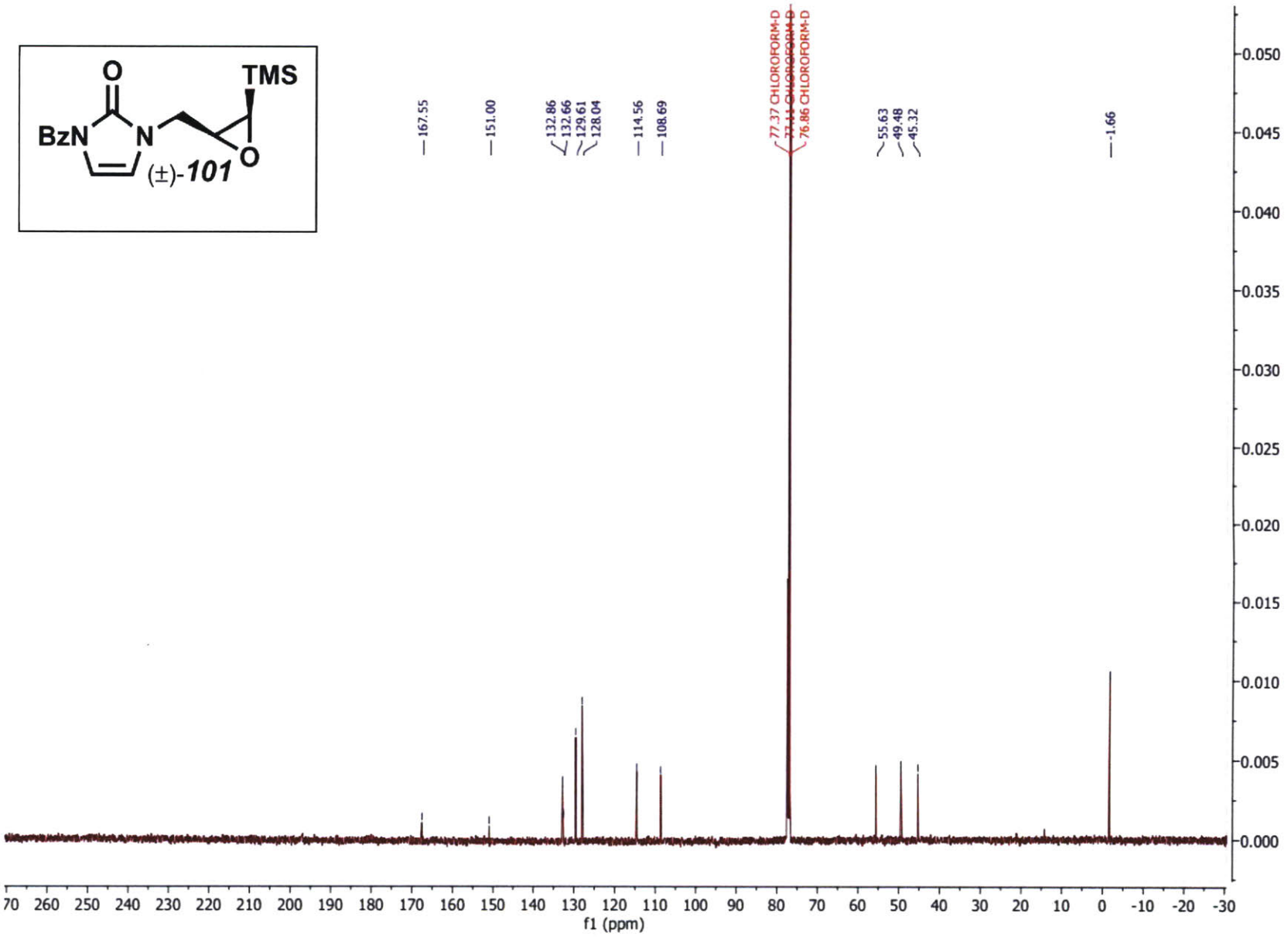
O
TMS
BzN
N
O
(±)-101
167.55
151.00
132.86
132.66
129.61
128.04
114.56
108.69
77.37 CHLOROFORM-D
77.11 CHLOROFORM-D
76.86 CHLOROFORM-D
55.63
49.48
45.32
1.66
f1 (ppm)

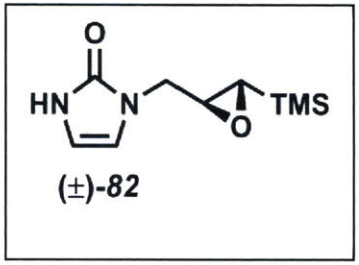
O
HN
N
O
TMS

(±)-*82*

6.44
6.43
6.37
6.37
4.87
4.01
4.00
3.98
3.98
3.57
3.56
3.54
3.53
3.05
3.04
3.03
3.03
3.02
2.10
2.09
0.13
0.03
f1 (ppm)

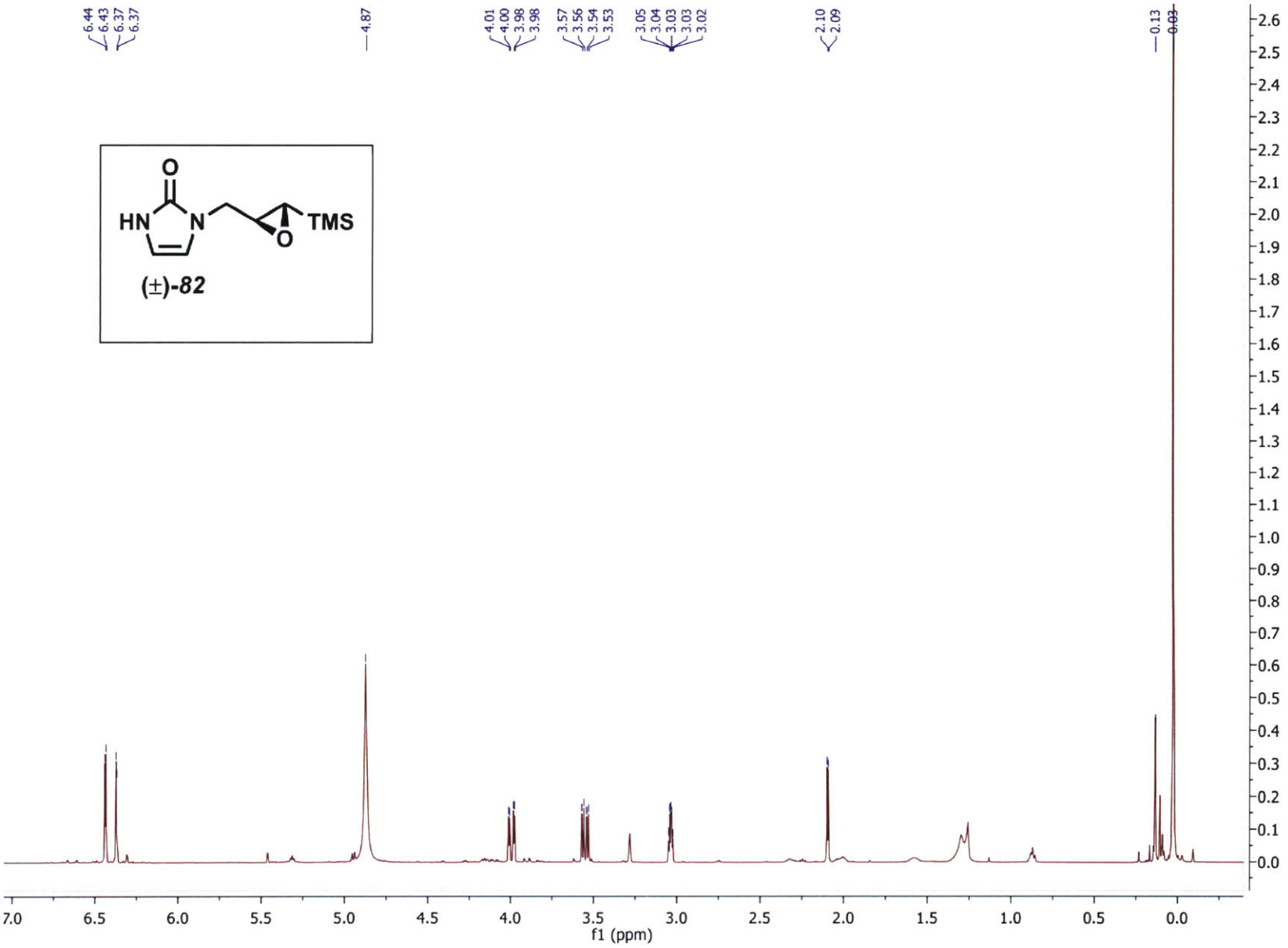
6.44
6.43
6.37
6.37
4.87
4.01
4.00
3.98
3.98
3.57
3.56
3.54
3.53
3.05
3.04
3.03
3.03
3.02
2.10
2.09
0.13
0.03
HN
N
O
O
TMS
(±)-82
f1 (ppm)

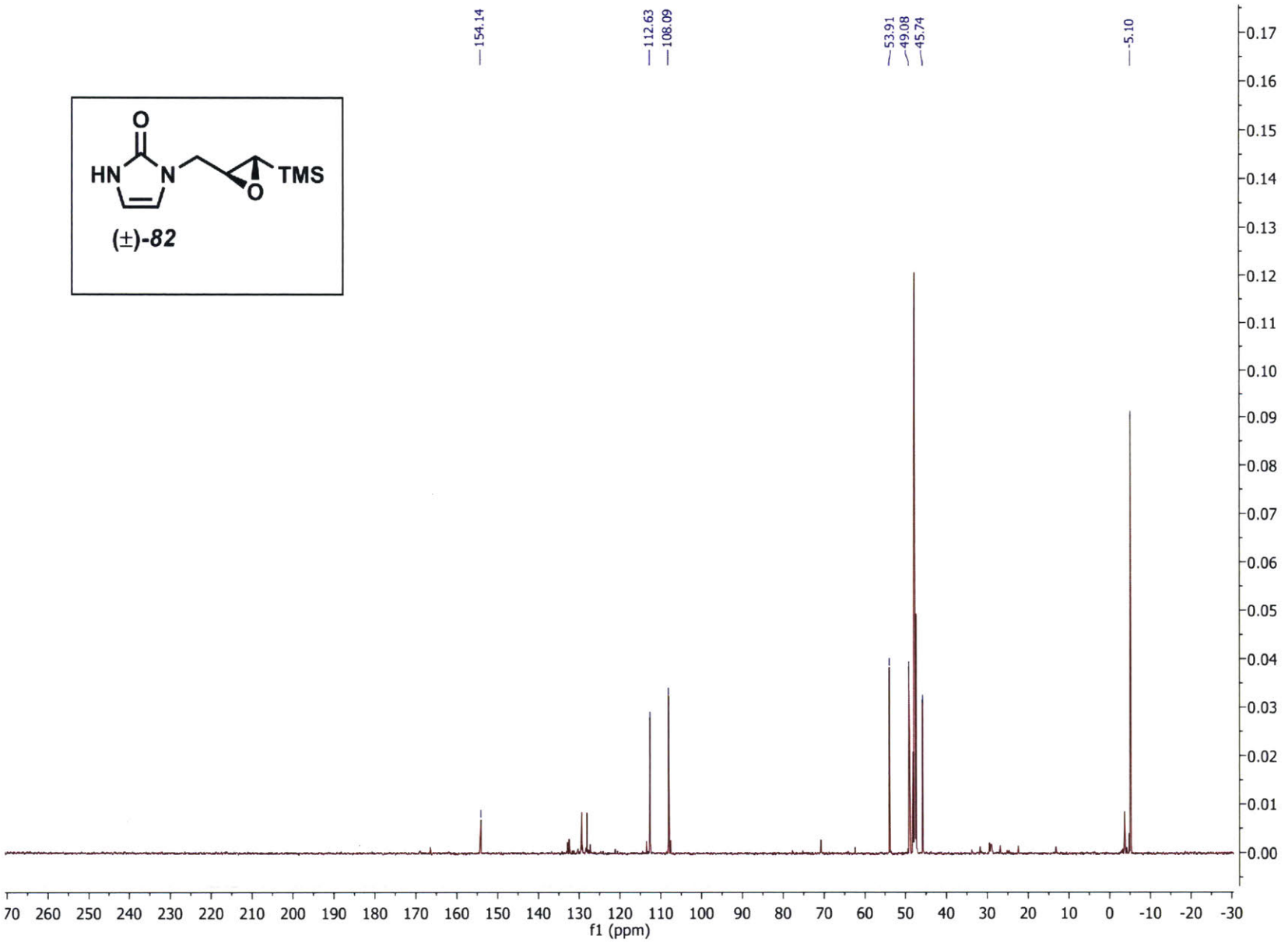
154.14
112.63
108.09
53.91
49.08
45.74
5.10
HN
N
O
O
TMS
(±)-82
f1 (ppm)

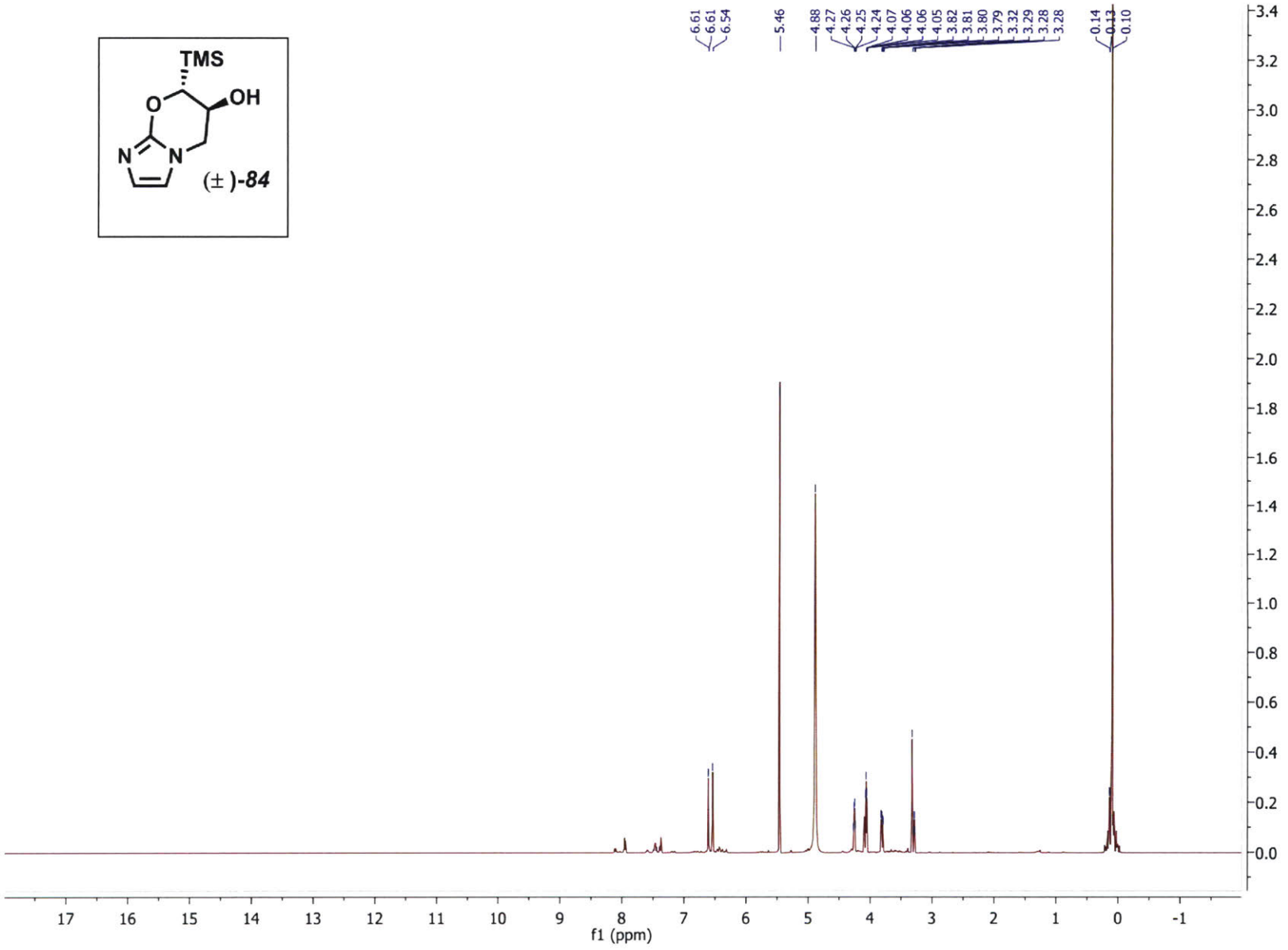
TMS
OH
O
N
N
(±)-84
6.61
6.61
6.54
5.46
4.88
4.27
4.26
4.25
4.24
4.07
4.06
4.06
4.05
3.82
3.81
3.80
3.79
3.32
3.29
3.28
3.28
0.14
0.13
0.10
f1 (ppm)

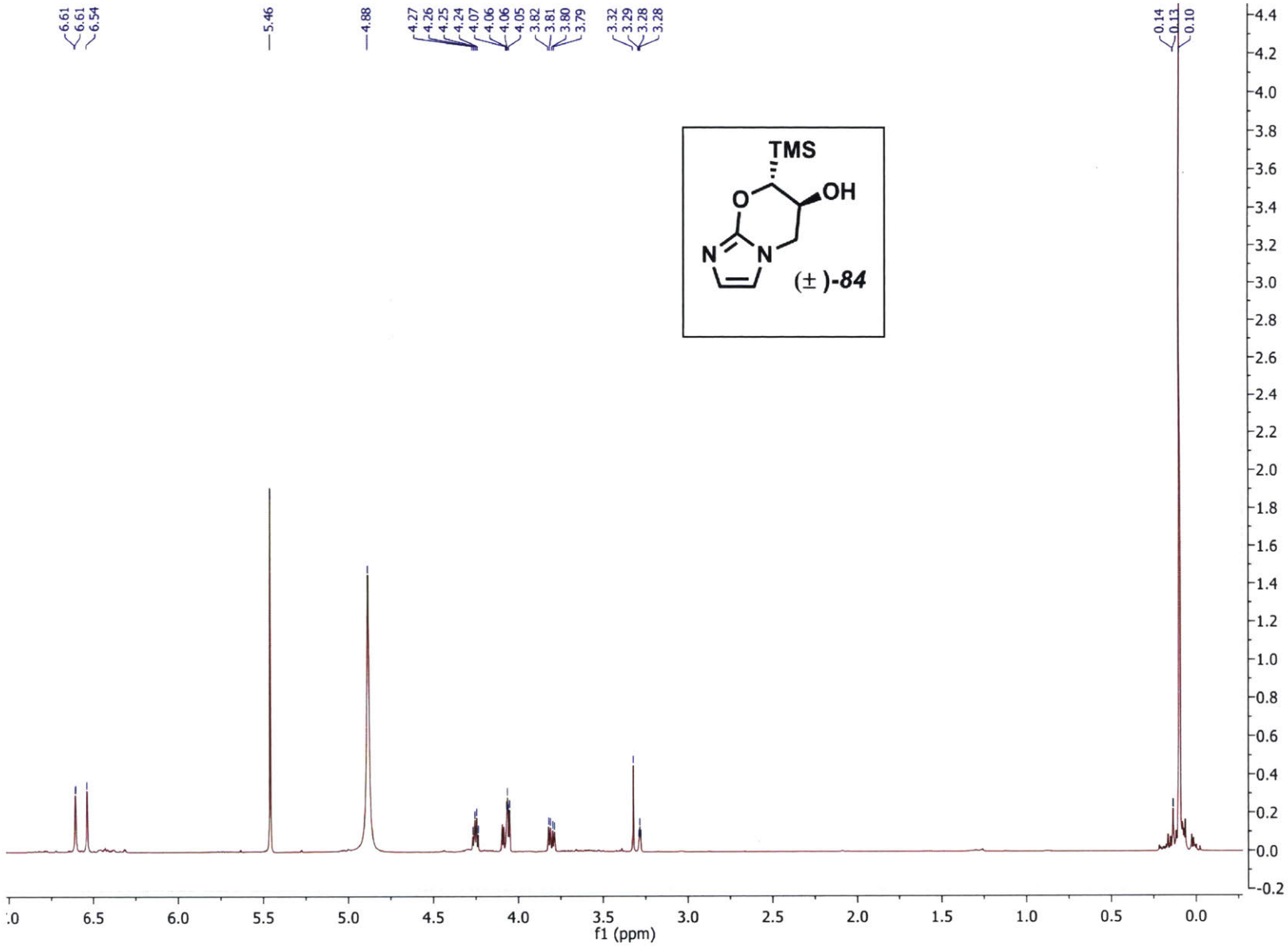
6.61
6.61
6.54
5.46
4.88
4.27
4.26
4.25
4.24
4.07
4.06
4.06
4.05
3.82
3.81
3.80
3.79
3.32
3.29
3.28
3.28
0.14
0.13
0.10
TMS
OH
O
N
N
(±)-84
f1 (ppm)

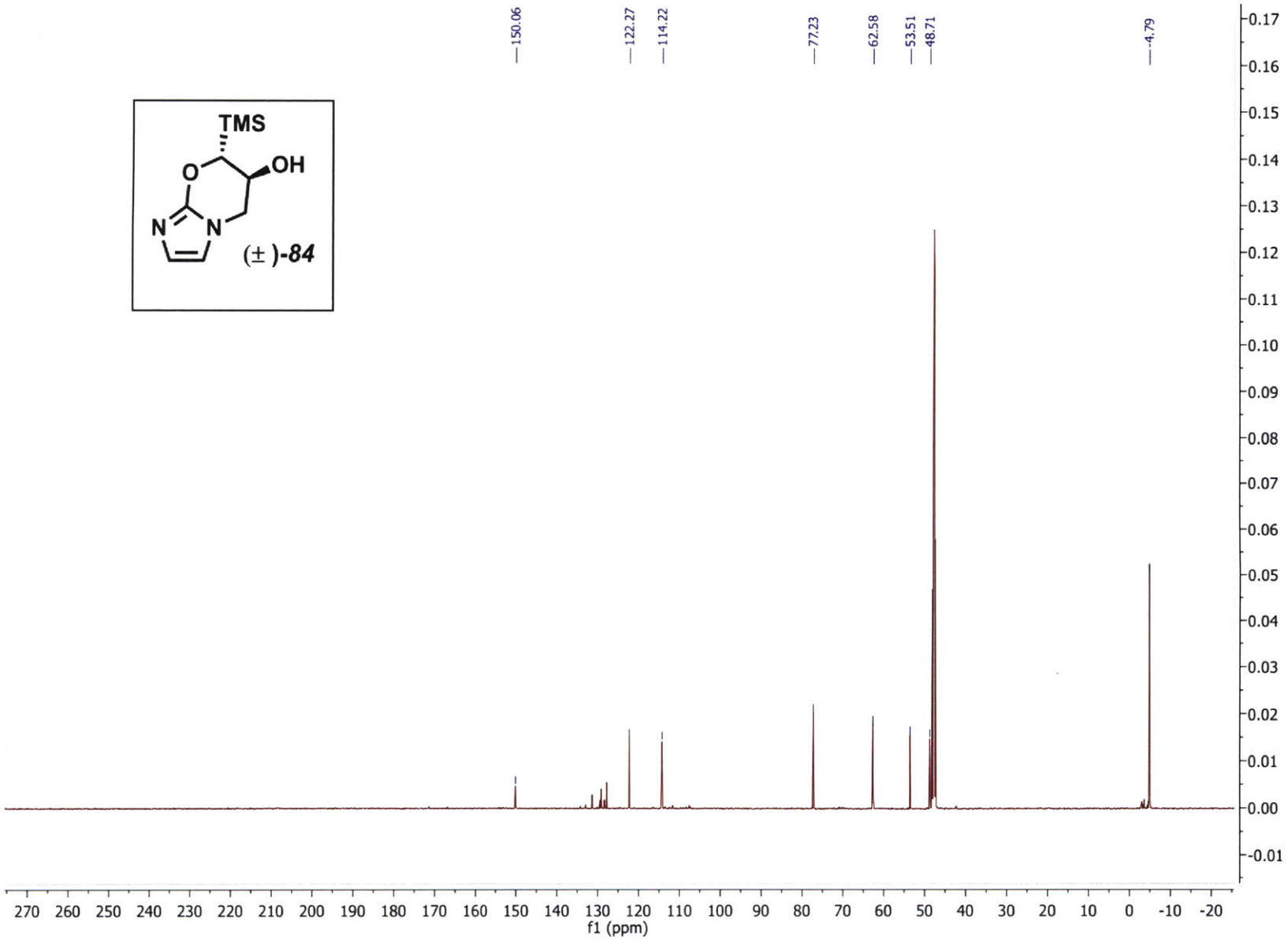
TMS
OH
O
N
N
(±)-84
150.06
122.27
114.22
77.23
62.58
53.51
48.71
4.79
f1 (ppm)

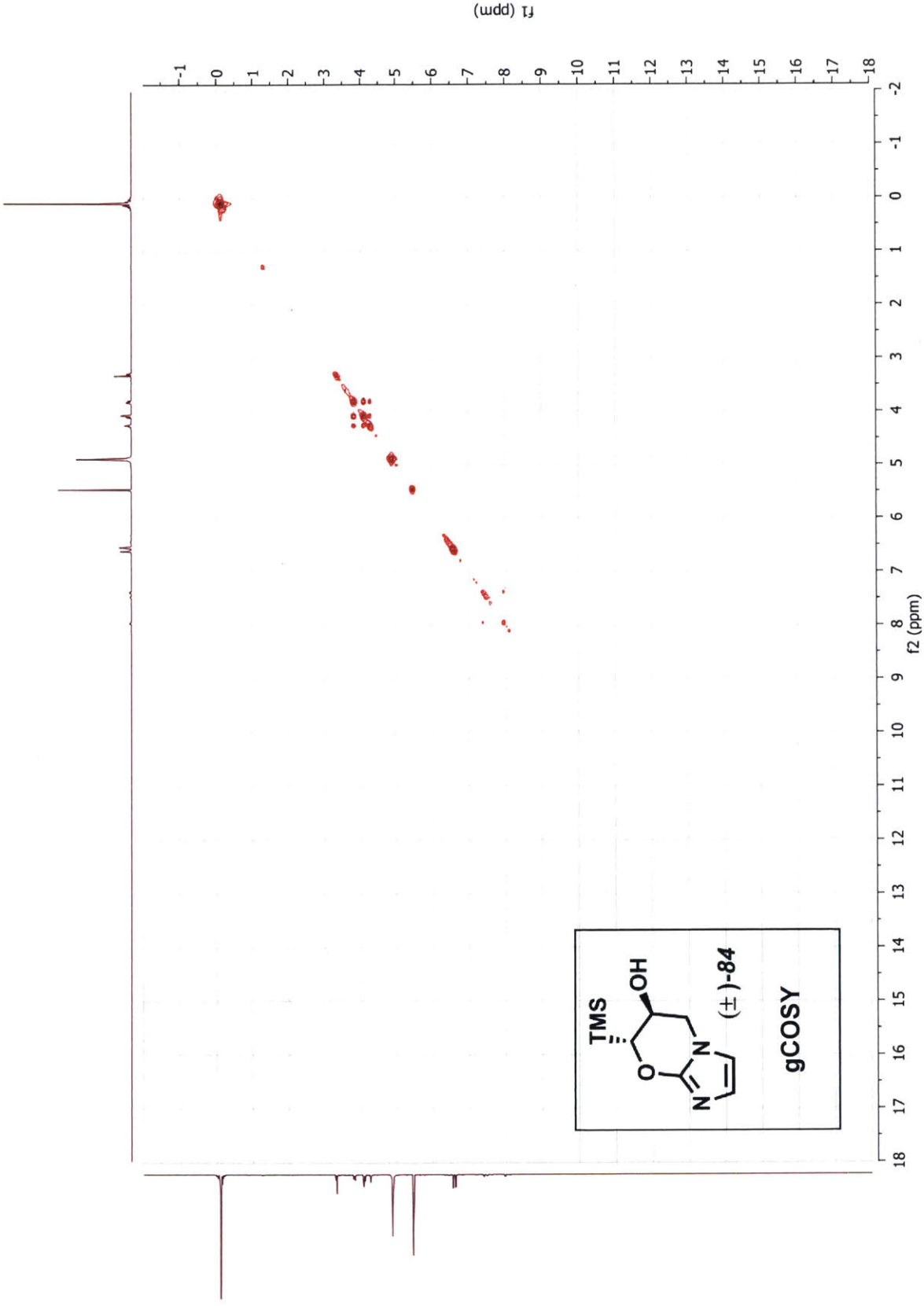
f1 (ppm)
f2 (ppm)
TMS
OH
O
N
N
(±)-84
gCOSY

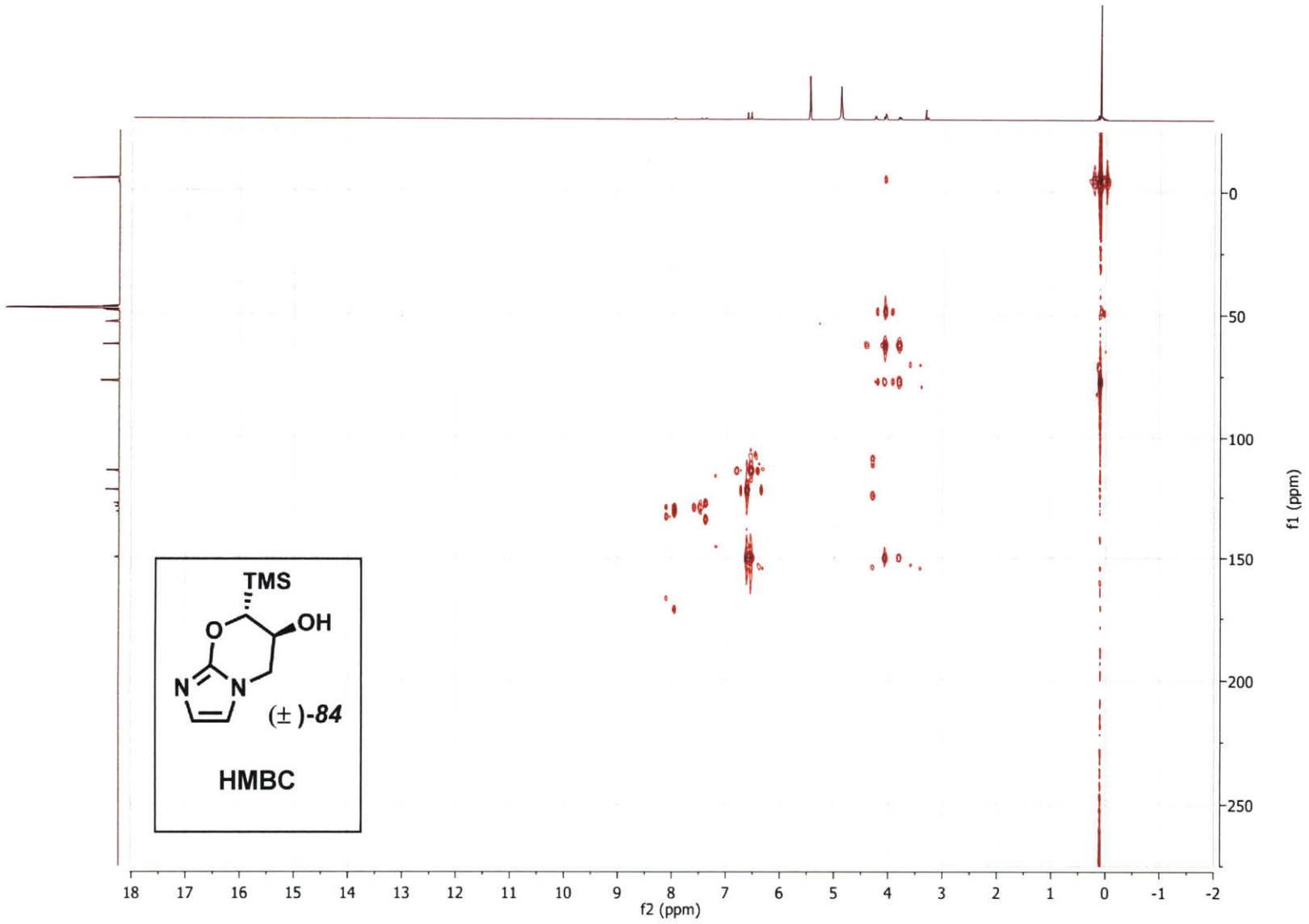
TMS
OH
O
N
N
(±)-84
HMBC
f2 (ppm)
f1 (ppm)

TMS
OH
O
N
N
(±)-84
HSQC
f2 (ppm)
f1 (ppm)
18
17
16
15
14
13
12
11
10
9
8
7
6
5
4
3
2
1
0
-1
0
50
100
150
200
250

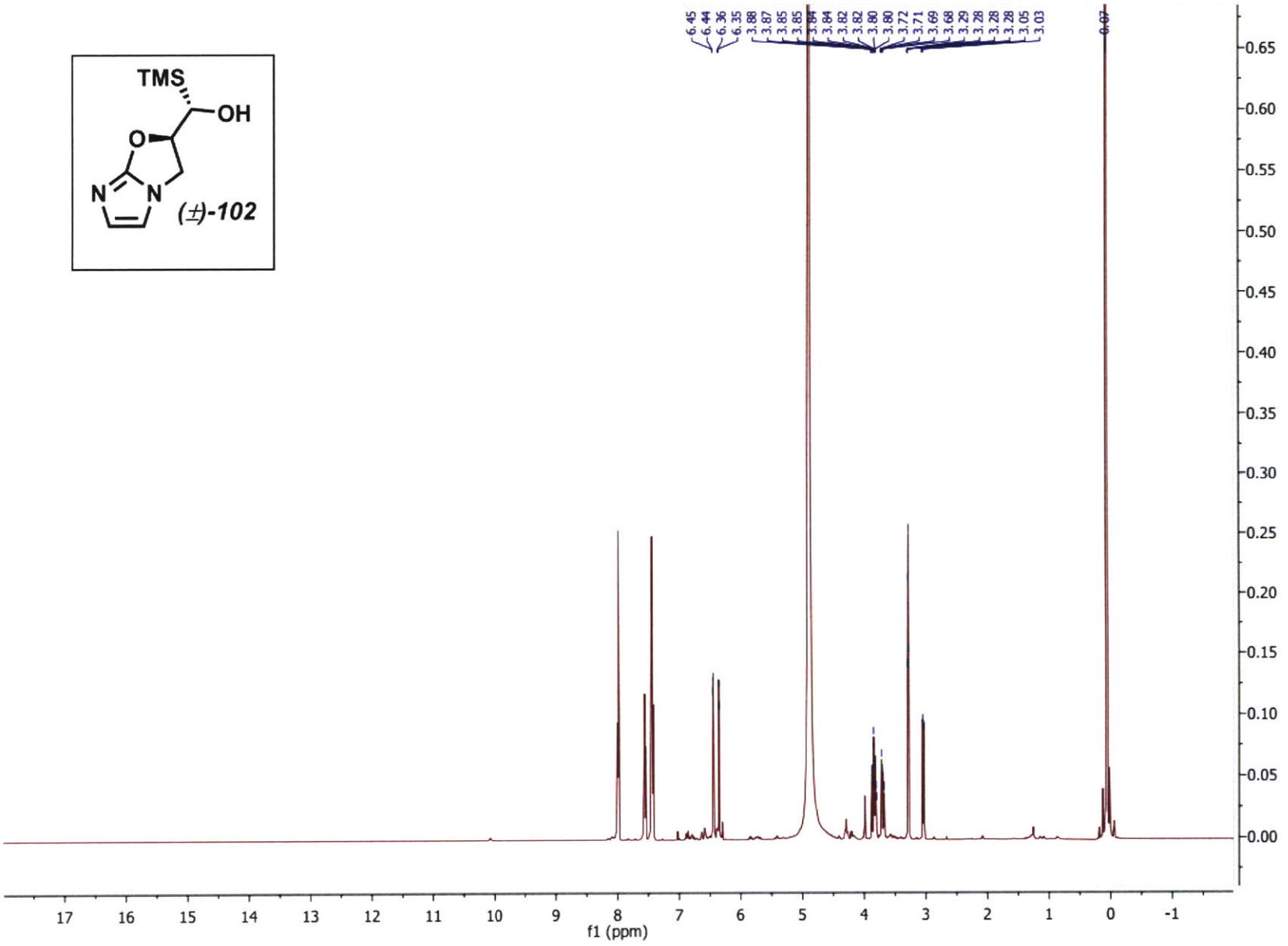
TMS
OH
O
N
N
(±)-102
6.45
6.44
6.36
6.35
3.88
3.87
3.85
3.85
3.84
3.84
3.82
3.82
3.80
3.80
3.80
3.72
3.71
3.69
3.68
3.29
3.28
3.28
3.28
3.05
3.03
0.07
0.65
0.60
0.55
0.50
0.45
0.40
0.35
0.30
0.25
0.20
0.15
0.10
0.05
0.00
17
16
15
14
13
12
11
10
9
8
7
6
5
4
3
2
1
0
-1
f1 (ppm)

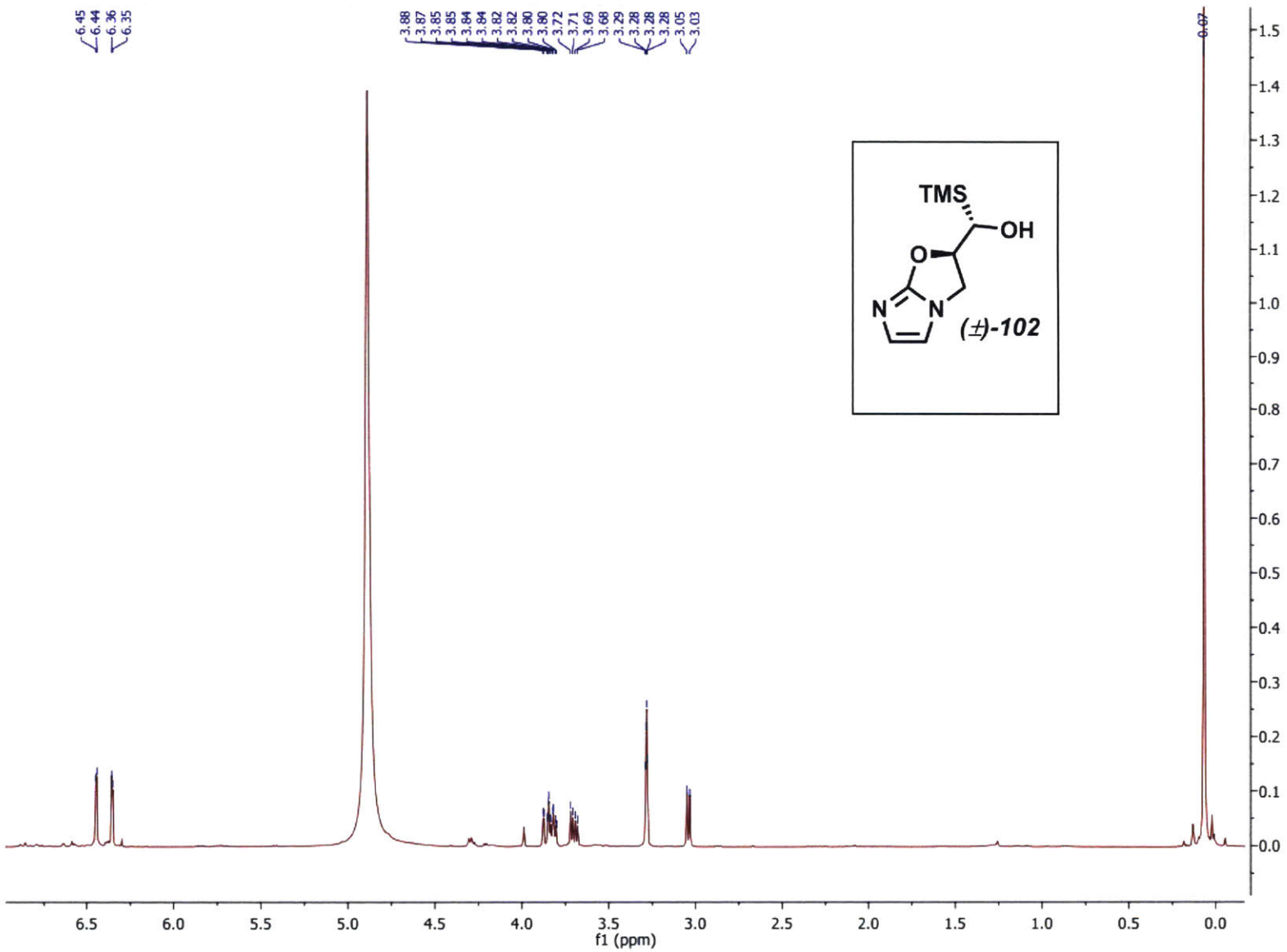
6.45
6.44
6.36
6.35
3.88
3.87
3.85
3.85
3.84
3.84
3.82
3.82
3.80
3.80
3.72
3.71
3.69
3.68
3.29
3.28
3.28
3.28
3.05
3.03
0.07
TMS
OH
O
N
N
(±)-102
f1 (ppm)

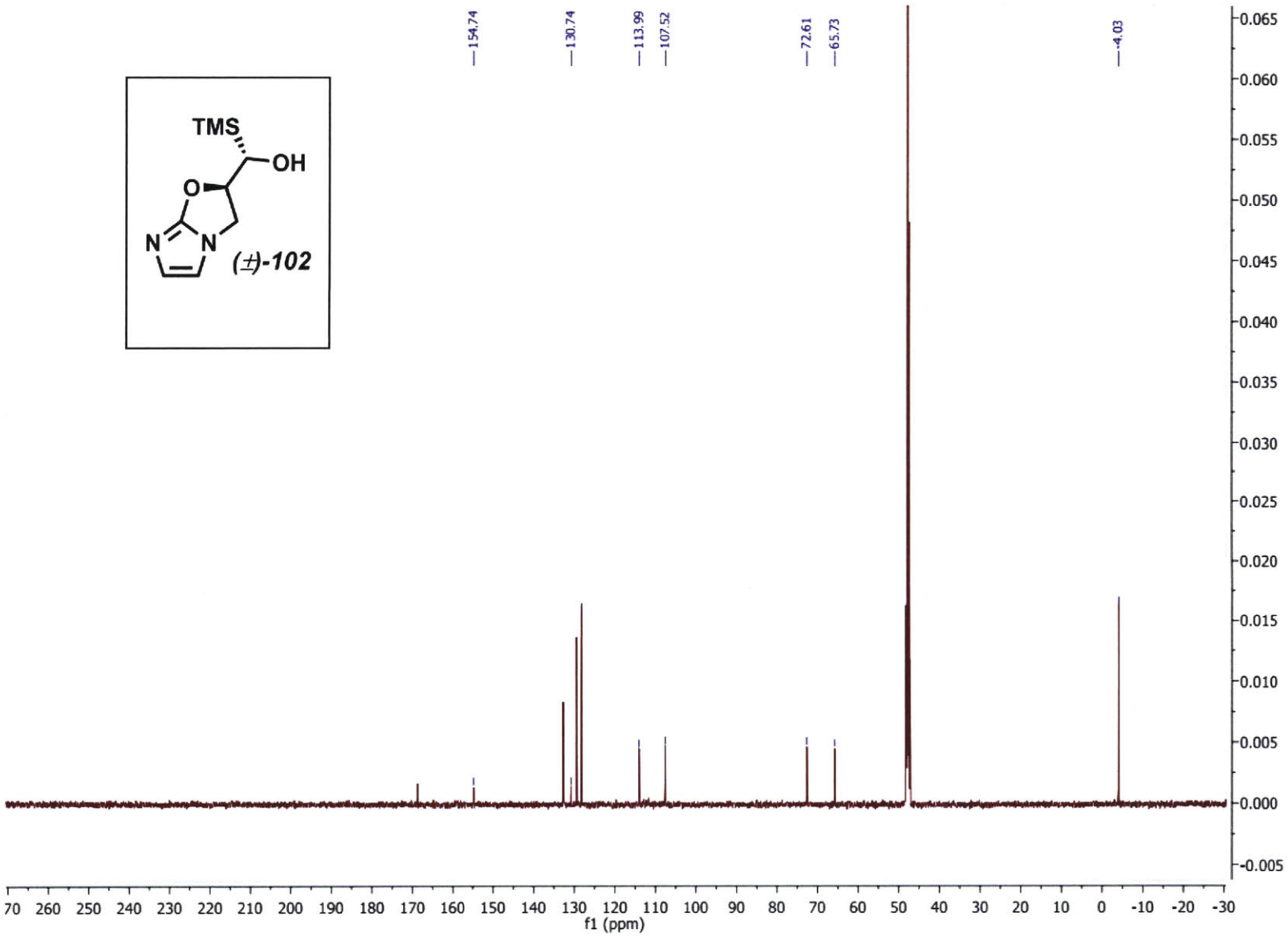
TMS
OH
O
N
N
(±)-102
154.74
130.74
113.99
107.52
72.61
65.73
4.03
0.065
0.060
0.055
0.050
0.045
0.040
0.035
0.030
0.025
0.020
0.015
0.010
0.005
0.000
-0.005
70 260 250 240 230 220 210 200 190 180 170 160 150 140 130 120 110 100 90 80 70 60 50 40 30 20 10 0 -10 -20 -30
f1 (ppm)

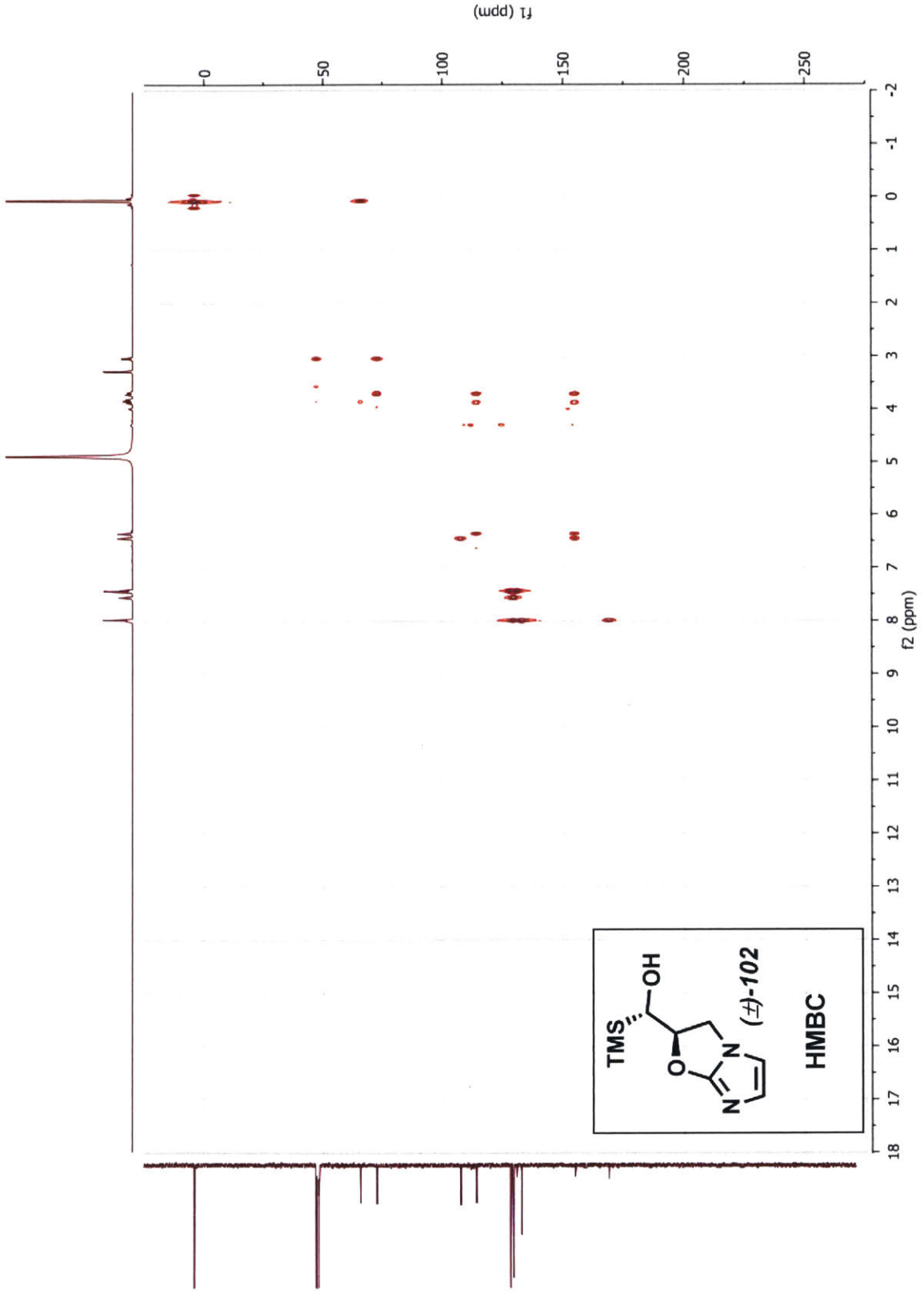
f1 (ppm)
0
50
100
150
200
250
f2 (ppm)
-2
-1
0
1
2
3
4
5
6
7
8
9
10
11
12
13
14
15
16
17
18
TMS
OH
O
N
N
(±)-102
HMBC

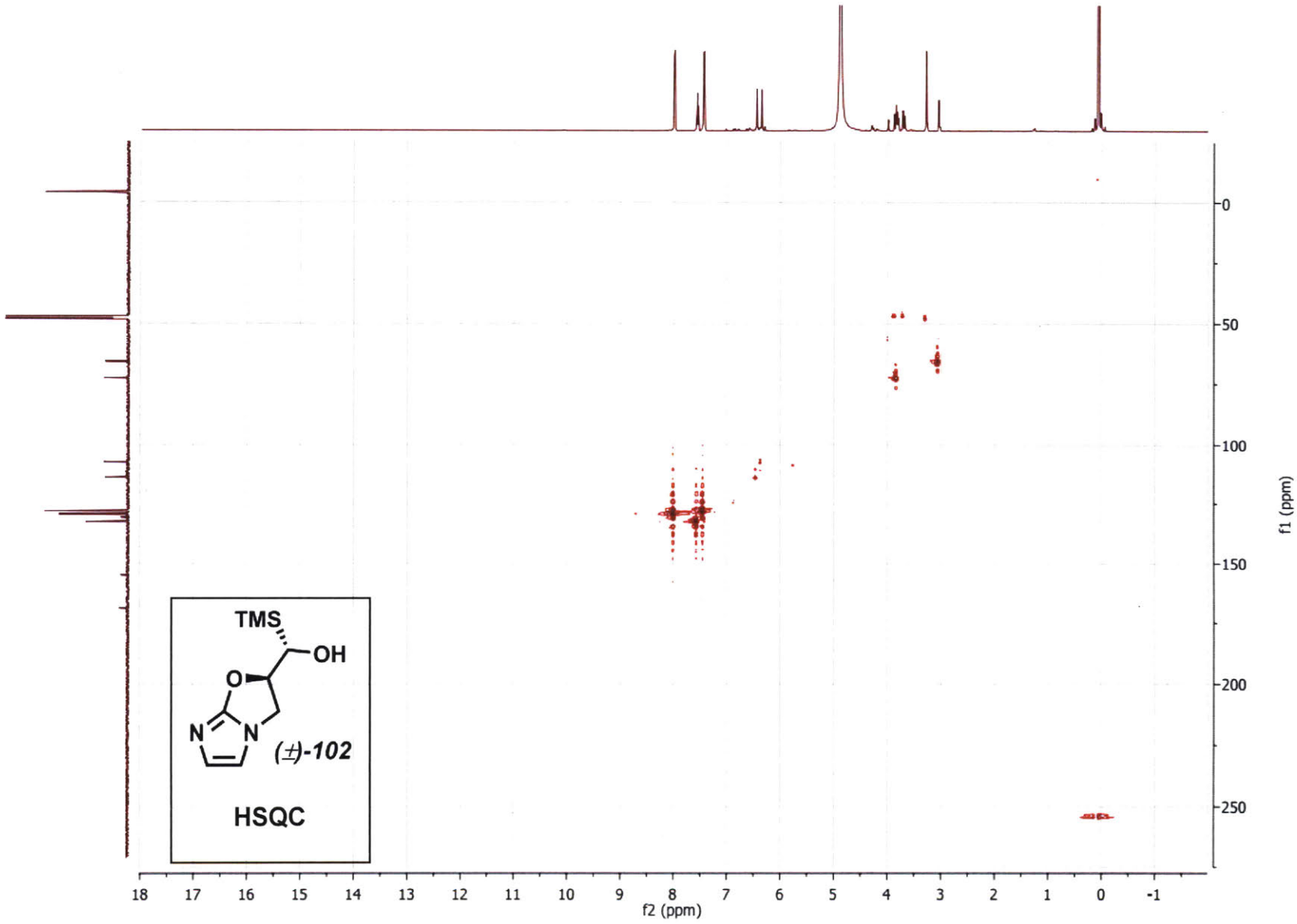
TMS
OH
O
N
N
(±)-102
HSQC
f2 (ppm)
f1 (ppm)

TMS
OH
O
N
N
(±)-102
gCOSY
f2 (ppm)
f1 (ppm)

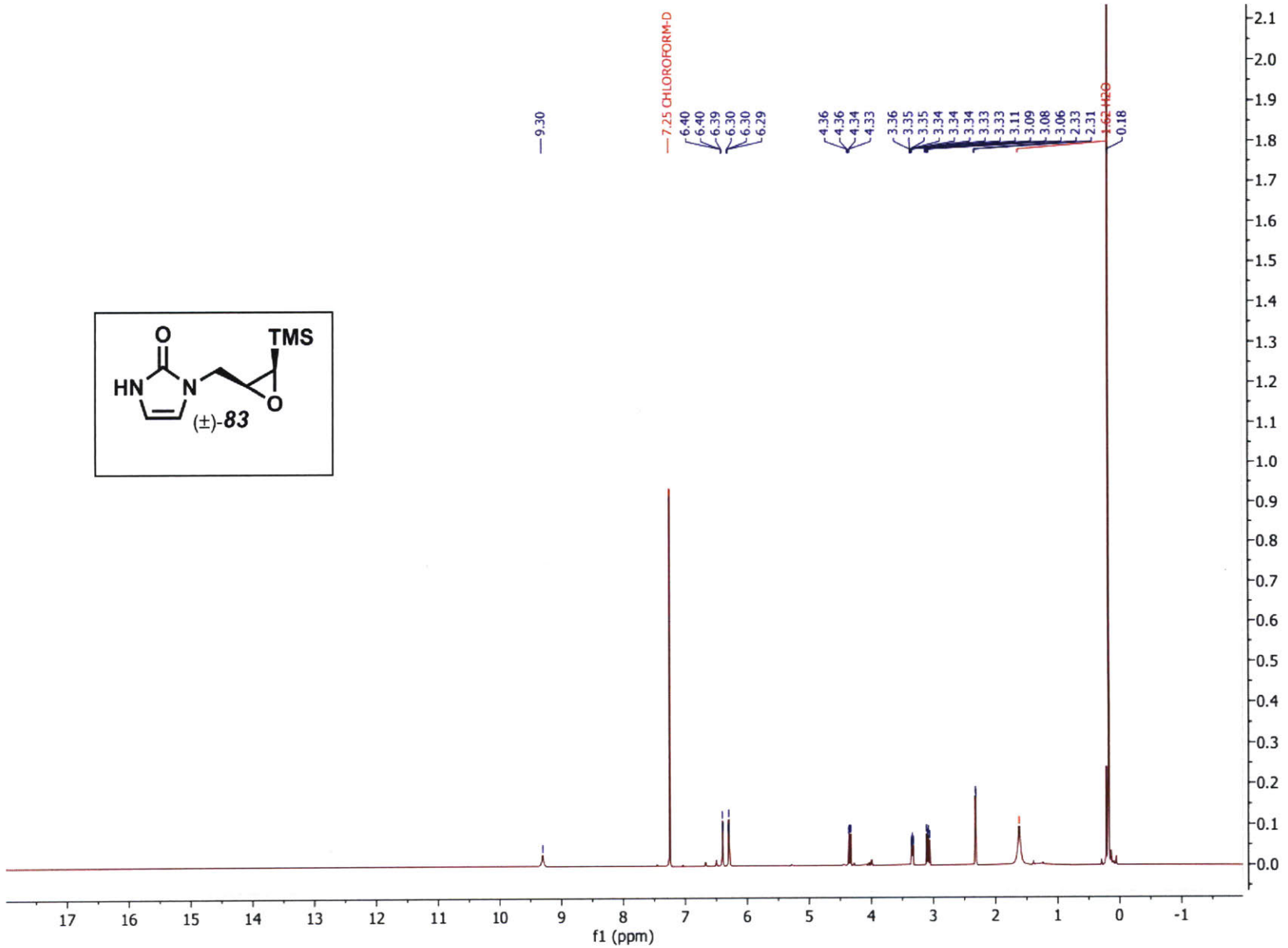
9.30
7.25 CHLOROFORM-D
6.40
6.40
6.39
6.30
6.30
6.29
4.36
4.36
4.34
4.33
3.36
3.35
3.35
3.34
3.34
3.34
3.33
3.33
3.33
3.11
3.09
3.08
3.06
2.33
2.31
1.62 H2O
0.18
O
TMS
HN
N
O
(±)-83
f1 (ppm)

9.30
7.25 CHLOROFORM-D
6.40
6.40
6.39
6.30
6.30
6.29
4.36
4.36
4.34
4.33
3.36
3.35
3.35
3.34
3.34
3.34
3.33
3.33
3.11
3.09
3.08
3.06
2.33
2.31
1.62 H2O
0.18
O
TMS
HN
N
O
(±)-83
f1 (ppm)

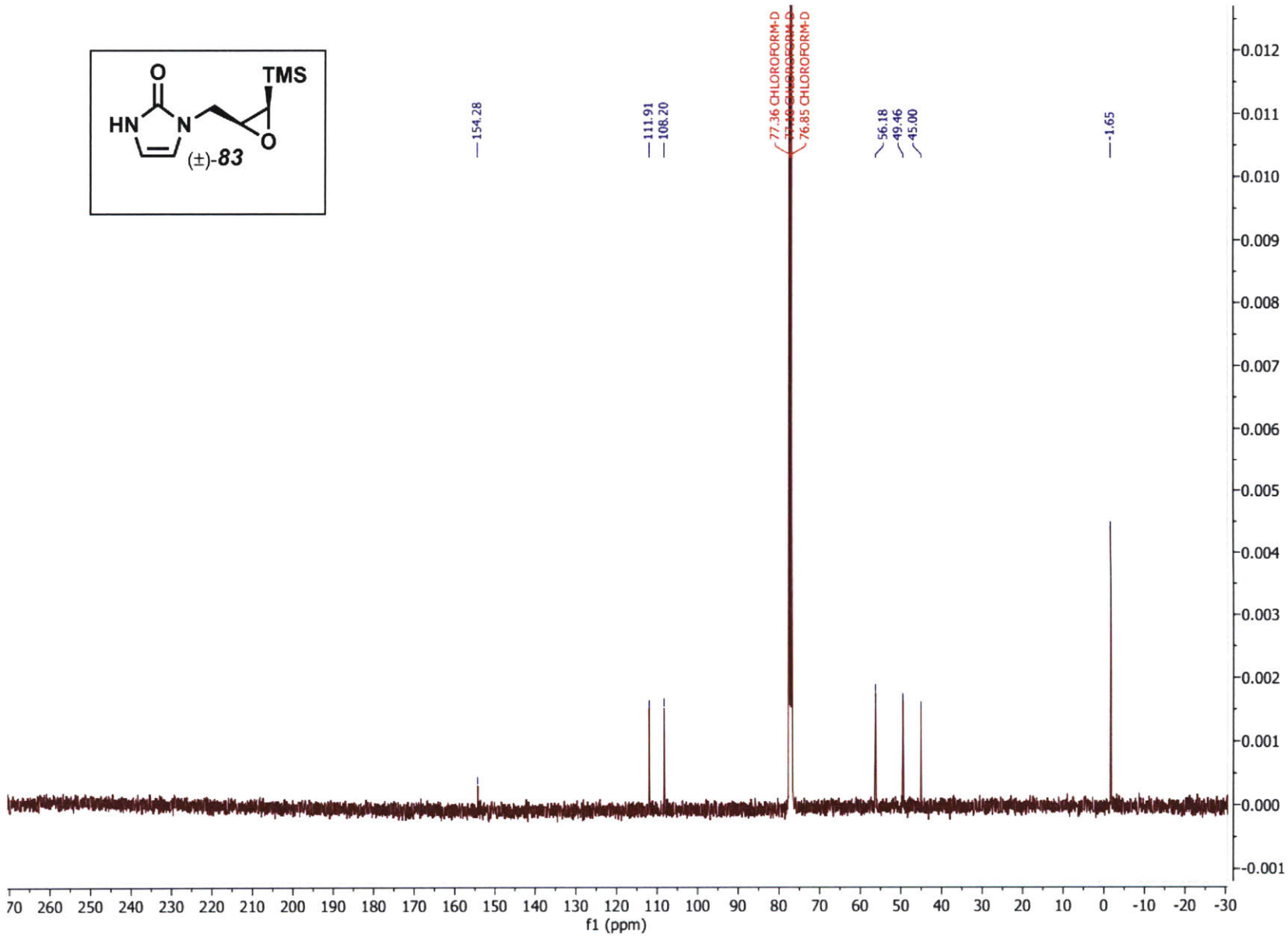
O
TMS
HN
N
O
(±)-83
154.28
111.91
108.20
77.36 CHLOROFORM-D
77.00 CHLOROFORM-D
76.85 CHLOROFORM-D
56.18
49.46
45.00
1.65
f1 (ppm)

TMS
O
HN
N
O
(±)-83
gCOSY
f2 (ppm)
f1 (ppm)

O
TMS
HN
N
O
(±)-83
HMBC
18 17 16 15 14 13 12 11 10 9 8 7 6 5 4 3 2 1 0 -1 -2
f2 (ppm)
0 50 100 150 200 250
f1 (ppm)

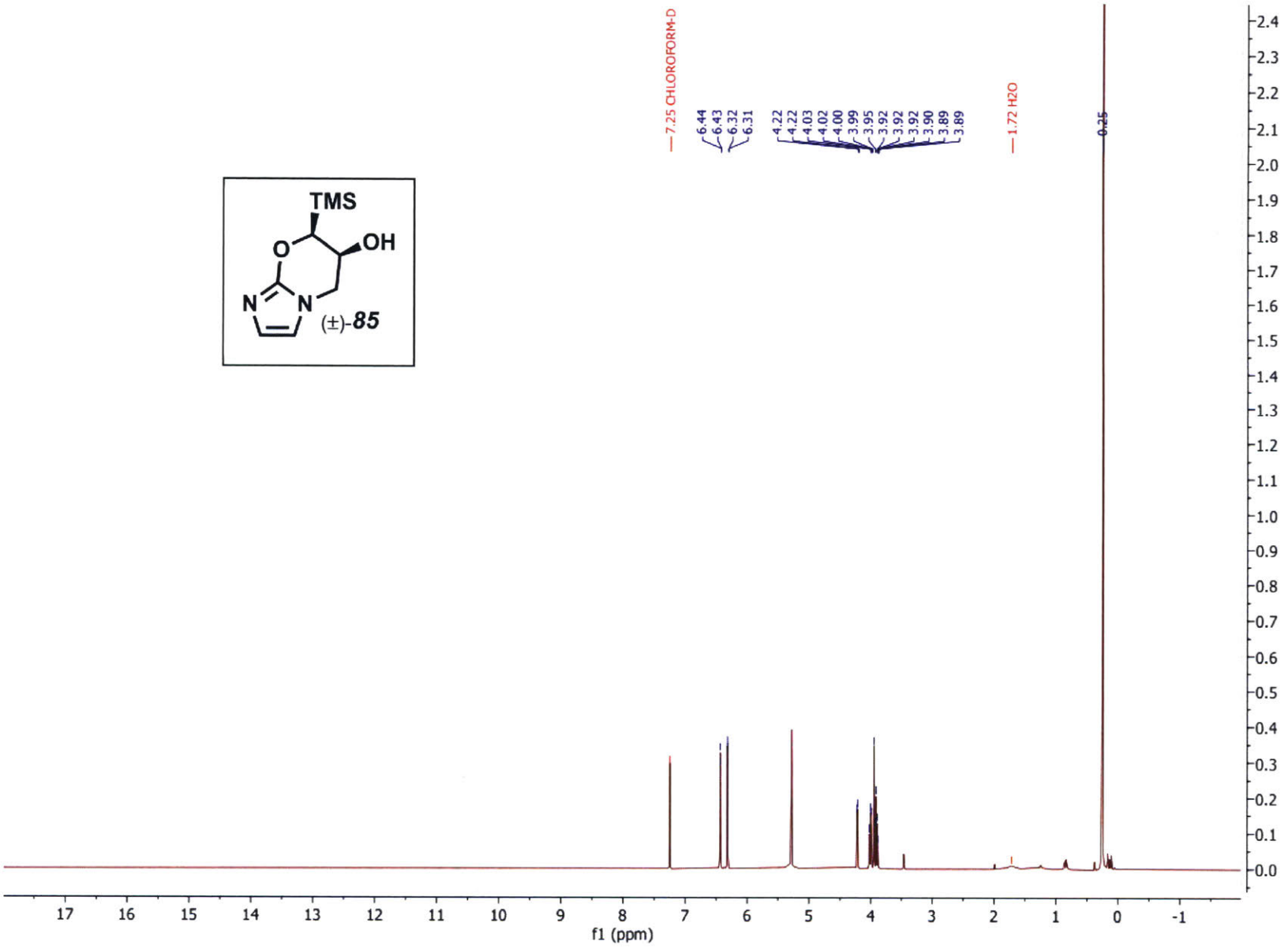
TMS
OH
O
N
N
(±)-85
7.25 CHLOROFORM-D
6.44
6.43
6.32
6.31
4.22
4.22
4.03
4.02
4.00
3.99
3.95
3.92
3.92
3.92
3.90
3.89
3.89
1.72 H2O
0.25
f1 (ppm)

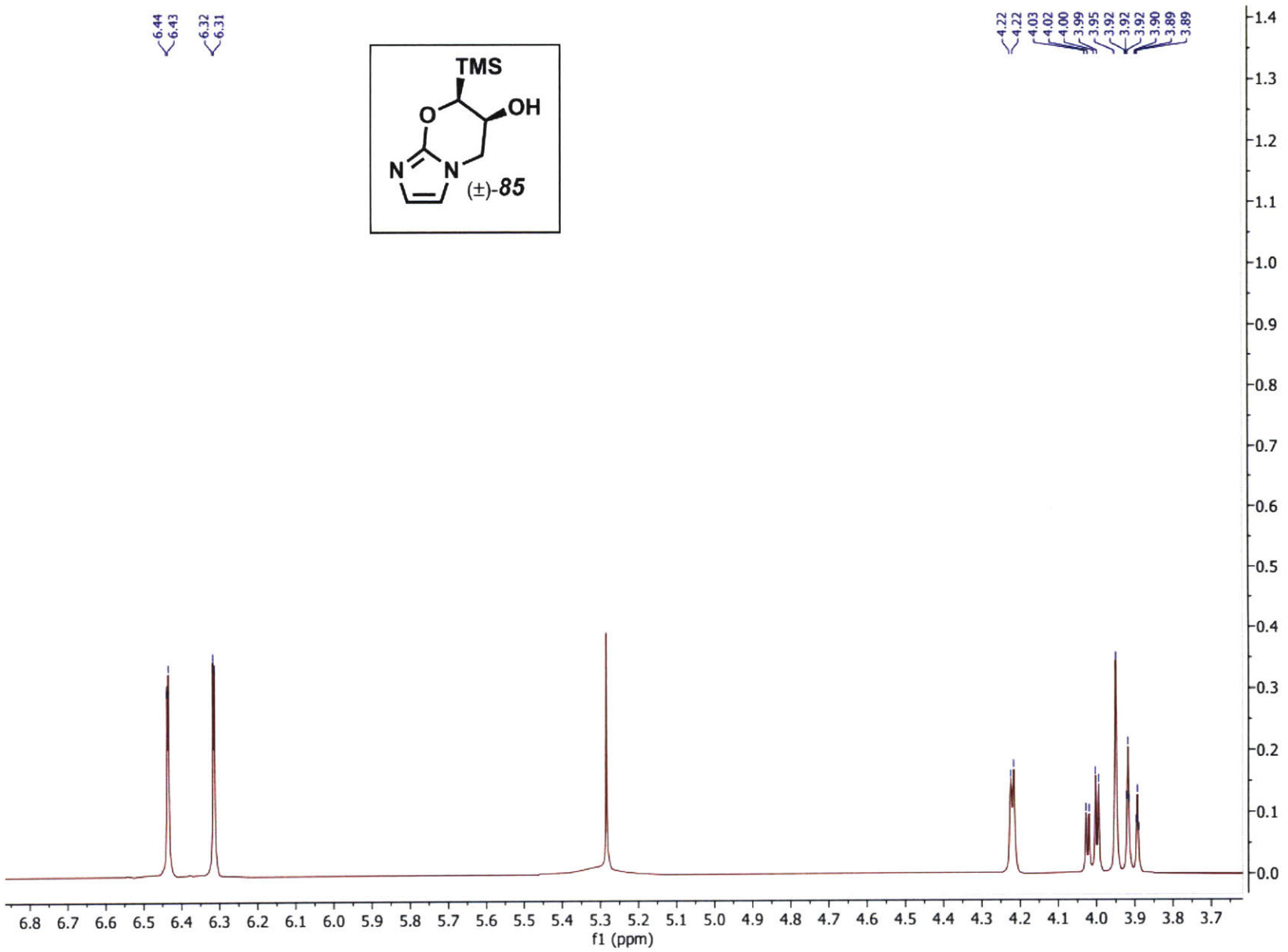
6.44
6.43
6.32
6.31
4.22
4.22
4.03
4.02
4.00
3.99
3.95
3.92
3.92
3.90
3.89
3.89
TMS
OH
O
N
N
(±)-85
1.4
1.3
1.2
1.1
1.0
0.9
0.8
0.7
0.6
0.5
0.4
0.3
0.2
0.1
0.0
6.8 6.7 6.6 6.5 6.4 6.3 6.2 6.1 6.0 5.9 5.8 5.7 5.6 5.5 5.4 5.3 5.2 5.1 5.0 4.9 4.8 4.7 4.6 4.5 4.4 4.3 4.2 4.1 4.0 3.9 3.8 3.7
f1 (ppm)

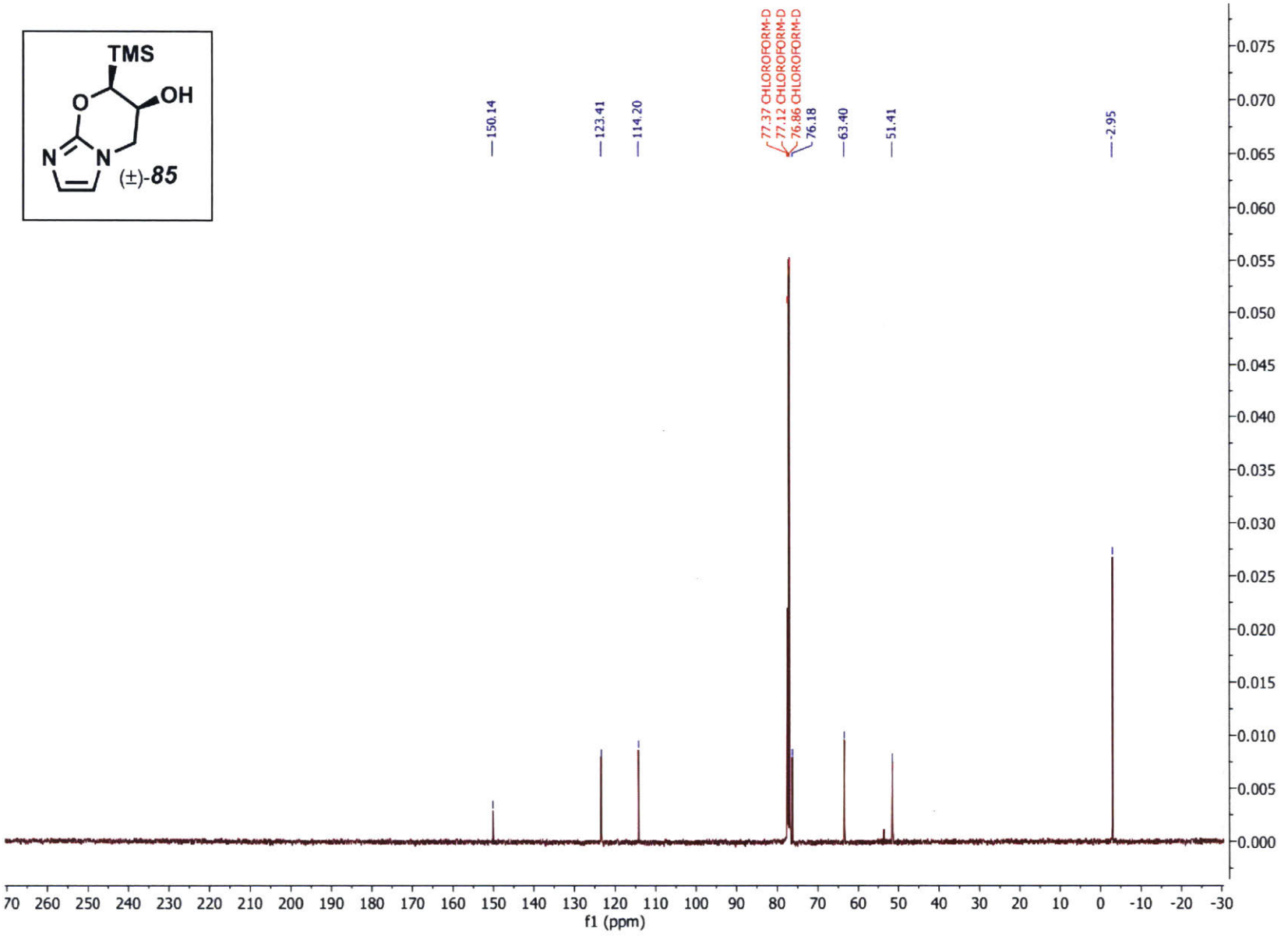
TMS
OH
O
N
N
(±)-85
150.14
123.41
114.20
77.37 CHLOROFORM-D
77.12 CHLOROFORM-D
76.86 CHLOROFORM-D
76.18
63.40
51.41
-2.95
f1 (ppm)

TMS
O
OH
N
N
(±)-85
gCOSY
f2 (ppm)
f1 (ppm)

TMS
OH
O
N
N
(±)-85
HMBC
f2 (ppm)
f1 (ppm)

Chapter Two

Investigations of Raman Spectroscopy for Through-Tube Monitoring of Continuous-Flow Reactions

Abstract

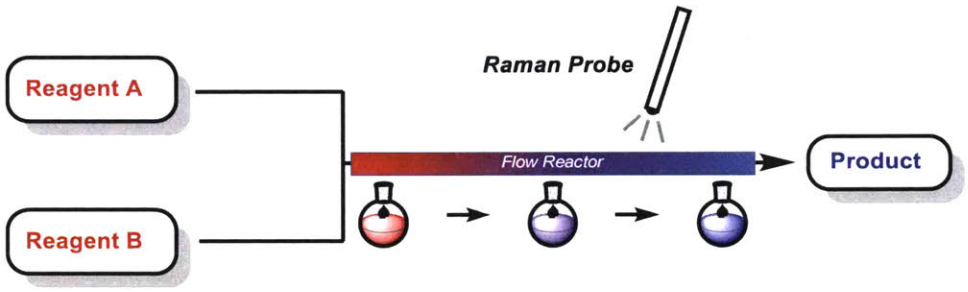

Continuous-flow chemistry has seen expansive growth and thus requires powerful new analytical techniques. The current commonly-used analytics involve inline analysis at a single point, which can hinder analysis. In this report, we demonstrate the utility of the MarqMetrix TouchRaman probe for reaction monitoring through a continuous-flow reactor. The reactions studied were ring-closing metathesis, benzyne generation, and ketene generation.

Dr. Justin Lummiss carried out Raman analysis through tubing. Dr. Justin Lummiss and Tho Tran performed experiments on ring-closing metathesis and in acquiring spectral data for all continuous-flow systems. Tho Tran carried out the synthesis of both ketene and benzyne precursors.

2.1 Continuous-flow chemistry and commonly used analytics

2.1.1 General Introduction

Continuous-flow processes have become vital for the chemist in the ever-increasing competitive landscape of the production of chemical goods and active pharmaceutical ingredients.[1,2] In this regard, the advantages of continuous-flow chemistry include safer handling of hazardous chemicals due to more efficient mass and heat transfer, and smaller production foot print from using tubing as reactors, among others.[3] Furthermore, as concern for the environment is becoming increasingly more important, continuous processes generally produce less waste when compared to batch counterparts.[4,5] The importance of this growing field is thus exemplified by the variety of commercial equipment that exist. [6,7] In a recent review of the patent literature, flow chemistry utilized in the drug development pipeline resulted in improved regio- and diastereoselectivity, higher throughput, and many of the advantages highlighted earlier.[8] As this technology increases, there will be a paralleled demand for better analytics to monitor and study these processes.

In continuous-flow chemistry, there is an opportunity to study and monitor reactions inline. For example, Leadbeater and coworkers have analyzed organic transformations in line with Raman and NMR spectroscopy.[9,10] A similar analytical approach utilized both FT-IR and NMR for real-time monitoring of fluoroform consumption by Ley and coworkers.[11,12] In those studies, a ReactIR flow cell was developed to act as an operating window in the continuous-flow process. In many of these techniques, real time data is obtained and thus decreases time and resources

spent in optimization or troubleshooting chemical reactions.[13] A limitation, however, is that the full reaction profile cannot be obtained within an equilibrated system. One approach to solve this issue is through ramping of flow rates with a static sensor.[14,15,16,17] While this solution is viable in some cases, it is still limited by a single point. Furthermore, as the flow rates are changed, the entire system becomes inherently different as other factors such as heat transfer and mixing are consequently affected. This issue is further compounded as more operation steps are added to the process.

Herein, we describe the use of an external Raman probe sensor that in principle can be located to any point in a flow system. Raman spectroscopy seen a surge in use as a powerful spectroscopic technique in manufacturing, pharmaceuticals, and biomedical applications.[18,19,20,21] This heightened prominence could be attributed to the advent of more sophisticated optics and smaller, sensitive detectors. Aligned with this prospect, we will demonstrate the MarqMetrix TouchRaman that allows the user to have immediate access to data with minimal perturbation to a chemical system.[22] The advantages highlighted are that reactions can be monitored without the integration of a sensor and real-time analysis can be performed without affecting other factors mentioned earlier. Overall, these elements contribute to a decreased operational complexity when designing a continuous system.

2.1.2 What is continuous-flow chemistry?

Continuous-flow chemistry has provided the chemist with many tools that complement existing batch techniques. For example, a number of batch chemical transformations are typically dangerous or difficult to handle such as organometallic

reactions, oxidations, and nitrations.[23] These reactions can generate intermediates that could be hazardous, unstable, pyrophoric, highly reactive, toxic, or even explosive. However, when these transformations were adapted into continuous-flow conditions, great improvements were observed.

In recent years, chemical waste has been a larger concern as it heavily affects our environment.[4] Continuous-flow chemistry, due to its generally smaller footprint, offers a great solution in efforts for greener chemical processes.[24] In continuous-flow processes, the reactors offer precise control over residence times,[25] improved mixing,[26] and the ability to telescope multistep reactions.[3,27]

From the aforementioned benefits of continuous-flow chemistry, it is not surprising to see its adoption in industries such as pharmaceuticals where there has been intense pressure to improve efficiency to keep up with rising costs.[28] In 2013, MIT scientists and engineers demonstrated an end-to-end continuous process for the synthesis of aliskiren hemifumarate.[29] In this report, a chemical intermediate was put through a series of reactions, separations, crystallizations, drying, and formulation in one tightly controlled process that was monitored at several points throughout the single, continuous-process. The end result was a throughput of the API at 45 $g \cdot h^{-1}$.

An example of a general continuous-flow diagram is shown where reagents A and B are injected and met at a junction, "mixer" shown in purple (Figure 1). After the junction, the reaction mixture of A and B proceeds through the reactor, R_1, that is then met with reagent C at second junction. The streams are mixed at the second junction and subsequently flowed through a second reactor, R_2. The exiting stream then passes through a back-pressure regulator (BPR) that acts as a gate-keeper to the system to

maintain consistent flow rates and homogeneity.[3] After passing through the BPR, the product can be isolated in-line or collected as the crude mixture.

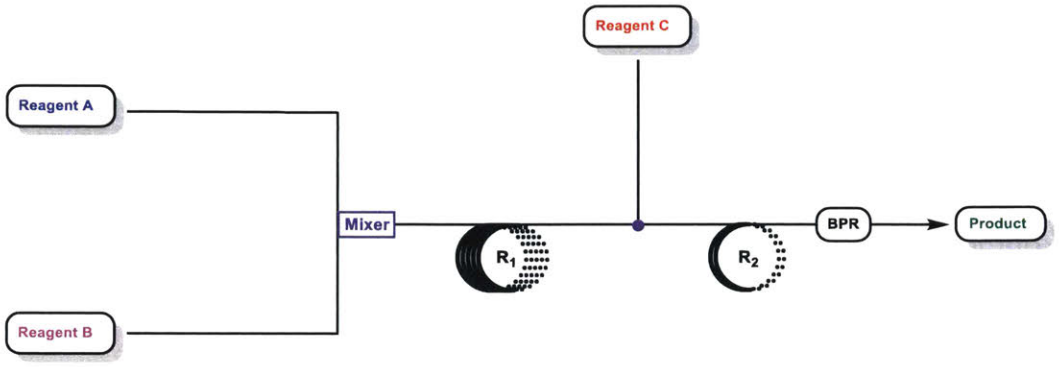

Figure 1. Simplified continuous-flow diagram.

The above continuous process can be related to a typical batch process. In both continuous-flow chemistry and batch chemistry, these reagents could be added with syringe pumps. With regard to batch chemistry, a round bottom flask, such as the one shown in Figure 2, is commonly used. A continuous-flow "round bottom flask" is the analogous perfluoroalkoxy (PFA) tubing, typically chosen for its chemical robustness, thermal stability, high pressure resistance, among others.[30] In almost all chemical reactions, mixing is incredibly important. In batch chemistry, there are many varieties of stir bars to choose from, depending on the scale or other needs of a chemical reaction.[31] Likewise, in continuous-flow chemistry, mixing can be controlled at the junction where streams at varying rates can meet through either a head-on collisions (T-mixer) or at an angle (Y-mixer). In batch chemistry, the contents of the reaction are kept separated from the atmosphere with a septum. Additionally, a condenser is often used in high temperature reactions to retain its contents. Similarly, a BPR can be considered to behave as a septum or a condenser.

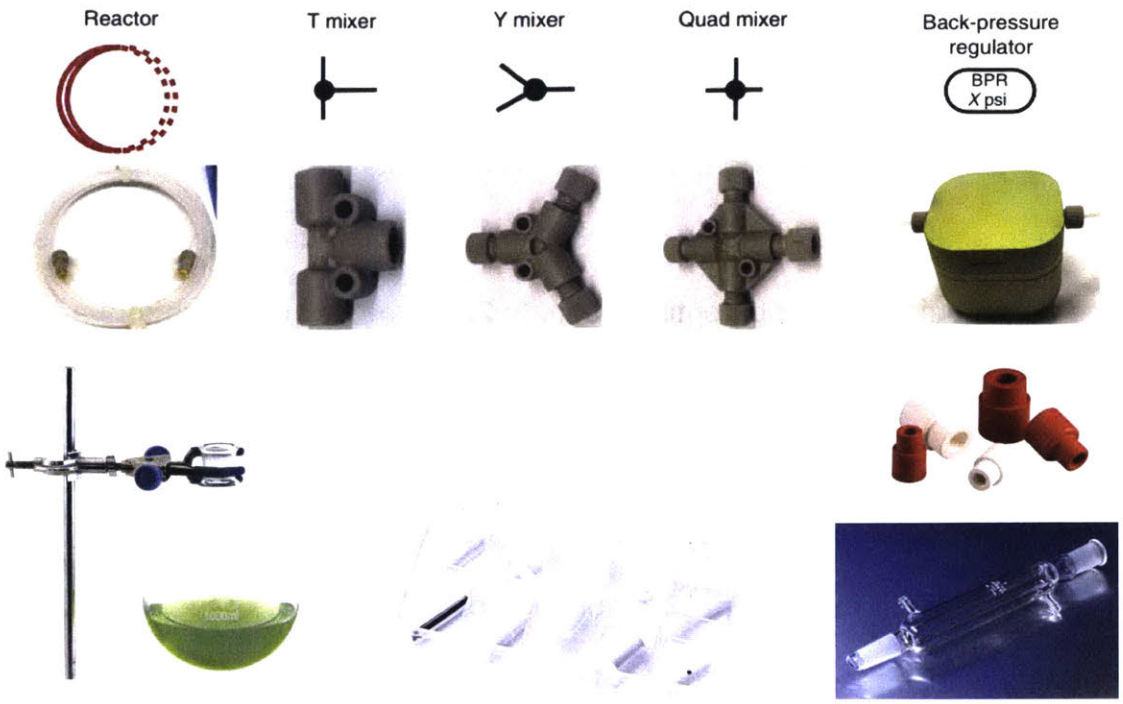

Figure 2. Representative analogous examples of flow diagram, flow equipment, and corresponding batch equipment. (Image retrieved from ref. 30)

2.1.3 Commonly used analytics in continuous-flow chemistry

Continuous-flow processes offers many opportunities for monitoring at multiple stages in real-time. At the industrial scale, process analytical tools (PATs) have become critical in maintaining stringent production quality standards.[32] Modern analytical tools have reached a level where it is possible to detect chemicals or intermediates at very low concentrations allowing for precise measurements. In continuous-flow chemistry, these tools are often used in line and must therefore be able to withstand a wide range of conditions such as high pressure fluctuations, corrosive conditions, and multiphasic mixtures.

Various inline detection techniques are available to the continuous-flow chemist such as near-infrared (NIR)[33], infrared (IR)[12], ultraviolet/visible light (UV/vis)[34], and

Raman.[9,10,19] Mass spectrometry (MS) or nuclear magnetic resonance (NMR) analytical methods have also been reported;[35]however, these techniques often require additional sample manipulations to remove undesirable components that could interfere with the signal. These analytical techniques can provide immediate data that can processed in real-time for automated reaction optimization. In 2014, the Ley research group used real-time data from an in-line IR to optimized methods for the synthesis of an important TB treatment component.[36] For the data analysis, they developed an algorithm through an open-source package software with a Raspberry Pi® as the computer. In another example, a reconfigurable system for automated optimization was developed by the Jensen and Jamison research groups.[37] The in-line analytics used for optimization included high-performance liquid chromatography (HPLC), MS, and vibrational spectroscopy.

In Figure 3, a ReactIR was used to analyze the fluorination of quinoline **3**.[12] The ReactIR flow cell (Figure 4) was placed in-line following a quench and workup with a $CaCO_3/SiO_2$ column. Consumption of reagent and product formation was analyzed using an iC IR software. While the example has the flow cell placed after the fluorination event, it can be placed further upstream. Therefore, short-lived reactive intermediates could be observed to provide insights into complex transformations, depending on where the ReactIR was positioned.

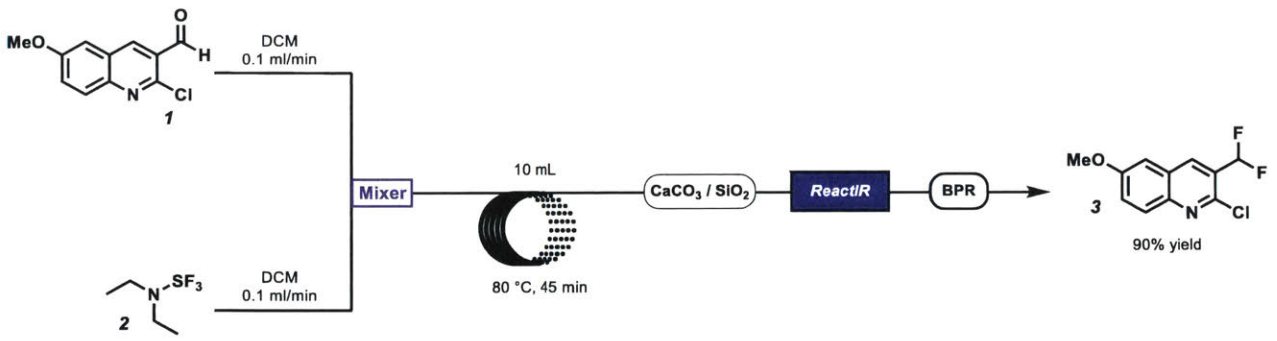

Figure 3. Fluorination reaction with in-line ReactIR analysis.

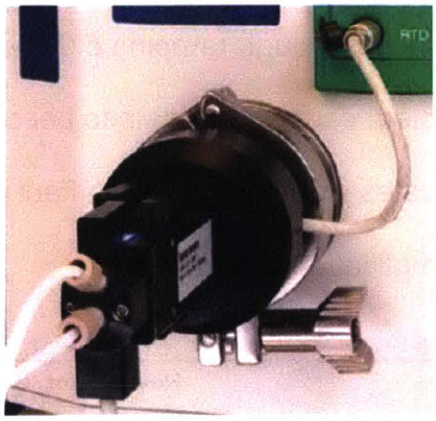

Figure 4. ReactIR with flow cell and tubing shown. (Image retrieved from ref. 36)

While in-line analytics offer many benefits, one limitation is the static nature of these devices. A roundabout solution could be to have multiple analysis windows placed throughout a continuous-process at critical points. However, this increases operational complexity, and ultimately, costs. Another setback is that many reaction conditions require cryogenic or high temperatures where the reactor is placed in the appropriate temperature bath. In order to have real-time data of the reaction profile, the circumstance dictates that the inline analytical tool must be compatible, which is often a challenging feat to accomplish.

A comparison between conversion and net yield is shown between a batch reactor and a continuous-flow reactor in Figure 5. For batch conditions, reaction progress is shown as a change in color from starting material (red) to product (blue), where the intermediacy is a combination of both (purple). In this case, the progress is a function of time. Analogously, the reaction progress can be viewed as a function of length along the reactor. Therefore, in-line analytics provide valuable data for reaction analysis; however, with the downside of only being capable of analyzing one point. A solution to circumvent this issue is through ramping of flow rates. The entire continuous-flow system is ultimately affected, causing the data to become possibly inconclusive. Moreover, changing the flow rates will consequently affect all unit operations downstream, thus, further complications can transpire.

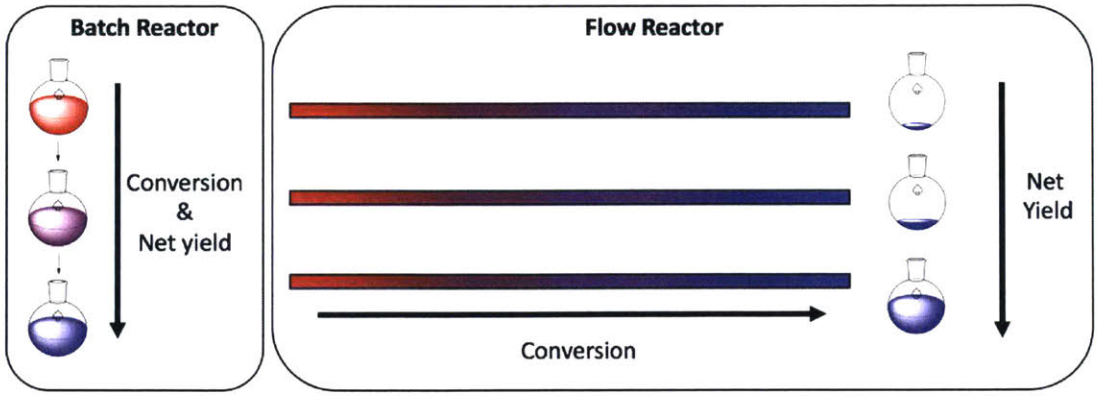

Figure 5. Reaction progress of batch process vs continuous-flow process. (I thank Dr. Justin Lummiss for this graphic.)

2.1.4 Raman spectroscopy probe

As the chemical industry expands and becomes more refined, there is an ever-increasing demand for better technology from the active chemist.[38,39] The MarqMetrix TouchRaman probe offers potential for applications in continuous-flow processes

(Figure 6). While other laser probes exist,[40] this handheld probe offers the convenience of portability through its small size with a powerful laser (500-1100 nm) source up to 500 mW. The Class 3b laser source is emitted from the all-in-one (AIO) unit that additionally functions as a computer that houses the analytical software.[41]

Figure 6. MarqMetrix TouchRaman Probe. (Image retrieved from MarqMetrix website[42])

The probe tip is a spherical, sapphire lens with the length of the probe being a Hastelloy C-276 alloy (Figure 7).[42] These specifications allow the probe to have a continuous operating temperature range from -100 °C to 300 °C, and to withstand pressures up to 6,000 PSI. Most importantly, the probe is resistant to harsh chemical conditions. With a small focal length, it can be used to analyze samples of liquids, solids, slurries, powders, and heterogeneous mixtures.

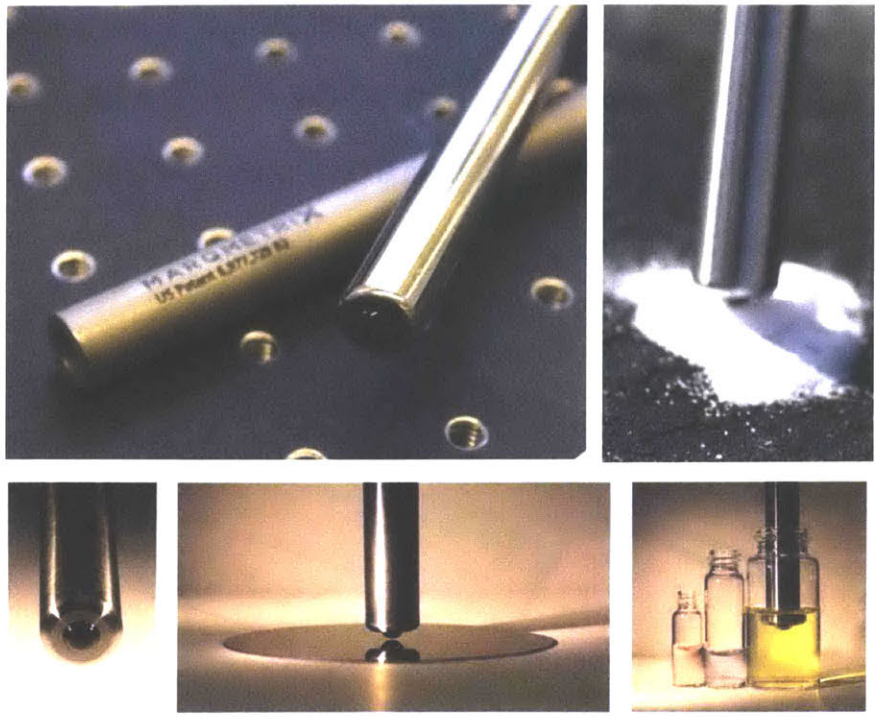

Figure 7. Possible applications of Raman probe. (Image retrieved from MarqMetrix website[42])

An advantage of the probe is seen through the use of Raman spectroscopy. The utilization of Raman spectroscopy in organic chemistry has been largely outpaced by other spectroscopic methods until recently.[43] Since Raman spectroscopy depends on the scattering of light, the laser source and detector can housed within the probe and, given the powerful laser, high resolutions of samples is possible. Furthermore, Raman spectroscopy offers a complement to existing FT-IR analytical tools.

2.2 Implementing Raman spectroscopy probe in continuous-flow systems

2.2.1 Obtaining Raman spectra through tubing

To implement this technology as a useful tool for continuous-flow chemistry, we first investigated the quality of spectra that can be obtained through various tubing. The tubing can be shaped into different designs depending on how long the reactor needs to be (Figure 8), For relatively short reactors, it can be in the free form and simply clamped (Figure 8A). For longer reactors, the design can exists as a helical coil or as a pancake coil (Figure 8B & C). Of note, the pancake coil or free form tubing is best for access to the entire reaction profile of a chemical transformation. The tubing type and select sizes (1/8" and 1/16") were then analyzed for possible operating windows at room temperature. A variety of materials exist that offer various levels of chemical robustness and compatibility ranging from quartz to PFA and HPFA (high quality perfluoroalkoxy). From Table 1, the operating windows are shown in green. In general, these regions lack any pervasive signal from the tubing material and thus allows us observe our analyte without any interference. The operating windows of PTFE, HPFA, and PFA are of particular interest given that the entire region past the fingerprint (>1450 cm^{-1}) display no competing signals. Likewise, Teflon-AF showed superior operating windows; however, its relatively high costs deter its use unless absolutely necessary. Silicon, and in particular, quartz displayed the smallest operating windows, but may be useful in niche cases.

Having established operating windows for tubing material, our next study was to establish Raman signal deviations on possible bath media that the probe and reactor will be submerged in. From Table 2, 1,2-dichloroethane (DCE) and its peak at 944 cm^{-1} was chosen as our standard for these studies. The "counts" on the y-axis are the relative intensity of signal. Of interest to the organic chemist are the common media: water, acetone, and silicone oil, all of which showed intensification of signal. Silicone oil, compared to air, showed a 26% average boost in signal. In addition, the signal intensities were overall more consistent. IPA also showed similar increases in signal with good consistency and thus offers an excellent alternative to acetone baths. Surprisingly, vegetable oil was the best bath media with the over 50% increase in signal. However, silicone is likely to be used more often due to its ubiquity in the laboratory. When a flow cell was used, the signal was increased by a factor of 2.5x. Therefore, a flow cell offers an excellent solution for reactions that are difficult to observe due to low concentration or weak signals.

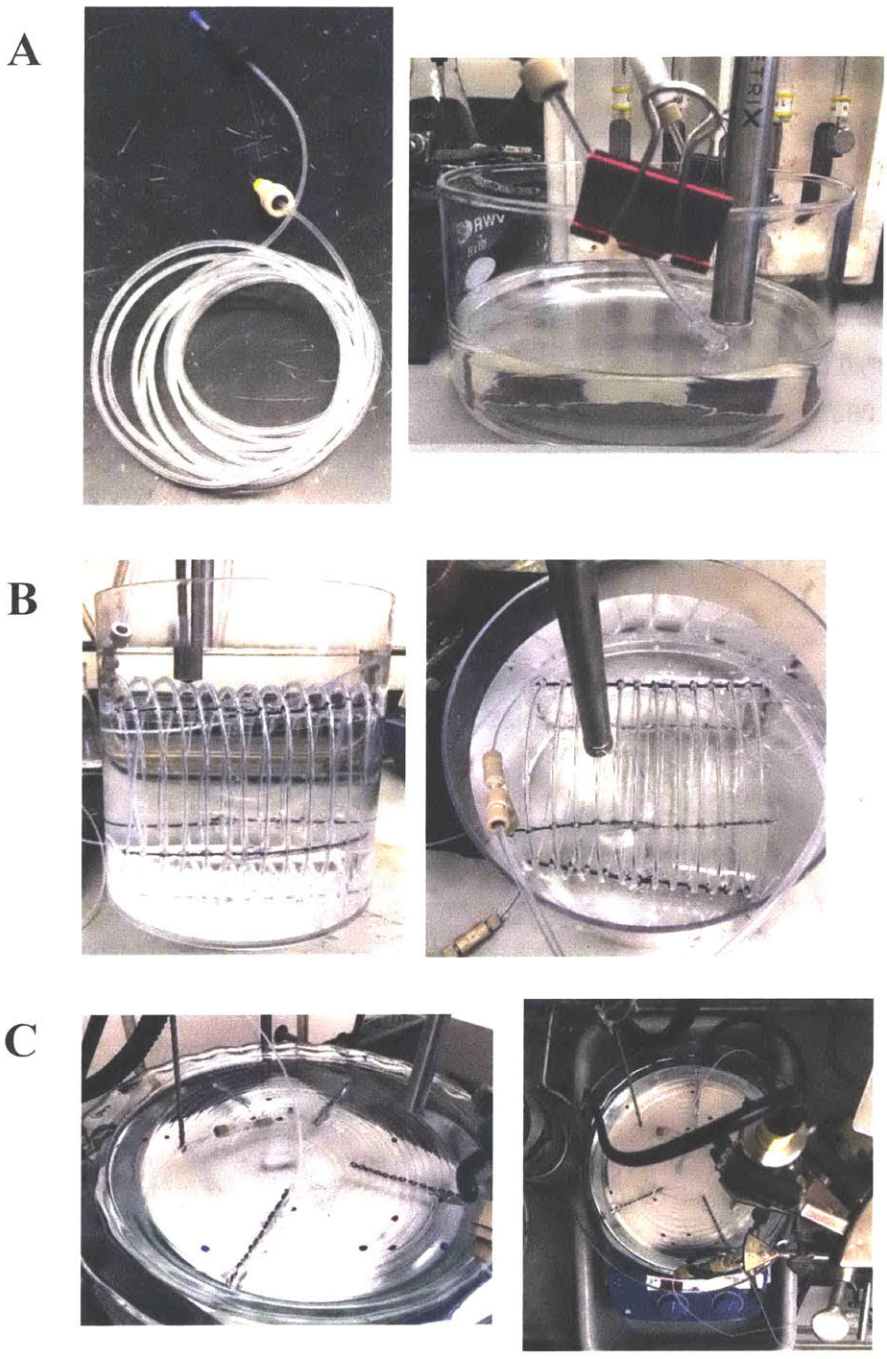

Figure 8. A) Free tubing (left), free tubing dispersed in oil bath (right). B) Helical coil side view (left), helical coil top view (right). C) Pancake coil side view (left), pancake coil (right).

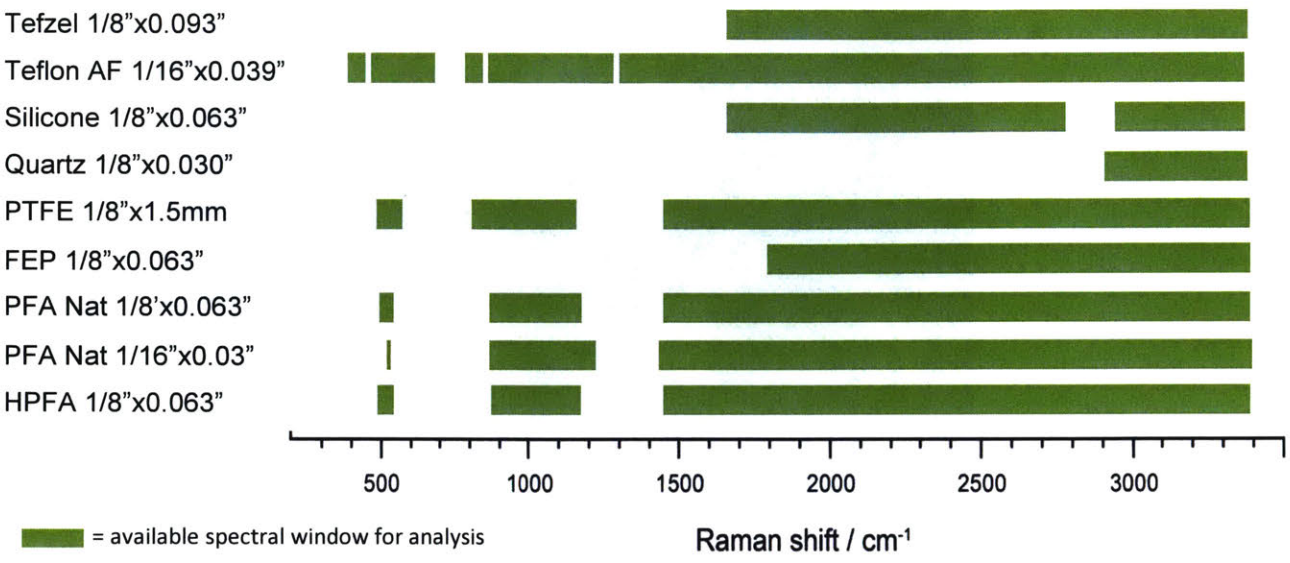

Table 1. Raman signal operating windows for various tubing types. (I thank Dr. Justin Lummiss for this graphic.)

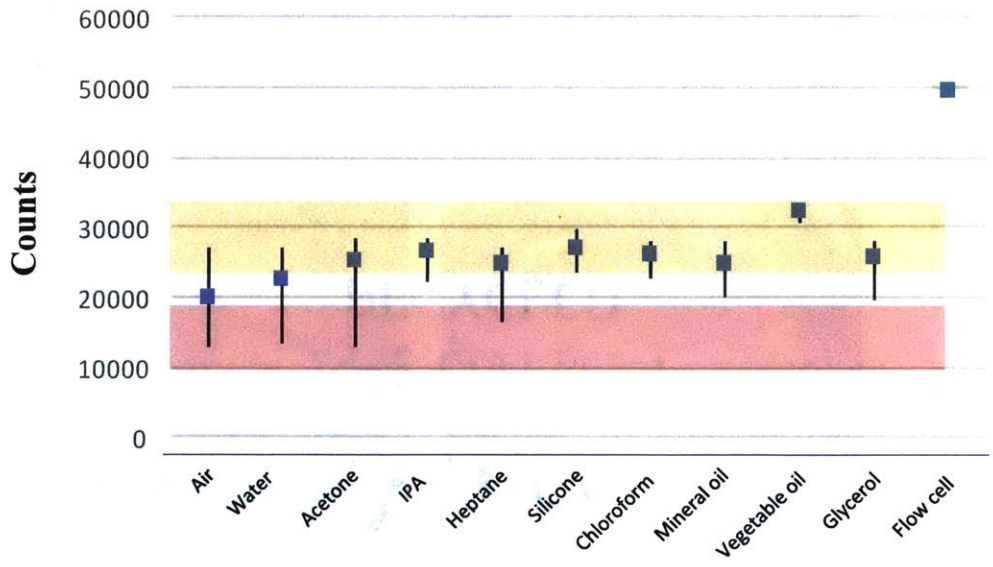

Table 2. Raman spectra signal from bath media. (I thank Dr. Justin Lummiss for this graphic.)

Our next investigation was into signal strength regarding tubing outer and inner diameter.[1] From Figure 9, the tubing were all commercial sizes from Idex.[44] Using DCE as the standard, PFA 1/16"x0.04" displayed the overall best signal. Furthermore, three out of four 1/16" outer diameter tubing displayed better signal overall when compared to 1/8" outer diameter tubing. From Figure 10, we observed an overall trend in loss of signal as wall thickness increases. This is likely caused by loss in signal from less scattered photons reaching detector as the thickness increases. While 1/16" tubing appeared to be the likely choice going forward, it was much more difficult to obtain reliable signal because of alignment issues with the probe tip and the tubing.

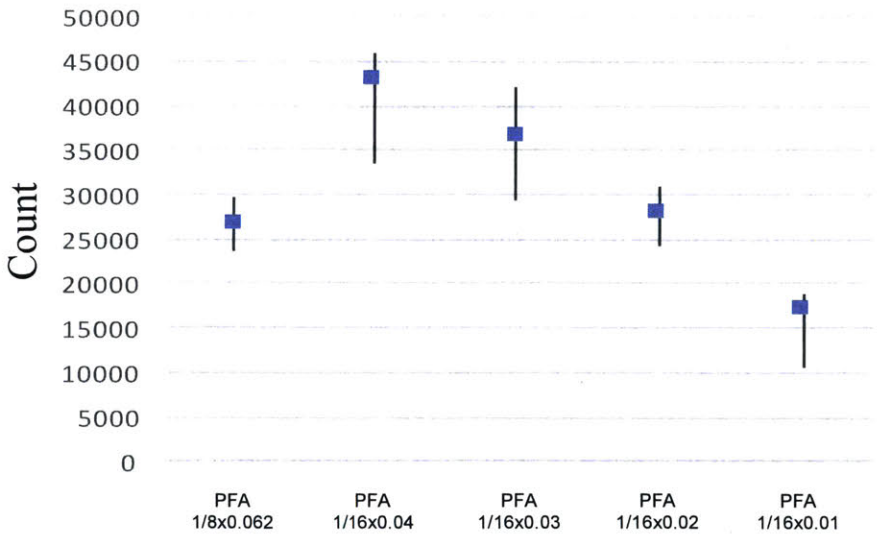

Figure 9. Signal intensity vs PFA wall thickness and outer diameter. (I thank Dr. Justin Lummiss for this graphic.)

[1] Typically reported as 1/8"x0.062" where 1/8" is the outer diameter and 0.062" is the inner diameter.

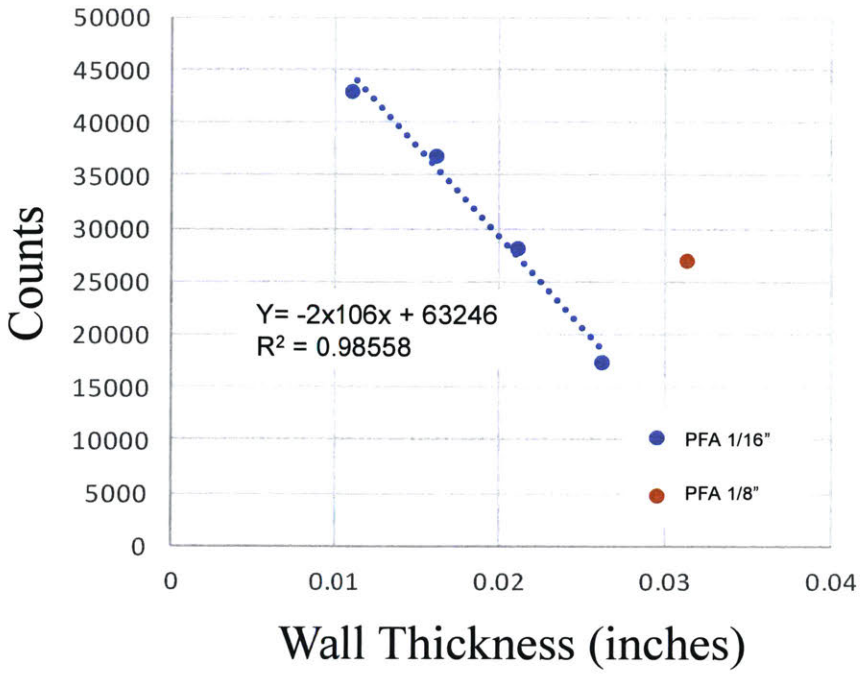

Figure 10. Trend in signal intensity vs wall thickness. (I thank Dr. Justin Lummiss for this graphic.)

Since thermally promoted reactions are vital in continuous-processes, we then investigated the effects of temperature on signal intensity. From Figure 11, it can be seen that from room temperature to 80 °C, there is little change in signal and spectrum quality. However, at 120 °C, there is a significant saturation of signal along the fingerprint region. A possible cause is that PFA polymer went through a glass transition at these temperatures and thus oversaturated the detector due to its structure no longer being uniform.[45] As mentioned earlier, PFA showed only signal at lower ranges of <1700 cm^{-1} and we can see that signals above that are not as affected.

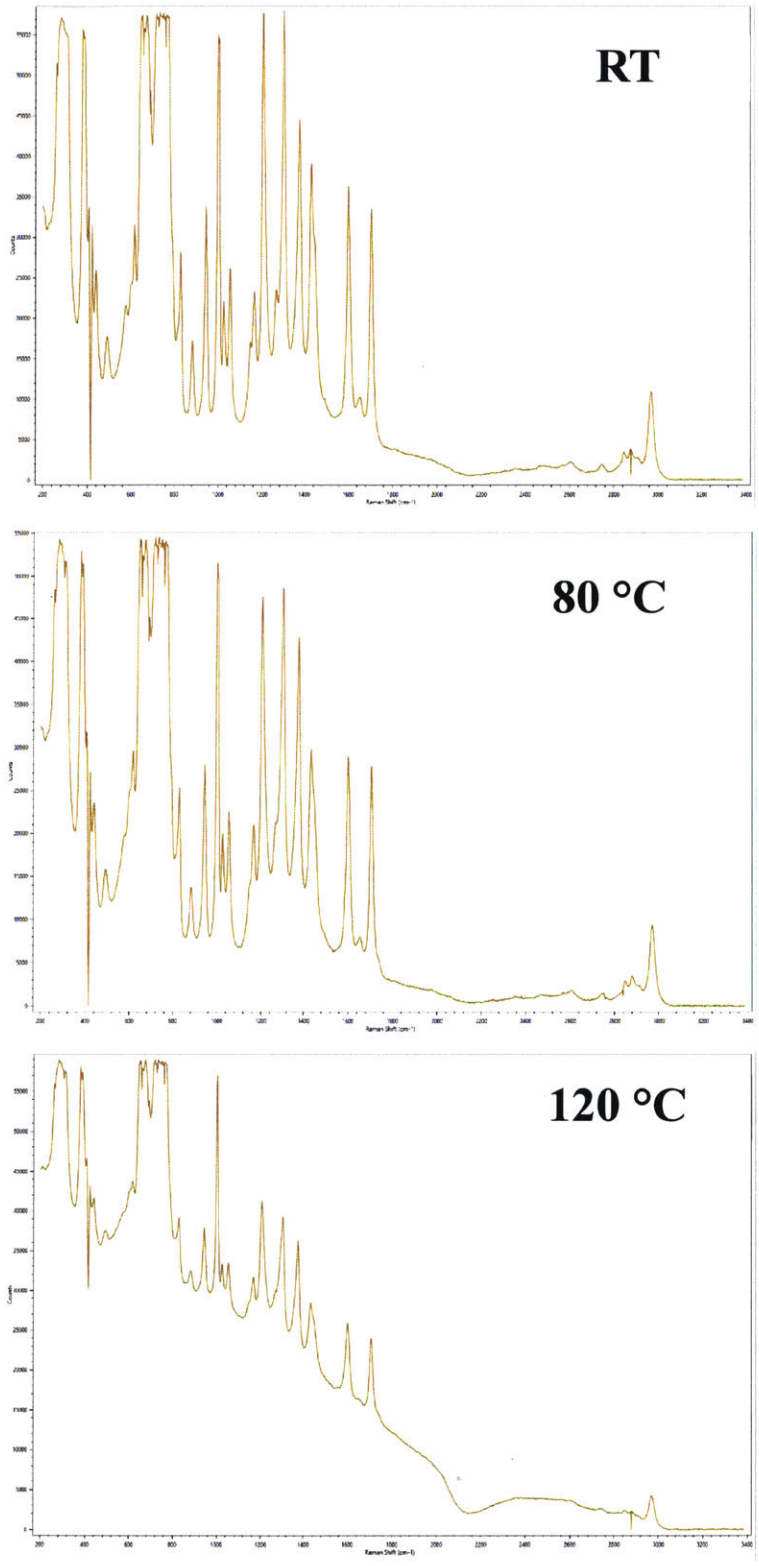

Figure 11. Effects of temperature on acquired spectra when Raman probe was used to analyze a solution through tubing.

Through our optimization studies, PFA or HPFA tubing was the best going forward. In particular, 1/8"x0.062" would be used as it is easier to align with the probe tip. Furthermore, the bath media overall increased signal when compared air with the ubiquitous silicone oil providing an increase in signal. While high temperatures may pose a challenge, it was seen that the fingerprint region was mostly affected. As a result, if the signal of interest lies above that region, such as olefins, alkynes, or nitriles, then data analysis would be minimally affected.[46]

2.2.2 Development of probe adapter

Throughout our experiments, we found that alignment issues were a common occurrence that often slowed data acquisition. While holding the probe in place with one's hand was adequate, there was a chance that inconsistencies resulted due to fatigue or small movements. Clamps to hold the probe in place were also used but would still require realignment between each change in position along the tubing.

Therefore, we sought to improve uniformity by creating an adapter for the probe. From Figure 12A, we can see the probe held in place with clamps and pressed firmly against the tubing. This ensured complete contact; however, slippage could occur. From Figure 12B and C, our first generation probe adapter was designed using two pieces of wood held in place with electrical tape. A notch was cut out to hold the tubing at the apex of the lens. While this design worked well for our studies, the materials were not chemically robust. From Figure 12D and E, we designed a PFA adapter that fit perfectly around the adapter with a laser-cut notch to hold in our tubing in place firmly. This PFA adapter has the potential of being 3D printed and would allow for wider availability.

With our probe optimized for analyzing data in continuous-flow chemistry conditions, we set forth with the analysis of chemical reactions.

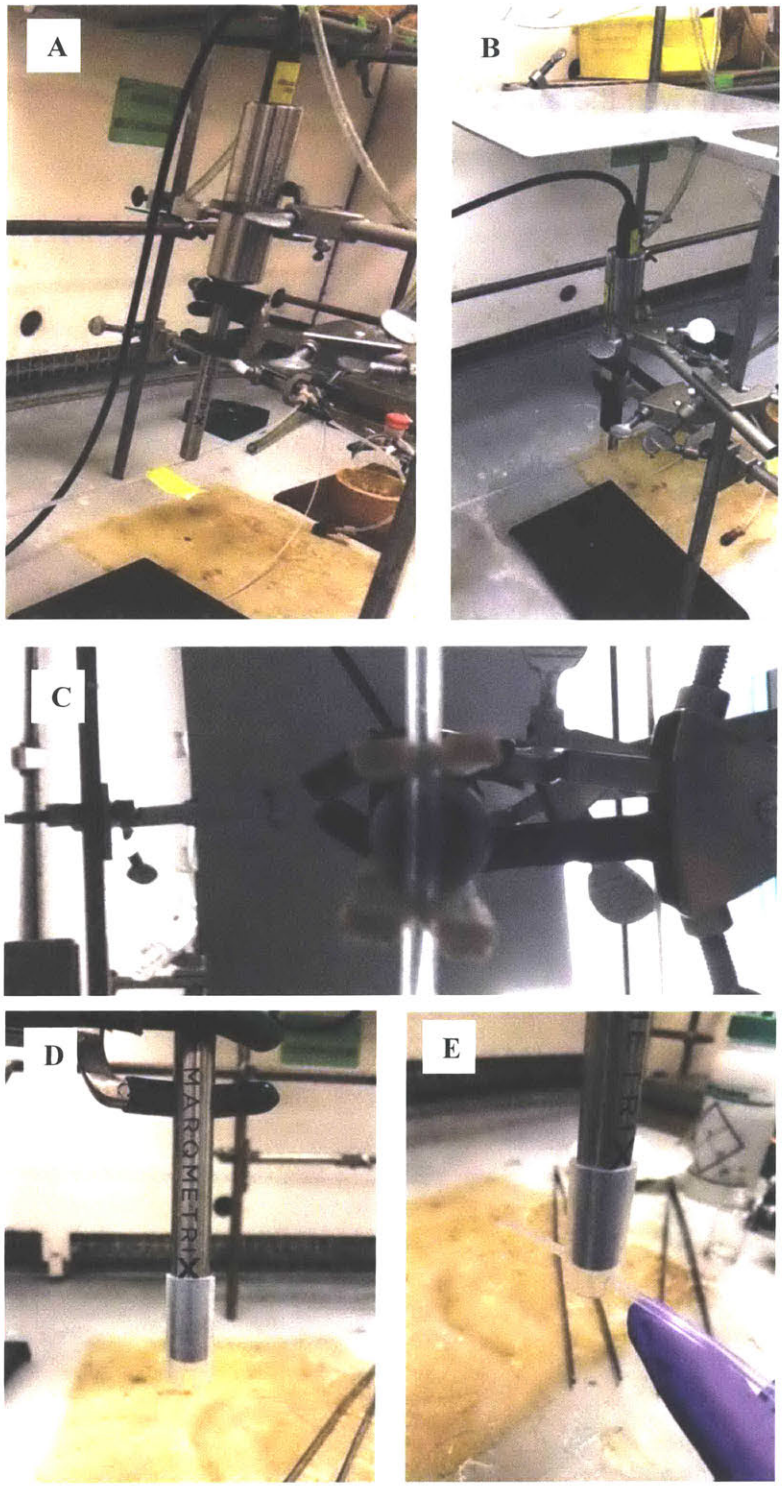

Figure 12. A) Probe clamped in place over tubing. B) First generation tubing adapter, side view. C) First generation tube adapter, bottom-up view. D) Second generation tube adapter, side view. E) Second generation tube adapter with tube in place.

2.3 Analysis of continuous-flow organic reactions with Raman spectroscopy probe

2.3.1 Raman analysis of a ring-closing metathesis reaction

To demonstrate the utility of the Raman probe, we chose a ring-closing metathesis (RCM) example. Through a standard system designed for characterizing olefin metathesis,[47] the reaction would involve diethyldiallyl malonate (DDM) **4** with a Hoveyda-Grubbs II (HG II, **5**) catalyst to form ring-closed DDM (R-DDM) **6** (Figure 13). This system was chosen due to the presence of olefin (~1600 cm^{-1}) and carbonyl (~1700 cm^{-1}) peaks that are easy to discern on the Raman spectrum.

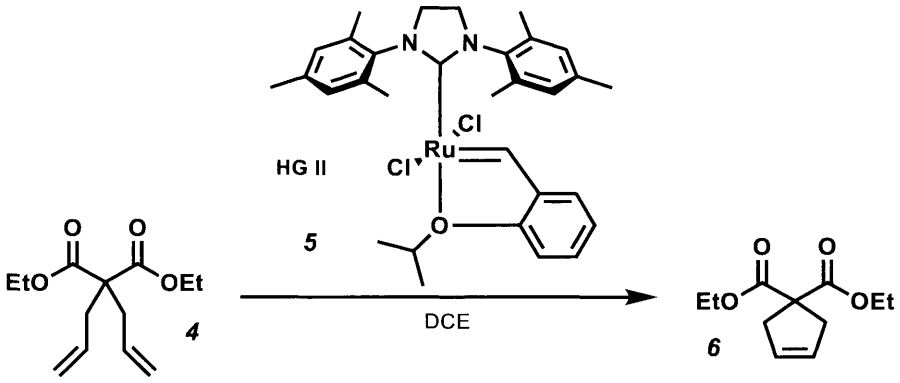

Figure 13. Ring-closing metathesis of diethylallyl malonate **4**.

Prior to studying the transformation in a continuous-process, we investigated the signal strength relative to concentration and their corresponding reproducibility. Various concentrations from 50 mM up to 1000 M of DDM (**4**) in DCE were examined (Figure 14). In each case, the olefin peak of DDM at 1642 cm^{-1} was compared to DCE peak at 944 cm^{-1}. This strategy provided a normalized data set as the DCE peak does not change in intensity as it is the solvent. From Figure 14, an expected increase of signal

was observed as concentration was increased. A calibration curve was then possible to obtain and would allow for determination of unknown concentrations (Figure 15). Importantly, the data was consistent from trial to trial with the properly aligned probe with the tubing. With regard to concentration threshold, it appears that 50 mM is the lower limit at which we can observe adequate spectra. This threshold may be higher or lower depending on the strength of the observed peak.

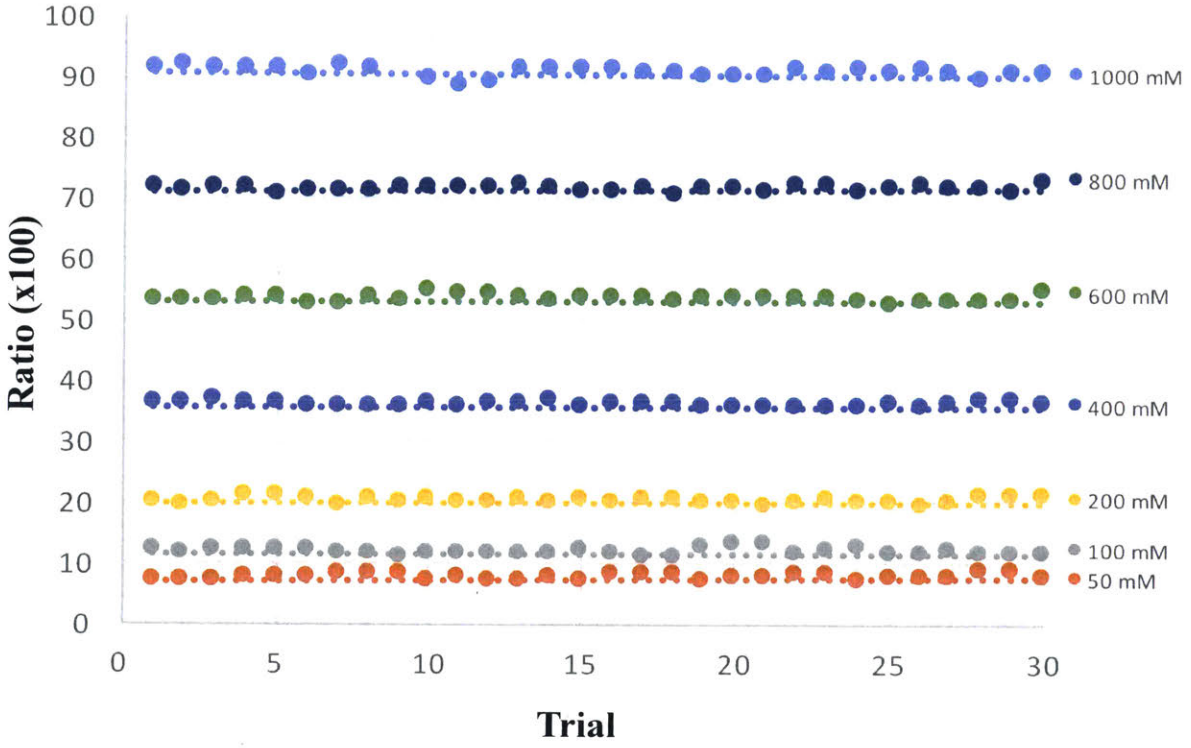

Figure 14. Signal intensity vs, concentration, and corresponding reproducibility. DDM (**4**) was dissolved in DCE at different concentrations and peaks at 1642 cm^{-1} of DDM and 944 cm^{-1} of DCE were compared. (I thank Dr. Justin Lummiss for this graphic.)

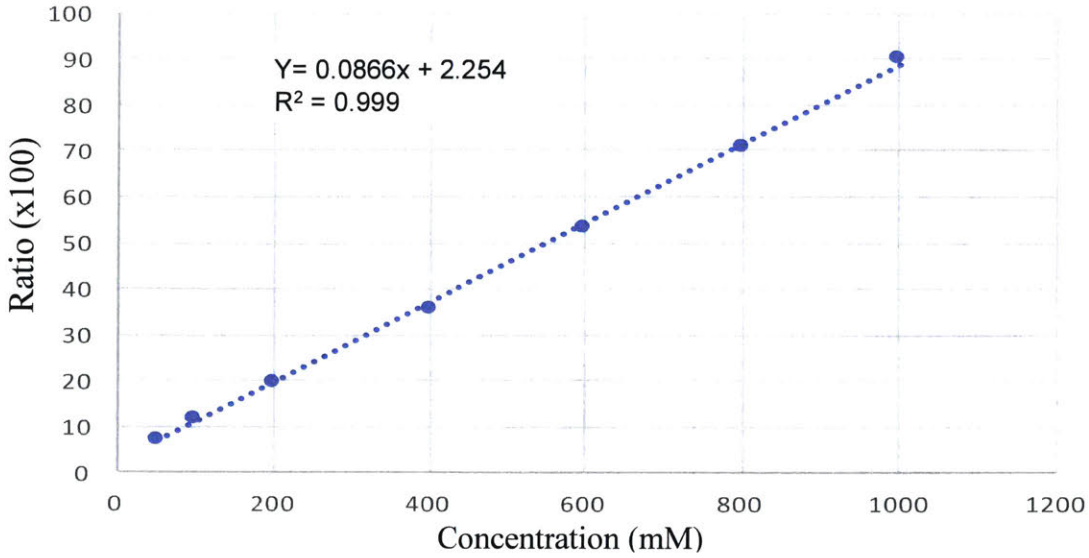

Figure 15. Calibration curve for DDM in DCE. (I thank Dr. Justin Lummiss for this graphic)

This transformation was implemented into a continuous-flow process and shown in Figure 16. A 2 M solution of DDM (**4**) in DCE was met with a 0.02 M solution of HG II (**5**) and flowed through a reactor at room temperature with a residence time of 45 minutes. The reactor was measured at multiple points that correlated with the appropriate residence times. From Figure 17, the conversion of **4** and yield of **6** was monitored throughout the reactor. The reaction was noticeably fast initially and plateaued at the 10 minute mark. Similarly, conversion stalled around 80% and no further starting material was observed to be consumed. In the continuous-flow system, ethylene is dissolved to a greater extent compared to the batch conditions given the presence of the BPR. Furthermore, ethylene does not escape the solution in our continuous flow process. Therefore, the stalled conversion of DDM could be from the presence of dissolved ethylene hindering the catalyst from releasing more ethylene through its catalytic cycle.[48] A complication that occurred was the overlap of ethylene peak (1620 cm^{-1}) with product olefin peak **6** at 1625 cm^{-1}. Nonetheless, we have

successful demonstrated the capability of the Raman probe to monitor continuous-flow reactions throughout a reactor without needing to be fixed to a single point.

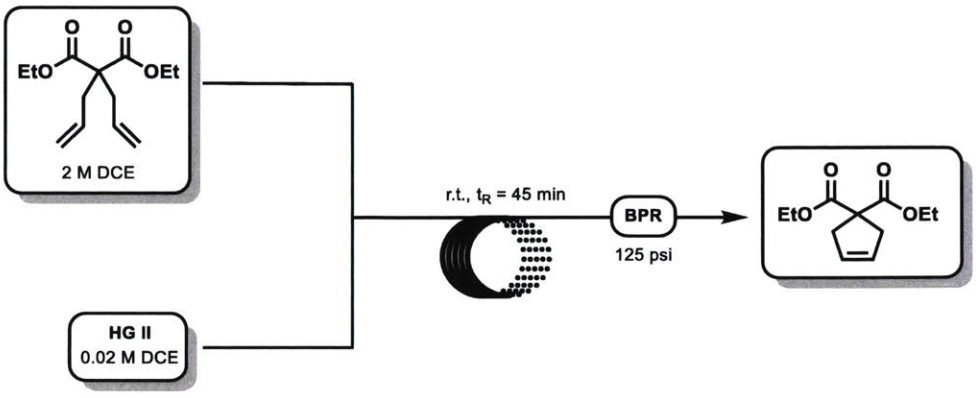

Figure 16. Continuous-flow process of DDM RCM.

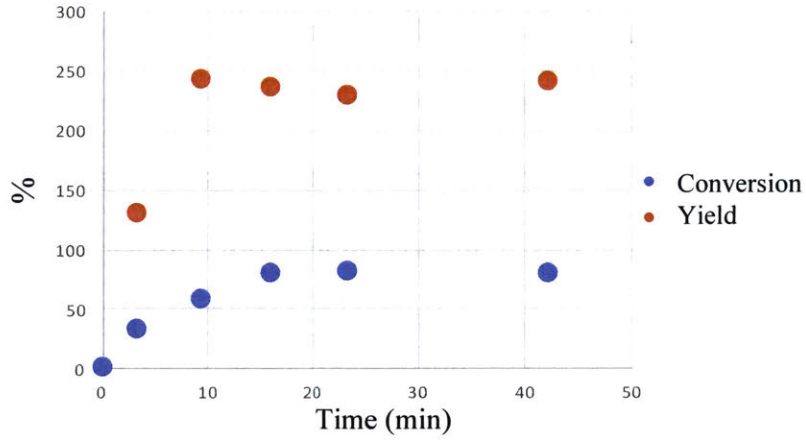

Figure 17. Conversion and yield along the reactor. (I thank Dr. Justin Lummiss for this graphic.)

2.3.2 Raman analysis of a benzyne intermediate

With our first example of reaction monitoring successful, our next objective was to observe possible benzyne intermediate **7**. Originally known as 1,2-dehydrobenzene (**1**), the term "benzyne" was finally coined by J.D. Roberts after half a century of research.[49] Since their discovery by Stoermer and Kahlert in 1902,[50] the unique

reactivity of these intermediates have fascinated chemists.[51,52,53] Benzynes undergo a variety of transformations including nucleophilic additions, multicomponent reactions, σ-bond insertion reactions, [4+2] cycloadditions, [2+2] cycloadditions, and metal-catalyzed reactions (Scheme).[54] These various transformations have been important tools for synthetic organic chemistry and have been implemented in a variety of total syntheses of natural products and active pharmaceutical ingredients (APIs).[55]

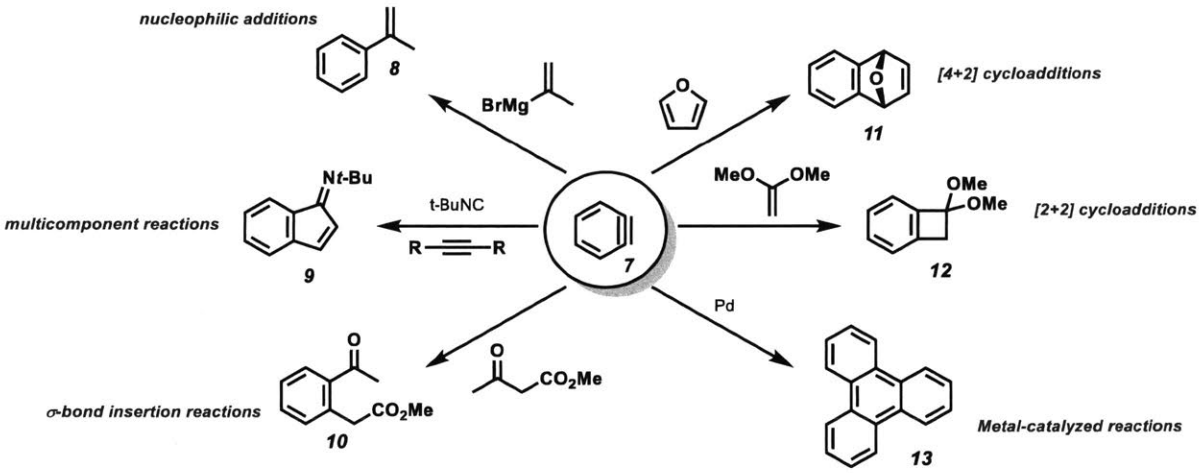

Scheme 1. Representative transformations of benzynes.

The highly reactive nature of benzynes is due to the very strained nature of the triple bond.[54] Unlike traditional alkynes, benzynes react as electrophiles. In an extended application of the Hückel theory, Hoffman[56] and Houk[57] explained that because the π-orbitals of the alkyne deviate considerably from 180°, the LUMO is significantly lowered allowing for better overlap between the HOMO of nucleophiles and dienes.[58] The alkyne present in benzyne has been assigned a band at 1846 cm^{-1} and is generally strong in Raman given its symmetry.[59]

There are various methods to generate benzyne such as through strong bases or entropically driven conditions.[54] We settled on using benzyne precursor 2-(TMS)phenyl trifluoromethanesulfonate **14** because the desired intermediate could be formed with a fluoride source and this would simplify the components within the reaction (Figure 18). While **14** was commercially available, it was expensive for the amount that was anticipated to be used given that high concentrations were ideal for good signal.

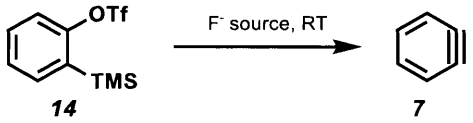

Figure 18. Benzyne generation via o-(TMS)phenyl triflate.

Shown in Figure 19, there exist various methods for the synthesis of **14**.[60] Many of these were lengthy and required multiple steps. As a result, we sought a quick synthesis that combined the benefits of the available methods. The final route that was established is shown in **Figure 20**. 2-Bromophenol (**18**) was reacted with HMDS to afford *o*-(TMS)phenyl bromide **25** in quantitative yield. Then, treatment of **25** with butyllithium afforded phenoxide **27** that was then quenched to give **19** in 93% yield. For this lithium-halide exchange reaction, the chloride was also explored due to its lower cost relative to the bromide variant. However, desilylation was observed primarily over lithium-halogen exchange, likey due to the stronger carbon-chlorine bond.[61] Last, triflation with Tf_2O provided benzyne precursor **14** in 83% yield. Telescoping was investigated and phenoxide **27** was possible to be trapped with Tf_2O to give **14** in 87% yield over 3 steps at a 5 g scale. This telescoped, one-pot method allowed us to access material relatively quickly without going through many purifications.

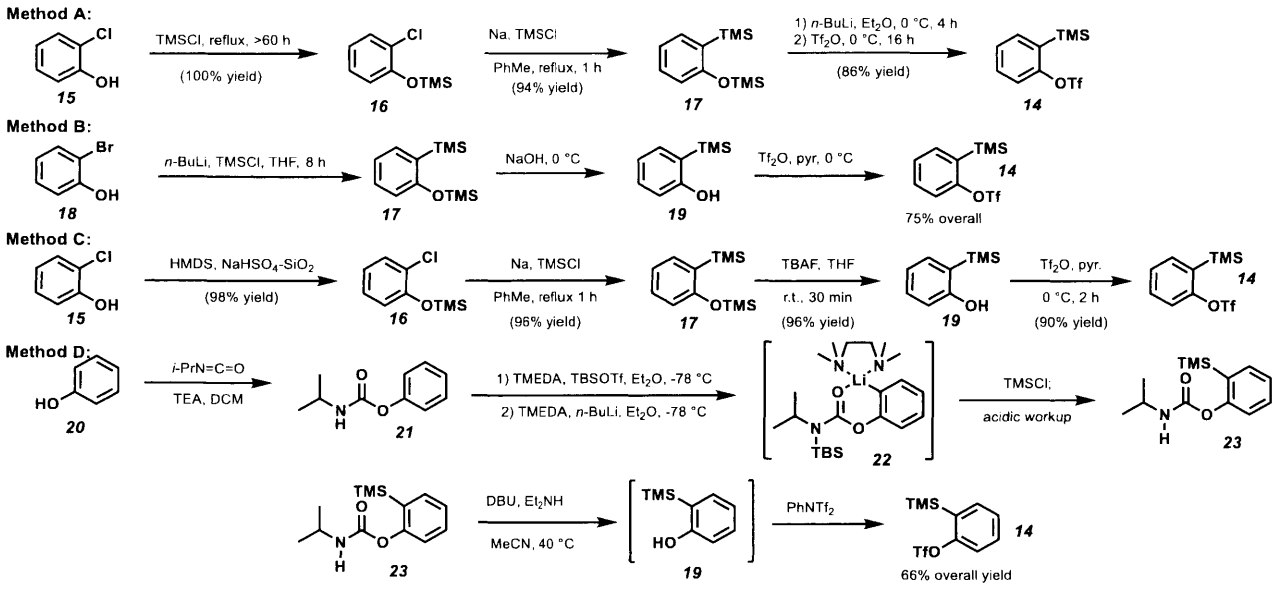

Figure 19. Various methods to synthesize o-(TMS)phenyl triflate.

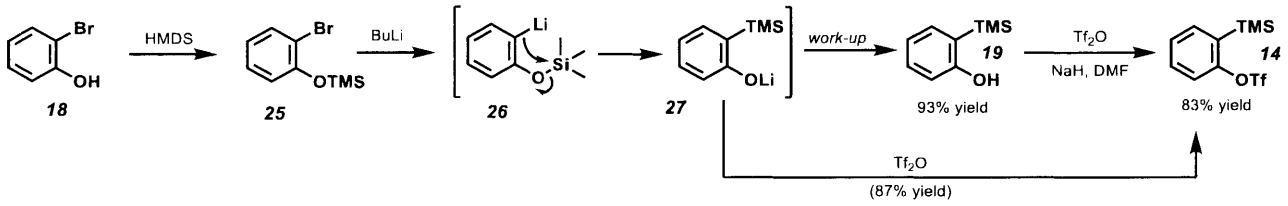

Figure 20. Established large-scale route of the synthesis of benzyne precursor **14**.

We then examined control experiments to validate formation of our desired benzyne intermediate. From Table 3, two common benzyne generation conditions were investigated with dimethyl furan **28** as the trapping reagent. Cesium fluoride is commonly used due to its low cost; however, it afforded the Diels-Alder (DA) product **29** in only 27% after 5 hours with 54% starting material (entry 1). In addition to its slow reactivity, CsF was also poorly soluble in MeCN and would not be amenable to a continuous-flow process. TBAF was then used and afforded DA product in 97% yield in under one minute, with every component being completely solubilized. Therefore, we chose TBAF desilylation conditions moving forward.

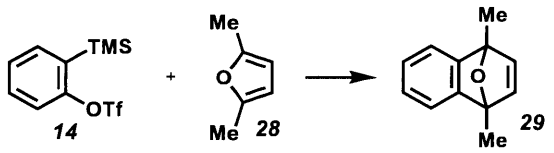

Entry	Conditions	Results
1	CsF (5 equiv), MeCN, 60 °C, 5 h	27% yield, 54% RSM
2	TBAF (1.1 equiv), THF, 0 °C, $<_1$ min	97% yield

Table 3. Benzyne generation conditions.

Having synthesized benzyne precursor **14**, we then designed the continuous-flow process according to Figure 21. In the system, two streams consisting of precursor **14** and TBAF would meet at a T-mixer fitted with a StaMixCo (See experimental section for more information) for better mixing due to the slow flow rates. From there, the reaction mixture will flow through the reactor and is then trapped with furan **28**. That resultant mixture will then go through a second reactor and the final product **29** is collected and purified via column chromatography. When we ran the system with reactor R_1 at 0 °C, we were unable to observe any benzyne peak among the many Raman spectra collected. This lack of signal was further confirmed by our low yield of product **29** (<10% yield). If we were to assume that complete generation of benzyne occurred, then we would have a maximum concentration of 91 mM in THF. This would be above the signal observance threshold mentioned earlier; however, we are likely generating significantly less benzyne than anticipated.

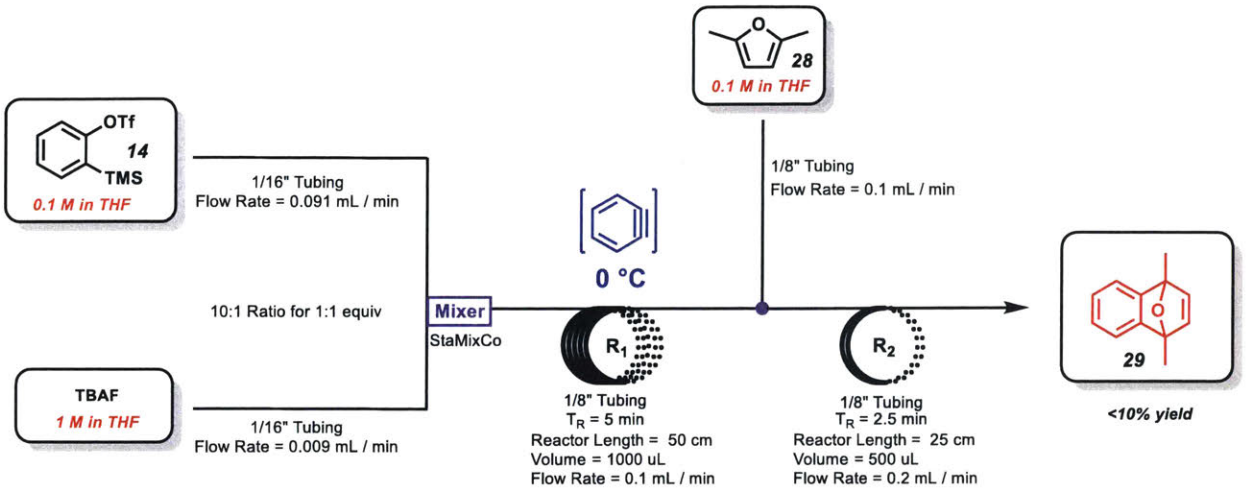

Figure 21. Continuous-flow process for benzyne observation.

To understand why benzyne was being formed at such low quantities, we compared the reaction conditions of both batch and continuous-flow. In batch conditions, the benzyne was being formed in the presence of the furan **28**. In continuous-flow conditions, the benzyne is generated and does not encounter any trapping reagent until after five minutes. It is possible that the benzyne is undergoing side reactivity pathways[62] and so control studies we performed according to Figure 22. As a parallel to our continuous-flow conditions, we generated benzyne intermediate **7** with TBAF and then added the trapping agent after 5 minutes at three different temperatures. At room temperature, we observed zero product formation with full conversion. Cooling down to 0 °C to mimic our continuous-flow conditions, we observed a low yield of 28% of **29**. At -78 °C in THF over MeCN, we were able to obtain product **29** in 71% yield. This 71% yield compared to the nearly quantitative yield from Table 3, entry 2 indicated that although some benzyne intermediate is being consumed, there should be enough present to observe at these temperatures. This yield also provided us with a rough idea of what concentration of benzyne could possibly be present as it

travels through the reactor. As it stood, the concentration was too low to be detected reliably and needed to be increased.

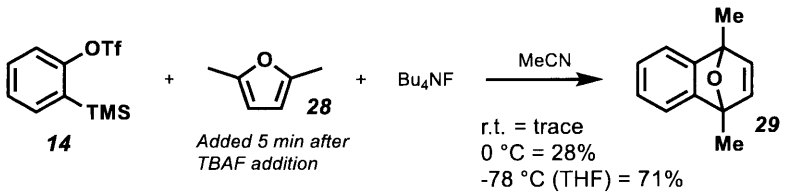

Figure 22. Control studies for benzyne trapping.

Our next continuous-flow conditions are shown in Figure 23, where the concentrations were doubled. The reactor, R_1, was submerged in a dry ice-acetone bath medium to reach -78 °C. From the cryogenics, we observed severe clogging as the stream of both precursor **28** and TBAF became submerged. This clogging was found to cause by precipitation of TBAF at these low temperatures. Solubility tests were then performed for TBAF solubility at low temperatures. TBAF in 3:1 THF:DMF was found to be completely solubilized at -78 °C. When these conditions were examined to generate benzyne **7**, side product **30** was formed in 32% yield. This side product is likely formed through a [2+2] cycloaddition with DMF followed by ring opening. Acetonitrile was then used as the cosolvent and it was found to completely solubilize TBAF at cryogenic temperatures without any side reactivity, as shown in Figure 25.

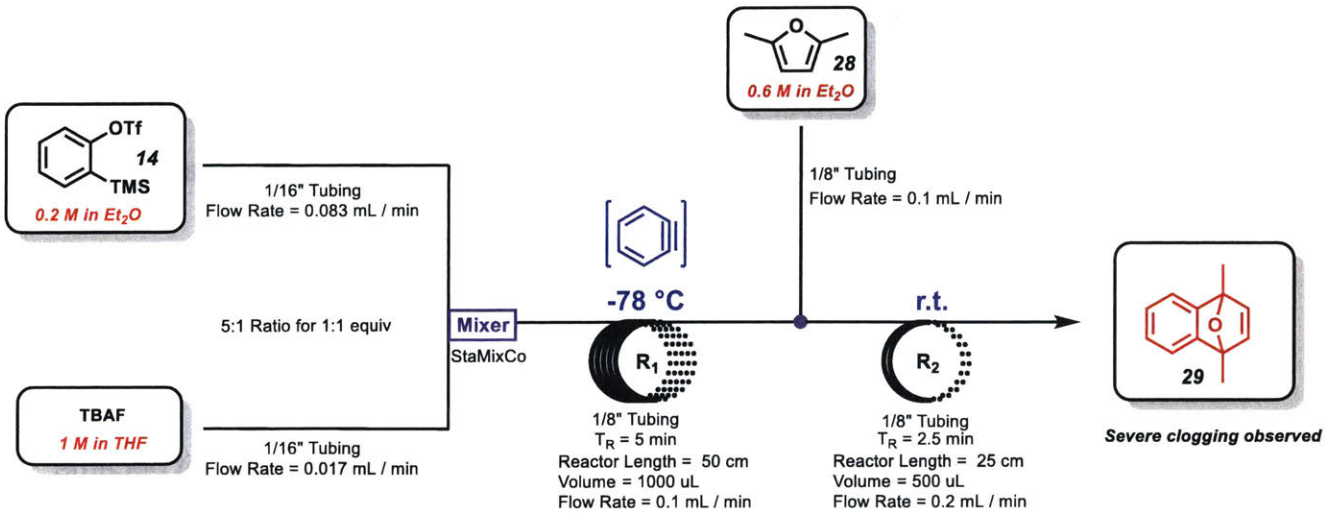

Figure 23. Low temperature benzyne generation in continuous-flow.

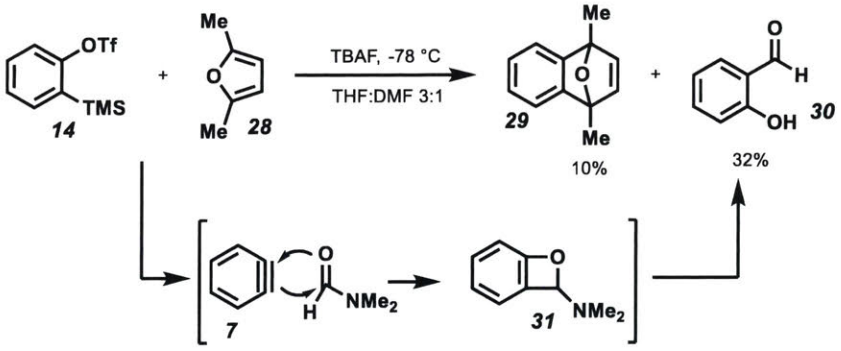

Figure 24. Side product observed with TBAF in 3:1 THF:DMF.

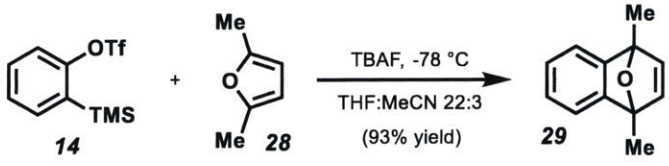

Figure 25. Conditions for full solubilized TBAF at cryogenic temperatures.

With the benzyne formation conditions now well-studied, we designed the updated flow system according to Figure 26. For this system, no clogging was observed throughout. Upon isolation, we were able to obtain DA product **29** in 36% yield,

indicating that at least 36% of benzyne traveled through reactor R_1 to be trapped with **28**. Since there was no presence of **28** in R_1, the benzyne could have gone through unwanted side reactions such as oligomerization.[62] Ultimately, we were unable to observe any benzyne intermediate. Some possibilities are that the benzyne intermediate was being generated slowly throughout the reactor and never reaching the threshold limit for detection. A likely complication could be from the fluorescence that was occurring under the reaction conditions.[63] As the reaction progressed, it became dark brown which likely saturated the detector with unwanted fluorescence.

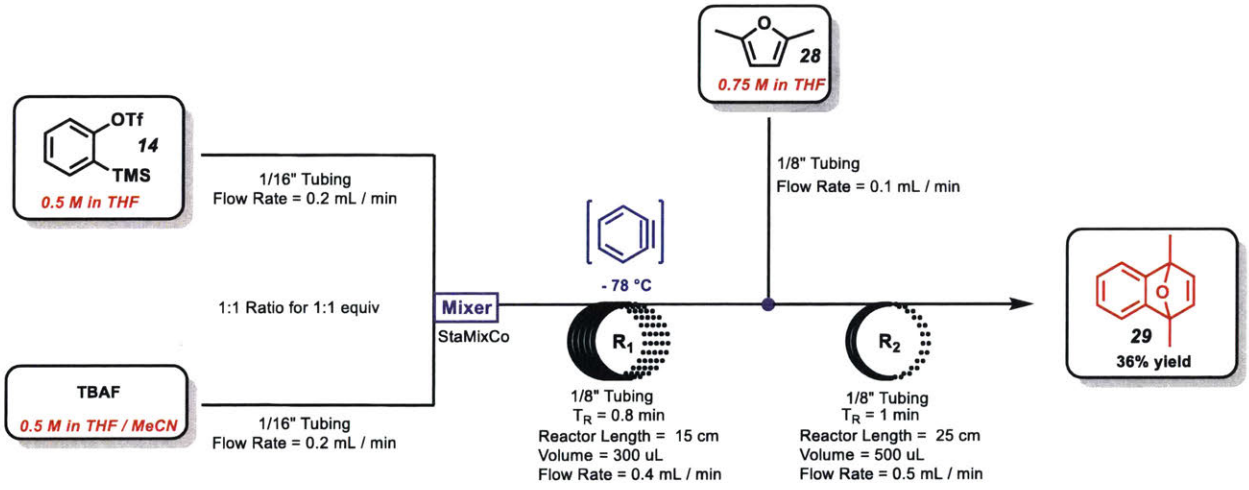

Figure 26. Updated flow system with new solvent system to prevent clogging, and higher concentration to observe benzyne.

The detection of benzyne intermediate in a continuous-flow process proved to be a challenging study. Several complications existed such as precipitation at low temperatures, low concentration of generated intermediate, and fluorescence. Furthermore, the dry-ice acetone bath media produced significant CO_2 and would affect signal acquisition by gas pocket formation within the probe adapter. This became evident as CO_2 peaks would be observed in certain spectra. At cryogenic temperatures, the PFA tubing became much stiffer and would interfere with alignment. As experiments

ran longer (>1 hr), signal quality was observed to diminished. While this reason is still unknown, we believe that it is caused by condensation of water within the probe that causes either signal degredation or laser source interference. From these issues discussed, we turned our attention to the investigation of ketenes.

2.3.3 Raman analysis of ketene **35**

Ketenes were first recognized in 1905 by Staudinger, when unexpected diphenyl ketene **34** was isolated.[64] Since then, ketenes have been widely studied and used in a variety of transformations such as [2+2] cycloadditions, nucleophilic additions, and rearrangements.[65] The fascinating structure of ketenes have spurred numerous development into its formation.[66]

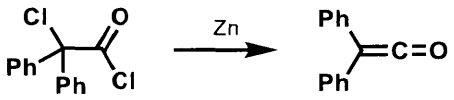

33 ***34***

Figure 27. First isolated ketene by Staudinger.

Of interest to us was the synthesis of ketenes through alkynyl ether precursors.[67] In particular, we chose ketene **37** for its stability upon isolation and storage (Figure 28). From Scheme 2, its batch synthesis started with volatile ethyl ethynyl ether (**36**) reacting with TMSCl after deprotonation with butyllithium to give TMS-alkyne **37** in 50% yield. Upon heating to 120 °C, retro-ene reaction occurs to release ethylene and our desired ketene in 63% yield.

For the batch synthesis, formation of TMS-alkyne **37** resulted in a dark, brown solution and may interfere greatly due to fluorescence. However, for the formation of

ketene **35**, there was minimal color change and would thus be ideal for the Raman probe. For the IR and Raman spectra of ketenes, we should expect characteristic bands around 2100 – 2200 cm^{-1}.[68] Furthermore, the alkyne starting material would likely have an absorbance band around 2200 – 2300 cm^{-1}. Of note, ketenes are often studied via IR while examples of Raman are far more limited.

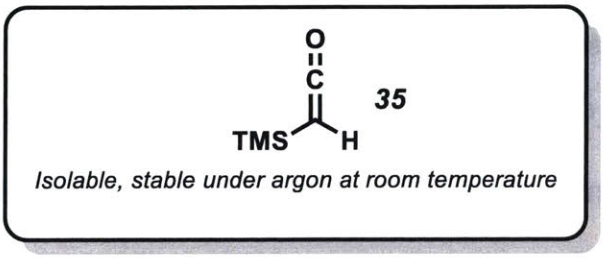

Figure 28. Target ketene for its stability at room temperature and under proper storage conditions.

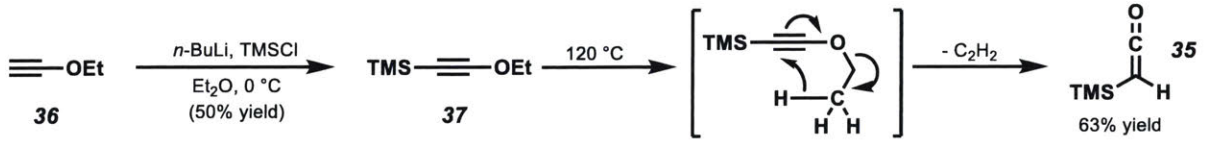

Scheme 2. Synthesis of ketene precursor.

With our batch conditions, we designed the following continuous-process, shown in Figure 29. In these conditions, ketene precursor **37** was in a 0.5 M solution in benzene to maximize signal while preserving material. Temperatures up to 140 °C was studied with our heating bath medium being silicone oil. The total residence time was 6 minutes. At the end of the reactor, 75 PSI BPR was used in anticipation of gaseous ethylene. Despite that, gasses were observed and resulted in inconsistent flow rates. Regardless, we were able to obtain valuable spectra of our ketene. From Figure 30, the Raman spectrum of ketene precursor **37** is shown. For this structure, there is minimal peaks present past 1600 cm^{-1} with its anticipated peak at near 2200 cm^{-1} being very

minor. From Figure 31, an overlay of all standards is shown. The most prominent peak that interested us was the rather large peak of ketene standard **35** around 2900 cm^{-1}. This peak is prevalent in this region while others of benzene, HPFA, and starting material **37** are not. From Figure 32, the continuous-flow system from Figure 29 was analyzed and shown to display a prominent band at the anticipated region around 2900 cm^{-1}. Therefore, we can conclude from these studies that ketene **35** had indeed been formed and was observed through our Raman probe.

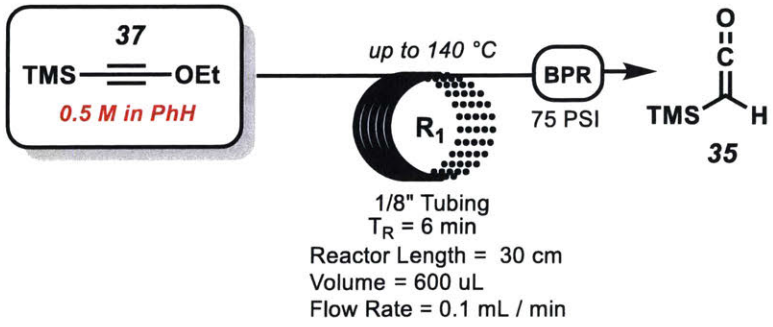

Figure 29. Ketene synthesis in continuous-flow.

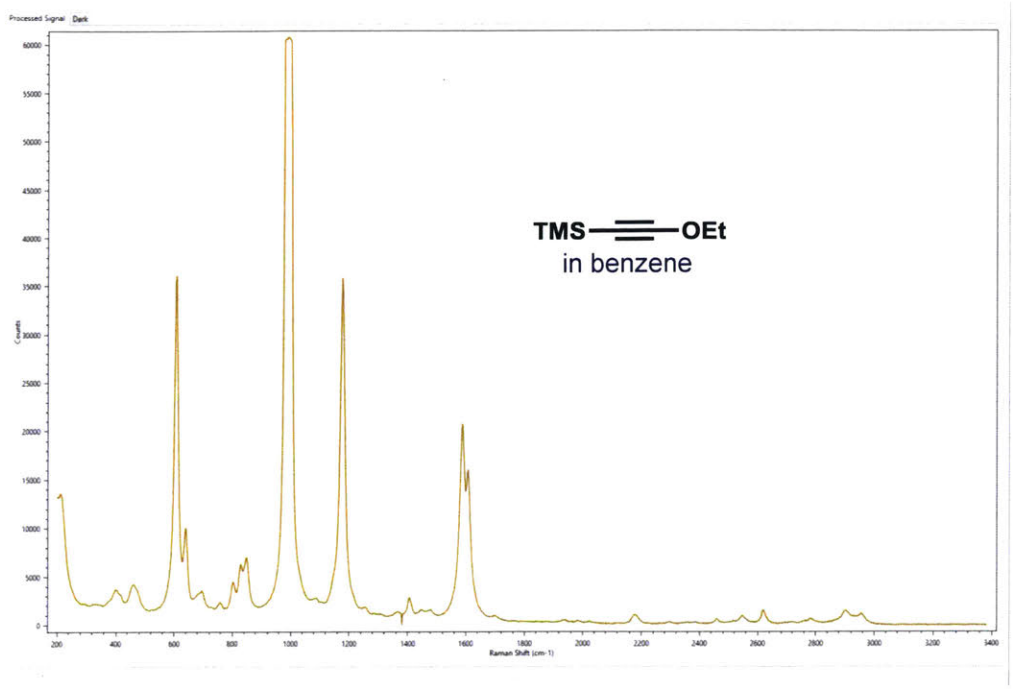

Figure 30. Raman spectrum of **37** in benzene.

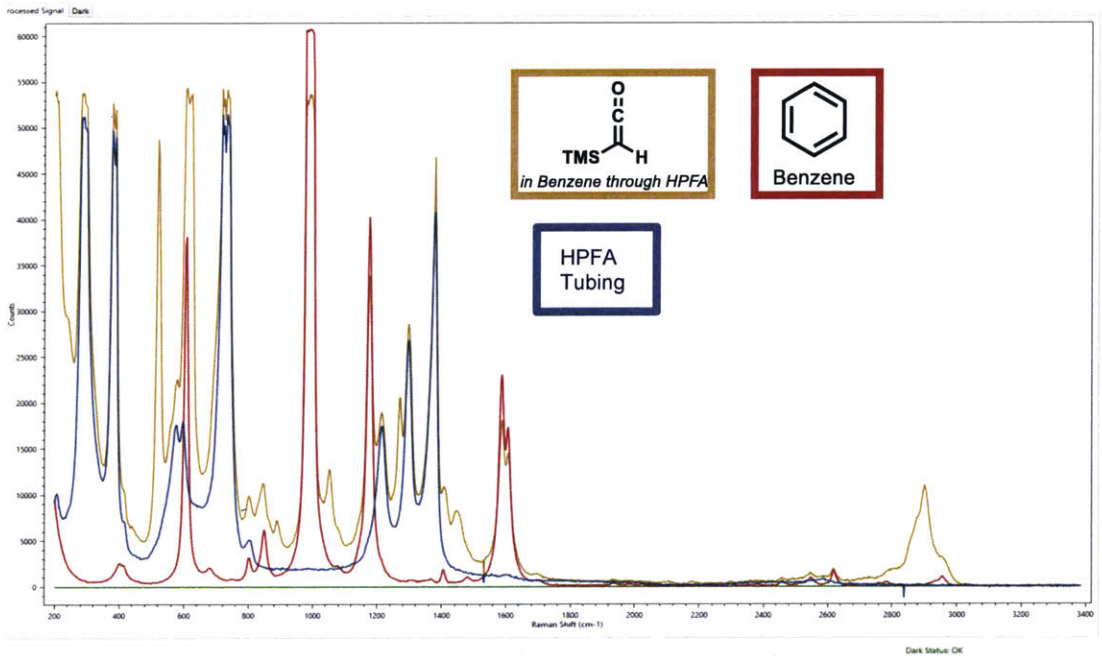

Figure 31. Spectra of compounds and materials used as standards.

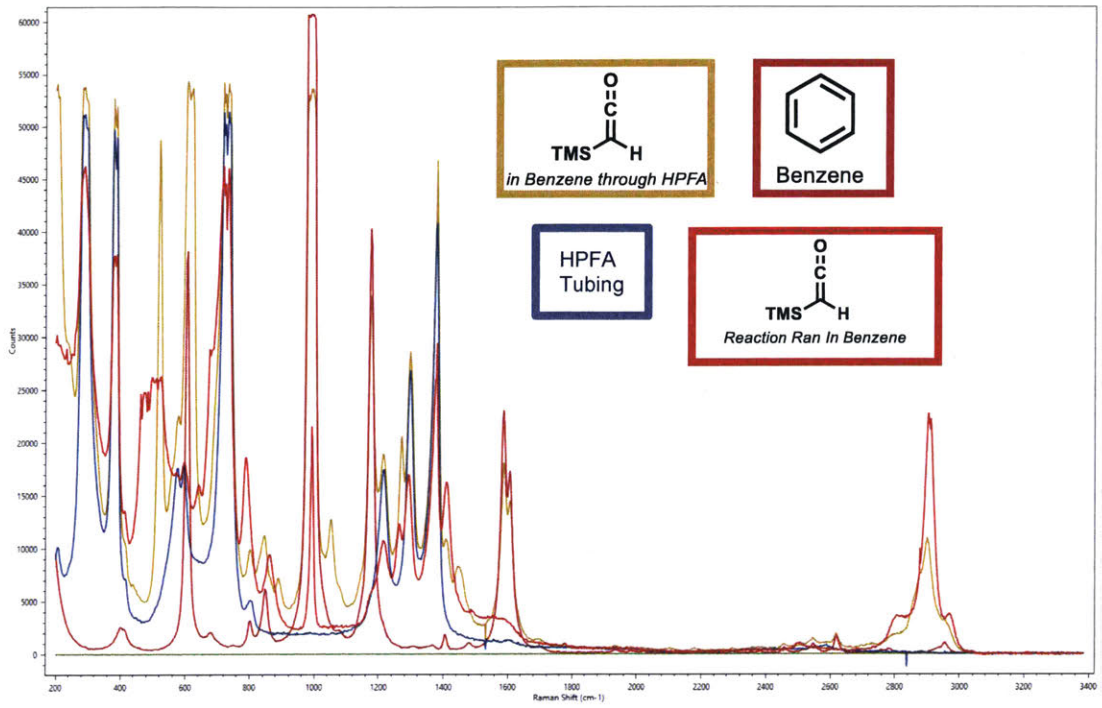

Figure 32. Spectra of ketene formation reaction, and compounds and materials used as standards.

2.4 Conclusion

Continuous-flow chemistry has been valuable for the growth of many chemical industries due to the many benefits such as simpler process scale-up, safer handling of hazardous chemicals, smaller production foot print, among others. These advantages often complement existing batch processes, and therefore, provides with a competitive edge if utilized properly. In these continuous processes, there exists a unique opportunity to have real-time analytics. Many of these existing techniques involve using inline analytics and are thus limited to a single-point.

Recently, the Raman spectroscopy probe has emerged as a powerful tool to analyze data in a continuous-flow system. The chemically robust probe employs Raman spectroscopy, which has seen a surge in the past years due to better laser technology.

In our studies, we demonstrated the benefits of this probe as a handheld device. Spectra acquired through various tubing material and heating bath media were shown to be consistent. PFA and HPFA were the most practical choice given its Raman operating window and cost. While excellent spectra could be obtained by hand, we found that having an adapter was much easier to reliably obtain a working spectrum.

After our thorough investigations into the various methods to utilize the Raman probe, we then investigated three reactions: ring-closing metathesis, benzyne generation, and ketene generation. For the ring-closing metathesis, we successfully monitored conversion and yield along the reactor at room temperature. Future studies of this reaction could be utilizing this technology to compare the reaction rates of various catalyst through the continuous-flow system. For our benzyne generation conditions, we found that fluorescence ultimately hindered our ability to observe the intermediate. Furthermore, the benzyne could have been formed under our detection threshold or that the benzyne absorbance band was too weak to observe. Future studies for this intermediate could be expanding to other more stable or long-lived benzyne intermediates. Lastly, we were successful in observing the ketene **35**. While quantitative data was not possible due to the inconsistent flow rates, we were able to show ketene formation within the reactor. Future studies for ketene analysis could be to expand to other stable ketene derivatives or to different methods where formation of ethylene is limited or not present altogether.

2.5 Works Cited

[1] Lévesque, F.; Rogus, N. J.; Spencer, G.; Grigorov, P.; McMullen, J. P.; Thaisrivongs, D. A.; Davies, I. W.; Naber, J. R. Advancing flow chemistry portability: a simplified approach to scaling up flow chemistry. *Org. Process Res. Dev.* **2018**, *22*, 1015.

[2] Porta, R.; Benaglia, M.; Puglisi, A. Flow chemistry: recent developments in the synthesis of pharmaceutical products *Org. Process Res. Dev.* **2016**, *20*, 2.

[3] Plutschack, M. B.; Piebar, B.; Gilmore, K.; Seeberger, P. H. The hitchhiker's guide to Flow Chemistry. *JACS* **2017**, *117*, 11796.

[4] Horvath, I. T.; Anastas, P. T. Innovations and Green Chemistry *Chem. Rev.* **2007**, *107*, 2169.

[5] Sheldon, R. A. The E-factor 25 years on: the rise of green chemistry and sustainability. *Green Chem.* **2017**, *19*, 18.

[6] Bogden, A. R.; Dombrowski, A. W. Emerging trends in flow chemistry and applications to the pharmaceutical industry. *J. Med. Chem.* **2019**, *ASAP*, DOI: 10.1021/acs.jmedchem.8b01760.

[7] McWilliams, J. C.; Allian, A. D.; Opalka, S. M.; May, S. A.; Journet, M.; Braden, T. M. The evolving state of continuous processing in pharmaceutical API manufacturing: a survey of pharmaceutical companies and contract manufacturing organizations. *OPRD* **2018**, *22*, 1143.

[8] Applications of flow chemistry in drug development: highlights of recent patent literature. *OPRD Highlights* **2018**, *22*, 13.

[9] Schmink, J. R.; Holcomb, J. L.; Leadbeater, N. E. Use of Raman spectroscopy as an *in situ* tool to obtain kinetic data for organic transformations. *Chem. Eur. J.* **2008**, *14*, 9943.

[10] Hamlin, T. A.; Leadbeater, N. E. Raman spectroscopy as a tool for monitoring mesoscale continuous-flow organic synthesis: equipment interface and assessment in four medicinally – relevant reactions. *Beilstein J. Org. Chem.* **2013**, *9*, 1843.

[11] Musio, B.; Gala, E.; Ley, S. V. Real-time spectroscopic analysis enabling quantitative and safe consumption of fluoroform during nucleophilic trifluoromethylation in flow. *ACS Sustainable Chem. Eng.* **2018**, *6*, 1489.

[12] Carter, C. F.; Lange, H.; Ley, S. F.; Baxendale, I. R.; Wittkamp, B.; Goode, J. G.; Gaunt, N. L. ReactIR flow cell: a new analytical tool for continuous-flow chemical processing *OPRD* **2010**, *14*, 393.

[13] Giraudeau, P.; Felpin, F. Flow reactors integrated with in-line monitoring using benchtop NMR spectroscopy *React. Chem. Eng.* **2018**, *3*, 399.

[14] Schaber, S. D.; Born, S. C.; Jensen, K. F.; Barton, P. I. Design, execution, and analysis of time-Varying experiments for model discrimination and parameter estimation in microreactors. *Org. Process Res. Dev.* **2014**, *18*, 1461.

[15] Moore, J. S.; Jensen, K. F. "Batch" kinetics in flow: Online IR analysis and continuous control. *Angew. Chem. Int. Ed.* **2014**, *53*, 470.

[16] Abolhasani, M.; Coley, C. W.; Jensen, K. F. Multiphase oscillatory flow strategy for *in situ* measurement and screening of partition coefficients. *Anal. Chem.* **2015**, *87*, 11130.

[17] Bedermann, A. A.; McTeague, T. A. Jamison, T. F. Automated on-demand titration of organometallic reagents in continuous flow," *Org. Process. Res. Dev.* **2019**, DOI: 10.1021/acs.oprd.8b00434.

[18] Hendra, P. J.; Stratton, P. M. Laster-raman spectroscopy. *Chem. Rev.* **1969**, *69*, 325.

[19] Acevedo, D.; Yang, X.; Mohammad, A.; Pavurala, N.; Wu, W-L.; O'Connor, T. F.; Nagy, Z. K.; Cruz, C. N. Raman spectroscopy for monitoring the continuous crystallization of carbamazepine. *Org. Process Res. Dev.* **2018**, *22*, 156.

[20] Bocklitz, T. W.; Guo, S.; Ryabchykov, O.; Vogler, N.; Popp, J. Raman based molecular imaging and analytics: a magic bullet for biomedical applications!? *Anal. Chem.* **2016**, *88*, 133.

[21] Esmonde-White, K. A.; Cuellar, M.; Uerpmann, C.; Lenain, B.; Lewis, I. R. Raman spectroscopy as a process analytical technology for pharmaceutical manufacturing and bioprocessing. *Anal. Bioanal. Chem.* **2017**, *409*, 637.

[22] MarqMetrix TouchRaman Probe. https://www.marqmetrix.com/products/all-in-one/ (accessed May 4, 2019).

[23] Movsisyan, M.; Delbeke, E. I.; Berton, J. K. E.; Battilocchio, C.; Ley, S. V.; Stevens, C. V. Taming hazardous chemistry by continuous-flow technology. *Chem. Soc. Rev.* **2016**, *45*, 4892.

[24] A) Yoshida, J. I.; Kim, H.; Nagaki, A. Green and sustainable chemical synthesis using flow microreactors. *ChemSusChem* **2010**, *4*, 331. B) Newman, S. G.; Jensen, K. F. The role of flow in green chemistry and engineering. *Green Chem.* **2013**, *15*, 1456.

[25] Yoshida, J. I.; Takahashi, Y.; Nagaki, A. Flash chemistry: flow chemistry that cannot be done in batch. *Chem. Commun.* **2013**, *49*, 9896.

[26] A) Morse, P. D.; Beingessner, R. L.; Jamison, T. F. Enhanced reaction efficiency in continuous flow. *Israel Journal of Chemistry* **2017**, *57*, 218. B) Gobert, S. R.; Kuhn, S.; Braeken, L.; Thomassen, L. C. J. Characterization of milli- and microflow reactors: mixing efficiency and residence time distribution. *Org. Process Res. Dev.* **2017**, *21*, 531.

[27] Webb, D.; Jamison, T. F. Continuous-flow multistep organic synthesis. *Chem. Sci.* **2010**, *1*, 675.

[28] A) DiMasi, J. A.; Hansen, J. A.; Grabowski, H. G. The price of innovation: new estimates of drug development costs. *J. Health Econ.* **2003**, 22, 151–185. B) Suresh, P.; Basu, P. Improving pharmaceutical product development and manufacturing: impact on cost of drug development and cost of goods sold of pharmaceuticals. *J. Pharm. Innov.* **2008**, 3,175.

[29] Mascia, S.; Heider, P. L.; Zhang, H.; Lakerveld, R.; Benyahia, B.; Barton, P. I.; Braatz, R. D.; Cooney, C. L.; Evans, J. M. B.; Jamison, T. F.; Jensen, K. F.; Meyerson, A. S.; Trout, B. L. End-to-end continuous manufacturing of pharmaceuticals: Integrated synthesis, purification, and final dosage formulation. *Angew. Chem. Int. Ed.* **2013**, *52*, 12359.

[30] Britton, J.; Jamison, T. F. The assembly and use of continuous flow systems for chemical synthesis. *Nat. Protocols* **2017**, *12*, 2423.

[31] Bayer, T.; Himmlen, K. Mixing and organic chemistry. *Chem. Eng. Technol.* **2005**, *28*, 285.

[32] Price, A. G.; Mallik, D.; Organ, M. A. Process analytical tools for flow analysis: A perspective. *J. Flow Chem.* **2017**, *7*, 82.

[33] Mitic, A.; Cervera-Padrell, A. E.; Mortensen, A. R.; Skovby, T.; Dam-Johansen, K.; Javakhishvili, I.; Hvilsted, S.; Gernaey, K. V. Implementation of near-infrared spectroscopy for in-line monitoring of a dehydration reaction in a tubular laminar reactor. *Org. Process Res. Dev.* **2016**, *20*, 395.

[34] McAfee, T.; Leonardi, N.; Montgomery, R.; Siqueira, J.; Zekoski, T.; Drenski, M. F.; Reed, W. F. Automatic control of polymer molecular weight during synthesis. *Macromolecules* **2016**, *49*, 7170.

[35] Archambault, C. M.; Leadbeater, N. E. A benchtop NMR spectrometer as a tool for monitoring mesoscale continuous-flow organic synthesis: equipment interface and assessment in four organic transformations. *RSC Adv.* **2016**, *6*, 101171.

[36] Ingham, R. J.; Battilocchio, C.; Hawkins, J. M.; Ley, S. V. Integration of enabling methods for the automated flow preparation of piperazine-2-carboxamide. *Beilstein J. Org. Chem.* **2014**, *10*, 641–652.

[37] Bédard, A.-C.; Adamo, A.; Aroh, K. C.; Russell, M. G.; Bedermann, A. A.; Torosian, J.; Yue, B.; Jensen, K. F.; Jamison, T. F. Reconfigurable system for automated optimization of diverse chemical reactions. *Science* **2018**, *361*, 1220.

[38] BASF. Outlook for the chemical industry. https://report.basf.com/2017/en/managements-report/forecast/economic-environment/chemical-industry.html (accessed May 4, 2018).

[39] Guidance for Industry: Advancement of Emerging Technology Applications for Pharmaceutical Innovation and Modernization. FDA, Ed. **2017**.

[40] Bruker. BRAVO Handheld Raman Spectrometer https://www.bruker.com/products/infrared-near-infrared-and-raman-spectroscopy/raman/bravo/overview.html (accessd May 5, 2019).

[41] Laser Safety Facts. Class 3B (IIIb) laser safety information. https://www.lasersafetyfacts.com/3B/ (accessed May 1, 2019).

[42] MarqMetrix. The process ballprobe – 0.5 in. https://www.marqmetrix.com/products/ballprobes/ (accessed May 5, 2019).

[43] A) Rivera-Hainaj, R. E. Raman spectroscopy in the organic chemistry laboratory: The formation of N-carboxy-2-imidazolidone. *J. Chem. Educ.* **2009**, *86*, 1319. B) Bowen, R. D.; Edwards, H. G. M.; Farwell, D. W.;Rusike, I.; Saun-ders, D. M. Analytical applications of raman spectroscopy in organic chemistry: Influence of the position, stereochemistry and substitution pattern of the double bond on the ν(C=C) and ν(sp^2-CH) stretching bands in the Raman spectra of alkenyl methyl ethers. *J. Chem. Res.* **1998**, *8*, 426.

[44] IDEX Health & Science. PFA tubing. https://www.idex-hs.com/store/fluidics/fluidic-connections/tubing/fluoropolymer-tubing/teflonr-pfa-tubing.html (accessed May 6, 2019).

[45] Dargaville, T. R.; George, G. A.; Hill, D. J. T.; Whittaker, A. K. An investigation of the thermal and tensile properties of PFA following γ-radiolysis. *Macromolecules* **2003**, *36*, 7132.

[46] Badertscher, M.; Bühlmann, P.; Pretsch, E. *Structure determination of organic compounds*; Springer: Berlin, 2009.

[47] Ritter, T.; Hejl, A.; Wenzel, A. G.; Funk, T. W.; Grubbs, R. H. A standard system of characterization for olefin metathesis catalysts. *Organometallics* **2006**, *25*, 5740.

[48] Dias, E. L.; Nguyen, S.-B. T.; Grubbs, R. H. Well-defined ruthenium olefin metathesis catalysts: mechanism and activity. *J. Am. Chem. Soc.* **1997**, *119*, 3887.

[49]Wittig, G. 1,2-Dehydrobenzene *Angew. Chemie. Int. Ed.* **1965**, *4*, 731.

[50] Stoermer, R.; Kahlert, B. Ueber das 1- und 2-Brom-cumaron. *Ber. Dtsch. Chem. Ges.* **1902**, *35*, 1633.

[51] Wenk, H. H.; Winkler, M.; Sander, W. One Century of Aryne Chemistry. *Angew. Chem. Int. Ed.* **2003**, *42*, 502.

[52] Roberts J. D.; Simmons Jr., H. W.; Carlsmith, L. A.; Vaughan, C. W. Rearrangement in the reaction of chlorobenzene-1-C^{14} with potassium amide. *J. Am. Chem. Soc.*, **1953**, *75*, 3290.

[53] Roberts, J. D.; Vaughan, C. W.; Carlsmith, L. A.; Semenow, D. A. Orientation in aminations of substituted halobenzenes. *J. Am. Chem. Soc.*, **1956**, *78*, 611.

[54] A) Pellisier, H.; Santelli, M. The use of arynes in organic synthesis. *Tetrahedron*, **2003**, *59*, 701. B) Tadross, P. M.; Stoltz, B. M. A Comprehensive history of arynes in natural product total synthesis. *Chem. Rev.* **2012**, *112*, 3550.

[55] Prajapati, S. M.; Patel K. D.; Vekariya, R. H.; Panchal, S. N.; Patel, H. D. Recent advances in the synthesis of quinolines: a review. *RSC Adv.* **2014**, *4*, 24463.

[56] Hoffman, R.; Imamura, A.; Hehre, W. J. Benzynes, dehydroconjugated molecules, and the interaction of orbitals separated by a number of intervening sigma bonds. *J. Am. Chem. Soc.* **1968**, *90*, 1499.

[57] Rondan, N. G.; Domesmith, L. N.; Houk, K. N., Levin, R. H. The relative rates of electron-rich and electron-deficient alkene cycloadditions to benzyne. Enhanced electrophilicty as a consequence of alkyne bending distortions. *Tetrahedron Lett.* ***1979**, 20,* 3237.

[58] Gampe, C. M.; Carreira, E. M. Arynes and cyclohexyne in natural product synthesis. *Angew. Chem. Int. Ed.* **2012**, *51*, 3766.

[59] A) Orendt, A. M.; Facelli, J. C.; Radziszewski, J. G.; Horton, W. J.; Grant, D. M.; Michl, J. ^{13}C dipolar NMR spectrum of matrix-isolated *o*-benzyne-*1,2*-$^{13}C_2$. *J. Am. Chem. Soc.* **1996**, *118*, 846-852. B) Warmuth, R. Inner-phase stabilization of reactive intermediates. *Eur. J. Org. Chem.* **2001**, 423.

[60] A) Atkinson, D. J.; Sperry, J.; Brimble, M. A. Improved synthesis of the benzyne precursor 2-(trimethylsilyl)phenyl trifluoromethansulfonate. *Synthesis* **2010**, *6*, 911. B) Bronner, S. M.; Garg, N. K. Efficient synthesis of 2-(trimethylsilyl)phenyl trifluoromethanesulfonate: A versatile precursor to *o*-benzyne. *J. Org. Chem.* **2009**, *74*, 8842.

[61] Bailey, W.F.; Patricia, J. J. The mechanism of the lithium halogen interchange reaction - A review of the literature. *J. Organomet. Chem.* **1988**, *352*, 1.

[62] A) Heaney, H. The benzyne and related intermediates. *Chem. Rev.***1962**, *62*, 81. B) Fishtik, I. Biphenylene: stabilization or destabilization? *J. Phys. Org. Chem.* **2011**, *24*, 263. C) Ihara, E.; Kurokawa, A.; Koda, T.; Muraki, T.; Itoh, T.; Inoue, K. Benzyne as a monomer for polymerization: alternating copolymerization of benzyne and pyridine to give novel polymers with o-phenylene and 2,3-dihydropyridine units in the main chain. *Macromolecules* **2005**, *38*, 2167.

[63] Beier, B. D.; Berger, A. J. Method for automated background subtraction from Raman spectra containing known contaminants. *Analyst* **2009**, 134, 1198.

[64] Staudinger, H. Ketene, eine neue Körperklasse. *Chem. Ber.* **1905**, *38*, 1735.

[65] Allen, A. D.; Tidwell, T. T. Ketenes and other cumulenes as reactive intermediates. *Chem. Rev.* **2013**, *113*, 7287.

[66] A) Tidwell, T. T. The first century of ketenes (1905–2005): the birth of a versatile family of reactive intermediates. *Angew. Chem. Int. Ed.* **2005**, *44*, 5778. B) Science of Synthesis (Houben-Weyl); Danheiser, R. L., Ed.; Georg Thieme Verlag: Stuttgart, 2006; Vol. 23. C) Fu, N.; Tidwell, T. T. Cycloaddition and electrocyclic reactions of vinylketenes, allenylketenes, and alkynylketenes. *Organic Reactions* **2015**, *87*, 257.

[67] Kita, Y. ; Fu, N.; Tidwell, T. T. Ethoxy(trimethylsilyl)acetylene. In Encyclopedia of Reagents for Organic Synthesis, 2009. doi:10.1002/047084289X.re036.pub2

[68] Kwiatkowskia, J. S.; Leszczyhski, J. Molecular structure and vibrational IR spectrum of ketene. Comparison of conventional ab initio post-Hartree-Fock and density functional theory calculations. *Journal of Molecular Structure (theochem)* **1995**, *342*, 43.

Chapter Two

Investigations of Raman Spectroscopy for Through-Tube Monitoring of Continuous-Flow Reactions – Experimental Section

General Information

Reactions were performed under an inert argon atmosphere unless otherwise stated. Commercially available chemicals were purchased from either Sigma-Aldrich Chemical Company (Milwaukee, WI), Alfa Aesar (Ward Hill, MA), Acros Organics (Pittsburgh, PA), or TCI America (Portland, OR). Anhydrous tetrahydrofuran (THF), dimethylformamide (DMF), toluene, benzene, and acetonitrile were purified via an SG Water USA solvent column system (Nashua, NH) before use. All reactions were monitored with thin-layer chromatography (TLC), which was performed using EMD 60-F254 silica glass plates and visualized with a UV lamp (254 nm). Products were purified on SNAP Ultra columns utilizing the Biotage® IsoleraTM flash purification system.

NMR spectra were obtained in $CDCl_3$ purchased from Cambridge Isotope Laboratories and used as received. Norell 5 mm NMR tubes with standard septa caps were used. ^1H NMR Spectra were obtained on Bruker Avance 400 (400 MHz for 1H, 100 MHz for 13C), JEOL 500 MHz (500 MHz for ^1H, 126 MHz ^{13}C), and Bruker AVANCE 600 MHz (600 MHz for ^1H, 151 MHz for ^{13}C) equipped with TXI Cryoprobe. ^{13}C spectra were obtained with ^1H decoupling. ^1H chemical shifts are reported in parts per million relative to TMS (δ = 0.00 ppm) and were referenced to the residual solvent peak. The following designations are used to describe multiplicities: s (singlet), brs (broad singlet), d (doublet), t (triplet), q (quartet), dd (doublet of doublets), dt (doublet of triplets), m (multiplet). Unless otherwise noted, NMR spectra were collected at room temperature (23–27 °C).

For the continuous-flow setup, all parts were commercially purchased and include Harvard Apparatus PHD 2000 syringe pump, Syrris Asia pump, stainless-steel

syringes from Harvard Apparatus, tubing and connections from Upchurch Scientific® and IDEX, PEEK T-mixer & union from Upchurch Scientific, and back-pressure regulator from Zaiput Flow Technologies. All parts list are given under general procedure for Raman analysis.

Preparation of starting materials

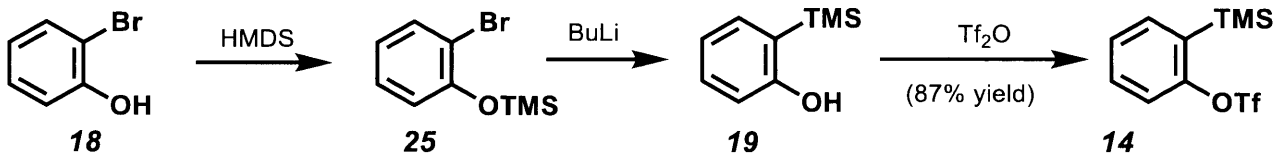

18 ***25*** ***19*** ***14***

2-(Trimethylsilyl)phenyl trifluoromethanesulfonate (14): To a flame-dried flask containing **18** (5 g, 3.36 mL, 28.9 mmol) in 29 mL DCM, HMDS (14 g, 18.17, 86.7 mmol) was added and the reaction was refluxed at 60 °C over night. The reaction mixture was concentrated and carried to the next step.

To a flame-dried flask containing crude **25** in 72 mL THF at −78 °C, butyllithium (2.5 M in hexanes, 2.78 g, 17.35 mL, 43.37 mmol) was added dropwise and the reaction was allowed to stir until disappearance of starting as monitored by TLC. Tf_2O (16.32 g, 9.71 mL, 57.83 mmol) was added slowly and reaction was warmed to rt and stirred overnight. The reaction was cooled to 0 °C and quenched with 100 mL of sat. $NaHCO_3$. The reaction was extracted twice with ether, dried over Na_2SO_4, and purified via column chromatography to give **14** (7.51 g, 25.17 mmol, 87% yield) as a clear oil. Spectral data are in agreement with the literature.[1]

[1] Atkinson, D. J.; Sperry, J.; Brimble, M. A. Improved synthesis of the benzyne precursor 2-(trimethylsilyl)phenyl trifluoromethansulfonate. *Synthesis* **2010**, *6*, 911.

Solubility Table for TBAF in continuous-flow at -78 °C

TBAF Solubility with THF:DMF at - 78 °C

Entry	Soluble?	TBAF Conc. (M)	THF:DMF Ratio
1	X	1	THF only
2	X	0.1	THF only
3	Y	0.083	10:2
4	Y	0.154	11:2
5	Y	0.214	12:2
6	Y	0.266	13:2
7	~	0.375	15:2
8	X	0.962	25:1
9	X	0.909	10:1
10	X	0.833	10:2
11	Y	0.769	10:3

Table SI- 1. Conditions for TBAF to be fully solubilize at -78 °C within a flow reactor. Entries 1-7 describes maximum concentration with *minimal* DMF co-solvent, entries 8-11 are maximum concentrations possible with DMF co-solvent. *Y = fully soluble, ~ = thick slurry that precipitates slowly if left undisturbed, thus possible to maintain stream at constant flow, X = precipitates readily.*

TBAF Solubility with THF:MeCN at - 78 °C

Entry	Soluble?	TBAF Conc. (M)	THF:MeCN Ratio
1	X	1	THF only
2	X	0.1	THF only
3	Y	0.095	20:1
4	~	0.174	22:1
5	Y	0.167	22:2
6	Y	0.231	23:2
7	~	0.286	26:2
8	~	0.333	15:1
9	X	.92	12:1
10	Y	0.91	10:1
11	Y	0.89	10:3
12	Y	0.67	2:1

Table SI- 2. Conditions for TBAF to be fully solubilize at -78 °C within a flow reactor. Entries 1-7 describes maximum concentration with *minimal* MeCN co-solvent, entries 8-12 are maximum concentrations possible with MeCN co-solvent. *Y = fully soluble, ~ = thick slurry that precipitates slowly if left undisturbed, thus possible to maintain stream at constant flow, X = precipitates readily.*

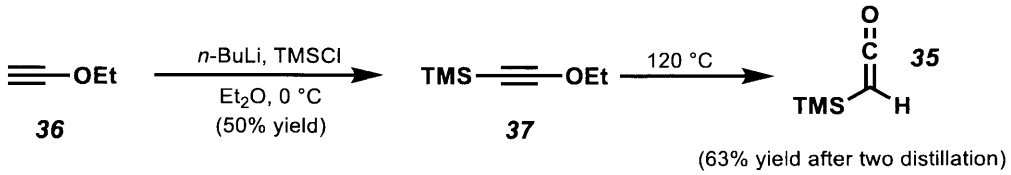

2-(Trimethylsilyl)ethen-1-one (35): 35 was prepared according to literature procedure.[2] To a solution of **36** (10.0 g, 143 mmol) in Et_2O (143 mL) at 0 °C was added

[2] A) Kita, Y. ; Fu, N.; Tidwell, T. T. Ethoxy(trimethylsilyl)acetylene. In Encyclopedia of Reagents for Organic Synthesis, 2009. doi:10.1002/047084289X.re036.pub2 B) Ruden, R. A. Trimethylsilylketene. Acylation and olefination reactions. *J. Org. Chem.* **1974**, *39*, 3607. C) Loebach, J. L.; Danheiser, R. L.; Adams, J. A. Trimethylsilylketene. *Encyclopedia of Reagents for Organic Synthesis*; Wiley, New York, 2009. doi:10.1002/047084289X.rt311.pub2

n-butyllithium (10.05 g, 157 mmol, 63 mL, 2.5 M solution in hexanes) dropwise. After addition was complete, the reaction was stirred for 5 min at 0 °C followed by dropwise addition of TMSCl (17.1 g, 19.9 mL, 157 mmol). The reaction was allowed to warm to rt and stirred overnight. The reaction was then cooled down to 0 °C and slowly quenched 100 mL sat. NH_4Cl solution. The layers were separated and the aqueous layer was extracted 3 times with 100 mL Et_2O. The combined organic layers were then washed with 250 mL brine and dried over Na_2SO_4. Solvent was removed slowly at 200 Torr at rt followed by distillation at 35 °C at 1 Torr to give **37** (10.2 g, 71.5 mmol, 50% yield) as a clear oil. Spectral data were in agreement with reported literature.[2] Neat **37** was then heated to 120 °C and distillate **35** (5.17 g, 45.3 mmol, 63% yield) was collected as a clear oil. A second distillation was performed if starting material was present. Spectral data were in agreement with reported literature.[2]

General Procedure for Raman Analysis of Continuous-Flow Systems and Data Acquisition with MarqMetrix TouchRaman probe

The continuous-flow process described in this section is shown in Figure 23, where the generation of benzyne was performed with precursor **14** and TBAF at -78 °C.

Continuous-flow set up

From Figure SI- 1, we used both a Harvard Apparatus PHD 2000 syringe pump and a Syrris Asia syringe pump. The Harvard pump is considered a "single" syringe pump while the Syrris pump is a pair of "dual" syringe pumps. We chose the Harvard single pump for delivery of TBAF because it is generally more accurate at lower flow

rates.[3] However, the pump is limited by the volume of the syringe used. Analogously, the Syrris dual pump offers a truly continuous-process from having alternating chambers pump in solution. However, this pumping nature results in a parabolic velocity profile and we can expect that the flow rate to be the *average* of a range of fluctuating flow rates.[3] From Figure SI- 2, the PFA tubing are connected to both syringe pumps present on the Syrris pump. The left pump was used pump a solution of the benzyne trapping reagent **15** and the right pump was used to deliver benzyne precursor **14**.

The tubing and connectors, purchased from IDEX unless otherwise noted, were used for both Harvard and Syrris pumps, and are as follows:

- PFA (perfluoroalkoxy alkane) tubing 1/16 inch O.D. x 0.03 inch I.D. (part# 1514L)
- PFA tubing 1/8"x0.062" tubing from Upchurch Scientific (cat. 05-701-216)
- PEEK (polyether ether ketone) connectors
- Tee Assembly High Pressure PEEK .050 (P-716)
- Standard Union Tefzel™ ¼-28 (part# P-623)
- Super Flangeless™ Nut PEEK, Short, ¼-28 Flat-Bottom, for 1/16 inch O.D. Natural (part # LT-115X)
- Super Flangeless™ Nut PEEK, 1/4-28 Flat-Bottom, for 1/8" (part# P-331Y)
- Super Flangeless™ Ferrule Tefzel™ (ETFE), 1/4-28 Flat-Bottom, for 1/8" OD (part # P-359X)
- Super Flangeless™ Ferrule w/SST Ring, Tefzel™ (ETFE), ¼-28 Flat-Bottom, for 1/16 inch O.D. Yellow (part# P-259X)

---

[3] Plutschack, M. B.; Piebar, B.; Gilmore, K.; Seeberger, P. H. The hitchhiker's guide to Flow Chemistry. *JACS* **2017**, *117*, 11796.

- BPR from Zaiput Flow Technologies [not shown in this example]
- StaMixCo helical static mixer for 1/8"x0.062" PFA tubing

Figure SI- 1. (top) Harvard Apparatus PHD 2000 Infusion syringe pump. (bottom) Syrris Asia Syringe Pump. Both were used in the continuous-process for benzyne generation.

Figure SI- 2. Closer examination of Syrris Asia syringe pump with tubing connected. Shown are a pair of "dual" pumps, i.e., one pump refills from a source while the other pumps solution out.

From Figure SI- 3, we can see the two steams from the Harvard pump and Syrris pump meet at a T-mixer junction that leads into a StaMixCo chamber prior to entering reactor, R_1. This set-up was chosen increase mixing and maximize benzyne formation. Of note, if the reactor is ran at room temperature, then it can be held taught at two

points with the Raman probe held firmly with clamps (Figure SI- 4). The second T-mixer junction can be seen where the exiting stream from R_1 is met with the trapping reagent **15** stream from the Syrris pump to through the last reactor, R_2, and into a collection flask. The full system, if ran at room temperature, can be seen in Figure SI- 5. For our system, our reactor needs to be submerged in a dry ice-acetone bath to reacth -78 °C temperature and the completed system with stock solutions and syringes are shown in Figure SI- 6 and Figure SI- 7 (top-down view.). The reactor is fully submerged with the StaMixCo to maximize stirring and potential benzyne formation. The Raman probe can be moved throughout the system as needed. For better alignment, the first generation adapter was used and shown in Figure SI- 8, which held well in this situation and represents a simple solution if a more robust adapter is not available. The 2nd generation adapter that was designed is shown in Figure SI- 9 with a side view and in Figure SI- 10 from the probe tip.

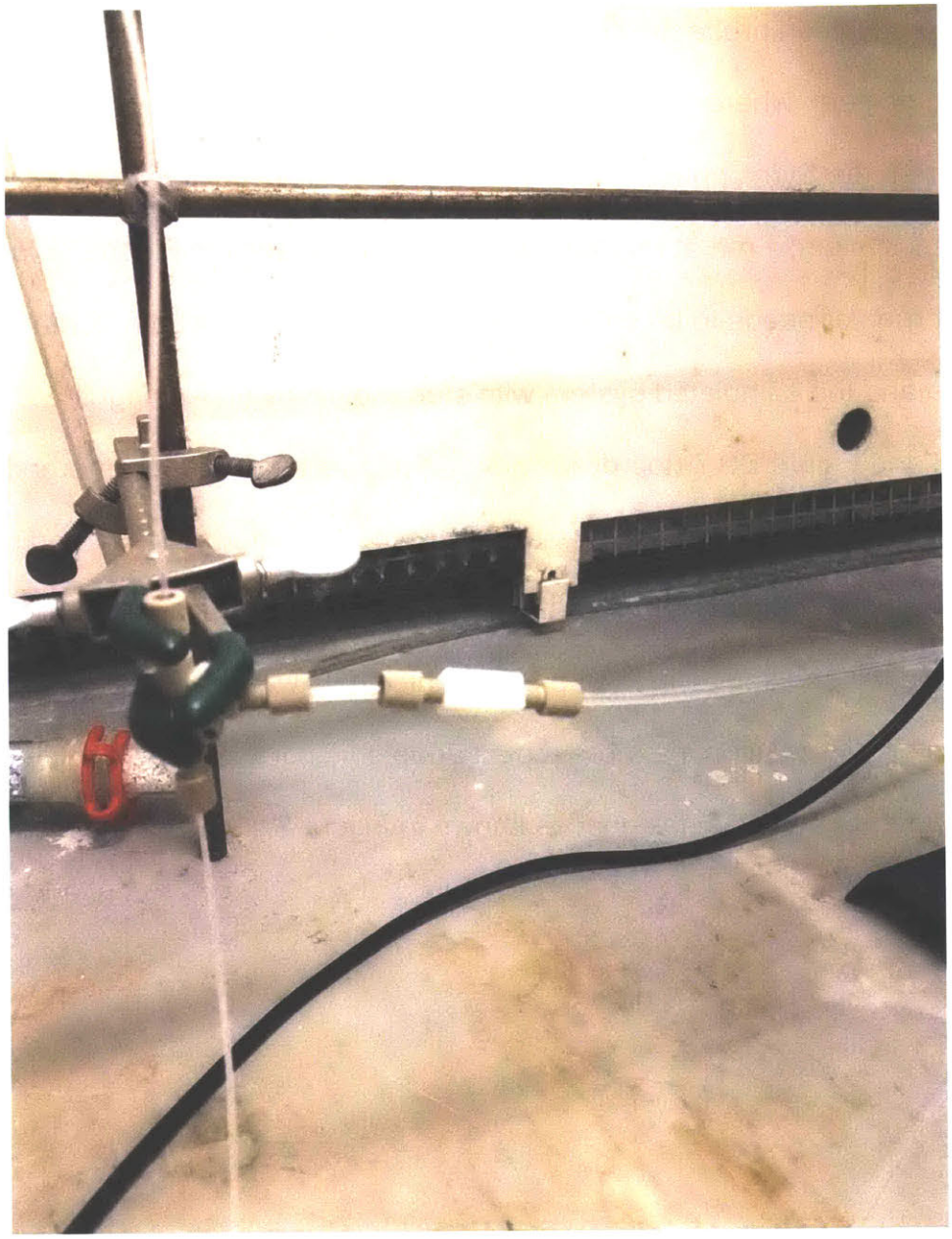

Figure SI- 3. Two streams of benzyne precursor 14 (from bottom) and TBAF (from top) meet at a T-mixer and the combined exiting stream passes through a StaMixCo chamber connected to the reactor, R_1, through a union (white, rectangular portion).

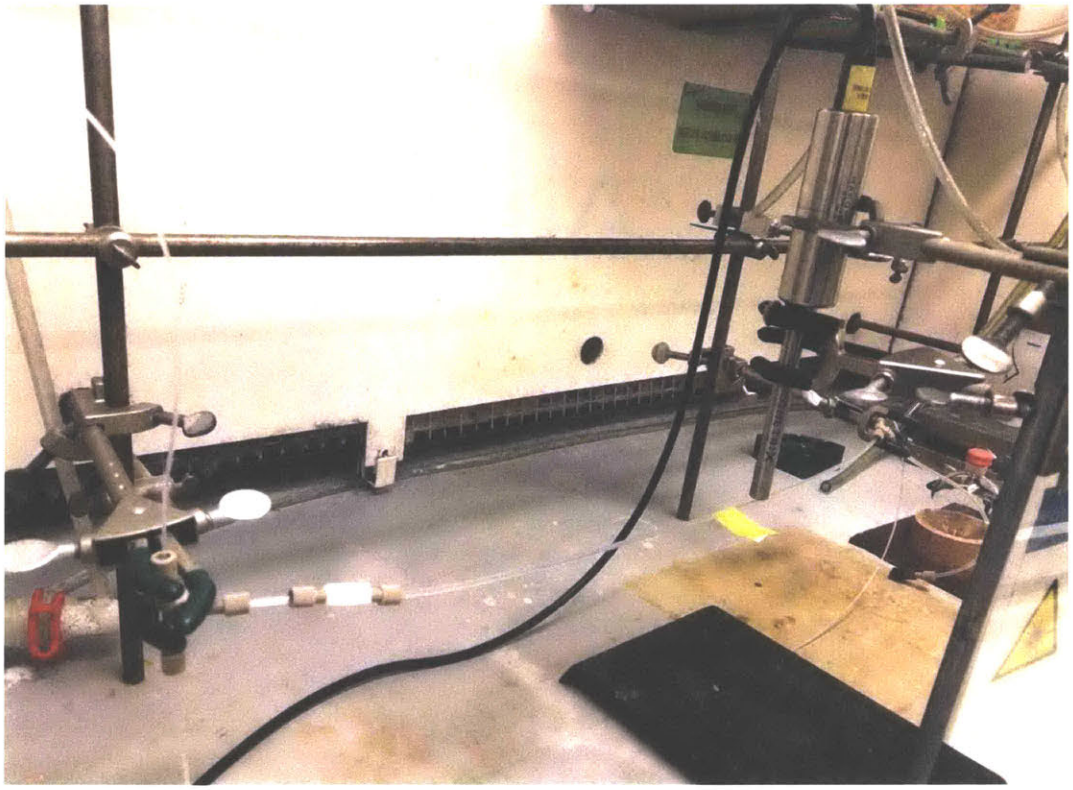

Figure SI- 4. MarqMetrix TouchRaman probe shown in contact with reactor, R_1, for spectra acquisition.

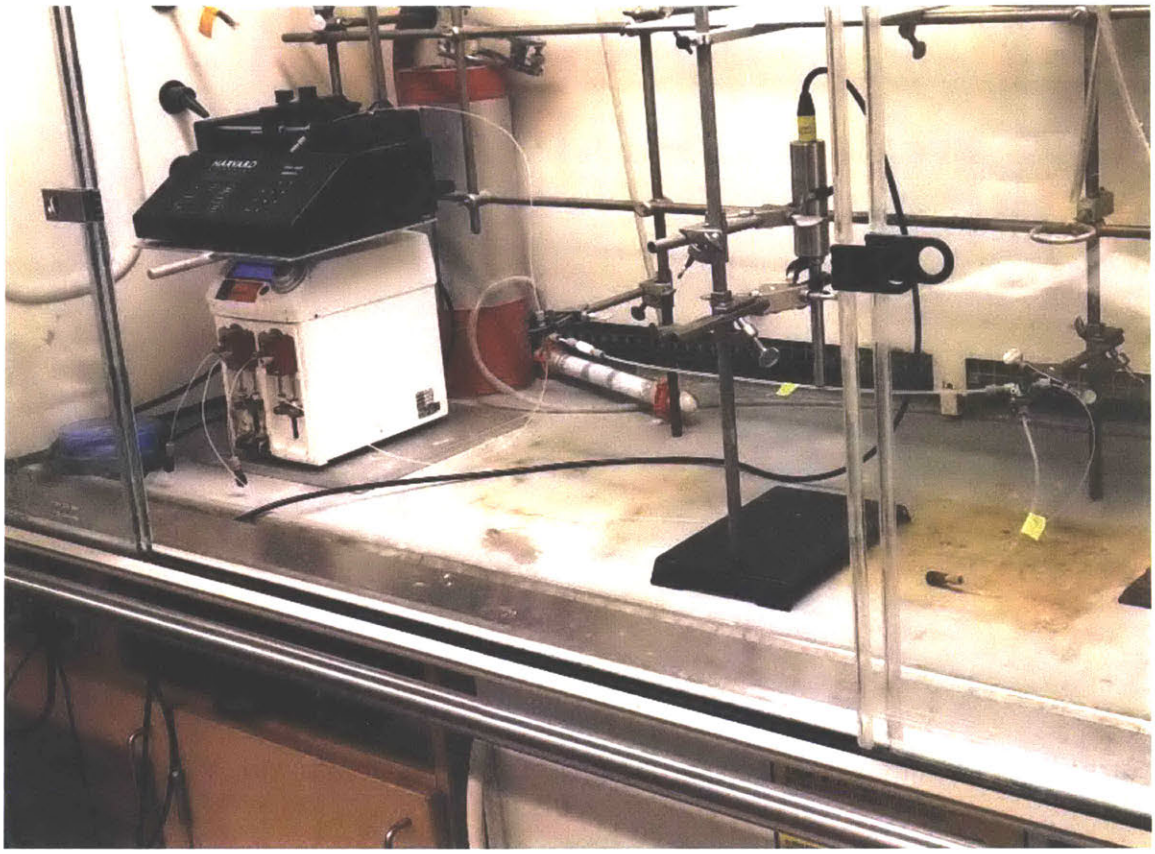

Figure SI- 5. Full system set up for a continuous-flow system with Raman probe at room temperature. Not shown are the connections of the pumps to their stock solutions.

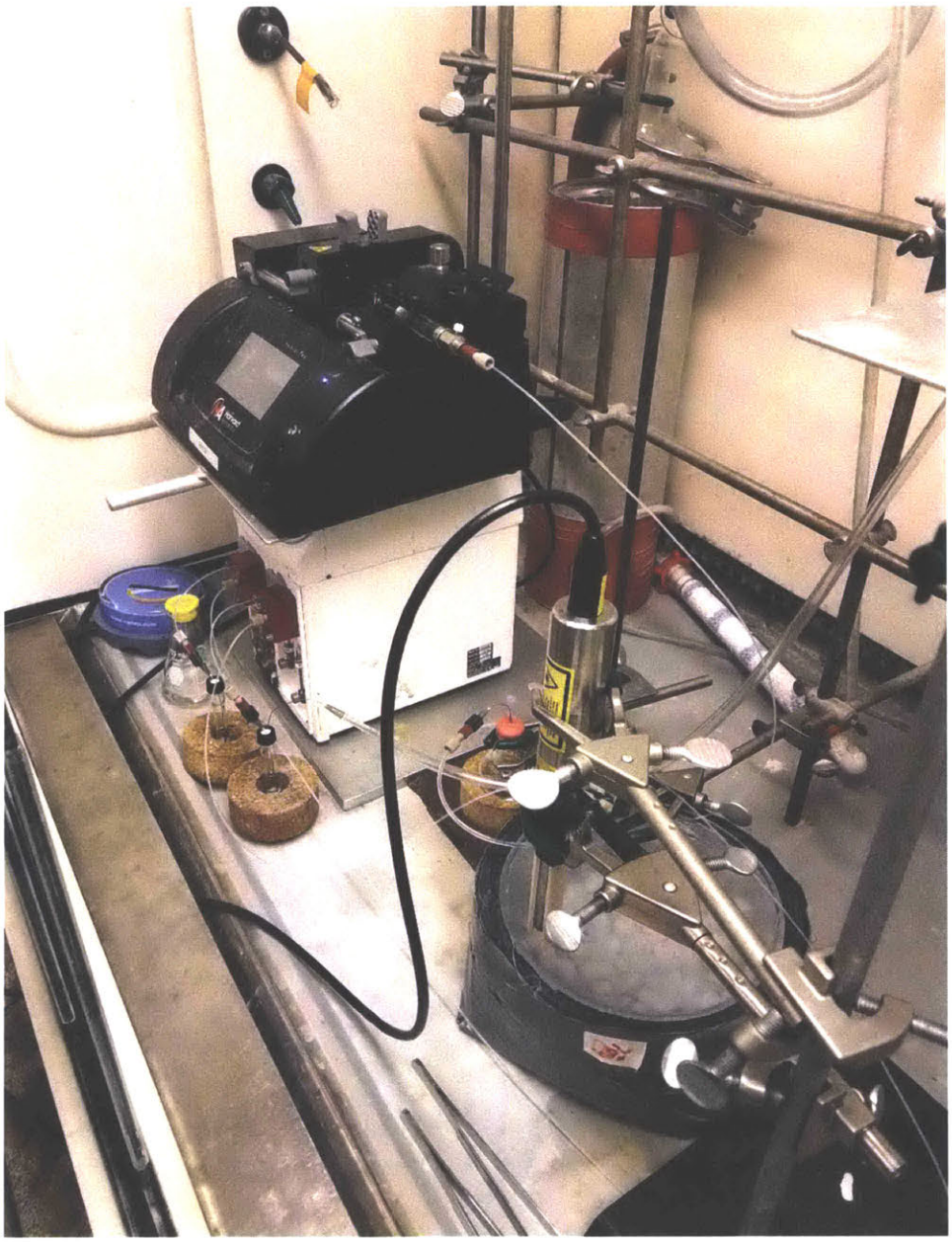

Figure SI- 6. Final system at -78 °C. All stock solutions and syringes are filled. The Raman probe can been seen held in place with clamps for stability. The reactor is submerged into the acetone bath. Large tongs are used to manipulate the reactor.

Figure SI- 7. Top-down view of reactor, R_1, with Raman probe. The reactor is fully submerged in the acetone bath and the probe is capable of being moved throughout the system.

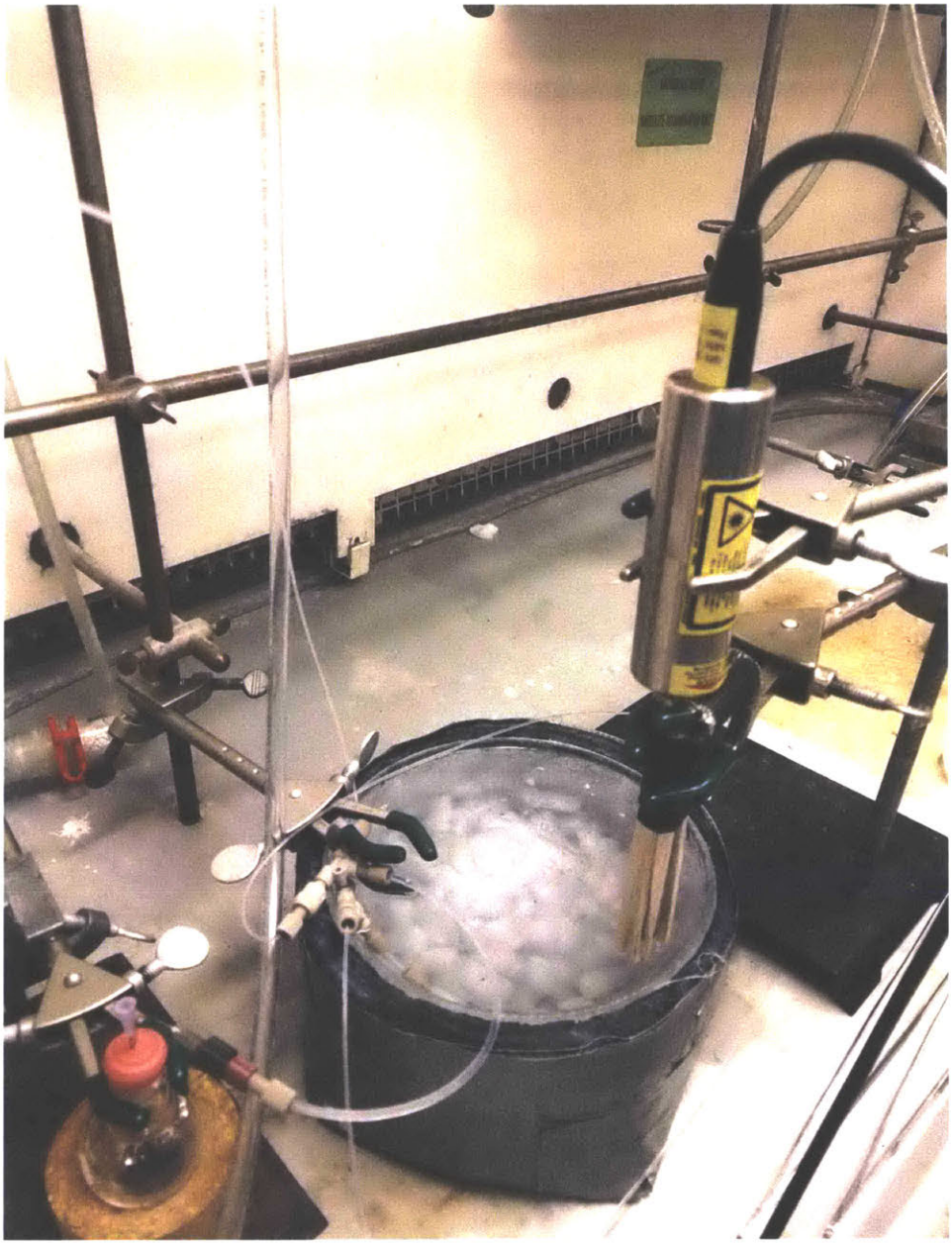

Figure SI- 8. First generation adapter for more consistent alignment of probe with reactor tubing.

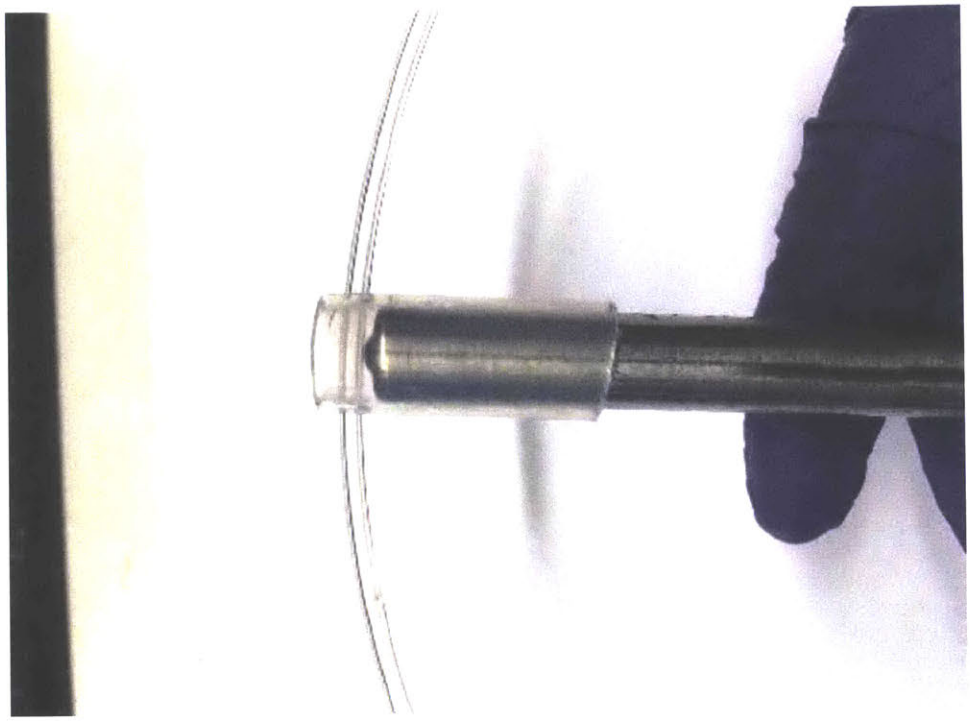

Figure SI- 9. 2nd generation adapter shown as a side view.

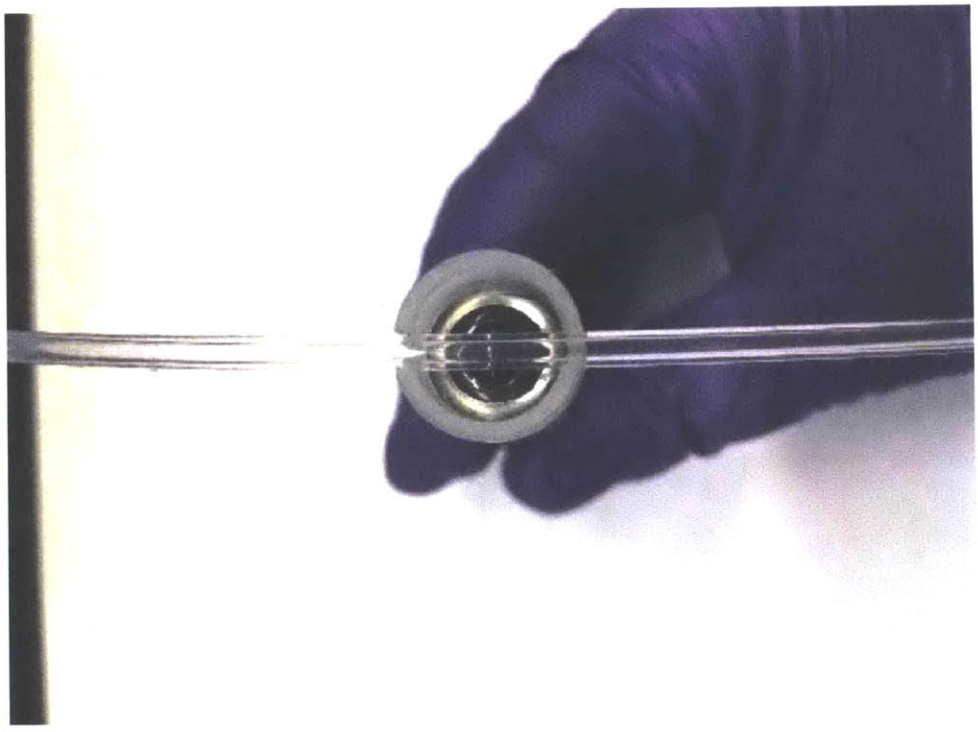

Figure SI- 10. 2nd generation adapter shown from probe tip.

Data Acquisition with MarqMetrix TouchRaman probe

Throughout the example shown in this section, the Raman probe can be seen. The probe is connected to an all-in-one (AIO) unit that also houses the laser source (Figure SI- 11). The connection is composed of fiber optics so care should be taken when operating the instrument. Given that the laser is a class 3B, the user should have proper laser training before handling the probe. As the laser can potentially damage the eye, special precaution must be taken and laser safety goggles should be worn while the laser is in operation. Furthermore, the area should be cleared from others not wearing proper laser goggles and caution signs should be placed around the perimeter (Figure SI- 12).

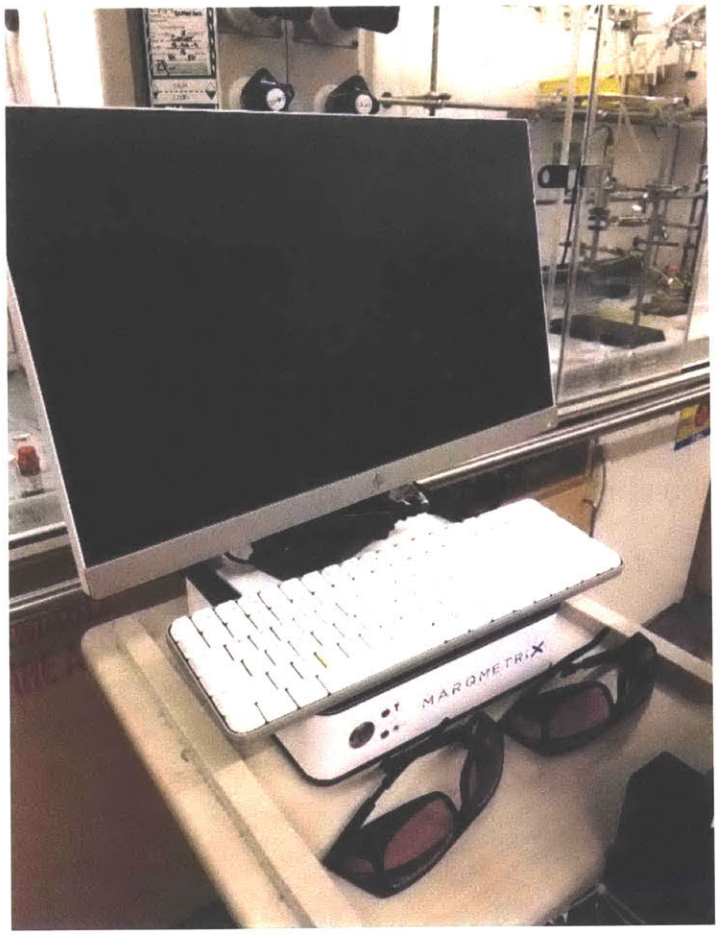

Figure SI- 11. Raman all-in-one unit that houses the operating system and laser source. Laser-safety goggles are used to protect the eyes from potential stray lasers from the probe.

Figure SI- 12. Laser caution signs that warns non-Raman workers without proper laser safety goggles to stay clear from the area.

For the software used to operate the probe and to examine the spectral data, there are three interfaces that can be accessed via tabs near the top of the window. The first interface, *Acquisition*, is shown Figure SI- 13. In the top left corner, there are various parameters can be set by the user.

- *Int. Time* – Integration time in milliseconds for each scan by the detector.
- *Averages* – Allows the user to decide how many scans to perform per spectrum.
- *Delay* – The delayed time after initiating an experiment for the laser to fire. This may be useful continuous mode. (See continuous mode for more details)
- *#Acqs* – A unique file can be saved *after each* Int. Time and Averages settings are completed. Changing this value allows the user to run experiments in tandem with the option to save each automatically (if Auto Save is checked).
- *Continuous* – Checking this allows the user to run experiments (i.e. laser constantly on) continuously until stopped by the user.
- *Dark Subtract* – Subtract a blank spectrum obtained when the laser is off.
- *Auto New Dark* – Automatically acquires a new black spectrum before each experiment.
- *Acquire* – Run experiment
- *New Dark* – Acquire new blank spectrum.
- *Path / File Name* – Allows the user to select where to save their files and what to name the files.

- *Cancel* – Stops currently running experiment.
- *Auto*-save – saves automatically after each completed experiment.

For the second interface, *Load*, the user has the option to access previous data via the dropdown menu or the "add" functionality (. The other options allows the user to remove single or all files that have been added. For the last interface, *Setup*, the initialization menu allows the user to change the detector settings. The scale menu allows the user to select between reporting the data as wavenumber (cm^{-1}) or as wavelengths (nm), and the option to view full scale. The laser menu allows the user to change the power of the laser with 450 mW being 100%. The system menu allows the user to open file explorer to access files on the AIO and to turn off the instrument.

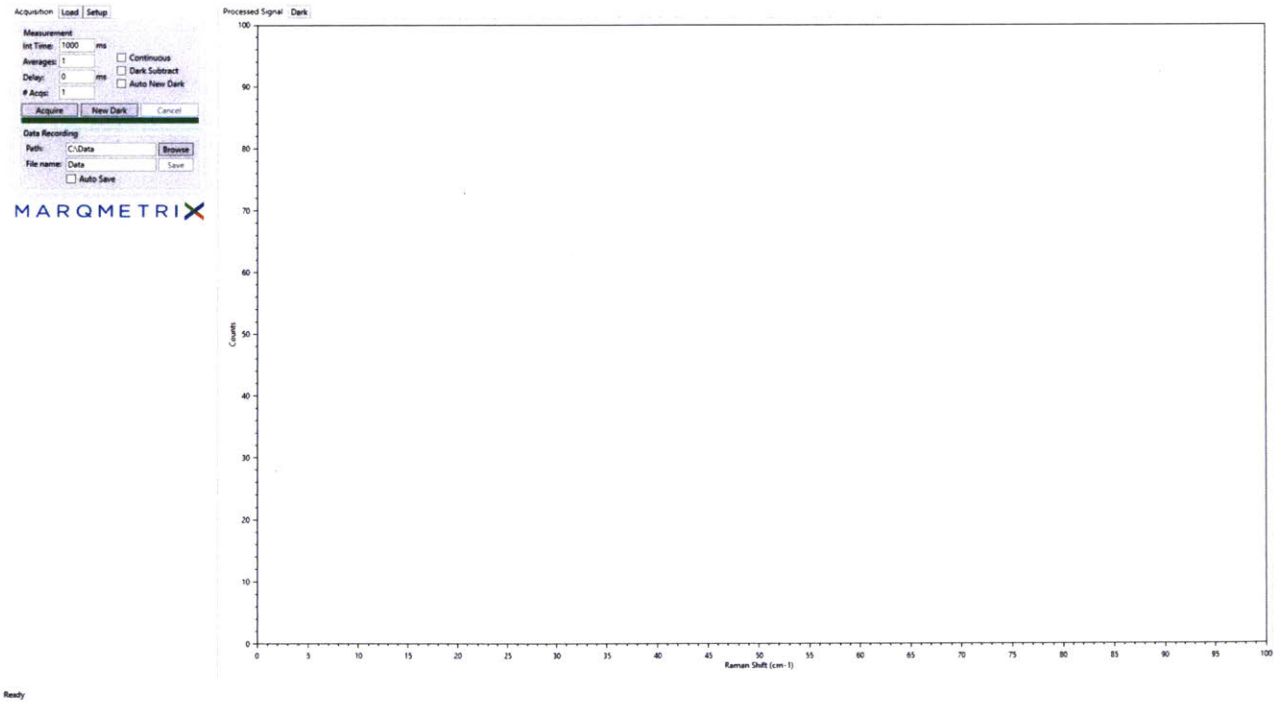

Figure SI- 13. First interface of the included Raman operating software in AIO. Various parameters are provided, see above for more details.

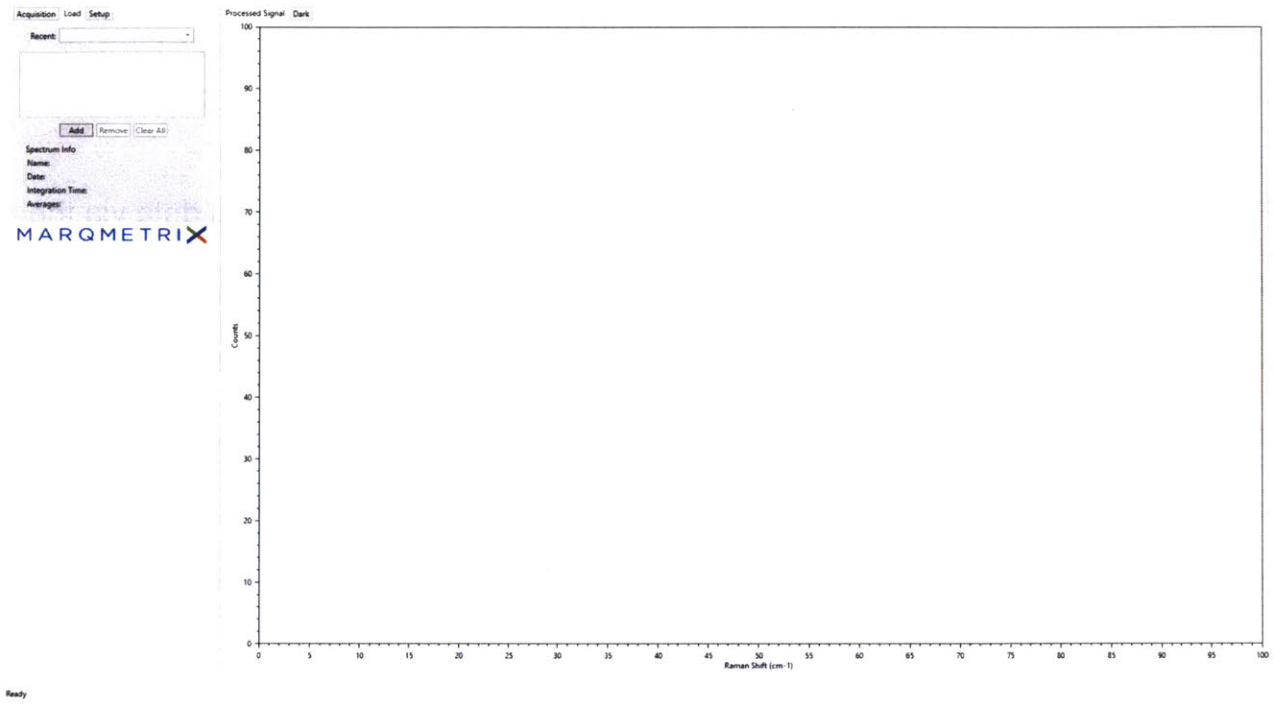

Figure SI- 14. Second interface of Raman operating software that allows the user to view and compare previous experiments.

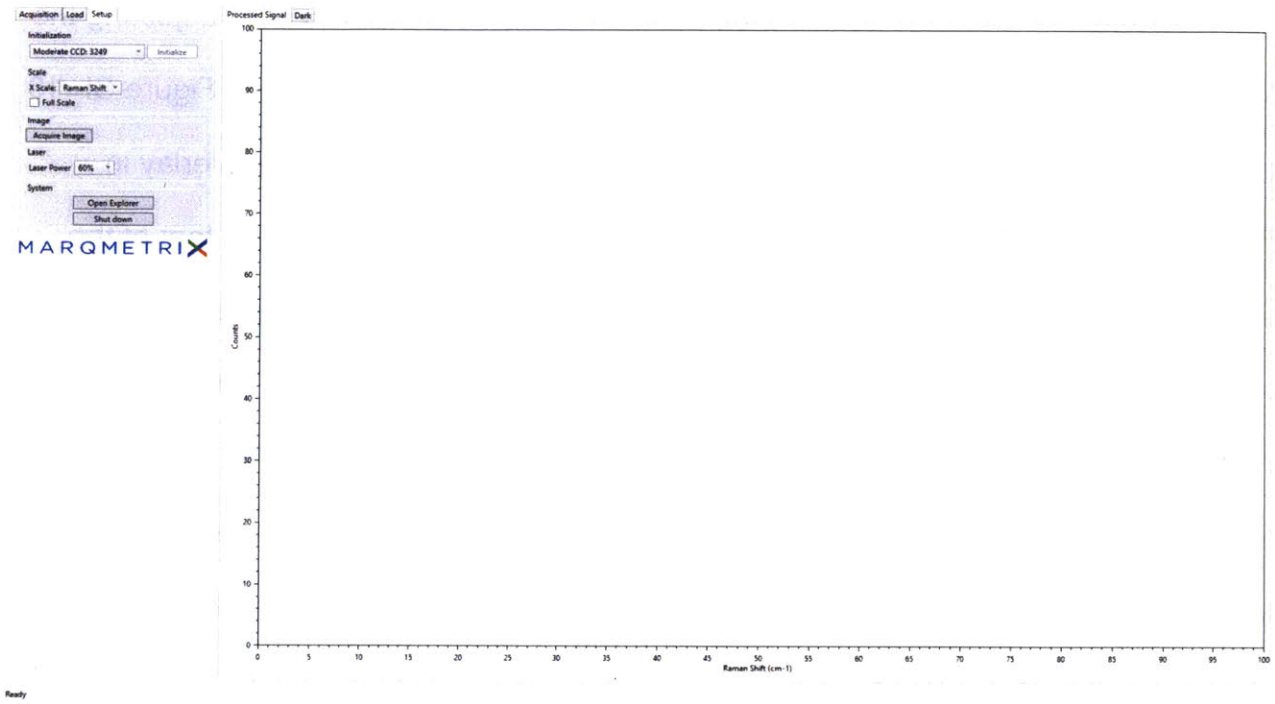

Figure SI- 15. Last interface of the Raman operating software. This interface allows the user to choose different modes of initialization, Raman spectrum display range, acquire a picture file, control the laser power, view files on AIO, and shut down instrument.

With the interface and set-up examined, general reaction monitoring methodology will be discussed. The example will be the reaction monitored that was shown in Figure 17 involving the RCM of DDM **4** and product **6**. The reactor used an 8 ft long, PFA 1/8"x0.062" tubing with a flow rate 53 μL/min and residence time of 45 minutes. Six data points were collected at equidistance from beginning to end and correlated to residence time. To mark these points, nail polish remover was used and applied the day prior to ensure that it was completely dried. Nail polish remover was found best to survive oil bath mediums and remain on the PFA tubing. Shown in Figure SI- 16, markings along a reactor were performed with the 2nd generation adapter in mind. The center of the adapter is the point of interest along the reactor. From Figure SI- 17, the reactor can be seen submerged in an oil bath.

Finding the ideal parameters for a given trial can be achieved after adjusting the parameters: int. time, averages, and laser power. From Figure SI- 18 and Figure SI- 19, spectra of DDM **4** and ring-closed product **6** are shown, with both being overlay in Figure SI- 20. From the spectra, we can see that the peaks of interest are that of the alkene region with DDM **4** at 1641 cm^{-1} and R-DDM **6** at 1625 cm^{-1} (Figure SI- 21). The carbonyl peaks (1751 cm^{-1}) of both are nearly identical. The difference in alkenyl peak intensity can be attributed to the likely presence of two olefins on DDM **4**, which effectively doubles the concentration, and the possibility that the olefin of R-DDM **6** absorbs less strongly compared to DDM **4**. These two peaks were monitored along the reactor and the data is plotted with excel. In each case, the actual concentration was calibrated to a known reference peak, such as DCE (see discussion).

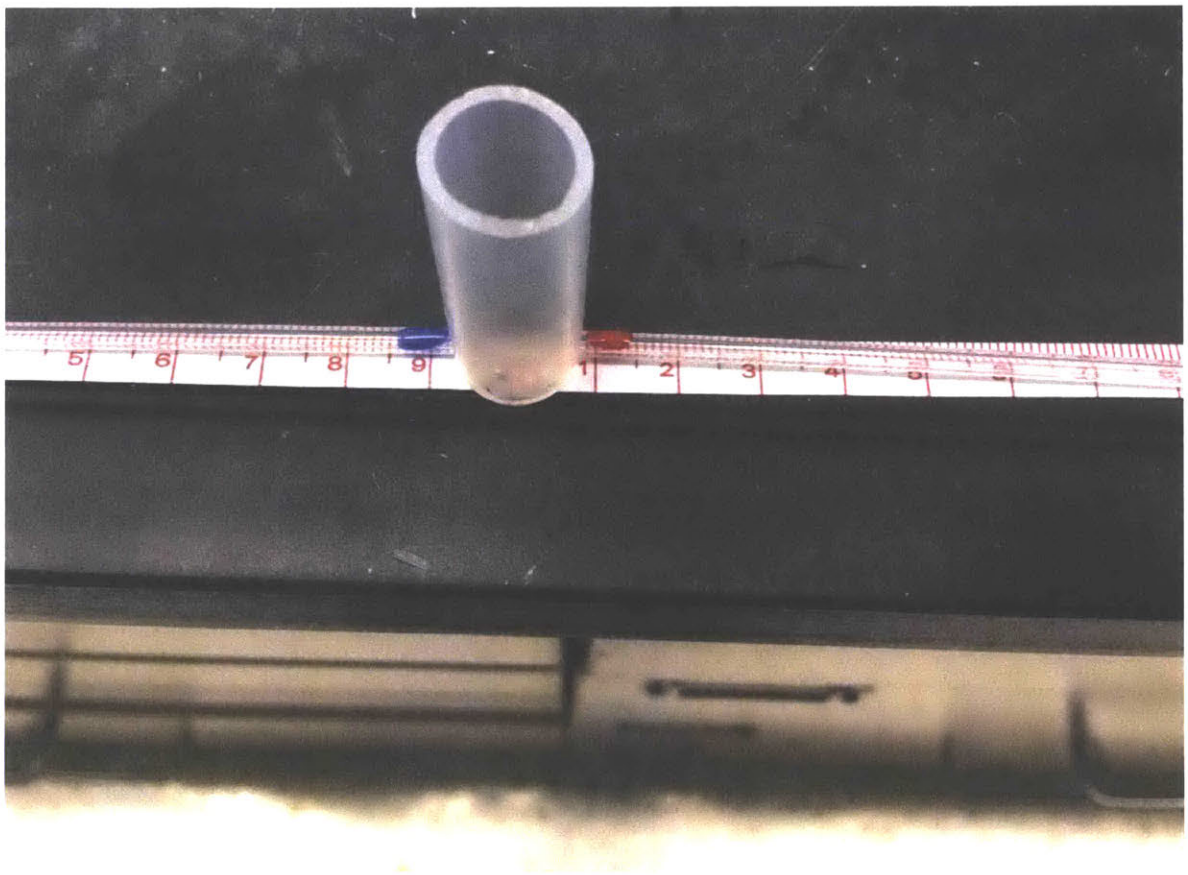

Figure SI- 16. Markings along a reactor to accurately measure distance. Nail polish was used to make these marks and allowed to dry overnight. Also shown is the 2nd generation adapter with the center at the distance of interest.

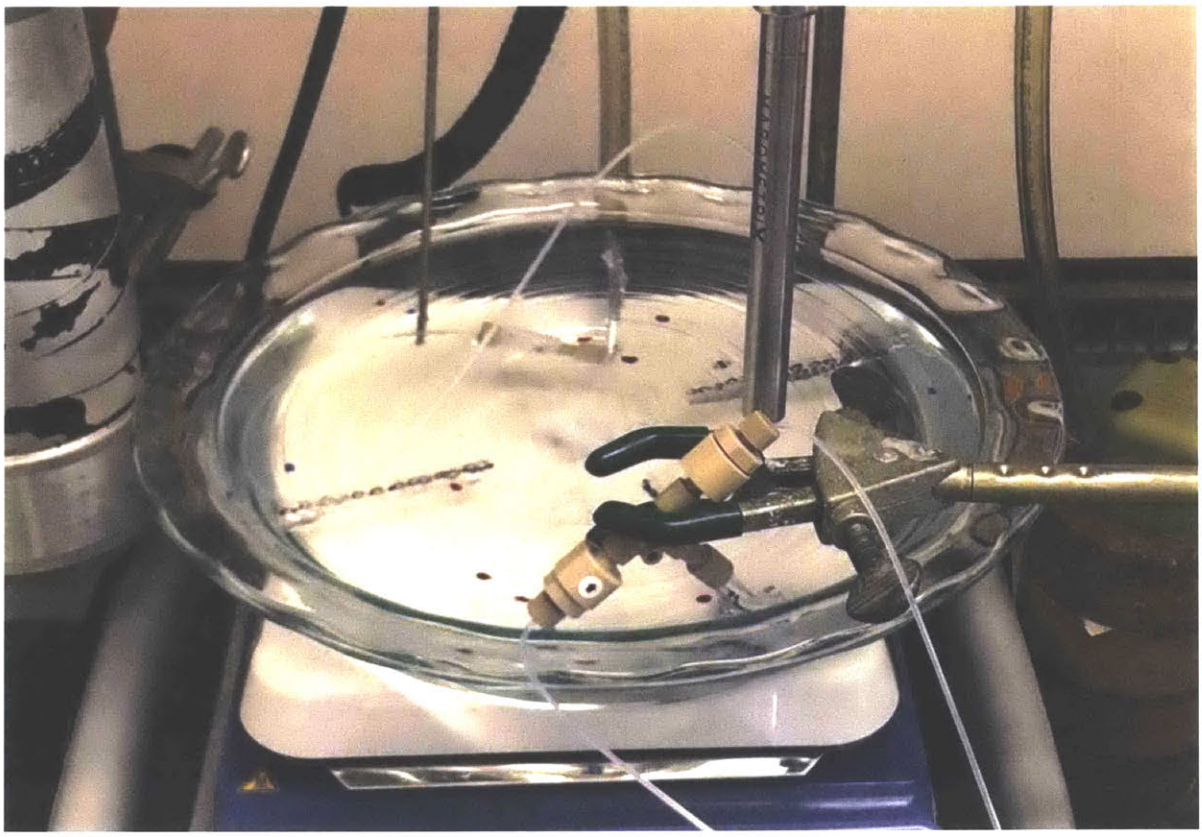

Figure SI- 17. Reactor submerged in an oil bath with markings made with nail polish remover. The probe is moved throughout the reactor with these markings to keep track of distance.

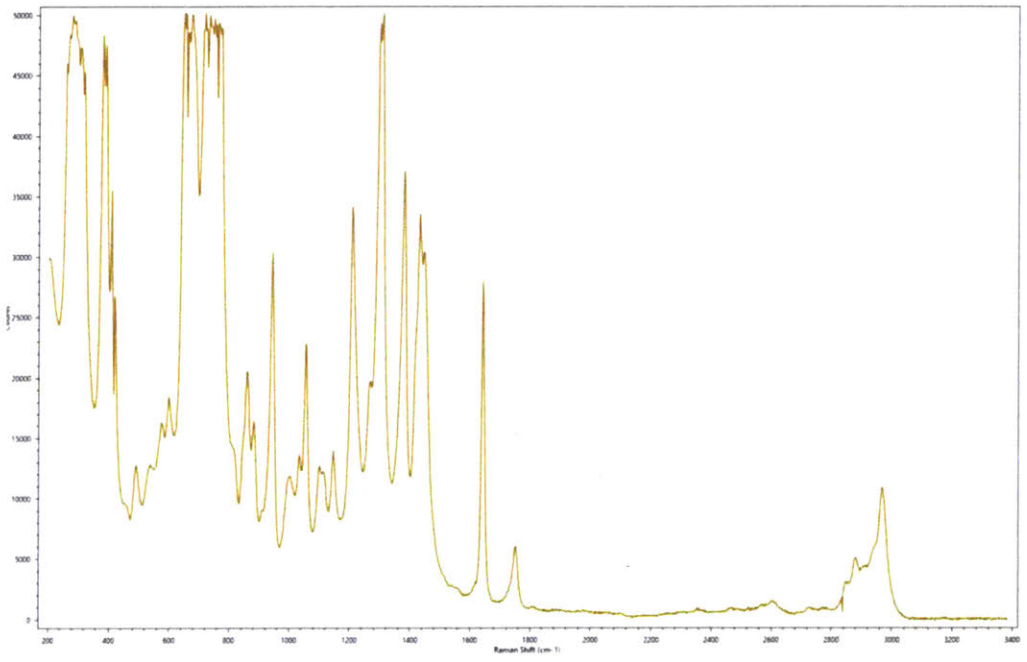

Figure SI- 18. Raman spectrum of DDM **4** at 1 M, 1000 Int. Time, 2 averages.

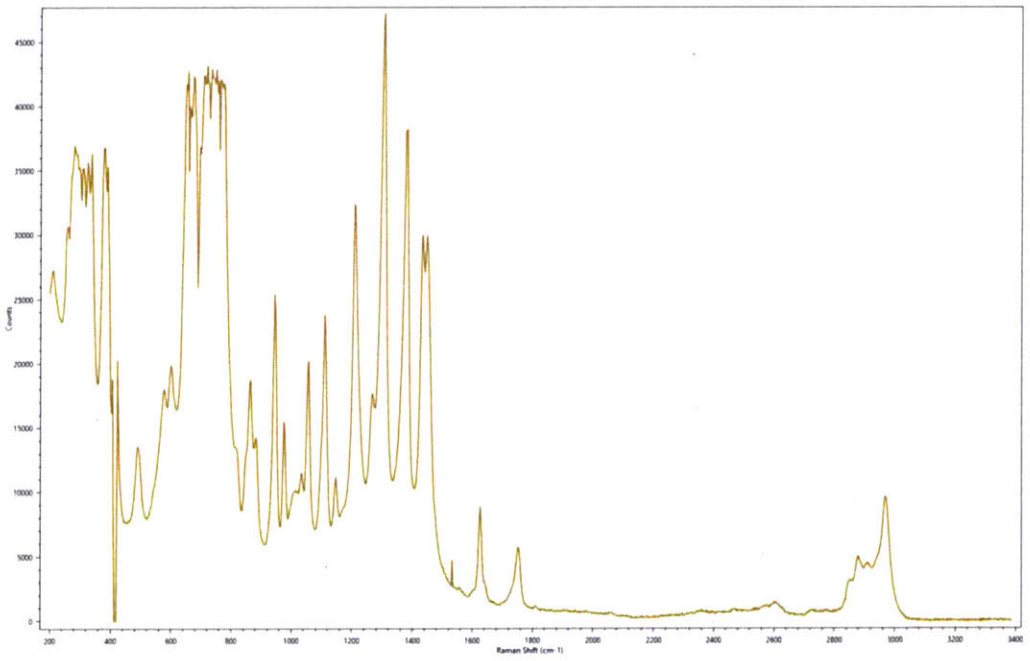

Figure SI- 19. Raman spectrum of R-DDM **6** at 1 M, 1000 Int. Time, 2 averages.

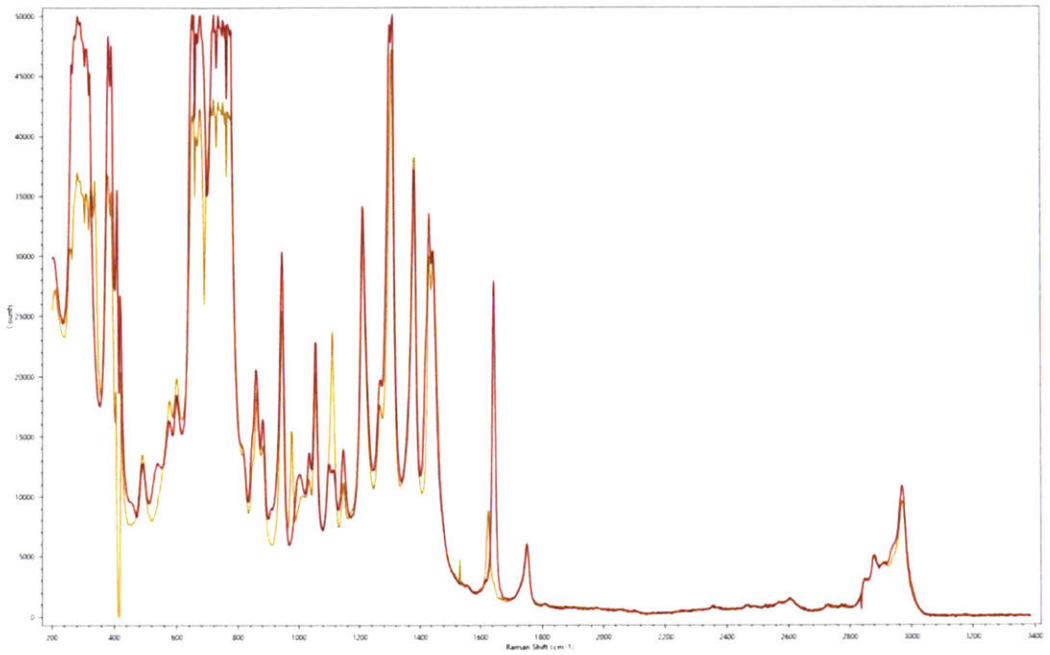

Figure SI- 20. Overlay of spectra of **4** and **6**.

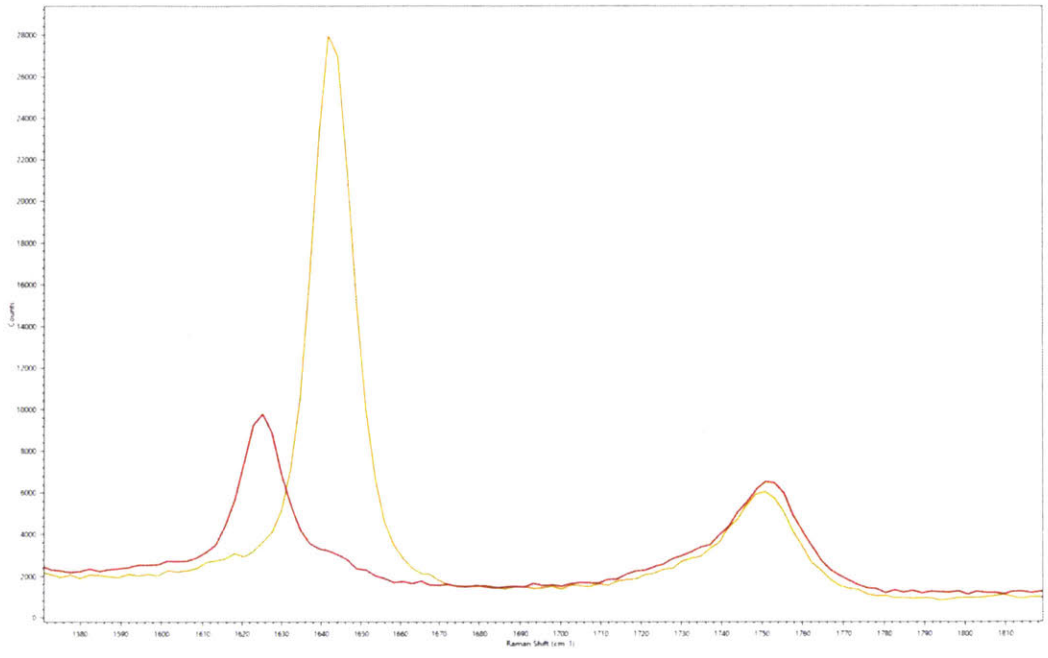

Figure SI- 21. Zoomed in region of alkenyl peaks of **4** (1641 cm^{-1}) and 6 (1625 cm^{-1}). The carbonyl stretches (1751 cm^{-1}) are also shown.

Chapter Two

Investigations of Raman Spectroscopy for Through-Tube Monitoring of Continuous-Flow Reactions – Raman Spectral Data

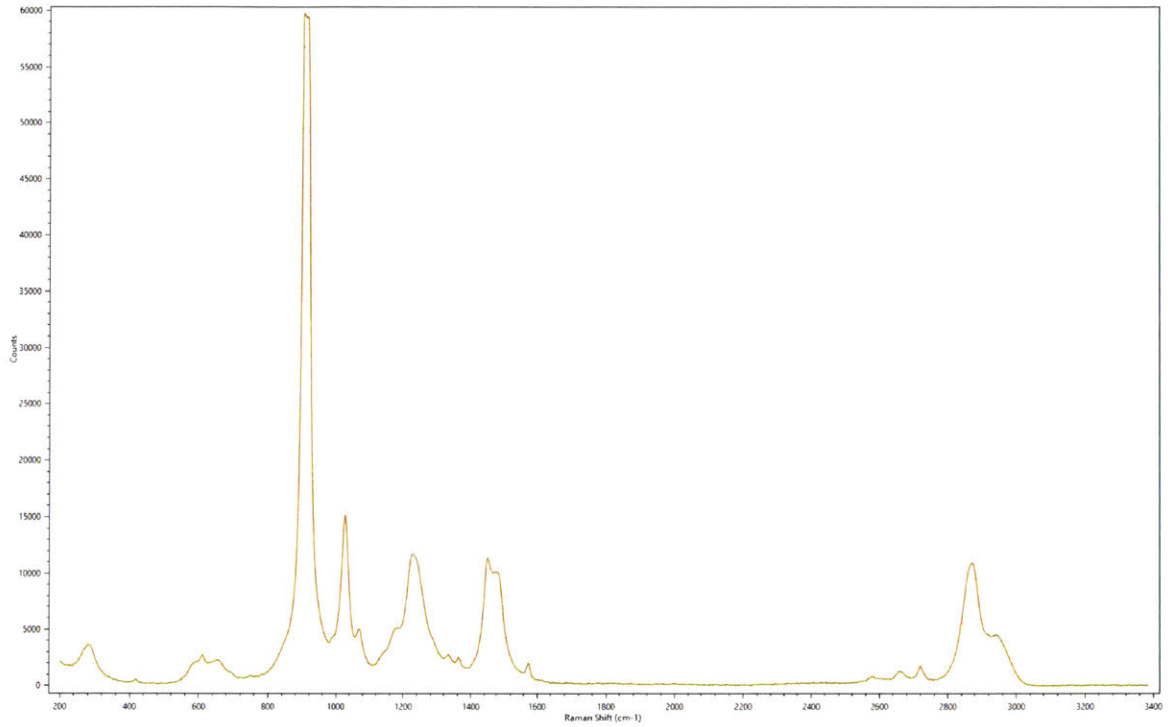

Raman Spectrum 1. Neat dimethylfuran **28**; 2000 ms Int. Time, 2 averages.

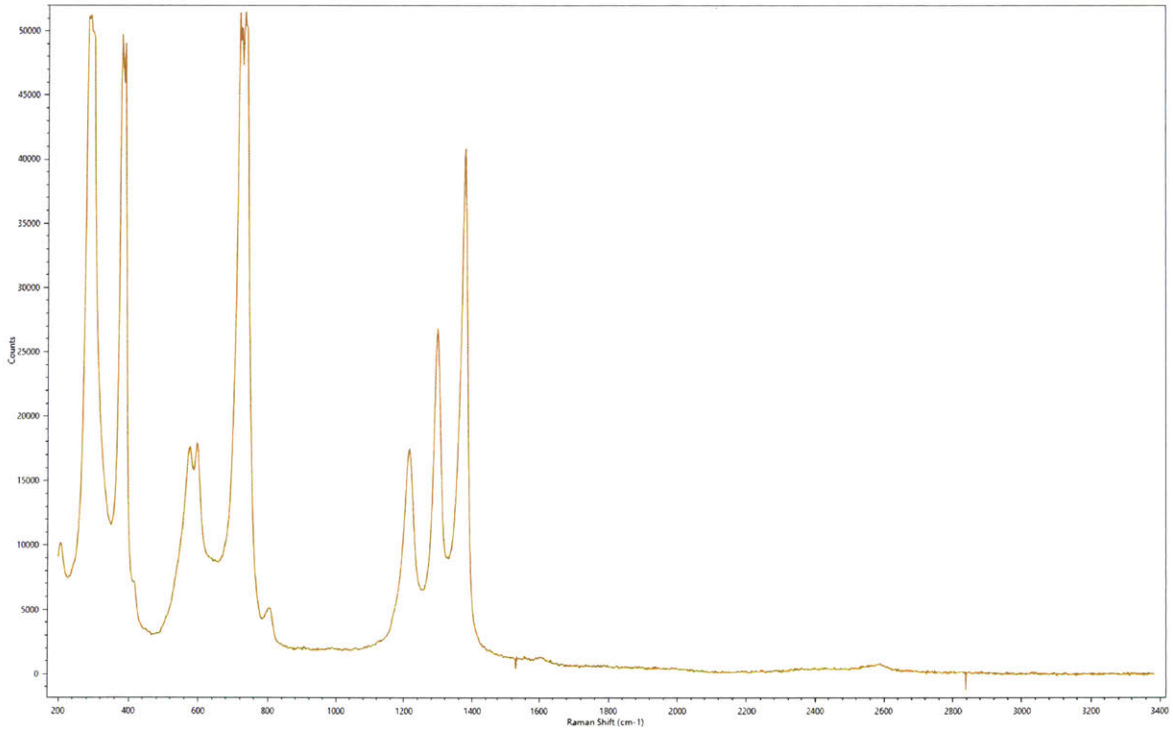

Raman Spectrum 2. PFA tubing; 10000 ms Int. Time, 2 averages.

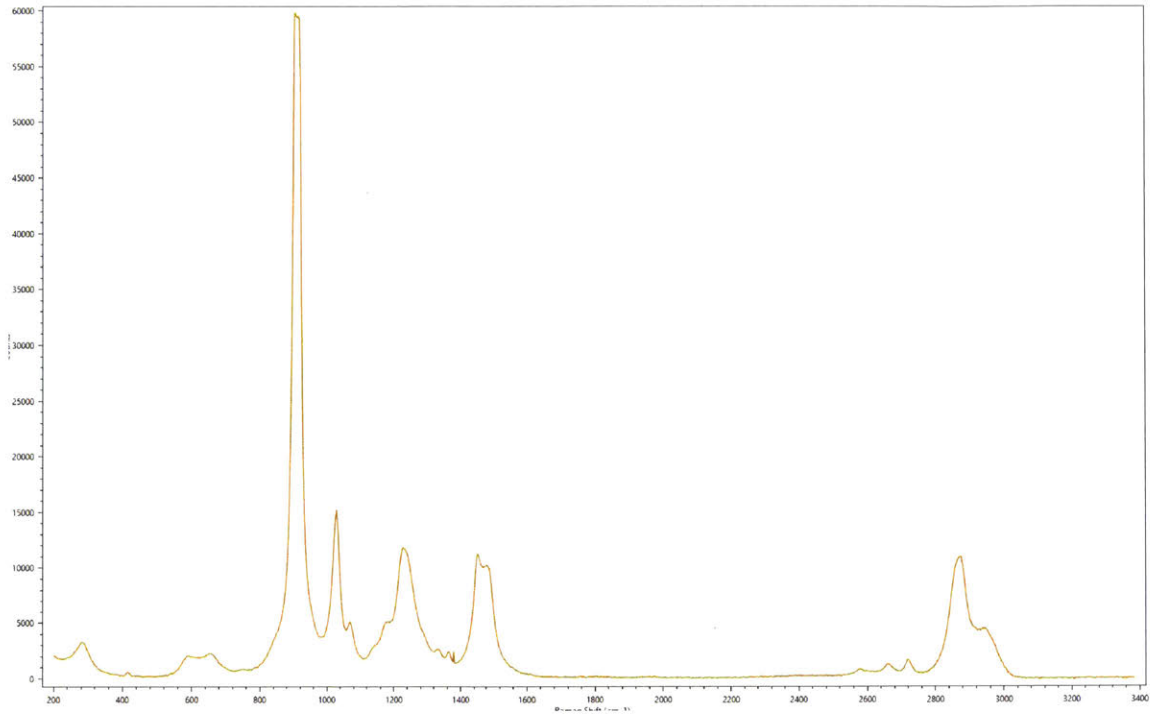

Raman Spectrum 3. THF solvent; 2000 ms Int. Time, 2 averages.

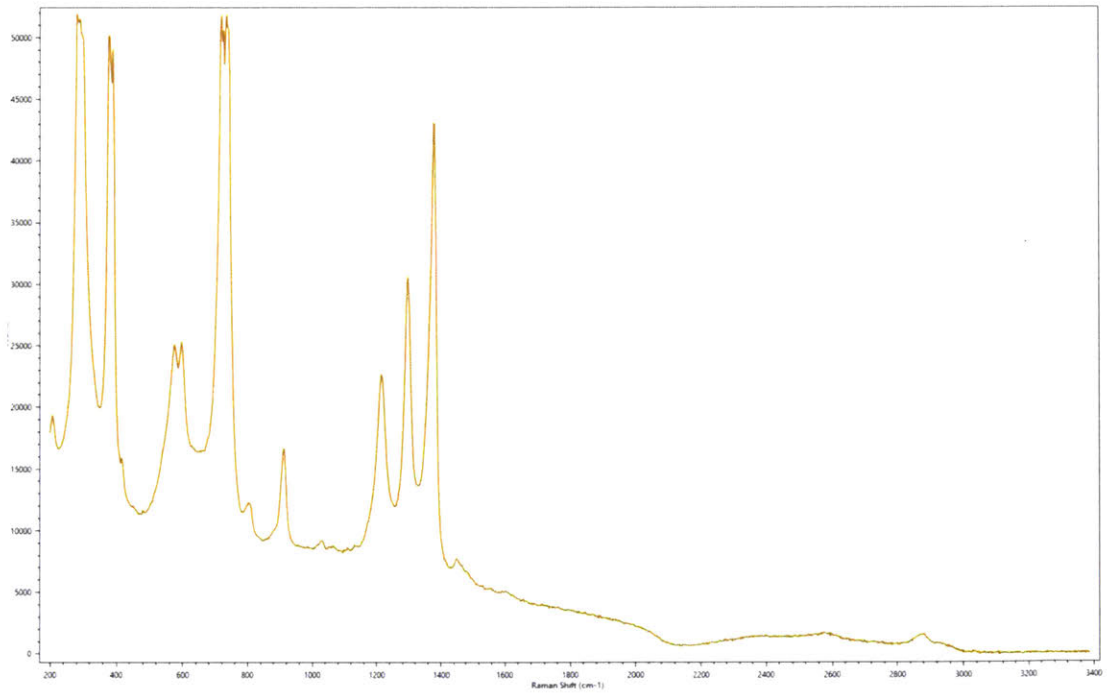

Raman Spectrum 4. TBAF in 1M THF through PFA tubing; 10000 ms Int. Time, 2 averages.

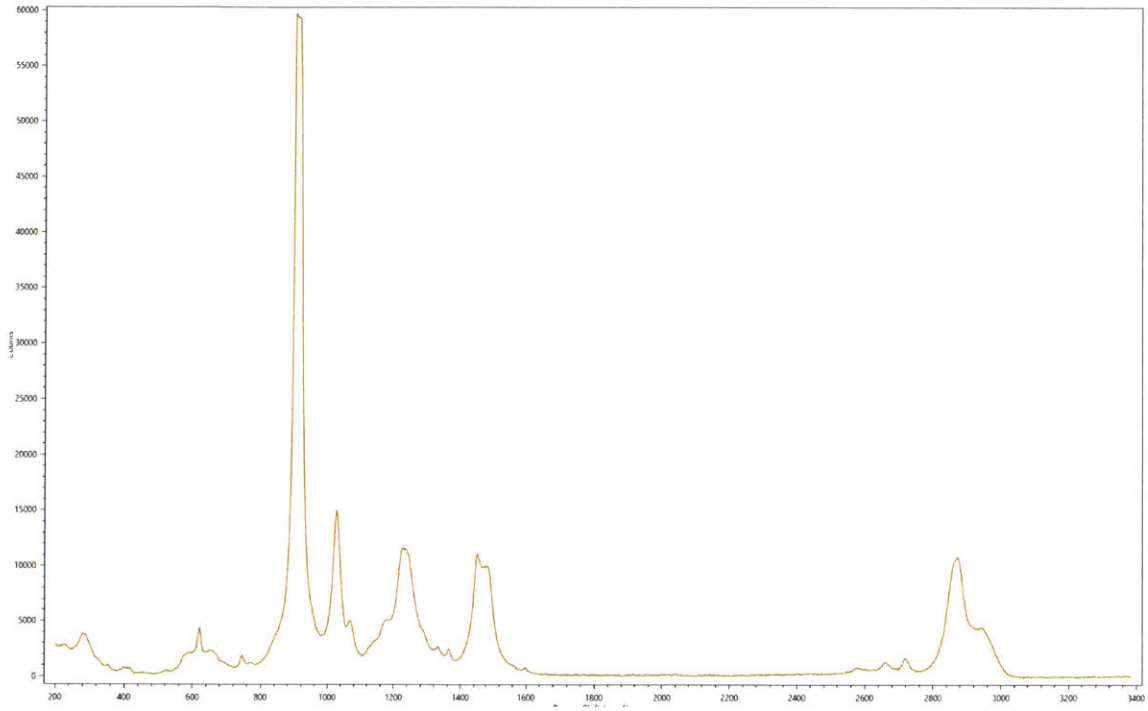

Raman Spectrum 5. Neat Benzyne precursor **14**; 2000 ms Int. Time, 2 averages.

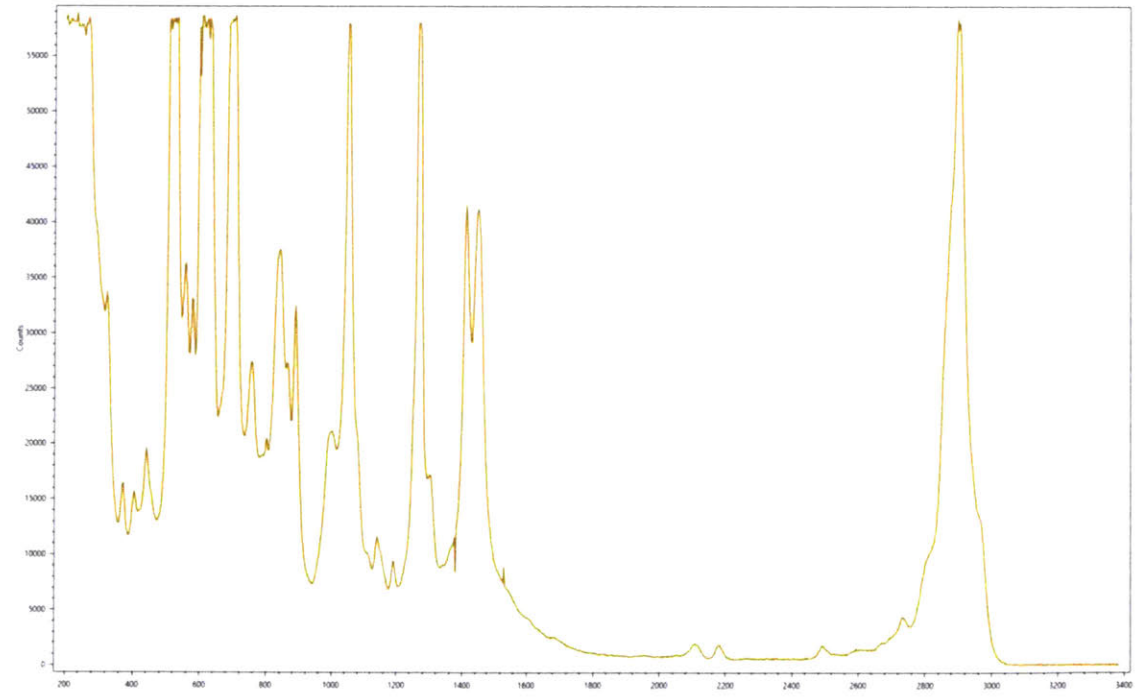

Raman Spectrum 6. Neat ketene **35**; 10000 ms Int. Time, 2 averages.

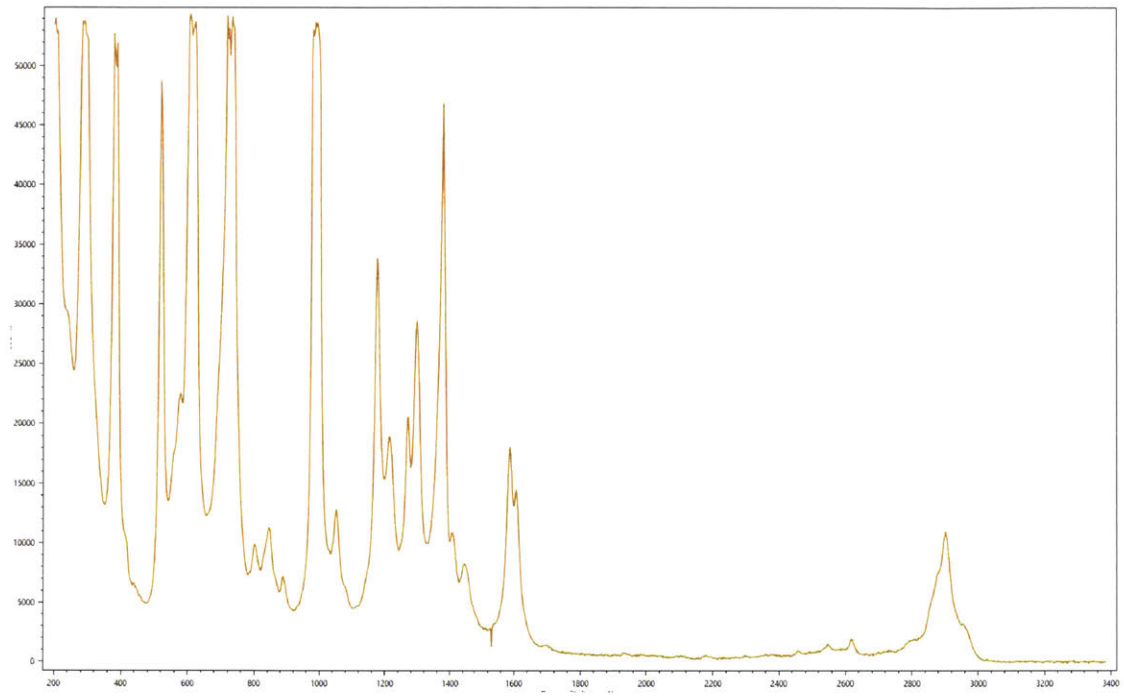

Raman Spectrum 7. Ketene **33** in benzene through PFA tubing; 10000 ms Int. Time, 2 averages.

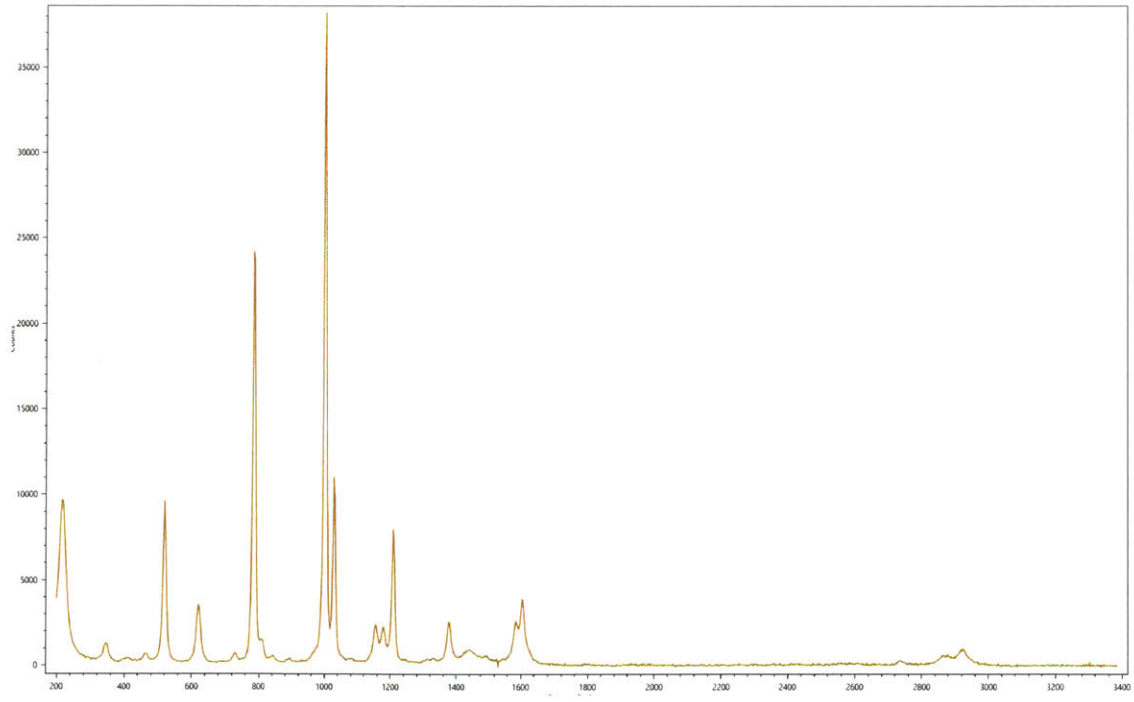

Raman Spectrum 8. Toluene; 10000 ms Int. Time, 2 averages.

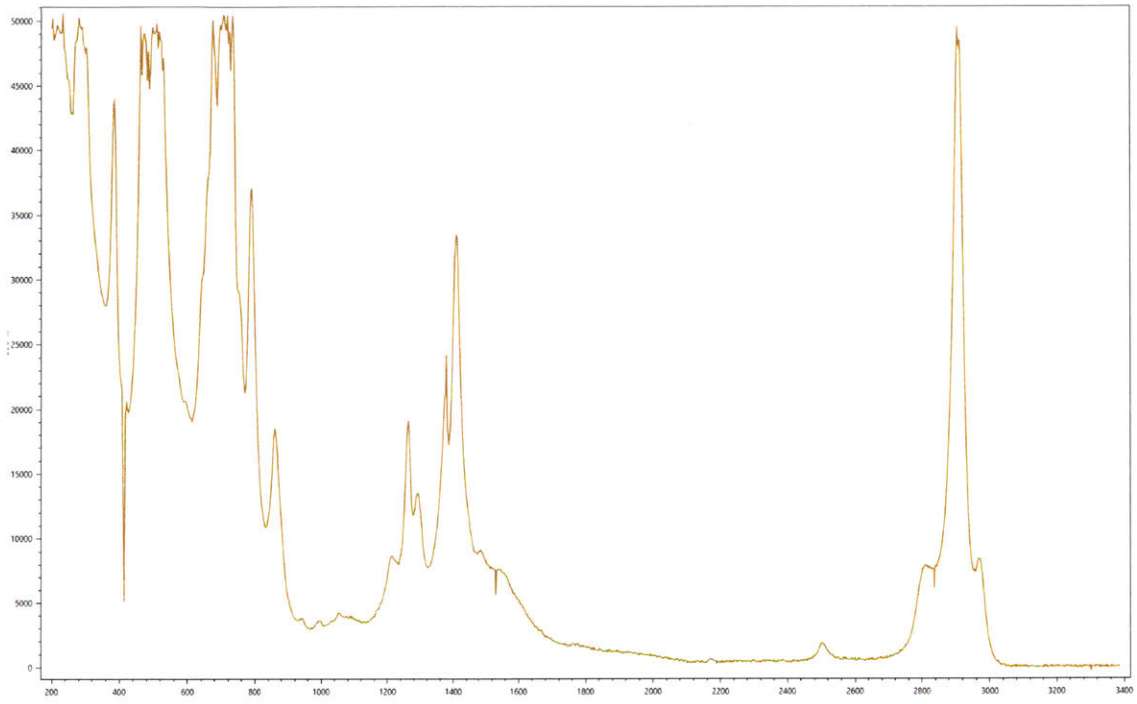

Raman Spectrum 9. Ketene formation in continuous-flow with DCE solvent at 120 °C; 10000 ms Int. Time, 2 averages.

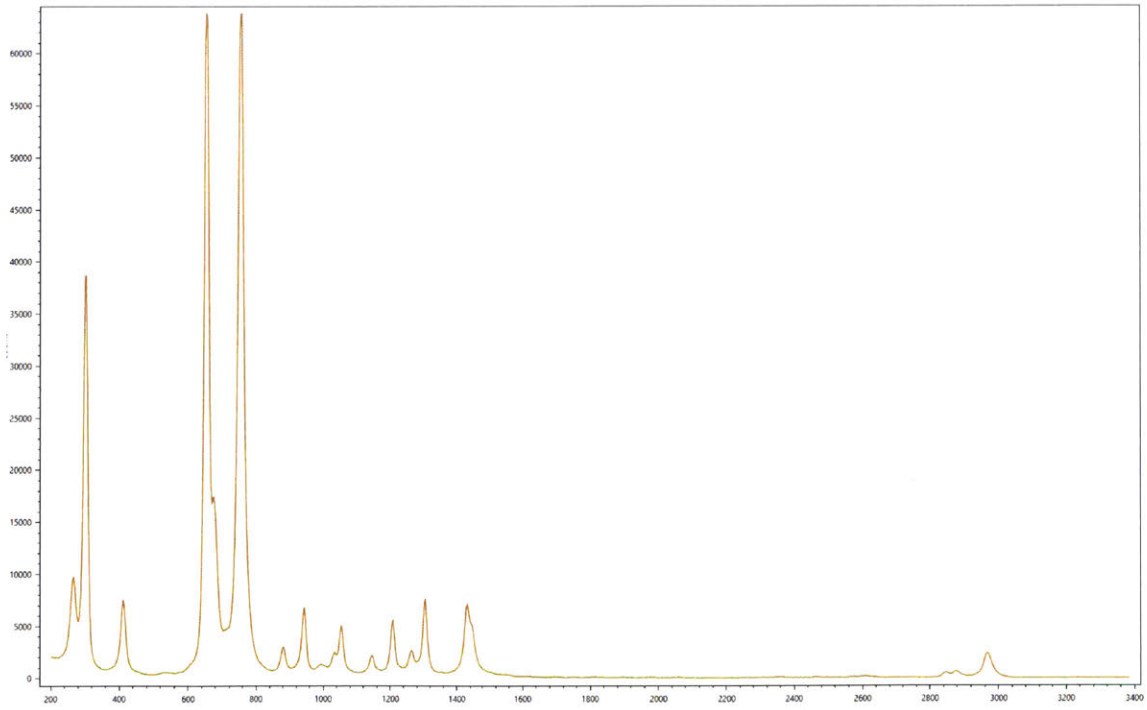

Raman Spectrum 10. DCE solvent; 1000 ms Int. Time, 2 averages.